

Computational Insights into Proton and Hydride Transfer Chemistry

by

Subhrashis Banerjee

10CC18A26012

A thesis submitted to the
Academy of Scientific & Innovative
Research for the award of the degree of

DOCTOR OF PHILOSOPHY

In

SCIENCE

Under the supervision of

Dr. Kumar Vanka



CSIR-National Chemical Laboratory, Pune



Academy of Scientific and Innovative Research

AcSIR Headquarters, CSIR-HRDC campus

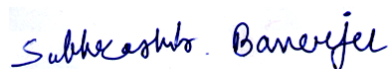
Sector 19, Kamla Nehru Nagar,

Ghaziabad, U.P. - 201002, India

March 2022

Certificate

This is to certify that the work incorporated in this Ph.D. thesis entitled, "Computational Insights into Proton and Hydride Transfer Chemistry" submitted by Subhrashis Banerjee to the Academy of Scientific and Innovative Research (AcSIR) in fulfillment of the requirements for the award of the Degree of Doctor of Philosophy In Science embodies original research work carried-out by the student. We, further certify that this work has not been submitted to any other University or Institution in part or full for the award of any degree or diploma. Research material(s) obtained from other source(s) and used in this research work has/have been duly acknowledged in the thesis. Image(s), illustration(s), figure(s), table(s) etc., used in the thesis from other source(s), have also been duly cited and acknowledged.



(Signature of Student)

Name: Subhrashis Banerjee

Date: 31-03-2022

(Signature of Co-Supervisor)

No



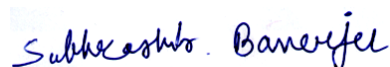
(Signature of Supervisor)

Name: Dr. Kumar Vanka

Date: 31-03-2022

STATEMENTS OF ACADEMIC INTEGRITY

I, **Subhrashis Banerjee**, a Ph.D. student of the Academy of Scientific and Innovative Research (AcSIR) with Registration No. **10CC18A26012** hereby undertake that, the thesis entitled "**Computational Insights into Proton and Hydride Transfer Chemistry**" has been prepared by me and that the document reports original work carried out by me and is free of any plagiarism in compliance with the UGC Regulations on "*Promotion of Academic Integrity and Prevention of Plagiarism in Higher Educational Institutions (2018)*" and the CSIR Guidelines for "*Ethics in Research and in Governance (2020)*".



Signature of the Student

Date: 31-03-2022

Place: CSIR-NCL, Pune

It is hereby certified that the work done by the student, under my/our supervision, is plagiarism-free in accordance with the UGC Regulations on "*Promotion of Academic Integrity and Prevention of Plagiarism in Higher Educational Institutions (2018)*" and the CSIR Guidelines for "*Ethics in Research and in Governance (2020)*".



Signature of the Supervisor

Name: Dr. Kumar Vanka

Date: 31-03-2022

Place: CSIR-NCL, Pune

Dedicated to my beloved parents

Acknowledgement

At the concluding stage of PhD journey, I ponder back and wonder how did it all started and how did it evolved so graciously. This journey, a rare learning curve of my life, is a complex amalgamation of several factors and altruistic values of numerous people. I am bound with my duty to at least acknowledge those people who tangibly or intangibly contributed for this doctorate journey.

First, I would like to express my gratefulness to my research supervisor, Dr. Kumar Vanka, for his constant guidance and support. Without him, it would have been impossible to reach this point. His undying inclination for the scientific insights has always amazed me. His nature of being perfect, unidirectional, liberal thinking and possession over the subject has inspired me a lot. As an individual, his mentor-ship is not restricted to research, but span beyond measures. He is generous, empathetic, yet humble and down to the earth person. Furthermore, I am also grateful for the academic freedom he has given me, which motivated me to grow as an independent researcher. Also, his teaching, writing and communication skills have always been inspirational to me throughout my doctoral research.

I would also thank Doctoral Advisory Committee members, Dr. Sakya S. Sen, Dr. Sailaja Krishnamurty and DAC chairperson Dr. Benudhar Punji for their insightful suggestions and feedback. I am grateful to Director Dr. Ashish Lele for his support. I am also grateful to former directors Dr. Ashwini Kumar Nangia, and Dr. Sourav Pal. Moreover, I take the opportunity to thank the present and former heads of the Physical and Materials Chemistry Division for their support and providing all facilities during my Ph.D.

I want to extend my gratitude to Dr. Suman Chakrabarty, who was my first research guide, whose support and encouragement helped me to start thinking the researcher related problems in entire different perspective. I am grateful to all the teachers who had taught me during my Ph.D. course work at CSIR-NCL: Dr. Kumar Vanka, Dr. Suman Chakrabarty, Dr. Sayan Bagchi, Dr. Debashree Ghosh, Dr. Rajesh Gonnade and Dr. T.G. Ajithkumar as well as other scientists in NCL. Let me extend my warm thanks to my research collaborators Dr. Rahul Banerjee, Dr.

Sakya S. Sen, Dr. Nitin Patil, Dr. Shabana Khan, Dr. Moumita Majumdar and Dr. Paresh Dhepe. Moreover, I owe to thank my University and school teachers for teaching me the basics of chemistry, physics, mathematics and biology which helped me a lot in understanding research problems.

I also acknowledge all the non-academic staff of CSIR-NCL, and AcSIR, for their support and help during my work. Without the funding, this Ph.D. journey would not have been possible; hence I would like to express my gratitude to the Council of Scientific & Industrial Research (CSIR) for the fellowship. Moreover, I want to thank the whole scientific community for being a source of inspiration and motivation.

I feel myself to be lucky to have dearest friends and roommates Tamal, Tapas, and Debranjana. I am immensely thankful to them for being there with me during my ups and downs during my whole Ph.D tenure. I thank them for their company and support.

It is my pleasure to thank my past labmates Shantanu, Nisha, Manoj, Amrita, Jugal, Yuvraj, Mrintyunjay, Shailja, Anagh and present labmates Vipin, Ruchi, Siddharth, Soumyaranjan, Himanshu and Priyam. It was fun working with them together. I express special thanks to Ruchi, Vipin and Soumyaranjan for helping me through many ways. My entire journey of Ph.D was associated with so many friends and seniors. Some of them are Sajal da, Santu da, Turbasuda, Achintyada, Susantada, Himadrida, Aaryada, Sayantan da, Sudip da, Atryee di, Gargi di, Monalisa di, Chayanika di, Vrushali, Amit, Pranab, Samik, Ravi, Abhijit, Koushik, Ashis, Saibal, Sibaprasad, Subrata, Suvendu, Rahul, Pronoy, Narugopal, Milan, Sutanu, Abdul, Srijan, Shibam, Tubai, Arindam, Sanjukta, Gargi, Susmita and many more. I am blessed to have them through fun, up and downs in this journey. The seniors from my M.Sc Atanu da and Shantanu da helped me lot in initial stages of my research. I want to thank Kabir, Pooja and Chhaya with whom I had lot of fun throughout my M.Sc and PhD days. I spent lot of good times with them. I want to thank Shrreya for the friendship we shared all through my PhD journey. I also want to thank Animesh and Sourosree for supporting and encouraging me in the last few days of my Ph.D. I had lot of beautiful days and nights partying with them. The long discussions about society, life, nature and many others topic helped me to gain knowledge outside my research. I

enjoyed a lot playing football with Shabeeb, Vidyanand, Ajith, Amarnath, Pranab, Sarath, Sandy, Kiran, Arindam and many others.

At this nostalgic junction, I feel content towards few important people in my life, my family. No words are sufficient to describe their love, blessings and support. I am highly indebted to my mother (Uma) and father (Pranab) for their unconditional love and the sacrifices they have made for me. I want to thank my sister (Soumi) and brother-in-law (Anindya) for their love and blessings. Also, I wish to thank my brother (Sourav) and sister-in-law (Dolon) for support and encouragement. My brother always encouraged me to do good things in life. I learnt lot of positivity from him. Furthermore, I would like to thank my all family members, cousin brothers and sisters for their mental and emotional support. I consider myself blessed to have such a beautiful family around me.

Finally, I express my gratitude to the Almighty for the blessings and for providing special challenges in my entire Ph.D journey.

-Subhrashis Banerjee

Table of Contents

| | |
|--|-----------|
| Abbreviations | ii |
| Physical Constants | iii |
| Chapter 1: A Brief Overview of the Importance in Hydride and Proton Transfer Chemical Transformations | 1 |
| 1.1 Introduction..... | 2 |
| 1.2 Hydride Transfer..... | 3 |
| 1.3 Hydride Transfer in Main Group Catalysis..... | 5 |
| 1.3.1 Hydrosilylation..... | 6 |
| 1.3.2 Tris(pentafluorophenyl)borane (B(C ₆ F ₅) ₃)..... | 7 |
| 1.3.3 Autocatalysis..... | 9 |
| 1.3.4 Hydroboration..... | 10 |
| 1.4 Stannylenes and Germylenes | 11 |
| 1.5 Proton Transfer..... | 14 |
| 1.6 Asymmetric Organocatalysis..... | 15 |
| 1.6.1 Brønsted Base Catalysis..... | 16 |
| 1.6.2 <i>Cinchona</i> Alkaloids..... | 17 |
| 1.6.3 Non-Covalent Interactions | 20 |
| 1.7 Objective of the Thesis..... | 22 |
| 1.8 Organization of the Thesis..... | 22 |
| 1.9 References..... | 25 |
| Chapter 2: History and Fundamentals of Computational Chemistry | 35 |
| Abstract..... | 36 |
| 2.1 Introduction to Computational Chemistry..... | 37 |
| 2.2 Quantum Mechanics and the Wave Function..... | 38 |
| 2.2.1 Schrodinger Equation and Hamiltonian Operator..... | 38 |
| 2.2.2 The Born-Oppenheimer Approximation..... | 40 |

| | |
|--|------------|
| 2.2.3 Wave Function, Probability and Normalization..... | 41 |
| 2.2.4 The Variational Principle..... | 42 |
| 2.2.5 Functional..... | 43 |
| 2.3 The Fundamentals of Density Functional Theory..... | 44 |
| 2.3.1 The Electron Density..... | 45 |
| 2.3.2 The Pair Density..... | 47 |
| 2.3.3 The Thomas-Fermi Model..... | 47 |
| 2.3.4 Hohenberg-Kohn (HK) Theorems..... | 49 |
| 2.3.5 The Kohn-Sham (KS) Approach..... | 56 |
| 2.4 Natural Bond Orbital Analysis (NBO)..... | 61 |
| 2.5 Free Volume Correction for Translational Entropy..... | 62 |
| 2.6 Non-Covalent Interaction Plot..... | 63 |
| 2.7 Quantification of Selectivity from Computation..... | 65 |
| 2.8 References..... | 67 |
| Chapter 3: B(C₆F₅)₃ Catalyst or Initiator? Insights from Computational Studies | 70 |
| Abstract..... | 71 |
| 3.1 Introduction..... | 72 |
| 3.2 Computational Details..... | 77 |
| 3.2.1 The Conformational Exploration..... | 79 |
| 3.2.2 The Energetic Span Model..... | 80 |
| 3.3 Results and Discussion..... | 80 |
| 3.3.1 Investigation of B(C ₆ F ₅) ₃ Involving in Normal Catalytic Pathway..... | 80 |
| 3.3.2 Investigation of B(C ₆ F ₅) ₃ Involving in Autocatalytic Pathway..... | 82 |
| 3.4 Conclusion..... | 90 |
| 3.5 References..... | 91 |
| Chapter 4: The Role of Ion-pair in B(C₆F₅)₃ Catalyzed Zwitterionic Chemistry..... | 100 |
| Abstract..... | 101 |

| | |
|---|------------|
| 4.1 Introduction..... | 102 |
| 4.2 Computational Details..... | 104 |
| 4.2.1 The Energetic Span Model..... | 106 |
| 4.3 Results and Discussion..... | 106 |
| 4.3.1 The Formation of Different Favorable and Unfavorable Ion-Pairs as mentioned in the Table 4.1..... | 115 |
| 4.4 Conclusion..... | 121 |
| 4.5 References..... | 123 |
| Chapter 5: The Role of Hydride Transfer in Stannylenes and Germylenes Initiated Catalysis..... | 127 |
| Abstract..... | 128 |
| 5.1 Introduction..... | 129 |
| 5.2 Computational Details..... | 132 |
| 5.3 Results and Discussion..... | 134 |
| 5.3.1 Calculations According to the Newly Proposed Mechanism..... | 142 |
| 5.4 Conclusion..... | 147 |
| 5.5 References..... | 148 |
| Chapter 6: Unraveling the Role of Organocatalysis in Modified Cinchona Alkaloid Catalyst via Proton Transfer..... | 159 |
| Abstract..... | 160 |
| 6.1 Introduction..... | 161 |
| 6.2 Computational Details..... | 166 |
| 6.2.1 Enantiomeric Ratio (er) Calculations..... | 168 |
| 6.2.2 Non-Covalent Interaction (NCI) Plot Analysis..... | 169 |
| 6.3 Results and Discussion..... | 169 |
| 6.3.1 Conformational Analysis of BzCPD..... | 169 |
| 6.3.2 Mechanistic study of the BzCPD Catalyzed Thiocyanation Reaction with Oxindole as Nucleophile, N-Thiocyanatophthalimide as Electrophile and 2-naphthol as Additive..... | 171 |
| 6.3.3 Origin of Enantioselectivity for Reaction with Additive and Oxindole..... | 179 |

| | |
|---|------------|
| 6.3.4 Mechanistic study of the thiocyanation reaction with BzCPD as catalyst, β -keto ester as nucleophile, and N-thiocyanatophthalimide as electrophile..... | 185 |
| 6.3.5 Origin of Enantioselectivity for reaction without Additive and β -keto ester | 186 |
| 6.3.6. Determining why there is change in enantioselectivity when the nucleophile is changed..... | 188 |
| 6.4 Conclusion..... | 190 |
| 6.5 References..... | 192 |
| Chapter 7: Summary and Future Outlook..... | 201 |
| 7.1 Focus of the Thesis..... | 202 |
| 7.2 Methodology Employed..... | 203 |
| 7.3 Summary of Results..... | 204 |
| 7.4 Future Outlook..... | 206 |
| 7.5 References..... | 208 |
| ABSTRACT..... | 211 |
| Details of the publications emanating from the thesis work..... | 212 |

List of Figures

| | |
|--|----|
| Figure 1.1 The simplest reaction for hydride transfer mechanism..... | 3 |
| Figure 1.2 The simplest reaction of the intermolecular hydride transfer mechanism. | 4 |
| Figure 1.3 The general scheme for the hydrosilylation of different unsaturated compounds | 6 |
| Figure 1.4 An idealized mechanism for the metal catalysed hydrosilylation of alkene. | 7 |
| Figure 1.5 Comparison of the Lewis acidity between different boron species..... | 8 |
| Figure 1.6 Hydroboration of a terminal alkene to a trialkylborane, showing an idealized image of the cyclic transition state | 11 |
| Figure 1.7 The ability of low valent main group compounds to act as both electrophiles and nucleophiles..... | 14 |
| Figure 1.8 Simplified model for Chiral Brønsted bases catalyst design..... | 17 |
| Figure 1.9 The relevant angles and dihedrals for the cinchona alkaloid catalyst | 18 |
| Figure 1.10 Different modified cinchona alkaloid catalysts..... | 19 |
| Figure 1.11 Non-covalent interactions of a model system are shown | 21 |
| Figure 2.1 The flow chart for Kohn Sham iterations for the single point or the single step during optimization | 61 |
| Figure 3.1 The role of $B(C_6F_5)_3$ in homogeneous olefin polymerization has been that of a co-catalyst or initiator, while the cation formed performs as the actual catalyst..... | 73 |
| Figure 3.2 The <i>in situ</i> generation of SiH_4 , as proposed by Simonneau and Oestreich. | 74 |
| Figure 3.3 The Lewis acid $B(C_6F_5)_3$ catalysed mechanism for the formation of SiH_4 from tri(cyclohexa-2,5-diene-1-yl)silane..... | 75 |
| Figure 3.4 The currently proposed autocatalytic mechanism for the formation of di(cyclohexa-2,5-diene-1-yl)silane, which is a lower surrogate of tri(cyclohexa-2,5-diene-1-yl)silane. The $[BH(C_6F_5)_3]^-$ anion remains as a spectator, and shifts to the cation formed to create a new ion-pair..... | 75 |
| Figure 3.5 <i>In situ</i> generation of SiH_4 : the currently proposed autocatalytic approach. The $[BH(C_6F_5)_3]^-$ anion remains as a spectator. In each step it forms the ion pair with the new cation which formed from the autocatalytic mechanism. In one step the R' generates and comes out as a cation in the very next step..... | 76 |
| Figure 3.6 The free energy profile (ΔG) in kcal/mol for the proposed mechanism by Simonneau and Oestreich. R =cyclohexa-1,4-diene. The blue profile is for the PTC(DCM) level of theory and the brown profile is for the TDC(DCM) level of theory | 82 |

| | |
|---|-----|
| Figure 3.7. The free energy profile (ΔG) in kcal/mol for the autocatalytic mechanism. The $[\text{BH}(\text{C}_6\text{F}_5)_3]^-$ anion remains as a spectator. R=cyclohexa-1,4-diene. The blue profile is for the PTC(DCM) level of theory and the brown profile is for the TDC(DCM) level of theory..... | 83 |
| Figure 3.8 The comparison of the free energy profiles (ΔG , kcal/mol) between a) the conventional mechanism with mono(cyclohexa-2,5-dien-1-yl)silane and $\text{B}(\text{C}_6\text{F}_5)_3$, and b) our proposed autocatalytic mechanism. The blue profile is for the PTC(DCM) level of theory and the brown profile is for the TDC(DCM) level of theory for conventional pathway. The deep green species are the ones pertaining to newly proposed autocatalytic pathway..... | 86 |
| Figure 3.9 Flowchart for the formation of SiH_4 through (a) the conventional $\text{B}(\text{C}_6\text{F}_5)_3$ catalyzed pathway and (b) the newly proposed autocatalytic pathway. The autocatalytic pathway is shown in green..... | 88 |
| Figure 3.10 The dissociation of benzene from the $[\text{SiHR}_2\text{R}']^+$ complex..... | 89 |
| Figure 3.11 The dissociation of benzene from the $[\text{SiH}_3\text{R}']^+$ complex..... | 89 |
| Figure 3.12. c) The dissociation of benzene from the $[\text{SiH}_3\text{R}']^+$ complex..... | 89 |
| Figure 4.1 Showing possibilities of ion-pair in solvent bounded systems..... | 103 |
| Figure 4.2 The free energy profile (ΔG) in kcal/mol for the proposed mechanism by Simonneau and Oestreich. R=cyclohexa-1,4-diene. The blue profile is for the PTC(DCM) level of theory and the brown profile is for the TDC(DCM) level of theory | 107 |
| Figure 4.3 The separation of the ion-pair is favorable for the borane-silane zwitterionic complex shown in this figures (experimentally studied by Oestreich <i>et al. Angew. Chem., Int. Ed.</i> 2017, 56, 3712): the ΔG for this has been calculated to be 25.2 kcal/mol for the PTC(toluene) level of theory and 28.5 kcal/mol for the TDC(toluene) level of theory..... | 108 |
| Figure 4.4 The separation of the ion-pair is favorable for the borane-silane zwitterionic complex shown in this figures (experimentally studied by Oestreich <i>et al. Angew. Chem., Int. Ed.</i> 2017, 56, 3712): the ΔG for this has been calculated to be 28.3 kcal/mol for the PTC(toluene) level of theory and 30.8 kcal/mol for the TDC(toluene) level of theory..... | 109 |
| Figure 4.5 The separation of the ion-pair is favorable for the borane-silane zwitterionic complex shown in this figures (experimentally studied by Oestreich <i>et al. Angew. Chem., Int. Ed.</i> 2017, 56, 3712): the ΔG for this has been calculated to be 30.8 kcal/mol for the PTC(toluene) level of theory and 22.3 kcal/mol for the TDC(toluene) level of theory..... | 109 |
| Figure 4.6 The separation of the ion-pair is unfavorable for the borane-silane zwitterionic complex shown in this figures (experimentally studied by Piers <i>et al. Nature Chem.</i> 2014, 6, 983): the ΔG for this has been calculated to be 63.5 kcal/mol for the PTC(toluene) level of theory and 68.8 kcal/mol for the TDC(toluene) level of theory..... | 111 |

| | |
|--|-----|
| Figure 4.7 The separation of the ion-pair is favorable for the borane-silane zwitterionic complex shown in this figures (experimentally studied by Hou <i>et al. J. Am. Chem. Soc.</i> 2016, 138, 3663): the ΔG for this has been calculated to be 14.2 kcal/mol for the PTC(cholorobenzene) level of theory and 4.8 kcal/mol for the TDC (cholorobenzene) level of theory..... | 111 |
| Figure 4.8 The separation of the ion-pair is favorable for the borane-silane zwitterionic complex shown in this figures (experimentally studied by Oestreich <i>et al. Angew. Chem., Int. Ed.</i> 2015, 54, 1965): the ΔG for this has been calculated to be 34.7 kcal/mol for the PTC(toluene) level of theory and 36.0 kcal/mol for the TDC(toluene) level of theory..... | 112 |
| Figure 4.9 The separation of the ion-pair is favorable for the borane-silane zwitterionic complex shown in this figures (experimentally studied by Chang <i>et al. Angew. Chem., Int. Ed.</i> 2015, 54, 14805): the ΔG for this has been calculated to be 14.2 kcal/mol for the PTC(choloroform) level of theory and 13.3 kcal/mol for the TDC(choloroform) level of theory..... | 113 |
| Figure 4.10 The separation of the ion-pair is unfavorable for the borane-silane zwitterionic complex shown in this figures (experimentally studied by Chang <i>et al. Angew. Chem., Int. Ed.</i> 2015, 54, 14805): the ΔG for this has been calculated to be 40.6 kcal/mol for the PTC(choloroform) level of theory and 42.3 kcal/mol for the TDC(choloroform) level of theory..... | 113 |
| Figure 4.11 The separation of the ion-pair is unfavorable for the borane-silane zwitterionic complex shown in this figures (experimentally studied by Hou <i>et al. J. Am. Chem. Soc.</i> 2016, 138, 3663): the ΔG for this has been calculated to be 48.7 kcal/mol for the PTC(cholorobenzene) level of theory and 52.2 kcal/mol for the TDC(cholorobenzene) level of theory..... | 116 |
| Figure 4.12 The separation of the ion-pair is favorable for the borane-silane zwitterionic complex shown in this figures (experimentally studied by Stephan <i>et al. Organometallics</i> 2011, 30, 4497): the ΔG for this has been calculated to be 31.4 kcal/mol for the PTC(toluene) level of theory and 16.1 kcal/mol for the TDC(toluene) level of theory..... | 116 |
| Figure 4.13 The separation of the ion-pair is favorable for the borane-silane zwitterionic complex shown in this figures (experimentally studied by Piers <i>et al. Org. Lett.</i> 2000, 2, 3921): the ΔG for this has been calculated to be 24.8 kcal/mol for the PTC(toluene) level of theory and 29.1 kcal/mol for the TDC(toluene) level of theory..... | 116 |
| Figure 4.14 The separation of the ion-pair is unfavorable for the borane-silane zwitterionic complex shown in this figures (experimentally studied by Oestreich <i>et al. Angew. Chem., Int. Ed.</i> 2015,54, 1965): the ΔG for this has been calculated to be 40.8 kcal/mol for the PTC(toluene) level of theory and 49.7 kcal/mol for the TDC(toluene) level of theory | 117 |

| | |
|--|-----|
| Figure 4.15 The separation of the ion-pair is unfavorable for the borane-silane zwitterionic complex shown in this figures (experimentally studied by Stephan <i>et al. J. Am. Chem. Soc.</i> 2009, <i>131</i> , 3476): the ΔG for this has been calculated to be 31.9 kcal/mol for the PTC(toluene) level of theory and 28.0 kcal/mol for the TDC(toluene) level of theory. | 117 |
| Figure 4.16 The proposed mechanism by Oestreich and co-workers ⁷⁵ for the hydrogenation of imine by $B(C_6F_5)_3$ | 118 |
| Figure 4.17 The mechanism that I propose, for the same reaction: hydrogenation of imine by $B(C_6F_5)_3$ based on the facile separation of the cation from the ion-pair..... | 119 |
| Figure 4.18 The comparison of the free energy profiles (ΔG , kcal/mol) for the formation of [PhNH(HC(CH ₃)(Ph))] between a) the conventional mechanism with [PhNH(C(CH ₃)(Ph)] ⁺ cation and [BH(C ₆ F ₅) ₃] ⁻ anion, and b) our proposed autocatalytic mechanism. The blue profile is for the PTC(DCM) level of theory and the brown profile is for the TDC(DCM) level of theory. The autocatalytic mechanism is more favourable than the conventional mechanism..... | 120 |
| Figure 5.1 The ability of low valent main group compounds to act as both electrophiles and nucleophiles..... | 129 |
| Figure 5.2 The germylene and stannylene systems considered in this work..... | 132 |
| Figure 5.3 The free energy profile for the hydroboration reaction with germylene catalyst: mechanism proposed in the literature by Khan and coworkers..... | 135 |
| Figure 5.4 The free energy profile for the hydroboration reaction with the stannylene catalyst: mechanism proposed in the literature by Khan and coworkers..... | 136 |
| Figure 5.5 The free energy profile for a new mechanism that we propose for the hydroboration of benzaldehyde by HBpin, in the presence of the germylene catalyst..... | 137 |
| Figure 5.6 The free energy profile for a new mechanism that we propose for the hydroboration of benzaldehyde by HBpin, in the presence of the stannylene catalyst..... | 138 |
| Figure 5.7 The catalytic cycle and reaction mechanism for the aldehyde hydroboration by Catalyst-3 (E=Ge) and Catalyst 4 (E=Sn), <i>via</i> a four membered cyclic transition state..... | 140 |
| Figure 5.8 The free energy profile for the catalytic aldehyde hydroboration by Catalyst-3 with a four-membered cyclic transition state. The values (in kcal/mol) have been calculated at the PBE/TZVP level of theory..... | 141 |
| Figure 5.9 The free energy profile for the catalytic aldehyde hydroboration by Catalyst-4 with a four-membered cyclic transition state. The values (in kcal/mol) have been calculated at the PBE/TZVP level of theory..... | 142 |
| Figure 5.10 The catalytic cycle and reaction mechanism for aldehyde hydroboration by Catalyst-3 and Catalyst-4, <i>via</i> a six-membered cyclic transition state..... | 143 |

| | |
|---|-----|
| Figure 5.11 The free energy profile for the catalytic aldehyde hydroboration by Catalyst-3 passing through a six membered cyclic transition state. The values (in kcal/mol) have been calculated at the PBE/TZVP level of theory..... | 144 |
| Figure 5.12 The free energy profile for the catalytic aldehyde hydroboration by Catalyst-4 passing through a six-membered cyclic transition state. The values (in kcal/mol) have been calculated at the PBE/TZVP level of theory..... | 145 |
| Figure 5.13 The free energy profile for the catalytic aldehyde hydroboration without any catalyst through a six-membered cyclic transition state. The values (in kcal/mol) have been calculated at the PBE/TZVP level of theory..... | 146 |
| Figure 6.1 Alpha thiocyanation of oxindole using N-thiocyanatophthalimide. The BzCPD catalyst, with 2-naphthol employed as additive, works to provide the S-enantiomer as the major product..... | 164 |
| Figure 6.2 The three models shown above describe how the 2-naphthol additive participates in the reaction. The model in green (Model b) is the most correct mode of activation, where the additive serves to stabilize both the electrophile and nucleophile, along with the C6'-OH <i>cinchona</i> alkaloid catalyst. This is based on insights gained from the current work..... | 164 |
| Figure 6.3 Alpha thiocyanation of β -keto ester (nucleophile) using N-thiocyanatophthalimide (electrophile). BzCPD works as catalyst and the R-enantiomer is the major product..... | 165 |
| Figure 6.4 Transition state (TS) models show the TS from the favourable Wynberg ion-pair hydrogen bonding mechanism and from the unfavourable Houk-Grayson bifunctional Brønsted acid-hydrogen bonding mechanism, with the β -keto ester nucleophile. The reactions occur in the absence of additive. The catalyst and electrophile are BzCPD and N-thiocyanatophthalimide respectively..... | 166 |
| Figure 6.5 Different conformations (<i>anti</i> open, <i>anti</i> closed, <i>syn</i> open, <i>syn</i> closed) of the <i>Cinchona</i> alkaloid proposed by Wynberg and co-workers..... | 169 |
| Figure 6.6 The relevant angles and dihedrals in the BZCPD catalyst structure..... | 171 |
| Figure 6.7 The scheme for the new model where a molecule of the additive 2-naphthol plays an explicit role in the thiocyanation reaction along with the quinuclidine nitrogen of the catalyst. The blue coloured atoms are those participating in the transition states (TSs). The green coloured species is the major TS and the red coloured species is the minor TS..... | 172 |
| Figure 6.8 The optimized transition state structures for the <i>syn</i> -S and <i>anti</i> -S approach cases..... | 174 |
| Figure 6.9 Energy profile for the BzCPD catalyzed thiocyanation of oxindole. 2-naphthol acts as an additive, activating both the nucleophile as well as the electrophile. The free energy (ΔG) values are in kcal/mol, at the PBE-D3/TZVP+COSMO(CH ₃ CH ₂ Cl ₂) level of theory..... | 175 |
| Figure 6.10 Alpha thiocyanation of oxindole(nucleophile) using thiocyanatophthalimide (electrophile). No additive plays a role. BzCPD works as catalyst to give S-enantiomer as the major product..... | 177 |

| | |
|---|-----|
| Figure 6.11 Energy profile for the BzCPD catalyzed thiocyanation of oxindole. The free energy (ΔG) values are in kcal/mol, at the PBE-D3/TZVP+COSMO(CH_2Cl_2) level of theory..... | 178 |
| Figure 6.12 Energy decomposition analysis (EDA) for the newly proposed Wynberg ion-pair transition state model..... | 180 |
| Figure 6.13 The non-covalent interaction (NCI) plot showing extended $\pi\cdots\pi$ stacking interactions between 2-naphthol and the electrophile for the Wynberg ion-pair transition states (a and b). The Houk-Grayson model transition states (c and d) show no extended $\pi\cdots\pi$ stacking between 2-naphthol and the electrophile. $\pi\cdots\pi$ stacking between the electrophile and the benzyl group of the catalyst is not so predominant..... | 181 |
| Figure 6.14 Truncated model showing π - π stacking interactions for the transition states $\text{TS}_{\text{wyn}2\text{A}}(\text{S})$ and $\text{TS}_{\text{wyn}2\text{A}'}(\text{R})$. The $\Delta\Delta E$ ($\pi\cdots\pi$ stacking) is 1.7 kcal/mol favorable for $\text{TS}_{\text{wyn}2\text{A}}(\text{S})$ over $\text{TS}_{\text{wyn}2\text{A}'}(\text{R})$ | 183 |
| Figure 6.15 The quantification of the different non-covalent interactions in the transition state leading to the major S product..... | 184 |
| Figure 6.16 The quantification of the different non-covalent interactions in the transition state leading to the minor R product..... | 185 |
| Figure 6.17 The free energy profile for the BzCPD catalyzed thiocyanation of the β -keto ester. The free energy (ΔG) values are in kcal/mol, at the PBE-D3/TZVP+COSMO($\text{CH}_3\text{CH}_2\text{Cl}_2$) level of theory..... | 186 |
| Figure 6.18 Energy decomposition analysis for the Wynberg ion-pair transition state model..... | 187 |
| Figure 6.19 The optimized transition state structures showing different non-covalent interactions for the major and minor transition states. a) The R enantiomer as the major product with BzCPD as catalyst, β -keto ester as nucleophile, and N-thiocyanatophthalimide as electrophile. b) S enantiomer as minor product with BzCPD as catalyst, β -keto ester as nucleophile, and N-thiocyanatophthalimide as electrophile. c) S enantiomer as major product with BzCPD as catalyst, oxindole as nucleophile, and N-thiocyanatophthalimide as electrophile. d) R enantiomer as minor product with BzCPD as catalyst, oxindole as nucleophile, and N-thiocyanatophthalimide as electrophile..... | 189 |

List of Tables

| | |
|---|-----|
| Table 3.1 The calculated free energy barriers for all possible ways of the lower surrogate SiR_xH_y species formation through the conventional mechanism proposed in the literature and my proposed mechanism.. | 84 |
| Table 3.2 The values for the TOFs obtained for the stepwise and total autocatalytic pathways, as well as with the conventional $\text{B}(\text{C}_6\text{F}_5)$ catalyzed pathway. | 87 |
| Table 3.3 The calculated barriers (single point) for all possible ways of lower surrogate SiR_xH_y species formation through the conventional mechanism proposed in the literature and my proposed mechanism | 87 |
| Table 3.4 The calculated free energies (ΔG , in kcal/mol) for the dissociation of benzene from the respective cations. | 89 |
| Table 4.1 The calculated free energies, (ΔG , in kcal/mol) for the separation of the ion-pairs formed in the different experimentally studied reactions (references provided after the ion-pair formulae for each case) where $\text{B}(\text{C}_6\text{F}_5)_3$ has previously been considered to act as a catalyst. Cases where the separation is energetically non-feasible have been shown in shaded columns. | 114 |
| Table 4.2 The calculated free energy barriers for the formation of $\text{PhNH}(\text{HC})(\text{CH}_3)(\text{Ph})$ through the conventional mechanism proposed in the literature, and our proposed mechanism. | 120 |
| Table 5.1 HOMO-LUMO energy gap for the X_2E type germylene catalyst. For the first three cases, the hydroboration reaction has been investigated experimentally and for the last case, the hydroboration reaction has been investigated computationally in this current work, with a designed catalyst system. | 138 |
| Table 6.1 Energy values of the calculated conformations. The first and second values are calculated at the $\text{M06-2X/TZVP}+\text{COSMO}(\text{CH}_2\text{Cl}_2)$ and $\text{M06-2X/TZVP}+\text{COSMO}(\text{CH}_3\text{CH}_2\text{Cl}_2)$ level of theory respectively. | 171 |
| Table 6.2 An energy decomposition analysis(EDA) approach adopted for $\text{TS}_{\text{wyn}}2\text{A}(\text{S})$ and $\text{TS}_{\text{wyn}}2\text{A}'(\text{R})$. | 180 |
| Table 6.3 Energy decomposition analysis (EDA) for $\text{TS}_{\text{wyn}}5\text{A}'(\text{R})$ and $\text{TS}_{\text{wyn}}5\text{A}(\text{S})$. | 187 |

Abbreviations

| | |
|---------------------------------|--|
| DFT | Density Functional Theory |
| COSMO | Conductor-like Screening Model |
| CH ₂ Cl ₂ | Dichloromethane |
| CHCl ₃ | Chloroform |
| er | Enantiomeric Ratio |
| ee | Enantiomeric Excess |
| IRC | Intrinsic Reaction Coordinate |
| IE | Interaction Energy |
| KS | Kohn-Sham |
| MP2 | Second-order Møller–Plesset Perturbation Theory |
| MARIJ | Multipole Accelerated Resolution of Identity |
| B3LYP | Becke, 3-parameter, Lee-Yang-Parr |
| M06 | Minnesota 06 |
| TPSS | Tao-Perdew-Staroverov-Scuseria |
| NBO | Natural Bond Orbital |
| NCI | Non-covalent Interactions |
| PBE | Perdew, Burke and Ernzerhof |
| PCM | Polarizable Continuum Model |
| RI | Resolution of Identity |
| SCF | Self-consistent Field |
| TZVP | Triple Zeta Valence plus Polarization |
| TS | Transition state |
| DCM | Dichloromethane |
| TDTS | Turn Over Frequency Determining Transition State |

| | |
|------|--|
| TOF | Turn over Frequency |
| TON | Turn over Number |
| ESM | Energetic Span Model |
| TDI | Turn Over Frequency Determining Intermediate |
| FLP | Frustrated Lewis Pair |
| BCF | Tris(pentafluorophenyl)borane |
| HOMO | Highest Occupied Molecular Orbital |
| LUMO | Lowest Unoccupied Molecular Orbital |
| NHC | N-Heterocyclic Carbene |

Physical Constants

| | |
|----------------------|--|
| Avogadro's Constant | $(N_A) = 6.02214129 \times 10^{23} \text{ mol}^{-1}$ |
| Atomic Mass Unit | $(u) = 1.660538921 \times 10^{-27} \text{ kg}$ |
| Boltzmann's Constant | $(k) = 1.3806488 \times 10^{-23} \text{ JK}^{-1}$ |
| Bohr Radius | $(a_0) = 5.291772109 \times 10^{-11} \text{ m}$ |
| Elementary Charge | $(e) = 1.602176565 \times 10^{-19} \text{ C}$ |
| Gas Constant | $(R) = 8.3144621 \text{ JK}^{-1} \text{ mol}^{-1}$ |
| Mass of Electron | $(m_e) = 9.10938291 \times 10^{-31} \text{ kg}$ |
| Mass of Proton | $(m_p) = 1.672621777 \times 10^{-27} \text{ kg}$ |
| Mass of Neutron | $(m_n) = 1.674927351 \times 10^{-27} \text{ kg}$ |
| Rydberg Constant | $(R) = 1.097373157 \times 10^5 \text{ cm}^{-1}$ |
| Speed of Light | $(c) = 2.99792458 \times 10^8 \text{ ms}^{-1}$ |
| Planck's Constant | $(h) = 6.62606957 \times 10^{-34} \text{ Js}$ |

Chapter 1

A Brief Overview of the Importance in Hydride and Proton Transfer Chemical Transformations

Chapter 1

A Brief Overview of the Importance in Hydride and Proton Transfer Chemical Transformations

1.1 Introduction

The hydrogen nucleus can migrate from one atom to another with zero, one, or two electrons attached, a process known as proton, hydrogen atom, or hydride transfer respectively. Hydride and proton transfer transformations are not only important to biology but also play a very crucial role in chemistry. There is always a donor and an acceptor species in all the hydride and proton transfer chemical reactions. However the exact role of the donor and acceptor species in all the transformations is not always clear. So, it is always challenging and intriguing to find out how the donor and acceptor species participate in the chemical transformations. In this chapter, I will provide a brief overview on the importance of hydride and proton transfer. I will also provide a overview on the different terms associated with hydride and proton transfer.

1.2 Hydride Transfer

The term "hydride-transfer" is used to describe the acquisition in a single step of a hydrogen nucleus, together with a pair of electrons, by one electrophilic centre at the expense of another, either in the same or in another molecule. This process is distinguished from proton-transfer by the absence of isotopic exchange with the labile protons of the medium and by the nature of the polarity at the point of the reaction.

Hydride-transfers are currently regarded as one of organic chemistry's processes, and they've been used to explain a variety of complex and well-known reactions. The most crucial of these are the Meerwein-Ponndorf-Verley reaction,¹ the Oppenauer oxidation,² the Cannizzaro reaction,³ the Leuckart reaction,⁴ and the Tishchenko reaction.⁵ Intramolecular and intermolecular hydride transfer reactions are the two types of hydride transfer processes. Carbonium ions are commonly produced as intermediates in intramolecular transfer, which isomerize and give rise to anomalous products. Whitmore proposed this to explain how isopropanol and n-propanol are formed when n-propylamine is treated with nitrous acid (see **Figure 1.1** below).⁶

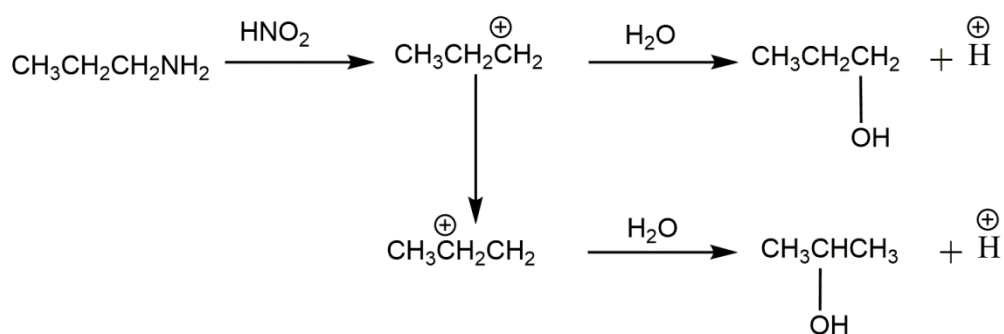


Figure 1.1 The simplest reaction for hydride transfer mechanism.

Intermolecular hydride-transfer was first proposed by Bartlett. Taryl bromide and isobutane were the results of a reaction between t-butyl chloride and isopentane in the presence of aluminium bromide and in a relatively short reaction time (see **Figure 1.2** below).⁷

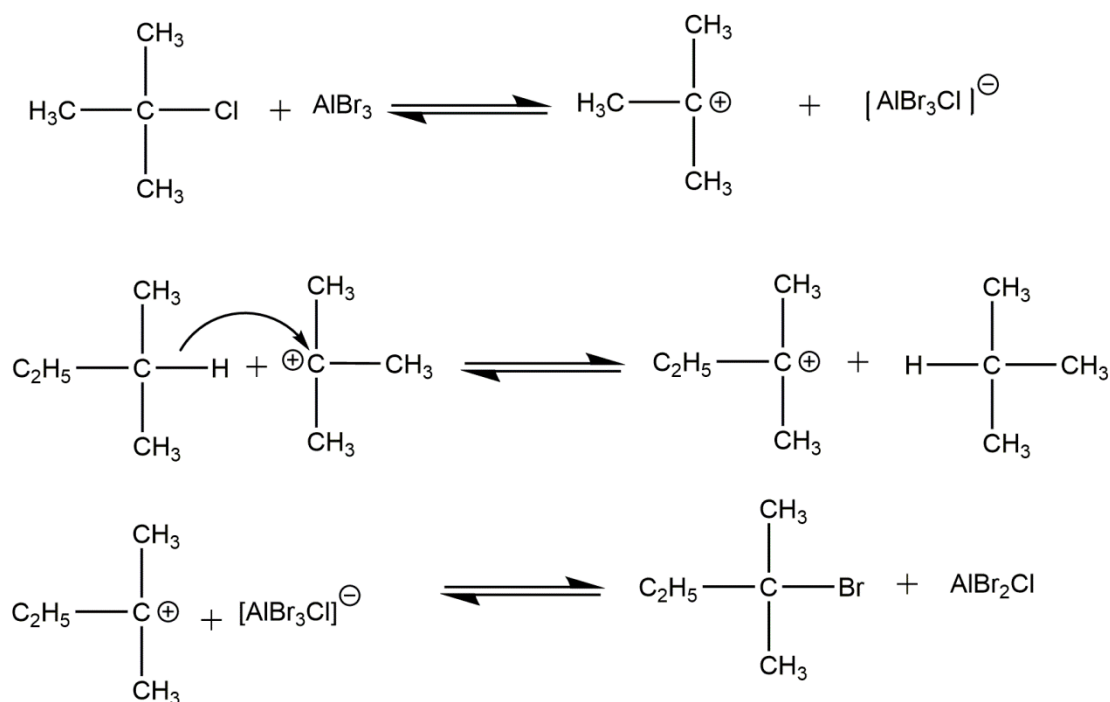


Figure 1.2 The simplest reaction of the intermolecular hydride transfer mechanism.

Except in few circumstances when the hydride is transferred to an electronegative atom that afterwards swaps the hydrogen as a proton, such as N, O, S, or halogen, hydride transfers occur without exchange with solvent protons.⁸ The existence of radical traps has little effect on hydride reactions because radical intermediates are either missing or very tiny. Although hydride transfer entails the transfer of a proton and two electrons at the same time, the word "simultaneous" only refers to the absence of a discernible time delay between the two electrons.⁹ The probability of two electrons moving at the same time in quantum mechanics is nearly zero, but because the nucleus moves so much slower than the electrons, one of the electrons can accompany the proton, while the other precedes or follows, and still be "simultaneous" in terms of practical mechanism determination. Thus, hydride transfer may be used in organic and biological oxidation reductions without proving or disproving the one-electron transfer principle. The difference between hydride and hydrogen atom transfer may end up being purely semantic, as the two methods are only distinguished by the detectability or non-detectability of radical intermediates. The ideal conditions for hydride anion transfer would include the following: The

donor molecule is a reducing agent having a hydrogen atom capable of leaving the donor site, as well as a negative charge. The acceptor molecule has a positive charge, is an oxidising agent, and has an electron-deficient core that is either present or potential. Because there are no bulky groups in the donor and acceptor molecules to produce steric hindrance with the near proximity of donor and acceptor sites, the hydride anion can move straight from donor to acceptor. With comparable circumstances, hydride transfer might occur between various parts of the same molecule. In practice, neutral acceptors and negatively charged donors, or neutral donors and positively charged acceptors, have been shown to be the most common hydride transfer reactions.¹⁰

1.3 Hydride Transfer in Main Group Catalysis

Hydride transfer is one of the important processes in main group catalysis and so, in order to elucidate the associated reaction mechanism, it is important to understand the hydride transfer mechanism. In previous works, the hydride transfer mechanisms in main group catalysis has been investigated using either experimental or theoretical approaches.¹¹⁻²² Although these mechanisms have not yet been fully explained due to the variety of possible pathways involving the overall transfer of two electrons and one proton, the following hydride transfer mechanisms have been proposed: (1) direct transfer of a hydride ion (H^-) in a single step, (2) a two-step transfer of an electron before or after the transfer of a hydrogen atom and (3) the transfer of two electrons and one proton in three separate steps. Several experimental studies have provided evidence for the single-step mechanism,²³⁻²⁶ although the multi-step mechanism has also been suggested.^{17,23,27} Therefore, although the hydride transfer mechanism has been researched over a significant period of time, there is little agreement as to the detailed reaction steps. Theoretical studies aimed at understanding the hydride transfer mechanism have also been conducted, focusing on the effects of the charge density, ionization potential and proton affinity of the reactant and the transition state.^{11-16,19,21,22} Silanes should donate a hydride more readily than alkanes, because of the increased electropositive nature of silicon relative to carbon. Thus, silanes generally evolve hydrogen in strong acids. The reaction of

several alkyl chlorides with triethylsilane in the presence of aluminum chloride to form the alkane demonstrates that hydride transfer from silicon to carbon²⁸ can take precedence over the formation of hydrogen.

1.3.1 Hydrosilylation

Hydrosilylation, also known as hydrosilation, is one of the most useful catalytic reactions leading to the formation of organosilanes and organosilicones, which have a variety of applications in industry and as intermediates in organic chemistry (see **Figure 1.3 below**). Hydrosilylation occurs *via* the addition of H-Si to an unsaturated bond such as a carbon-carbon bond, a carbon-oxygen bond, a carbon-nitrogen bond, a nitrogen-nitrogen bond and a nitrogen-oxygen bond using a metal catalyst, Lewis acid, or a radical initiator.

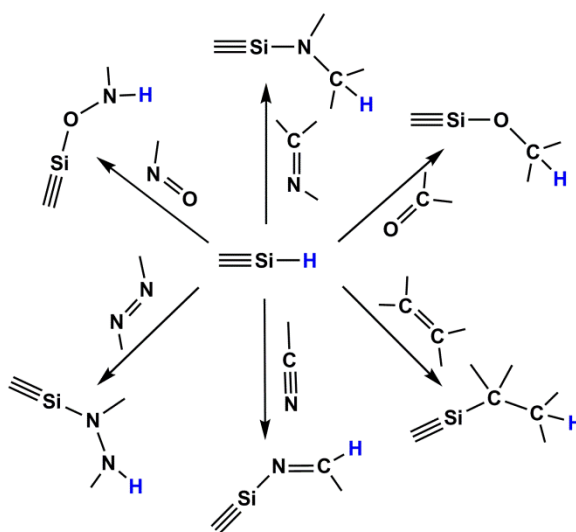


Figure 1.3 The general scheme for the hydrosilylation of different unsaturated compounds.

Ordinarily, the reaction is conducted catalytically, and usually the substrates are unsaturated organic compounds. Alkenes and alkynes give alkyl and vinyl silanes; aldehydes and ketones give silyl ethers. Hydrosilylation has been called the "most important application of platinum in homogeneous catalysis."²⁹ Hydrosilylation of alkenes represents a commercially important method for preparing organosilicon compounds. The process is mechanistically similar to the hydrogenation of alkenes. In

fact, similar catalysts are sometimes employed for the two catalytic processes. The prevalent mechanism, called the Chalk-Harrod mechanism, assumes an intermediate metal complex that contains a hydride, a silyl ligand (R_3Si), and the alkene substrate. Oxidative addition proceeds by the intermediacy of a sigma-complex, wherein the Si-H bond is not fully broken.

Hydrosilylation of alkenes usually proceeds *via* anti-Markovnikov addition, i.e., silicon is placed at the terminal carbon when hydrosilylating a terminal alkene.³⁰ Variations of the Chalk-Harrod mechanism exist. Some cases involve insertion of alkene into the M-Si bond followed by reductive elimination, the opposite of the sequence in the Chalk-Harrod mechanism (see **Figure 1.4 below**). In certain cases, hydrosilylation results in vinyl or allylic silanes due to beta-hydride elimination.³¹

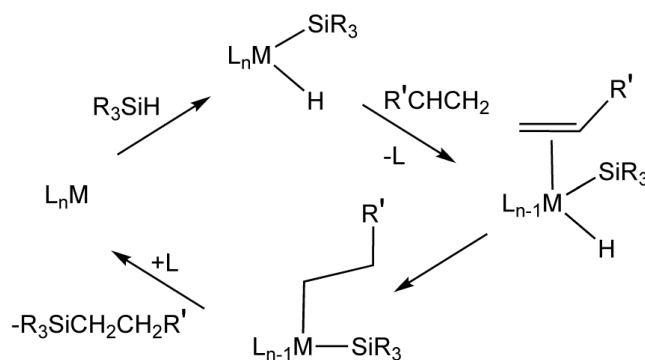


Figure 1.4 An idealized mechanism for the metal catalysed hydrosilylation of alkene.

Hydrosilylation can also occur through the addition of an alkene or an alkyne to a silyl group and by employing a Lewis acid. Generally, aluminum and boron based Lewis acids are the ones employed in most of the reactions.³²

1.3.2 Tris(pentafluorophenyl)borane ($B(C_6F_5)_3$)

Boron reagents are often employed as Lewis acids because of their ubiquitous electrophilic nature. Tris(pentafluorophenyl)borane $B(C_6F_5)_3$ ³³ is a powerful Lewis acid because of the electron-withdrawing effects of the three perfluorinated aryl rings and was first synthesized in the 1960s.³⁴ Experimental studies probed the Lewis acidity of this borane, the results of which determined that it was comparable to BF_3 ,

although it was weaker than BCl_3 , falling somewhere between the two (see **Figure 1.5** below)³⁵

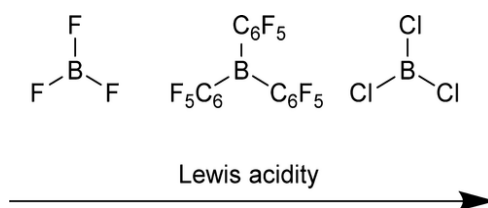


Figure 1.5 Comparison of the Lewis acidity between different boron species.

Furthermore, a multitude of boron Lewis acids, including $\text{B}(\text{C}_6\text{F}_5)_3$, have been studied by examining their hydride- and fluoride-ion affinities.^{36,37} These methods give insight into the relative stability and reactivity of a range of Lewis acids, both experimentally and computationally. Such methodologies are useful because they provide scales upon which a variety of reagents can be placed, allowing the selection of a specific Lewis acid and thus providing a more tailored approach when planning reactions. The inherent electrophilicity of $\text{B}(\text{C}_6\text{F}_5)_3$ makes it suitable for a wide range of reactions, including borylation, hydrogenation, hydrosilylation, frustrated Lewis pair (FLP) chemistry, Lewis acid catalysis, and more. The high Lewis acidity of $\text{B}(\text{C}_6\text{F}_5)_3$ is derived from the electronic effects of its three C_6F_5 rings, rendering it a versatile reagent for a great number of reactions. In addition, the steric bulk of these rings also allows it to function as the Lewis acid in a FLP, granting this reagent yet another synthetically useful application. The boron Lewis acid $\text{B}(\text{C}_6\text{F}_5)_3$ is one of those potent Lewis acid molecules that revealed its relevance to synthetic chemistry long after its discovery. The role of $\text{B}(\text{C}_6\text{F}_5)_3$ behaving as a co-catalyst³⁸ is quite different from the frustrated Lewis pair behaviour. It has also been observed that $\text{B}(\text{C}_6\text{F}_5)_3$ act as a catalyst in multiple organic transformations. It has also been observed that the presence of different donor ligands attached with the central atom of Lewis acid alter the rate and yield of the reactions.

1.3.3 Autocatalysis

A *set* of chemical reactions can be said to be "collectively autocatalytic" if a number of those reactions produce, as reaction products, catalysts for enough of the other reactions such that the entire set of chemical reactions is self-sustaining.

Perhaps the simplest autocatalytic reaction can be written as:



with the rate equations (for an elementary reaction)

$$\begin{aligned} d/dt[A] &= -k_+[A][B] + k_-[B]^2 \\ d/dt[B] &= +k_+[A][B] - k_-[B]^2 \end{aligned} \quad 1.2$$

This reaction is one in which a molecule of species A interacts with a molecule of species B. The A molecule is converted into a B molecule. The final product consists of the original B molecule plus the B molecule created in the reaction. The key feature of these rate equations is that they are nonlinear; the second term on the right varies as the square of the concentration of B.

In chemistry, autocatalysis is an interesting natural occurrence. In an autocatalytic reaction, the reaction's products increase the rate at which they are produced. These products are called autocatalysts. The mechanics driving the amplification may differ significantly, yet the isothermal autoamplification kinetic signature is largely retained.³⁹ Autoamplified processes are extremely important in physics and biology. The cornerstone of nuclear energy generation is nuclear chain reactions. All living things, from viruses to people, are capable of biological self-replication. Autocatalytic reactions are more unusual than the main processes in chemical sciences, making chemistry an outlier. Autocatalytic reactions, on the other hand, are important in industrial processes including photolithography,⁴⁰ electroless plating,⁴¹ and photography.⁴² Autocatalysis is a broad area that includes everything from chemical kinetics to inorganic and organic chemistry. Autocatalysis is a part of systems

chemistry, which is a young and rapidly expanding subject.⁴³ The importance of autocatalysis in hypotheses about the beginning of life on Earth has piqued people's interest.⁴⁴ Life arose from autocatalytic, self-replicating RNA molecules, according to the RNA world hypothesis.⁴⁵ The creation of autocatalytic cycles such as the reverse Krebs cycle and the formose reaction is proposed in the first metabolism scenario.⁴⁶ Autocatalysis is a cause of chemical instabilities (e.g., in chemical oscillations)⁴⁷ and symmetry breaking (e.g., during pattern development in an originally homogeneous layer of reactants solution) as a nonlinear process. As a result, research into out-of-equilibrium, dissipative chemical systems is quite interesting.⁴⁸ Building synthetic life is a lofty objective that necessitates the creation of complicated de novo autocatalytic systems.

1.3.4 Hydroboration

The addition of a hydrogen-boron bond to C-C, C-N, and C-O double bonds, as well as C-C triple bonds, is known as hydroboration. This chemical process is beneficial for production of boron containing compounds. Herbert C. Brown was awarded the Nobel Prize in Chemistry for his contributions to the invention of this reaction and the principles that underpin it.⁴⁹ In 1979, he and Georg Wittig shared the Nobel Prize in chemistry for their pioneering work on organoboranes as crucial synthetic intermediates.⁵⁰ Hydroboration can also be used to produce organoborane compounds, which are chemical compounds that have carbon-boron bonds and are derivatives of BH_3 . These organoboranes can be reacted with some reagents to give alkyl halides, alcohols, and amines. Alcohols are produced from the oxidation of the organoboranes with the help of hydrogen peroxide.

The electronegativity of carbon is 2.55 and the electronegativity of boron is 2.04. This is why the carbon-boron bond has a relatively low polarity. The low polarity of the B-C bond makes the alkyl boron compounds quite stable. On the other hand, alkyl boron compounds are also easily oxidizable. Due to the low electronegativity of boron, it tends to form electron deficient compounds. An example for the type of compounds produced by boron are triorgano boranes. The carbon boron bond gets some double bond characteristics from the donation of electrons by the vinyl and aryl groups. This

causes it to be less electrophilic. In the hydroboration process, it is observed that the hydrogen is added to the most substituted carbon of the double bond. Therefore, hydroboration can be considered as an anti Markovnikov process. This process proceeds *via* a four membered transition state. In this state, there is a same-face addition of the boron and hydrogen atoms on the double bond. The carbon boron bond is formed slightly faster than the carbon hydrogen bond. Therefore, the boron gains a partial negative charge whereas the more substituted carbon gains a partial positive charge in the four membered transition state. An example explaining the hydroboration of a given terminal alkene to a trialkylborane *via* the four membered transition state is shown below(see **Figure 1.6** below).

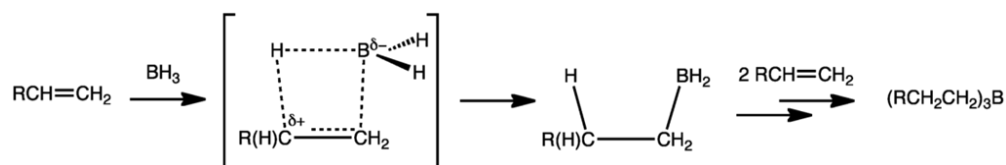


Figure 1.6 Hydroboration of a terminal alkene to a trialkylborane, showing an idealized image of the cyclic transition state.

1.4 Stannylenes and Germylenes

G. N. Lewis proposed the "octet rule" in 1916, which asserts that when non-transition elements establish bonds in a molecule, they tend to create an 8-electron valence shell by sharing electrons.⁵¹ Compounds containing atoms with less than eight valence electrons are very reactive because they tend to increase this number. Tetrylenes (the term originates from the words "tetrel" meaning heavy analogues of carbon and the suffix "ylene" signifying a group 14 divalent atom), derivatives of group 14 elements in the formal oxidation state 2+, have a particular position among such compounds. For a long time, the presence of heavy carbene analogues as stable compounds that can be handled under circumstances characteristic of organometallic compounds (at least for Sn and Ge) has been debated. Of course, the simplest inorganic compounds of germanium and tin in the oxidation state 2+ have long been known (all have a polymer structure in the solid phase),^{52,53} while compounds of lead in the oxidation state 2+ are more stable than those in the oxidation state 4+. Note that the

characteristics of lead derivatives, as well as of carbon compounds, differ greatly from those of the group's core trio, notably silicon, germanium, and tin. Stable compounds of group 14 divalent elements with organic replacements were first stated in 1956, with dicyclopentadienyltin (Cp_2Sn)₃ being mentioned for the first time. However, in the 1970s, the Lappert group published a series of papers on the synthesis of $\text{M}[\text{CH}(\text{SiMe}_3)_2]_2$ ($\text{M} = \text{Sn}, \text{Pb}$),⁵⁴ $\text{M}[\text{N}(\text{SiMe}_3)_2]_2$, and $\text{M}[\text{N}(\text{SiMe}_3)(\text{CMe}_3)]_2$ ($\text{M} = \text{Ge}, \text{Sn}, \text{Pb}$)⁵⁵ in the realm of molecular tetrylenes. The study of group 14 metal derivatives in a low-valent state has now become a wide topic of research in contemporary chemistry.

Tetrylenes are known to be intermediates in a variety of processes involving silicon, germanium, and tin compounds. They may be stable enough to handle at room temperature with the normal precautions in organometallic chemistry in some circumstances. The employment of different ligands to promote the stability of heavy carbenes has been extensively studied, and the factors stabilising a low-valent core have been established during the last three decades. The presence of bulky substituents near the low-valent centre (kinetic stabilisation) or the donation of electron density to the vacant orbital of the group 14 metal atom (thermodynamic stabilisation) both through transannular interaction, have been studied, as well as the case when the element's atom is directly bonded to the heteroatom containing an unshared electron pair (i.e., the ligand is an n- or a π -donor).^{56,57} N-heterocyclic stannylene and germylene, as previously stated, are very reactive. They are distinguished by a variety of reactions that involve both the formal oxidation state change (typically from 2+ to 4+) and the retention of the oxidation state 2+.

In contrast to carbenes, the heavier congeners R_2E (with $\text{E} = \text{Si}, \text{Ge}, \text{and Sn}$) frequently have a singlet ground electronic state, which results in a high energy lone pair (HOMO) and an energetically accessible unoccupied p-orbital (LUMO).⁵⁸ This orbital configuration resembles the transition metals' frontier d-orbitals and contributes to the dual donor and acceptor character required for bond activation. The nature of the R substituents, which influence the orbital energies, has a significant impact on the reactivity of tetrylenes towards small molecules and strong bonds. To date, a variety

of substituents with various steric and electronic characteristics have been used to adjust tetrylene's capacity to engage in bond activation events.^{59,60} The singlet-triplet gap and the HOMO-LUMO separation have been discovered to be useful indicators of carbene and related species' potential to engage in bond activation processes. In general, tetrylenes with narrow HOMO-LUMO gaps have stronger activity towards small molecules, as Bertrand and coworkers have demonstrated by comparing the behaviour of N-heterocyclic carbenes (NHCs) and cyclic alkyl(amino)carbenes (CAACs) towards dihydrogen.⁵³ The angle at the group 14 element and the donor/acceptor characteristics of the substituents are two important elements that determine this energy separation.⁶¹ Due to the increased p-character of the lone pair, which leads to an elevation of the HOMO energy, large angles are linked with short HOMO-LUMO gaps.⁶² As a result, acyclic tetrylenes are often more reactive than their cyclic counterparts. Bulky groups are also advantageous for small molecule activation because they enhance the R-E-R angle. For electronic manipulation, a wide range of substituents have been employed, especially for the heavier group 14 carbene analogues. While amino groups are favoured substituents for stabilizing tetrylenes because of their -I and + M donor characteristics, they frequently generate a substantial HOMO-LUMO separation. Strongly donating (i.e. more electropositive) groups provide more reactive species that are ideal for small molecule activation, leaving the empty p-orbital unoccupied, lower in energy, and open for interactions with bonding orbitals of other substrates. As a result, in addition to alkyl moieties, silyl or, more recently, boryl groups have been utilized in this chemistry.⁵⁵ The heavier group 14 carbene counterparts appear to be more favourable from a thermodynamic standpoint for developing reversible, and hence catalytic, reactions. While carbene E-H activation events are very exothermic and hence irreversible, reversible bond activations for their heavier equivalents have been found, while catalytic applications are still limited.^{63,64} Bond activation reactions often occur directly at the metal centre due to the unusual electronic structure of tetrylenes and the existence of a full and unfilled orbital at the group 14 element (single site).^{65,66} Aside from single-site reactivity, literature has revealed E-H bond activation methods including the active engagement of the σ -substituent (cooperative).

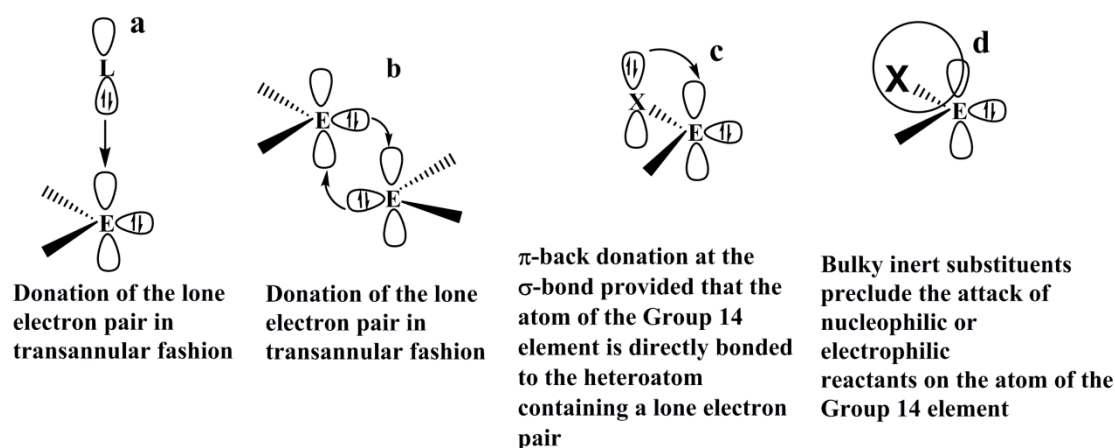


Figure 1.7 The ability of low valent main group compounds to act as both electrophiles and nucleophiles.

1.5 Proton Transfer

One of the most studied processes in chemistry is proton transfer from one molecule to another. This is what acid–base chemistry is all about. A hydrogen-bonded compound can be an intermediate phase in this process; therefore it is connected to hydrogen bonding,⁶⁷ where $A-H\cdots B$ is a hydrogen-bonded complex and $A\cdots H-B^+$ is an ionic pair held together primarily by Coulombic attraction. When compared to the energies of hydrogen bonds, proton transfer necessitates the breaking of the chemical bonds, which is a more energy intensive process. As a result, proton transfer processes are separate from the remainder of the processes discussed in this article, which focus solely on hydrogen bond breaking and formation. In the gas phase, almost all neutral dimers form just one stable complex, the neutral complex $A-H\cdots B$. As a result, proton transfer will be an uncommon occurrence. In solution, the situation changes because solvation stabilises both complexes. Some solvents will stabilise the ionic complex more than the neutral complex, until it reaches the global minimum on the proton transfer path. The acidity of $A-H$ and the basicity of B dictate the amount of proton transfer. The transition from neutral to ionic state may be detected experimentally as a considerable rise in the dipole moment of the complex. The dipole moments of the neutral forms are in the range of 1–3 Debye, whereas those of the ionic forms are approximately 10 Debye. Dissociation of the ionic complex into free solvated ions is

also possible. The entire proton transfer reaction is a multi-step process. The rate of proton transfer is determined by the barrier height(s) along the reaction path. There is a scarcity of accurate information on proton transfer barrier heights in solutions. Because the solvent effects are so powerful in some solvents (e.g., water), the process is simplified because neither the neutral complex nor the ionic complex are created, save as extremely short-lived intermediates. The reaction can thus be characterized as a one-step reaction.

1.6 Asymmetric Organocatalysis

The development of various analytical techniques for determining the stereochemical purity of chiral compounds, as well as the increasing demand for enantiopure chemicals and enantioenriched axially chiral compounds in asymmetric catalysis, led to significant progress in asymmetric synthesis^{68,69} and catalysis.⁷⁰ Considering recent advances in asymmetric catalysis, it is clear that current asymmetric catalysis is based on three main pillars: biocatalysis, metal catalysis, and organocatalysis. If one goes back in time, fully organic compounds such as acetaldehyde were the first catalysts utilised by organic chemists (Liebig in 1859).⁷¹ Lewis bases, Lewis acids, Brønsted bases, and Brønsted acids are the four broad groups of organocatalysts. These organocatalysts either provide or remove electrons or protons from a substrate or a transition state during chemical processes. Lewis base catalysts like amines and carbenes dominate organocatalysis, whereas Lewis acids like carbonyl compounds are rarely utilized. Iminium catalysis, first discovered by Macmillan in 2000⁷² and subsequently followed by asymmetric enamine catalysis published by List and collaborators, are two of the most often researched domains in organocatalysis.⁷³ Wurz's 4-dimethylaminopyridine (DMAP) analogues⁷⁴ made a significant contribution to asymmetric catalysis, followed by Gaunt and Johansson's contribution of ammonium enolates.⁷² With the discovery of an a^3-d^3 -type umpolung introduced separately by Glorius and Bode, organocatalysis by N-Heterocyclic Carbenes (NHC) has exploded in popularity in the field of asymmetric organocatalysis.⁷⁶ In asymmetric organocatalysis, Akiyama and Terada discuss the utilisation of stronger Brønsted acids. Depending on the acidity of the acid employed, Brønsted acids engage in the

process by creating hydrogen bonds or by protonating the reaction substrate, generating ion pairs as intermediates.⁷⁷⁻⁷⁸

1.6.1 Brønsted Base Catalysis

For enantioselective synthesis, chiral organic Brønsted bases have emerged as extremely selective and efficient catalysts (see **Figure 1.8 below**). The use of Brønsted base catalysts was first described in 1913 for enantioselective hydrocyanation to aldehydes.⁷⁹ Originally developed by Wynberg in the 1970s and 1980s for enantioselective hydrocyanation to aldehydes, chiral organic Brønsted base catalysis has progressed as a consequence of mechanistic insight and catalyst design to solve issues in synthetic technique.⁸⁰ Mechanistic research and perceptive observations on Brønsted base and hydrogen bond donor activation of substrates have aided novel catalyst development greatly during the last two decades.⁸¹⁻⁸⁴ During the bond formation process, bifunctional catalyst design has been ingeniously included into catalyst design to activate both nucleophiles and electrophiles. As a result of these advancements in mechanistic knowledge and catalyst design, a growing variety of innovative techniques and synthetic transformations have emerged.

The discovery that the *cinchona* alkaloids are efficient catalysts⁸⁵⁻⁹⁰ and favored structures⁹¹ led to the development of chiral Brønsted base catalysis. The features critical for enantioselective catalysis were better understood after a systematic study of structural variations. These investigations have revealed the relevance of a stiff backbone with fundamental activity, as well as the presence or absence of a hydrogen-bond donor within the same catalytic structure. As a result of these realisations, novel *cinchona* alkaloid-based catalysts with changed hydrogen-bond donor capabilities have been synthesised, expanding the area of their use. With the usage of the cyclohexane diamine by Jacobsen⁹² and Takemoto,⁹³ later studies have enhanced the knowledge of this motif. The emergence of chiral organic Brønsted bases for enantioselective catalysis, as well as the development of these catalysts, demonstrate the value of the mechanistic knowledge gained to date.

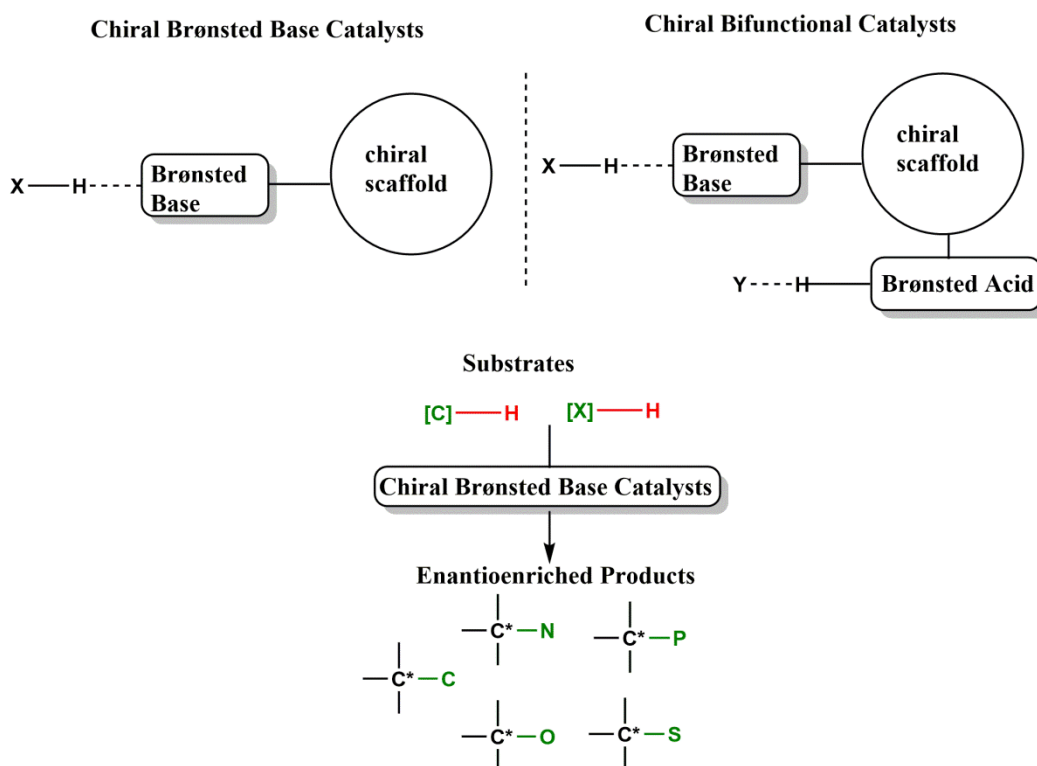


Figure 1.8 Simplified model for Chiral Brønsted bases catalyst design

1.6.2 *Cinchona* Alkaloids

The direct function of *cinchona* alkaloids in asymmetric synthesis demonstrates their flexibility as chiral base catalysts, promoters, and ligands. Pracejus,^{94,95} Morrison along with Mosher,⁹⁶ and Wynberg^{97,98} conducted early experiments on the utilization of *cinchona* alkaloids in asymmetric synthesis up to the late 1980s. Ketene chemistry, which was employed in asymmetric β -lactone synthesis⁹⁹⁻¹⁰⁰ during this period, as well as asymmetric induction in dihydroxylation and desymmetrization,¹⁰¹⁻¹⁰⁴ were important developments at the time. Wynberg's important work on *cinchona* alkaloid-catalyzed addition of cyclic β -ketoesters to methyl vinyl ketone was the first report of catalytic enantioselective conjugate addition.¹⁰⁵ *Cinchona* alkaloids have a bifunctional catalytic property due to the basicity of the quinuclidine nitrogen paired with the Brønsted acidic C(9)-OH. *Cinchona* alkaloids are important contributors to asymmetric reactions and enantioselective transformations because they behave as a bifunctional organocatalyst or ligand. The enantioselective transformation consist of

conjugate additions (Strecker, Baylis–Hillman, Michael, Mannich, Aldol, and Henry), cycloaddition reactions, phase-transfer reactions (PTC), β -lactone synthesis, aziridination, desymmetrization studies, decarboxylations, epoxidations, and hydrogenations.¹⁰⁶

Cinchona alkaloids' pseudoenantiomeric pairs, which may be used to make either enantiomer of chiral product, are a prominent mechanism of stereoselectivity. The quinuclidine nitrogen and the neighbouring C(9)–OH (the N–C(8)–C(9)–OH species) are important moieties in *cinchona* alkaloids.

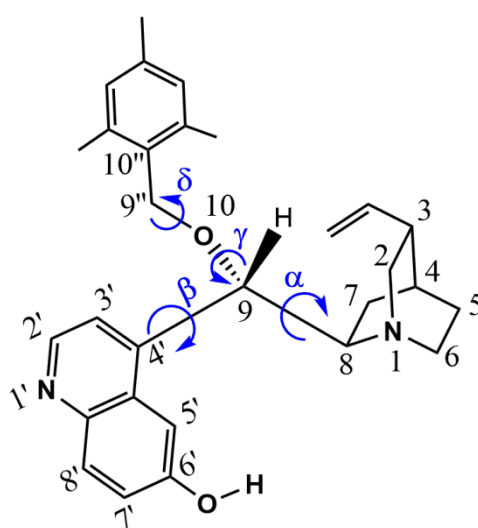


Figure 1.9 The relevant angles and dihedrals for the cinchona alkaloid catalyst.

The torsion angles N–C(8)–C(9)–O are opposite in sign in pseudoenantiomeric alkaloids in the normal open conformation: Q and CD are (-), and so induce selectivity for one enantiomer, whereas QD and C are (+), and thus afford the other enantiomer.^{107,108} Cupreines and cupreidines are pseudoenantiomers of *cinchona* alkaloids that have an OH–group in lieu of the quinoline C(6')–OCH₃. As a result, another hydrogen-bonding moiety becomes available. In asymmetric reactions like the Baylis–Hillman reaction, β -lactone synthesis, asymmetric α -halogenation, alkylations, carbocyanation of ketones, and Diels–Alder reactions, the quinuclidine nitrogen launches a nucleophilic assault on the substrate, making *cinchona* alkaloids Lewis basic.^{109–118}

Cinchona alkaloids have a lesser-known but equally important and recent role as Brønsted bases. *Cinchona* alkaloids are Brønsted bases when the nitrogen moiety combines with a proton (either by partial deprotonation or protonation), resulting in the chiral intermediate species required for stereodirection and facial selectivity. Hiemstra and Wynberg's¹¹⁹ 1,4-addition of thiophenols to cyclohexenones is the oldest example. The thiol is deprotonated by the quinuclidine nitrogen, which also stabilises the enolate by hydrogen-bonding with the C(9)–OH moiety of the catalyst. In the past two decades, modified *Cinchona* alkaloids catalysts have been created to improve the catalyst's bifunctional mode. The most important developments are C(9)–OH group derivations, quinoline C(6')–OCH₃ substitution with a hydroxyl group to improve hydrogen bonding, bis-*cinchona* alkaloids syntheses, and synthesis of thiourea-derived *cinchona* alkaloids. There are also other modified *cinchona* alkaloid catalysts, namely (see Figure 1.9 below)

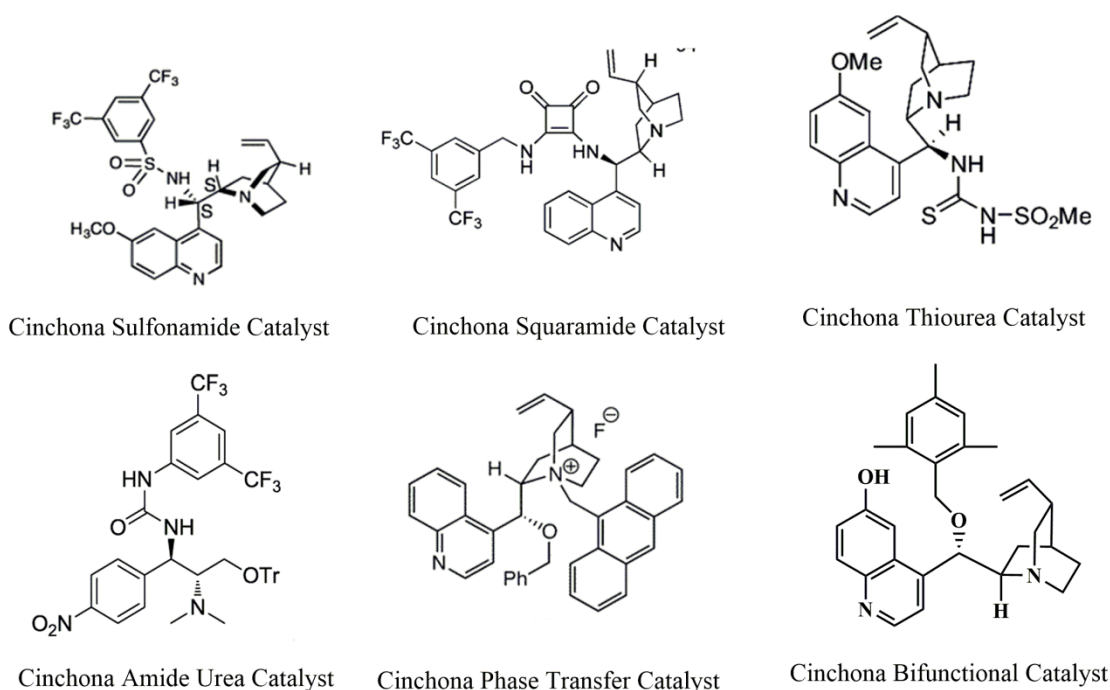


Figure 1.10 Different modified cinchona alkaloid catalysts.

1.6.3 Non-Covalent Interactions

Non-covalent interactions (NCIs) are common in nature and help to keep chemical systems together. Intramolecular and intermolecular non-covalent interactions are weaker locally than covalent connections and have lower energy and directionality. Nonetheless, in many circumstances, these interactions can play a dominant role in materials synthesis, catalysis, and design. NCIs are frequently divided into subclasses of bonds and interactions based on the nature of the individual elements or synthons involved. Chemical interactions are common between proteins and drugs, catalysts and substrates, nanomaterial self-assembly,¹²⁰ and many chemical processes.¹²¹ Non-covalent interactions like hydrogen bonding, dipole-dipole interactions, steric repulsion, and London dispersion dominate these interactions.¹²² In biochemical processes, non-covalent and electrostatic interactions are the driving factors. Although there are several tools for viewing and analysing covalent and electrostatic interactions, similar methods for non-covalent interactions have yet to emerge. The *cinchona* alkaloid and its modified bifunctional catalysts have been shown to have a prominent effect on stabilizing electrophiles and nucleophiles through non-covalent interactions.

Non-covalent interactions are common in organic systems, and they can have a big impact on how asymmetric organocatalytic events turn out. Their frequent occurrence, along with the sometimes indistinct boundary separating advantageous dispersion interactions from negative steric contacts, makes identifying the specific non-covalent interactions that cause stereoselectivity difficult. In most organocatalytic processes, stereoselectivity is ultimately determined by the balance of favourable and unfavourable non-covalent interactions in the stereocontrolling transition state (TS). Concerns about the relevance of non-covalent interactions in organocatalysis have altered lately. The consensus has shifted away from the steric-repulsion-centered perspective that dominated the asymmetric response debate for decades and towards a focus on the potentially crucial role of favorable non-covalent interactions. This has been primarily driven by two crucial developments. First, Copeland and Miller,¹²³ and Jacobsen and coworkers,¹²⁴ have argued that developing organocatalysts with

favorable non-covalent interactions that stabilise the transition state (TS) leading to the desired product is advantageous.

It is now commonly recognised that favorable non-covalent interactions can be critical in a variety of catalytic applications. Aromatic interactions as control components in catalysis, for example, were recently examined by Krenske and Houk.¹²⁵ Wagner and Schreiner¹²⁶ very recently published an eye-opening study of the influence of dispersion interactions on molecule structure and stability, as well as reactivity, catalysis and spectroscopy. The widespread availability of computational methods to reliably address favourable non-covalent interactions in organic chemistry, as well as the rising acknowledgment of their relevance in organic chemistry,¹²⁷⁻¹²⁹ has opened up new paths for the computational research of organic systems. In the context of asymmetric organocatalysis, it has also brought new hurdles for both experiment and theory. Most importantly, it has highlighted the question of how best to take advantage of non-covalent interactions in order to create more effective catalysts.

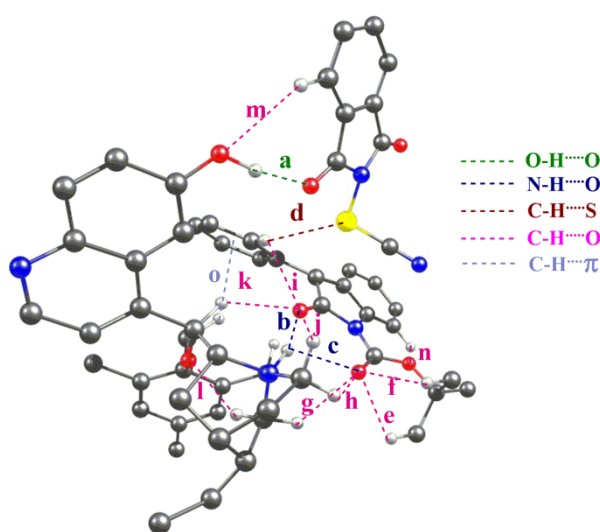


Figure 1.11 Non-covalent interactions of a model system are shown.

1.7 Objective of the thesis

Though the experimental studies have opened up insights towards the hydride and proton transfer organic transformations, still a lot of questions remain unanswered, such as (i) What could be the initiation step for hydride and proton formation? (ii) If the hydride transfer goes through an initiation step, then what would the actual mechanism be? (iii) How does the involvement of multiple hydroborating agents reduce the activation barriers for the hydroboration reactions? (iv) What are the challenges in asymmetric catalysis? (v) What are the plausible mechanistic pathways towards the formation of new asymmetric products? (vi) What is the deciding point between two comparable pathways? In this thesis, full quantum chemical calculations using density functional theory (DFT) have been utilized to provide interesting insights and address the above mentioned questions. In so doing, I have investigated the role of the hydride and proton transfer processes in different organic transformations. The thesis titled “**Computational Insights into Proton and Hydride Transfer Chemistry**” is divided into seven different chapters. A brief introduction to each chapter is provided below with the chapter titles.

1.8 Organization of the thesis

Chapter-1: A Brief Overview of the Importance in Hydride and Proton Transfer Chemical Transformations.

In this chapter, I have provided in brief details of how hydride and proton transfer play important roles in chemistry as well as in biology. In the later part of this chapter, I have highlighted how the hydride and proton transfer processes play an important role in my current research. This include mainly hydrosilylation and hydroboration reactions for hydride transfer and asymmetric organocatalysis for proton transfer reactions.

Chapter-2: The History and Fundamentals of Computational Chemistry.

This chapter deals with the history and fundamentals of computational chemistry, quantum chemical methods, density functional theory (DFT), non-covalent

interaction (NCI) plots, natural bond orbital analysis, and volume correction methods.

Chapter-3: B(C₆F₅)₃ Catalyst or Initiator? Insights from Computational Studies.

In this chapter, I have tried to look into a very important reaction i.e. *in situ* generation of SiH₄. First, we have looked into the earlier proposed mechanism, which is B(C₆F₅)₃ catalyzed. Then, I have looked at the autocatalytic mechanism. Then, I have compared both the mechanisms and come up with a new mechanism where B(C₆F₅)₃ plays the role of initiator and the rest of the mechanism goes *via* the autocatalytic way. In order to get more insights into the proposed idea, I have calculated the turn over frequency of the previous, as well as newly proposed mechanism. The turnover frequency suggests that the autocatalytic pathway is followed.

Chapter-4: The Role of Ion-pair in B(C₆F₅)₃ Catalyzed Zwitterionic Chemistry.

In this chapter, I have investigated the ion-pair separation energy of each of the ion-pairs formed in different experimentally proposed reactions. Then I have proposed a means of deciding whether B(C₆F₅)₃ acts as a catalyst or as an initiator, based on how easy or difficult it is to separate the ion-pair.

Chapter 5: The Role of Hydride Transfer in Stannylene and Germylene Initiated Catalysis.

In this chapter, I investigate the reaction mechanism and role of hydride transfer in stannylene and germylene initiated catalysis. I subsequently subjected these pathways to a full static quantum chemical study with density functional theory (DFT) and thus obtained all the barriers (ΔG^\ddagger) for the reactions involved in these processes, as well as the energies (ΔG) of the reactions. As will be discussed in this chapter, this has led to results that not only reveal interesting pathways for the formation of the hydroboration product but also indicate that these mechanistic routes would have been thermodynamically and kinetically feasible.

Chapter-6: Unraveling the Role of Organocatalysis in Modified *Cinchona* Alkaloid Catalyst *via* Proton Transfer.

In this chapter, I have shown the role of additive where a modified C6'-OH *cinchona* catalyst has been investigated for different alpha thiocyanation reactions. First, I have looked into the most stable conformation of the modified C6'-OH *cinchona* catalyst *via* a potential energy scan method. Then, I have looked into the reaction mechanism for the experimentally obtained asymmetric products. It has been observed that the additive plays a very crucial role in determining the major yield and enantioselectivity of a particular asymmetric product. Thus the mechanistic investigation discards the previous accepted mechanism and comes up with a new mechanistic pathway favoring the Wynberg model rather than the Houk-Grayson model. This provides new insights into modified bifunctional asymmetric organocatalysis.

Chapter-7: Summary and Future Outlook

In this chapter, I have summarized all the working chapters and concluding remarks in detail, as well as provided a pictorial representation. Further future aspects of the thesis work have been provided.

1.9 References

1. (a) Woodward, R. B.; Wendler, N. L.; Brutschy, F. J. *J. Am. Chem. Soc.* **1945**, *67*, 1425–1429. (b) Ebenezer D. Williams, Knut A. Krieger, and Allan R. Day, *J. Am. Chem. Soc.* 1953, *75*, 10, 2404–2407.
2. Oppenauer, R.V. *Recl. Trav. Chim. Pays-Bas.* **1937**, *56*, 137-144.
3. Hammett, X. P. *Physical Organic Chemistry*. McCraw-Hill, New York, 1940. pp 350. (b) Alexander E. R. *J. Am. Chem. Soc.* **1947**, *69*, 289–294.
4. Pollard, C. B.; Young, D. C. *J. Org. Chem.* **1951**, *16*, 661–672.
5. Pfeil, Bee., 1951, 229.
6. Whitmore, F. C. *J. Am. Chem. Soc.* 1932, *54*, 3274–3283.
7. Bartlett, P.D.; Condon, F. E.; Schneider, A. *J. Am. Chem. Soc.* **1944**, *66*, 1531–1539.
8. Freitag, F.; Irrgang, T.; Kempe, R. *J. Am. Chem. Soc.* **2019**, *141*, 11677–11685
9. Deno, N. C.; Peterson, H. J.; Saines, G. S. *Chem. Rev.* **1960**, *60*, 7–14.
10. Schellenberg, K.A. (1970). *The Mechanism of Hydride Transfer*. In: Sund, H. (eds) *Pyridine Nucleotide-Dependent Dehydrogenases*. Springer, Berlin, Heidelberg.
11. Tapia, O.; Andres, J.; Aullo, J. M.; Branden, C.-I. *J. Chem. Phys.* **1985**, *83*, 4673-4682.
12. Tapia, O.; Andres, J.; Aullo, J. M.; Cardenas, R. *J. Mol. Struct., Theochem.* **1988**, *167*, 395-412.
13. Mestres, J.; Lledo's, A.; Duran, M.; Bertra'n, J. *J. Mol. Struct. Theochem.* **1992**, *260*, 259–272.
14. Mestres, J.; Duran, M.; Bertra'n, J. *Theor. Chim. Acta.* **1994**, *88*, 325–338.
15. Mestres, J.; Duran, M.; Bertra'n, J. *Bioorg. Chem.* **1996**, *80*, 69–80.

16. Fradera, X.; Duran, M.; Mestres, J. *Can. J. Chem.* **2000**, *78*, 328–337.
17. Zhu, X. Q.; Liu, Y.; Zhao, B. J.; Cheng, J. P. *J. Org. Chem.* **2001**, *66*, 370–375.
18. Gębicki, J.; Marcinek, A.; Zielonka, J. *Acc. Chem. Res.* **2004**, *37*, 379–386.
19. Pankratov, A. N.; Drevko, B. I. *J. Serb. Chem. Soc.* **2004**, *69*, 431–439.
20. Buck, H. *Int. J. Quant. Chem.* **2005**, *101*, 389–395.
21. Pankratov, A. N.; Drevko, B. I. *Chem. of Het. Comp.*, **2005**, *41*, 1105–1111.
22. Khanna, S.; Kaur, D.; Kaur, R. *J. Phys. Org. Chem.* **2014**, *27*, 747–755.
23. Powell, M. F.; Wu, J. C.; Bruce, T. C. *J. Am. Chem. Soc.* **1984**, *106*, 3850–3856.
24. Miller, L. L.; Valentine, J. R. *J. Am. Chem. Soc.* **1988**, *110*, 3982–3989.
25. Powell, M. F.; Bruce, T. C. *J. Am. Chem. Soc.* **1983**, *105*, 1014–1021.
26. Cheng, J.-P.; Lu, Y.; Zhu, X.; Mu, L. *J. Org. Chem.* **1988**, *63*, 6108–6114.
27. Zhu, X. Q.; Liu, Y. C.; Cheng, J. P. *J. Org. Chem.* **1999**, *64*, 8980–8981.
28. Ashby, E. C.; Dobbs, F. R.; Hopkins, H. P. *J. Am. Chem. Soc.* **1975**, *97*, 3158–3162.
29. Renner, H., Schlamp, G., Kleinwächter, I., Drost, E., Lüscho, H.M., Tews, P., Panster, P., Diehl, M., Lang, J., Kreuzer, T., Knödler, A., Starz, K.A., Dermann, K., Rothaut, J., Drieselmann, R., Peter, C., Schiele, R., Coombes, J., Hosford, M. and Lupton, D.F. (2018). Platinum Group Metals and Compounds. In Ullmann's Encyclopedia of Industrial Chemistry.
30. Hydrosilylation A Comprehensive Review on Recent Advances" B. Marciniak (ed.), Advances in Silicon Science, Springer Science, 2009.
31. Troegel, D.; Stohrer, J. *Coordination Chemistry Reviews*, **2010**, *255*, 1440–1459.
32. Fry, J. L.; Rahaim Jr., R. J. Maleczka, Jr., R E. "Triethylsilane", *Encyclopedia of Reagents for Organic Synthesis*, John Wiley & Sons, 2007.

33. (a) Piers, W. E.; Chivers, T. *Chem. Soc. Rev.* **1997**, *26*, 345–354. (b) Piers, W. E. *Adv. Organomet. Chem.* **2004**, *52*, 1–76. (c) Erker, G. *Dalton Trans.* **2005**, 1883–1890. (d) Welch, G. C.; San Juan, R. R.; Masuda, J. D.; Stephan, D. W. *Science* **2006**, *314*, 1124–1126. (e) Stephan, D. W.; Erker, G. *Angew. Chem., Int. Ed.* **2010**, *49*, 46–76. (f) Piers, W. E.; Marwitz, A. J. V.; Mercier, L. G. *Inorg. Chem.* **2011**, *50*, 12252–12262. (g) Melen, R. L. *Chem. Commun.* **2014**, *50*, 1161–1174.
34. (a) Massey, A. G.; Park, A. J.; Stone, F. G. A. *Proc. Chem. Soc.* **1963**, 212–212. (b) Massey, A. G.; Park, A. J. *J. Organomet. Chem.* **1964**, *2*, 245–250.
35. Laszlo, P.; Teston, M. *J. Am. Chem. Soc.* **1990**, *112*, 8750–8754.
36. Clark, E. R.; Del Grosso, A.; Ingleson, M. J. *Chem. - Eur. J.* **2013**, *19*, 2462–2466.
37. Krossing, I.; Raabe, I. *Chem. - Eur. J.* **2004**, *10*, 5017–5030.
38. Stephan, D. W. *J. Am. Chem. Soc.* **2015**, *137*, 10018–10032.
39. Plasson, R.; Brandenburg, A.; Jullien, L.; Bersini, H. *J. Phys. Chem. A* **2011**, *115*, 8073–8085.
40. Ito, H. *IBM J. Res. Dev.* **1997**, *41*, 69–80.
41. Mallory, G. O.; Hajdu, J. B. *Electroless plating : fundamentals and applications*, The Society, Orlando, FL, **1990**.
42. James, T. H.; Mees, C. E. K. *The Theory of the photographic process*, 4th ed., Macmillan, New York, **1977**.
43. (a) Ludlow, R. F.; Otto, S. *Chem. Soc. Rev.* **2008**, *37*, 101–108. (b) Ashkenasy, G.; Hermans, S. Otto, T. M.; Taylor, A. F.; *Chem. Soc. Rev.* **2017**, *46*, 2543–2554. (c) Mattia, E.; Otto, S. *Nat. Nanotechnol.* **2015**, *10*, 111–119.
44. (a) C. De Duve, *Singularities Landmarks on the Pathways of Life*, Cambridge University Press, Cambridge, UK, **2005**. (b) C. De Duve, *Blueprint for a cell : the*

nature and origin of life, N. Patterson, Burlington, N. C., **1991**. (c) Pross, A.; Pascal, R.; Sutherland, D. *Open* **2013**, *3*, 120190. (d) Szostak, J. W. *Nature* **2009**, *459*, 171–172. (e) Dyson, F. J. *Origins of life*, Cambridge University Press, Cambridge Cambridgeshire; New York, **1985**.

45. (a) Pross, A. *Origins Life Evol. Biospheres* **2004**, *34*, 307–321. (b) Joyce, G. F.; Szostak, J. W. *Cold Spring Harbor Perspect. Biol.* **2018**, *10*. (c) Orgel, L. E. *Acc. Chem. Res.* **1995**, *28*, 109-118.

46. (a) Morowitz, H. J.; Kostelnik, J. D.; Yang, J.; Cody, G. D. *Proc. Natl. Acad. Sci. USA* **2000**, *97*, 7704–7708. (b) Zubarev, D. Y.; Rappoport, D.; Aspuru-Guzik, A. *Sci. Rep.* **2015**, *5*, 8009. (c) Boutlerow, A. M.; *C. R. Chim.* **1869**, *53*, 145–147.

47. (a) Zhabotinsky, A. M. *Biofizika* **1964**, *9*, 306–311. (b) Belousov, B. P. *Sbornik Referatov po Radiatsionni Meditsine* **1958**, *145*.

48. (a) Castets, V.; Dulos, E.; Boissonade, J.; P. Dekepper, *Phys. Rev. Lett.* **1990**, *64*, 2953–2956. (b) Epstein, I. R.; Pojman, J. A. *An introduction to nonlinear chemical dynamics : oscillations, waves, patterns, and chaos*, Oxford University Press, New York, 1998 (c) Epstein, I. R.; Xu, B. *Nat. Nanotechnol.* **2016**, *11*, 312–319.

49. Brown, H.C. *Tetrahedron*, **1961**, *12*, 117-138.

50. "The Nobel Prize in Chemistry 1979". www.nobelprize.org.

51. Lewis, G. N. *J. Am. Chem. Soc.*, **1916**, *38*, 762.

52. Neumann, W. P. *The Organic Chemistry of Tin*, Wiley, London, **1970**.

53. Powell, H. M.; Brewer, F. M. *J. Chem. Soc.*, **1938**, 197.

54. Davidson, P. J.; Lappert, M. F. *J. Chem. Soc., Chem. Commun.*, **1973**, 317.

55. Harris, D. H.; Lappert, M. F. *J. Chem. Soc., Chem. Commun.*, **1974**, 895.

56. Frey, G. D.; Lavallo, V.; Donnadiu, B.; Schoeller, W. W.; Bertrand, G. *Science* **2007**, *316*, 439.

58. Apeloig, Y.; Pauncz, R.; Karni, M.; West, R.; Steiner, W.; Chapman, D. *Organometallics* **2003**, *22*, 3250.
59. (a) Haaf, M.; Schmedake, T. A.; West, R. *Acc. Chem. Res.* **2000**, *33*, 704. (b) Asay, M.; Jones, C.; Driess, M. *Chem. Rev.* **2011**, *111*, 354. (c) Roy, M. D.; Rivard, E. *Acc. Chem. Res.* **2017**, *50*, 2017. (d) Fujimori, S.; Inoue, S. *Eur. J. Inorg. Chem.* **2020**, 2020, 3131. (e) Melen, R. L. *Science* **2019**, *363*, 479. (f) Yadav, S.; Saha, S.; Sen, S. S.; *ChemCatChem* **2016**, *8*, 486. (g) Chu, T.; Nikonov, G. I. *Chem. Rev.* **2018**, *118*, 3608. (h) Hadlington, T. J.; Driess, M.; Jones, C. *Chem. Soc. Rev.* **2018**, *47*, 4176. (i) Mizuhata, Y.; Sasamori, T.; Tokitoh, N. *Chem. Rev.* **2009**, *109*, 3479.
60. (a) Usher, M.; Protchenko, A. V.; Rit, A.; Campos, J.; Kolychev, E. L.; Tirfoin, R.; Aldridge, S.; *Chem. Eur. J.* **2016**, *22*, 11685. (b) Protchenko, A. V.; Birjkumar, K. H.; Dange, D.; Schwarz, A. D.; Vidovic, D.; Jones, C.; Kaltsoyannis, N.; Mountford, P.; Aldridge, S. *J. Am. Chem. Soc.* **2012**, *134*, 6500. (c) Kira, M.; Ishida, S.; Iwamoto, T.; Kabuto, C.; *J. Am. Chem. Soc.* **1999**, *121*, 9722. (d) Jutzi, P.; Kanne, K.; Krüger, C. *Angew. Chem. Int. Ed.* **1986**, *25*, 164.
61. (a) Munz, D.; *Organometallics* **2018**, *37*, 275. (b) Andrada, D. M.; Holzmann, N. T.; Frenking, H. G. *Beilstein J. Org. Chem.* **2015**, *11*, 2727.
62. Vignolle, J.; Cattoën, X.; Bourissou, D. *Chem. Rev.* **2009**, *109*, 3333.
63. Sen, N.; Khan, S. *Chem. Asian J.* **2021**, *16*, 705.
64. (a) Siwatch, R. K.; Nagendran, S. *Chem. Eur. J.* **2014**, *20*, 13551. (b) Hadlington, T. J.; Hermann, M.; Frenking, G.; Jones, C.; *J. Am. Chem. Soc.* **2014**, *136*, 3028. (c) Hadlington, T. J.; Kefalidis, C. E.; Maron, L.; Jones, C. *ACS Catal.* **2017**, *7*, 1853. (d) Erickson, J. D.; Lai, T. Y.; Liptrot, D. J.; Olmstead, M. M.; Power, P. P. *Chem. Commun.* **2016**, *52*, 13656.
65. (a) Wang, Y.; Ma, J.; *J. Organomet. Chem.* **2009**, *694*, 2567. (b) Denk, M.; Lennon, R.; Hayashi, R.; West, R.; Belyakov, A. V.; Verne, H. P.; Haaland, A.; Wagner, M.; Metzler, N. *J. Am. Chem. Soc.* **1994**, *116*, 2691. (c) Becerra, R.;

Bogdanov, S. E.; Egorov, M. P.; Faustov, V. I.; Nefedov, O. M.; Walsh, R. *Can. J. Chem.* **2000**, *78*, 1428.

66. Greb, L.; Ebner, F.; Ginzburg, Y.; Sigmund, L. M. *Eur. J. Inorg. Chem.* **2020**, *2020*, 3030.

67. Krzysztof Szalewicz, Hydrogen Bond, Editor(s): Robert A. Meyers, Encyclopedia of Physical Science and Technology (Third Edition), Academic Press, **2003**, pp 505-538.

68. (a) Helmchen, G.; Hoffmann, R. W.; Mulzer, J.; Schaumann, E. Stereoselective Synthesis in Methods of Organic Chemistry, Houben-Weyl, Vol. 21a-21f, 4th ed., Thieme, Stuttgart, **1995**. (b) Gawley, R. E.; Aube, J. Principles of Asymmetric Synthesis, Tetrahedron Organic Chemistry Series, Elsevier, New York, **1996**. (c) Ho, T.-L. Stereoselectivity in Synthesis, Wiley-VCH, New York, **1999**. (d) Lin, G.-Q.; Li, Y.-M.; Chan, A. S. C. Principles and Applications of Asymmetric Synthesis, Wiley-VCH, New York, **2001**. (e) Sharpless, K. B. *Angew. Chem., Int. Ed.* **2002**, *41*, 2024–2032. (f) Song, C. E.; Lee, S.-G. *Chem. Rev.* **2002**, *102*, 3495–3524. (g) Liu, M.; Sibi, M. P. *Tetrahedron* **2002**, *58*, 7991–8035.

69. (a) Jonathan, M. J. W. Catalysis in Asymmetric Synthesis, Sheffield Academic Press, Sheffield, **1999**. (b) Ojima, I. Catalytic Asymmetric Synthesis, 2nd ed., Wiley-VCH, New York, **2000**. (c) Noyori, R. *Angew. Chem., Int. Ed.* **2002**, *41*, 2008–2022 (d) Inanaga, J.; Furuno, H.; Hayano, T. *Chem. Rev.* **2002**, *102*, 2211–2225. (e) Mikami, K.; Terada, M.; Matsuzawa, H. *Angew. Chem., Int. Ed.* **2002**, *41*, 3554–3571.

70. List, B. *Chem. Rev.* **2007**, *107*, 5413–5415.

71. (a) Ahrendt, K. A.; Borths, C. J.; MacMillan, D. W. C. *J. Am. Chem. Soc.* **2000**, *122*, 4243–4244. (b) Erkkilä, A.; Majander, I.; Pihko, P. M. *Chem. Rev.* **2007**, *107*, 5416–5470.

72. Mukherjee, S.; Yang, J. W.; Hoffmann, S.; List, B. *Chem. Rev.* **2007**, *107*, 5471–5569.

73. (a) Wurz, R. P. *Chem. Rev.* **2007**, *107*, 5570–5595. (b) Wurz, R. P.; Lee, E. C.; Ruble, J. C.; Fu, G. C. *Adv. Synth. Catal.* **2007**, *349*, 2345–2352. (c) Fu, G. C. *Acc. Chem. Res.* **2004**, *37*, 542–547.
74. Gaunt, M. J.; Johansson, C. C. C. *Chem. Rev.* **2007**, *107*, 5596–5605.
75. (a) Enders, D.; Niemeier, O.; Henseler, A. *Chem. Rev.* **2007**, *107*, 5606–5655. (b) Mondal, S.; Yetra, S. R.; Mukherjee, S.; Biju, A. T. *Acc. Chem. Res.* **2019**, *52*, 425–436. (c) Zhong, R.; Lindhorst, A. C.; Groche, F. J.; Kühn, F. E. *Chem. Rev.* **2017**, *117*, 1970–2058. (d) Zhukhovitskiy, A. V.; MacLeod, M. J.; Johnson, J. A. *Chem. Rev.* **2015**, *115*, 11503–11532. (e) Flanigan, D. M.; Romanov-Michailidis, F.; White, N. A.; Rovis, T. *Chem. Rev.* **2015**, *115*, 9307–9387. (f) Perez, F.; Ren, Y.; Boddaert, T.; Rodriguez, J.; Coquerel, Y. *J. Org. Chem.* **2015**, *80*, 1092–1097. (g) Burstein, C.; Glorius, F. *Angew. Chem. Int. Ed.* **2004**, *43*, 6205–6208. (h) Sohn, S. S.; Rosen, E. L.; Bode, J. W. *J. Am. Chem. Soc.* **2004**, *126*, 14370–14371. (i) Hopkinson, M. N.; Richter, C.; Schedler, M.; Glorius, F. *Nature*, **2014**, *510*, 485–496.
76. (a) Sohn, SS.; Rosen, EL.; Bode, JW. *J. Am. Chem. Soc.* **2004** *126*, 14370 (b) Burstein, C.; Glorius, F. *Angew Chem, Int Ed.* **2004**, *43*, 6205. (c) Burstein, C.; Tschan, S.; Xie, X.; Glorius, F. *Synthesis* **2006**, 2418.
77. Akiyama, T.; Itoh, J.; Yokota, K.; Fuchibe, K. *Angew Chem Int Ed.* **2004**, *43*, 1566–1568.
78. Uruguchi, D.; Terada, M. *J. Am. Chem. Soc.* **2004**, *126*, 5356–5357.
79. Bredig, G. Fiske, P. *Biochem Z.* **1931**, *4*, 67.
80. Wynberg, H.; Heider, R. *Tetrahedron Lett.* **1975**, *16*, 4057.
81. Cannon, S. *Chem. –Eur. J.* **2006**, *12*, 5418.
82. Takemoto, Y. *Org. Biomol. Chem.* **2005**, *3*, 4299.
83. Taylor, M.; Jacobsen, EN. *Angew. Chem. Int. Ed.* **2006**, *45*, 1520.
84. Doyle, A.; Jacobsen, EN. *Chem. Rev.* **2007**, *107*, 5713.

85. Kacprazk, K. Gawronski, J. *Synthesis* **2001**, 7, 961.
86. Dalko, P.; Moisan, L. **2004**, 43, 5138.
87. Hoffman, HMR.; Frackenpohl, J. 2004, *Eur. J. Org.* 21, 4293.
88. Lygo, B. Andrews, BI. *Acc. Chem. Res.* **2004**, 37, 518.
89. Seeyad, J.; List, B. *Org. Biol. Chem.* **2005**, 3, 719.
90. Marcelli, T. van Maarseveen, JH. Kiemstra, H. *Angew. Chem. Int. Ed.* **2006**, 45, 7496.
91. Yoon, T.; Jacobsen, E. *Science* **2003**, 299, 1691.
92. Sigman, MS.; Jacobsen, EN. *J. Am. Chem. Soc.* **1998**, 120, 4901.
93. Okino, T.; Hoashi, Y.; Takemoto, Y. *J. Am. Chem. Soc.* **2003**, 125, 12672.
94. Pracejus, H. *Justs Liebigs Ann Chem.* **1960**, 634, 9.
95. Wynberg, H. *Fortswchr Chem Forsch.* **1967**, 8, 493.
96. Morrison, JD.; Mosher, HS; *Asymm organic reactions*, **1971**, Prentice-Hall, Englewood Cliffs.
97. Wynberg, H. *Top Stereochem*, **1986**, 16, 87.
98. Hermann, K.; Wynberg, H. *J Org Chem.* **1979**, 44, 2238.
99. Wynberg, H. Staring, EGJ. *J Am Chem Soc.* **1982**, 104, 166-168.
100. Wynberg, H.; Staring, EGJ. *J. Org. Chem.* **1985**, 50, 1977-1979.
101. Hiratake, J.; Yamamoto, Y.; Oda, J. *J Chem Soc Chem Commun.* **1985**, 1717.
102. Hiratake, J.; Inagaki, M.; Yamamoto, Y; Oda, J. *J. Chem. Soc. Perkin. Trans. 1*, 1053.
103. Kolb, HC.; VanNieuwenhuze, MS.; Sharpless, KB. *Chem. Rev.* **1994**, 94, 2483.

104. Sharpless KB (1998) Transition metal for organic synthesis, vol 2. Meller M, Colm C(eds).Wiley, VCH, Weinheim, pp 243–260.
105. Wynberg, H.; Heider, R. *Tetrahedron Lett.* **1975**, *16*, 4057.
106. Kacprazk, K.; Gawronski, J. *Synthesis* **2001**, *7*, 961.
107. Dijkstra, GHD.; Kellogg, RM.; Wynberg, H. *J. Org. Chem.* **1990**, *55*, 6121.
108. Dijkstra, GDH.; Kellogg, RM.; Wynberg, H.; Svendsen, JS.; Marko, I. Sharpless B. *J. Am. Chem. Soc.* **1989**, *111*, 8069.
109. France, A.; Guerin, DJ.; Miller, SJ.; Lectka, T. *Chem. Rev.* **2003**, *103*, 2985.
110. Tian SK, Chen Y, Hang J, Tang L, McDaid P, Deng L *Acc. Chem. Res.* **2004**, *37*, 621.
111. Paull, DH.; Abraham, CJ.; Scerba, MT.; Alden-Danforth, E. Lectka, T. *Acc. Chem. Res.* **2008**.
112. Iwabuchi, Y.; Nakatani, M.; Yokoyama, N.; Hatakeyama, S. *J. Am. Chem. Soc.* **1999**, *121*, 10219.
113. Cortez, GS.; Oh, SH.; Romo, D. **2001**, *11*, 1731.
114. Cortez, GS.; Tennyson, RL.; Romo, D. *J. Am. Chem. Soc.* **2001**, *123*, 7945.
115. Balan, D.; Adolfsson, H. *Tetrahedron Lett.* **2003**, *44*, 2521.
116. Kawahara, S.; Nakano, A.; Esumi, T.; Iwabuchi, Y. Hatakeyama, S. *Org Lett.* **2003**, *5*, 3103.
117. Papageorgiou, CD.; Cubillo de Dios, MA.; Ley, SV.; Gaunt, MJ. *Angew Chem Int Ed.* **2004**, *43*, 4641.
118. Kobbelgaard, S.; Brandes, S.; Jørgensen, KA. *Chem.-Eur. J.* **2008**, *14*, 1464.
119. Hiemstra, H.; Wynberg, H. *J. Am. Chem. Soc.* **1981**, *103*, 417.

120. (a) Fenniri, H.; Packiarajan, M.; Vidale, K. L.; Sherman, D. M.; Hallenga, K.; Wood, K. V.; Stowell, J. G. *J. Am. Chem. Soc.* **2001**, *123*, 3854–3855. (b) Kruse, P.; Johnson, E. R.; DiLabio, G. A.; Wolkow, R. A. *Nano Lett.* **2002**, *2*, 807–810. (c) Keinan, S.; Ratner, M. A.; Marks, T. J. *Chem. Phys. Lett.* **2004**, *392*, 291–296.
121. (a) Sheiko, S. S.; Sun, F. C.; Randall, A.; Shirvanyants, D.; Rubinstein, M.; Lee, H.; Matyjaszewski, K. *Nature* **2006**, *440*, 191–194. (b) DiLabio, G. A.; Piva, P. G.; Kruse, P.; Wolkow, R. A. *J. Am. Chem. Soc.* **2004**, *126*, 16048–16050.
122. Kollman, P. A. *Chem. Rev.* **1977**, *10*, 365–371.
123. Copeland, G. T.; Miller, S. J. *J. Am. Chem. Soc.* **2001**, *123*, 6496–6502.
124. Knowles, R. R.; Jacobsen, E. N. *Proc. Natl. Acad. Sci. U. S. A.* **2010**, *107*, 20678–20685.
125. Krenske, E. H.; Houk, K. N. *Acc. Chem. Res.* **2013**, *46*, 979–989.
126. Wagner, J. P.; Schreiner, P. R. *Angew. Chem., Int. Ed.* **2015**, *54*, 12274–12296.
127. Grimme, S. *Mol. Sci.* **2011**, *1*, 211–22.
128. Ehrlich, S.; Moellmann, J.; Grimme, S. *Acc. Chem. Res.* **2013**, *46*, 916–926.
129. Zhao, Y.; Truhlar, D. G. *Acc. Chem. Res.* **2008**, *41*, 157–167.

Chapter 2
**History and Fundamentals of Computational
Chemistry**

Chapter 2

History and Fundamentals of Computational Chemistry

Abstract: Density functional theory (DFT) as a tool has been exploited for investigating problems of interest in this thesis. The development and fundamental aspects of DFT have been briefly covered in this chapter. The DFT methods provide a means to computing energy and other attributes of atomic and molecular systems as a function of electron density, which is a physical observable that has direct implications for chemical and physical behaviour. For stationary point computations of ground state geometries, these approaches operate well under the Born-Oppenheimer approximation and provide an accurate and computationally less expensive alternative to wave function based methods. Due to their enormous scalability, they are practical for calculating attributes of actual (rather than model) molecular systems.



2.1 Introduction to Computational Chemistry

Computational chemistry entails employing a set of algorithms created over years of hard labour and research by science's forefathers to investigate chemical issues on a computer. It may be used to address issues in a variety of fields, including molecular geometries, molecule energies and transition states, chemical reactivity, interpreting IR, UV, and NMR spectra, substrate interaction with enzymes, and substrate physical characteristics. Computational chemistry entails the use of five distinct approaches to investigate various problems of chemical interest. (a) *Molecular Mechanics (MM)* is based on a collection of balls held together by springs. Molecular mechanics calculations are extremely quick and can be utilised to optimise huge molecules. (b) *Ab initio calculations* are based on solving the Schrodinger Equation. This approach solves the Schrodinger Equation for a molecule and returns the energy and wave function of the molecule. This procedure is computationally expensive. (c) *Semi-empirical (SE) calculations* is also based on the Schrodinger Equation and gives us the wave function of a molecule. The main distinction between the SE approach and the *ab initio* method is that it improves the findings using empirical data (taken from experimental outcomes). SE calculations are slower than MM, but faster than *ab initio* methods. (d) *Density functional* calculations, often called density functional theory (DFT), is based on the Schrodinger Equation, which derives the electron distribution directly. *DFT* is usually faster than *ab initio* calculations, but slower than SE. (e) *Molecular dynamics (MD)* is based on the laws of motion to molecules. It is used to study the structure of proteins, macromolecules and in drug design.

2.2 Quantum Mechanics and the Wave Function

Classical mechanics has looked into the models used to represent macroscopic systems. The laws controlling microscopic and macroscopic systems should be distinct, according to early chemists and physicists. Max Planck postulated in 1900 that blackbody radiation generated by minuscule particles had discrete or quantized values. It was discovered around the turn of the 20th century that quantization was not just a property of light, but also of the basic particles that make up matter. The ultraviolet and visible line spectra also revealed that bound electrons in atoms are constrained to distinct energy levels. However, in Newtonian mechanics, energy can only fluctuate continuously in classical mechanics. A distinct mechanics was then required to describe tiny systems. Surprisingly, matter may be proved to have wavelike qualities, as de Broglie initially hypothesised. It does, however, have particle-like qualities, and a new science, quantum mechanics, was invented to account for this paradox.

The fundamental premise of quantum mechanics is that a wave function Ψ exists for each chemical system, and that suitable operators or functions acting on Ψ yield the system's observable characteristics. In mathematical notation, it is represented as $\mathfrak{O}\Psi = e\Psi$ where \mathfrak{O} is an operator and e is a scalar value for some property of the system. Ψ is an eigenfunction and e is an eigenvalue. Importantly, the product of the wave function Ψ with its complex conjugate (i.e., $|\Psi|^2$) has units of probability density. The likelihood that a chemical system will be located inside some region of multi-dimensional space is equal to the integral for a real wave function of $|\Psi|^2$ over that region of space. For a bound particle, the normalized integral of $|\Psi|^2$ over all space must be unity such that Ψ must be continuous and single-valued.

2.2.1 Schrodinger Equation and Hamiltonian Operator

The energy of the wave function is given by an operator known as the Hamiltonian operator and is given by

$$\hat{H}\Psi = E\Psi \quad (2.1)$$

Equation (2.1) is the Schrodinger Equation (SE), where \hat{H} is the Hamiltonian operator and E is eigenvalue, which is actually the average energy of the system. The Hamiltonian operator takes into account five contributions to the total energy of a system: the kinetic energies of the electrons and nuclei, the attraction of the electrons to the nuclei, and the interelectronic and internuclear repulsions. The Hamiltonian operator can be written as:

$$\hat{H}\Psi(x_1, x_2, x_3, \dots, x_n, r_1, r_2, r_3, \dots, r_m) = E\Psi(x_1, x_2, x_3, \dots, x_n, r_1, r_2, r_3, \dots, r_m) \quad (2.2)$$

where $\hat{H}(x_n, r_m)$ denotes the molecular Hamiltonian operator, and x_n and r_m are the coordinates of respective electrons and nuclei, $\Psi(x_n, r_m)$ is a many particle wave function for a given system and is a function of the $3n$ space coordinates and n spin coordinates of electrons and $3m$ space coordinates of nuclei, and E is the total energy of the system. The wave function $\Psi(x_n, r_m)$ has to fulfill certain requirements, which defines $\Psi(x_n, r_m)$ to be well behaved, in order to be allowed for quantum chemical consideration.

The Hamiltonian operator in atomic unit is represented as,

$$\hat{H} = -\frac{1}{2} \sum_{i=1}^n \nabla_i^2 - \frac{1}{2} \sum_{a=1}^m \frac{\nabla_a^2}{m_a} - \sum_{a=1}^m \sum_{i=1}^n \frac{Z_a}{r_{ia}} + \sum_a \sum_{b>a}^m \frac{Z_a Z_b}{r_{ab}} + \sum_{i=1}^n \sum_{j>i}^n \frac{1}{r_{ij}} \quad (2.3)$$

The kinetic energy of electrons and nuclei are represented by the first two variables in the Hamiltonian. The nuclear-electron attraction, nuclear-nuclear repulsion, and electron-electron repulsion are the final three terms, respectively. Indices i and j indicate a total number of n electrons, whereas indices a and b denote a total of the m nuclei of the system. Other associated terms in the Equation have their usual meaning.

To apply QM theory to address real life chemical problems, we need to solve the SE for multi-electron multi-nuclear molecular systems. However, the exact solution to the SE is limited to only few simplistic ideal cases, such as a particle in a box, the harmonic oscillator, the rigid rotor and the hydrogen atom. Hence, to make

this theory applicable to larger systems, approximate methods have been proposed over the years. The first approximation that comes into consideration is the Born-Oppenheimer approximation, which is believed to be a good approximation for stationary point calculations.

2.2.2 The Born-Oppenheimer Approximation

The fact that nuclei are substantially heavier than electrons is self-evident. As a result, nuclei move significantly slower than electrons. As a result, we may assume that all electrons exist in a field of fixed nuclei. As a result, the nuclear kinetic energy can be set to zero, but the nuclear potential energy remains constant. This is known as the *Born-Oppenheimer approximation*. The Born-Oppenheimer approximation allows the electronic and nuclear components of the SE to be separated. Ultimately, the Hamiltonian shown in Equation (2.2) can be simplified to only the electronic part \hat{H}_{el} as,

$$\hat{H}_{el} = -\frac{1}{2} \sum_{i=1}^n \nabla_i^2 - \sum_{a=1}^m \sum_{i=1}^n \frac{Z_a}{r_{ia}} + \sum_{i=1}^n \sum_{j>i}^n \frac{1}{r_{ij}} = \hat{T} + \hat{V}_{ne} + \hat{V}_{ee} \quad (2.4)$$

The solution of the Schrödinger Equation with the electronic Hamiltonian \hat{H}_{el} yields the electronic energy E_{el} when \hat{H}_{el} is operated on the electronic wave function Ψ_{el} ,

$$\hat{H}_{el} \Psi_{el} = E_{el} \Psi_{el} \quad (2.5)$$

The total energy can be obtained as the sum of the electronic energy and the nuclear repulsion energy E_{nn} as follows:

$$E_{tot} = E_{el} + E_{nn} \quad (2.6)$$

Where E_{nn} is given by,

$$E_{nn} = \sum_a^m \sum_{b>a}^m \frac{Z_a Z_b}{r_{ab}} \quad (2.7)$$

2.2.3 Wave Function, Probability and Normalization

In the previous section, we saw how the energy may be derived by using a Hamiltonian \hat{H} on $\Psi(x_n, r_m)$. I will offer a basic description of the wave function in this section $\Psi(x_n, r_m)$. The Copenhagen interpretation provided the basis for the wave function definition. A wave function, according to this definition, is a function that includes all information of a particular system for the state represented by the wave function, and all information of that system for this state can be retrieved from the wave function using appropriate operators. However, because the wave function is not a physical observable, it has no physical meaning. It only returns the value of an observable when it is processed with an operator with classical mechanics roots. The physical interpretation of a wave function comes instead with the square of the $\Psi(x_n, r_m)$, which gives the probability density

$$\text{probability density} = |\Psi(x_1, x_2, \dots, x_n)|^2 \quad (2.8)$$

The probability density, on the other hand, cannot take on complex or negative values, whereas the wavefunction $\Psi(x_n, r_m)$ can. The following Equation can be used to calculate the chance of finding electrons in a given volume element:

$$|\Psi(x_1, x_2, \dots, x_n)|^2 dx_1 dx_2 \dots dx_n \quad (2.9)$$

Equation (2.9) represents the probability that electrons $1, 2, \dots, n$ are found simultaneously in volume $dx_1 dx_2 \dots dx_n$. Because electrons are indistinguishable, if two electrons swap places, the probability density remains constant,

$$|\Psi(x_1, x_2, \dots, x_i, x_j, \dots, x_n)|^2 = |\Psi(x_1, x_2, \dots, x_j, x_i, \dots, x_n)|^2 \quad (2.10)$$

However, electrons are fermions with spin $s=1/2$. Ψ According to the quantum mechanical version of Pauli's exclusion principle, it must be antisymmetric with regard to the exchange of the spatial and spin coordinates of any two electrons. ('no two electrons can occupy the same state').

$$\Psi(x_1, x_2, \dots, x_i, x_j, \dots, x_n) = -\Psi(x_1, x_2, \dots, x_j, x_i, \dots, x_n) \quad (2.11)$$

In addition, the chance of detecting n electrons in all of space should be one. Hence, the integral of Equation (2.9) over the entire space should be equal to 1.

$$\int \dots \int |\Psi(x_1, x_2, \dots, x_n)|^2 dx_1 dx_2 \dots dx_n = 1 \quad (2.12)$$

A normalised wave function is a wave function that meets this requirement.

2.2.4 The Variational Principle

We need the Hamiltonian operator to solve Equation 2.1 for any given molecule, and we must identify the eigenfunctions and accompanying eigenvalues for the Hamiltonian operator. However, there is no accurate solution to the Schrödinger Equation for this seemingly simple situation. The guess wave function may be used to solve this problem, since the variational principle states: ‘*The energy calculated using a guess wave function ψ is always an upper bound to the original ground state energy (E_0) of the system of interest*’

$$E[\psi] = \frac{\langle \Psi | \hat{H} | \Psi \rangle}{\langle \Psi | \Psi \rangle} \geq E_0 = \frac{\langle \Psi_0 | \hat{H} | \Psi_0 \rangle}{\langle \Psi_0 | \Psi_0 \rangle} \quad (2.13)$$

Here,

$$E[\psi] = \frac{\langle \Psi | \hat{H} | \Psi \rangle}{\langle \Psi | \Psi \rangle} \quad (2.14)$$

is called as the expectation value.

Here, Ψ_0 is true ground state wave function. A full minimization of the given functional $E[\Psi]$ with respect to all of the allowed n-electronic wave functions, under the Born-Oppenheimer approximation, will provide the true ground state Ψ_0 and the corresponding energy $E[\Psi] = E_0$. What “allowed” means in the present context is that the trial wave functions must follow certain criteria that ensure that these functions make physical sense. For instance, to be qualified as a wave function, Ψ

must be continuous everywhere and be square integrable. Otherwise, the normalization of Equation (2.13) would not be possible. This can be expressed as,

$$E_0 = \min_{\Psi \rightarrow n} E[\Psi] = \min_{\Psi \rightarrow n} \langle \Psi | \hat{T} + \hat{V}_{ne} + \hat{V}_{ee} | \Psi \rangle \quad (2.15)$$

where $\Psi \rightarrow n$ indicates that Ψ is an acceptable n-electron wave function. It is important to highlight, however, that a comprehensive search of all permitted functions is almost impossible. The variational principle, on the other hand, may be applied to subsets of all allowable functions. One alternative solution is to choose these subsets so that the minimization in Equation (2.15) can be performed using an algebraic technique, resulting in the best approximation to the precise wave function that can be achieved from that subset. The Hartree-Fock approximation is a good illustration of this strategy.

Furthermore, an antisymmetrized product of n numbers of orthonormal spin orbitals is $\chi_i(\mathbf{x})$, commonly used to describe the ground state n-electronic wave function, each of which is a product of spatial orbitals $\phi_i(\mathbf{x})$ and the spin functions $\sigma(s) = \alpha(s)$ or $\beta(s)$. The resulting formulation is called as the *Slater Determinant* and is expressed as

$$\Psi_0(\mathbf{x}_1, \mathbf{x}_2, \mathbf{x}_3, \dots, \mathbf{x}_n) = \frac{1}{\sqrt{n!}} \begin{vmatrix} \chi_1(\mathbf{x}_1) \chi_2(\mathbf{x}_1) \chi_3(\mathbf{x}_1) \dots \chi_n(\mathbf{x}_1) \\ \chi_1(\mathbf{x}_2) \chi_2(\mathbf{x}_2) \chi_3(\mathbf{x}_2) \dots \chi_n(\mathbf{x}_2) \\ \chi_1(\mathbf{x}_3) \chi_2(\mathbf{x}_3) \chi_3(\mathbf{x}_3) \dots \chi_n(\mathbf{x}_3) \\ \dots\dots\dots \\ \chi_1(\mathbf{x}_n) \chi_2(\mathbf{x}_n) \chi_3(\mathbf{x}_n) \dots \chi_n(\mathbf{x}_n) \end{vmatrix} \quad (2.16)$$

2.2.5 Functional

Before diving into the specifics of DFT, let us have a look at the definition of functional. A functional is a higher-order function. It is defined as a function of another function, i.e., a functional is a function whose argument itself is a function. A functional is commonly represented with the function in square brackets: $F[f] = a$.

For example, the integration of $|f|^2$ over all space, with each square integrable function $f(x)$, is a functional.

$$F[f] = \int_{-\infty}^{+\infty} f^*(x)f(x)dx \quad (2.17)$$

The total energy functional may alternatively be regarded the mathematical representation of the expectation value provided in Equation (2.14) ($E[\Psi]$) of Ψ as it takes the function Ψ as input and provides the value of energy, a number, for that particular state.

A functional may be distinguished from a function by noting the following distinction: a function takes a number as input and also produces a number as output, whereas a functional takes a function as input and produces a number as output. Functionals have qualities that are quite similar to functions. A functional, like a function, can have derivatives. The formulation is similar to the derivatives of functions. The differentiation of a functional $F[g]$ is defined as,

$$\delta F[g] = F[g + \delta x] - F[g] = \int \frac{\partial F}{\partial g(x)} \delta g(x).dx \quad (2.18)$$

The rules of differentiation are also similar to the functions,

$$\frac{\partial}{\partial f(x)} (c_1 F_1 + c_2 F_2) = c_1 \frac{\partial F_1}{\partial f(x)} + c_2 \frac{\partial F_2}{\partial f(x)} \quad (2.19)$$

$$\frac{\partial}{\partial f(x)} (F_1 \cdot F_2) = \frac{\partial F_1}{\partial f(x)} F_2 + \frac{\partial F_2}{\partial f(x)} F_1 \quad (2.20)$$

2.3 The Fundamentals of Density Functional Theory

The wave function is used as an input to compute the energy and other parameters of the system in traditional quantum mechanical methods that propose solutions to the SE. However, these approaches were shown to be extremely costly, prompting theoretical chemists to seek out alternative ways that are both accurate and

computationally efficient. Density functional theory (DFT) has emerged as the best alternative to wave function dependent approaches in terms of accuracy and efficacy. By using electron density as the basic parameter, DFT gives an alternate method for determining a system's attributes. To put it another way, the DFT makes use of the electron density as a fundamental variable that can be used to predict chemical and physical characteristics of any system. Using electron density as the primary parameter to calculate features of quantum mechanical systems has long piqued the interest of theoretical chemists due to the following benefits it offers over the wave function: (i) the electron density of a quantum mechanical system, unlike the wave function, is an empirically quantifiable quantity and (ii) the electron density is only affected by three spatial coordinates, but the wave function of a system with n particles is affected by $4n$ variables: $3n$ for coordinates and n for spin. When it comes to computational time and resources, density-based methods are expected to be more cost-effective than wave function-based methods, which is what has been achieved in recent developments with the help of smart and robust algorithms that have been implemented in many quantum chemical packages. As a result, DFT may now be used to compute a wide range of characteristics for a wide range of systems. We shall offer a quick introduction to density functional theory in the subsections that follow.

2.3.1 The Electron Density

We learned in Section 2.3 that DFT postulates using the electron density as a fundamental parameter to acquire all the important features of a quantum chemical system. The theoretical formulation of the electron density, a component on which the whole DFT recipe is built, has been discussed in this section. The likelihood of finding one electron of any spin within a certain volume element while the rest of the electrons are scattered throughout space is known as the electron density. The electron density is a physically observable quantity that may be determined by X-ray diffraction, transmission electron microscopy (TEM), scanning tunnelling microscopy (STM), and atomic force microscopy (AFM). The physical explanation of Equation (2.9) leads straight to the electron density in theory $\rho(\vec{r})$. The overall electron density of an n -electronic system may be expressed mathematically as the following multiple

integral of the modulus square of the wave function over all of the electrons' spin coordinates (s) and all but one of the spatial coordinates ($\overset{\perp}{r}$),

$$\rho(\overset{\perp}{r}) = n \int \dots \int |\Psi(\overset{\perp}{x}_1, \overset{\perp}{x}_2, \dots, \overset{\perp}{x}_n)|^2 ds_1 d\overset{\perp}{x}_2 \dots d\overset{\perp}{x}_n \quad (2.21)$$

Here $\overset{\perp}{x} = \overset{\perp}{r}.s$, and $\rho(\overset{\perp}{r})$ is the probability of finding any of the n electrons in the volume element $d\overset{\perp}{r}_1$ but with arbitrary spin. The rest of the n-1 electrons will have arbitrary positions and spins in the state represented by Ψ . Strictly speaking, $\rho(\overset{\perp}{r})$ represents the probability density, but calling it the electron density is a common practice. The multiple integral represents the probability of finding one particular electron in the volume element $d\overset{\perp}{r}_1$ (here, $\overset{\perp}{x}_1 = \overset{\perp}{r}_1.s_1$). However, since electrons are indistinguishable, the probability of finding any electron out of total n at this position is just n times the probability of finding one particular electron. $\rho(\overset{\perp}{r})$ follow some specific properties, which have been described below,

1. $\rho(\overset{\perp}{r})$ is a non-negative function of the three spatial variables, which integrates to the total number of electrons and vanishes at infinity,

$$\rho(\overset{\perp}{r}) \geq 0 \quad (2.22)$$

$$\int \rho(\overset{\perp}{r}) d\overset{\perp}{r}_1 = n \quad (2.23)$$

$$\rho(\overset{\perp}{r} \rightarrow \infty) = 0 \quad (2.24)$$

2. $\rho(\overset{\perp}{r})$ exhibits a maximum possessing a finite value at a given position of the atom due to the attractive force exerted by the positive nuclei. At this position, the gradient of density exhibits a discontinuity resulting in a *cusp* because of the singularity in the $-\frac{Z_a}{r_{ia}}$ part in the Hamiltonian (Equation (2.2)), as $r_{ia} \rightarrow 0$ at this position. The properties of the cusp are intimately related to the nuclear charge of the atom,

$$\lim_{r_a \rightarrow 0} \left[\frac{\partial}{\partial r} + 2Z_a \right] \bar{\rho}(\mathbf{r}) = 0 \quad (2.25)$$

where Z_a is the nuclear charge and $\bar{\rho}(\mathbf{r})$ is the spherical average of $\rho(\mathbf{r})$.

3. $\rho(\mathbf{r})$ shows an asymptotic exponential decay for large distances from the nuclei for any system,

$$\rho(\mathbf{r}) \propto \exp[-2\sqrt{2I} |\mathbf{r}|] \quad (2.26)$$

where I is the exact first ionization energy of the system.

2.3.2 The Pair Density

The pair density is the chance of discovering a pair of electrons with spins σ_1 and σ_2 in two separate volume elements $d\mathbf{r}_1$ and $d\mathbf{r}_2$ at the same time while the other $n-2$ electrons have arbitrary positions and spins. It is given as,

$$\rho(\mathbf{x}_1, \mathbf{x}_2) = n(n-1) \int \dots \int |\Psi(\mathbf{x}_1, \mathbf{x}_2, \dots, \mathbf{x}_n)|^2 d\mathbf{x}_3 \dots d\mathbf{x}_n \quad (2.27)$$

The pair density, like the electron density, is a positive value that is normalised to the total number of non-distinct electron pairs, *i.e.*, $n(n-1)^*$. In terms of coordinates, it is symmetric. Because it contains all information concerning electron correlation, the pair density is extremely important.

2.3.3 The Thomas-Fermi Model

Although contemporary DFT was only developed a few decades ago, the first effort to use electron density to gather information about atomic and molecular systems may be traced back to the early days of quantum chemistry, right after the Schrödinger Equation was introduced (1926). Llewellyn Thomas (1927) and Enrico Fermi proposed the first approximation of this type (1927). They replaced the wave function with electron density to better comprehend the electrical structure of many-body systems. The Thomas–Fermi (TF) model is the name given to this paradigm.⁴⁻⁶ In this quantum statistical model, Thomas and Fermi used the concept of a uniform electron

gas with a constant electron density. They went on to define the term "kinetic energy" for a quantum mechanical system. The following functional Equations can be used to find the kinetic energy expression in the TF model:

$$T_{TF}[\rho(\mathbf{r})] = \frac{3}{10}(3\pi^2)^{2/3} \int \rho^{5/3}(\mathbf{r}) d\mathbf{r} \quad (2.28)$$

According to this model, all additional electronic contributions owing to nuclear-electron attraction and electron-electron repulsion are addressed totally classically. As a result, the total energy may be expressed as:

*It is also common to use a different normalization coefficient $n(n-1)/2$, which corresponds to the distinct number of pairs of electrons.

$$E_{TF}[\rho(\mathbf{r})] = \frac{3}{10}(3\pi^2)^{2/3} \int \rho^{5/3}(\mathbf{r}) d\mathbf{r} - Z \int \frac{\rho(\mathbf{r})}{r} d\mathbf{r} + \frac{1}{2} \iint \frac{\rho(\mathbf{r}_1)\rho(\mathbf{r}_2)}{r_{12}} d\mathbf{r}_1 d\mathbf{r}_2 \quad (2.29)$$

The following are the limitations of this model. Because the electrons in this model are assumed to be part of a gas with a constant electron density, it yields a very imprecise approximation of the system's real kinetic energy. Furthermore, the impacts of exchange and correlation are completely overlooked. When the TF model for molecular systems is implemented, it is discovered that the model is unable to express the presence of a chemical bond. As a result, the TF model performs poorly when it comes to representing actual molecular systems. The true significance of the TF model, however, lies not in its correctness, but in the fact that it was the first prescription for depicting energy using only the electron density and no other information. It should be noted that the wave function was not used in this model.

The next step is to determine and identify the right density now that we have a functional that expresses energy solely in terms of electron density. Thomas and Fermi used the variational principle to determine the right density to utilise in Equation (2.27). They assumed that the system's ground state is proportional to its density, and that the expression of total energy is reduced under the following constraint $\int \rho(\mathbf{r}) d\mathbf{r} = n$. However, it was uncertain at the time whether describing a system's total energy in terms of density was physically warranted, or whether an

approach based on the variational principle on density was philosophically acceptable in this context. As a result, this paradigm is based more on intuition than on scientific evidence. As a result, this model is regarded a restricted model, and the TF technique has only historical value rather than any practical meaning in the current scenario.

2.3.4 Hohenberg-Kohn (HK) Theorems

Hohenberg and Kohn published a seminal work in Physical Review in 1964 that gave birth to the density functional theory we know and use today.⁷ They offered two easy proofs for two key theorems about the electron density of the system. These two theorems not only answer questions about the rationale of the approximations employed in the Thomas Fermi model, but they also lay the theoretical groundwork for rigorously constructing DFT in the ground state. These theorems are, in fact, the theoretical foundations upon which all current density functional theories are built. The two theorems are as follows: (1) every observable of a stationary quantum mechanical system, including energy, can be calculated, in principle exactly, from the ground state density alone, and (2) the ground state density can be calculated, in principle exactly, using the variational method involving only the density.⁴⁻⁵ It is worth noting that the HK theorems were originally designed for time-independent stationary ground states, but they were eventually extended to excited states and time-dependent systems as well.⁸⁻⁹ The details of the two HK theorems and their proof have been provided below.

Theorem 1 *‘The external potential $\hat{V}_{ext}(\mathbf{r})$ is (to within a constant) a unique functional of $\rho(\mathbf{r})$; since, in turn $\hat{V}_{ext}(\mathbf{r})$ fixes \hat{H} we see that the full many particle ground state is a unique functional of $\rho(\mathbf{r})$.*

In order to prove the validity of the first theorem, Hohenberg and Kohn contrived some legitimate assumptions based on the fundamental principles of quantum chemistry, which are as follows: under the Born-Oppenheimer approximation, the ground state of an electronic system is a direct consequence of the potential exerted by the nuclei. They called the potential exerted by nuclei as the *external potential*, \hat{V}_{ext}

. This assumption can further be clarified by analyzing the expression of the electronic Hamiltonian (\hat{H}_e) of Equation (2.3), which has been derived under the Born-Oppenheimer approximation. In Equation (2.3), the kinetic energy of electrons (\hat{T}_e) and the electron-electron repulsion term (\hat{V}_{ee}) simply adjust themselves to the external potential (which is represented as \hat{V}_{ne} in Equation (2.3)) so that the net energy of the system is minimized. Thus, for a specific value of \hat{V}_{ext} , every other variable of the system, including the electron density, accommodate themselves to provide the lowest possible ground state energy of the electronic system. Thus, one can consider \hat{V}_{ext} as the only variable term in the electronic Hamiltonian - the other parameters ultimately rely on it.

Based on the aforesaid assumption, Hohenberg and Kohn asked some very fundamental questions: "could the parameter \hat{V}_{ext} be uniquely determined just from the knowledge of electron density $\rho(\vec{r})$ alone? Is it possible (at least in principle) to get the information about the position and type of the nuclei if we accurately know the density $\rho(\vec{r})$ of the ground state? Does there exist a precise path for mapping from the density ($\rho(\vec{r})$) to the external potential (\hat{V}_{ext})?" The answers to all of the abovementioned questions were found to be positive. Essentially, the mapping of \hat{V}_{ext} from $\rho(\vec{r})$ has been observed to be accurate within the limit of a constant, which is not a big concern as it is well known that the SE with two different Hamiltonian of \hat{H}_e and $\hat{H}_e + const$ provides precisely the same eigenstates. The only thing that will vary in this case is the value of the energy, which will be shifted by the value of this constant. Thus, if this is true, the knowledge of only the density is enough to get complete information about the system. As $\rho(\vec{r})$ yields the total number of electrons, $n = \int \rho(\vec{r}) d\vec{r}$, as well determining the \hat{V}_{ext} , it is logical to conclude that the knowledge of $\rho(\vec{r})$ is an adequate substitute to the knowledge of Ψ , the wave function of the system.

The proof of Theorem 1 that has been provided by Hohenberg and Kohn is disarmingly simple and is based on the *reduction absurdum* principle. The proof runs as follows:

Let us consider that $\rho(\vec{r})$ represents the exact ground state density of a non-degenerate system* of n electrons and that Ψ is the wave function of the ground state. Let us also suppose that for this particular density $\rho(\vec{r})$, there exist two possible external potentials \hat{V}_{ext} and \hat{V}'_{ext} which differ with each other by more than a constant, since the wavefunction, and if just a constant is added to the potential, the electron density stays unchanged. Then, these two different external potentials will certainly correspond to two separate electronic Hamiltonian operators (\hat{H} and \hat{H}') and the two Hamiltonians \hat{H} and \hat{H}' belong to two different ground state wave functions, Ψ and Ψ' respectively.

*It is worth noting that later investigations have proven that HK theorems can easily be extended for degenerate ground states as well.¹⁰

ground state energies corresponding to the two wave functions are E_0 and E'_0 respectively, where $E_0 = \langle \Psi | \hat{H} | \Psi \rangle$, $E'_0 = \langle \Psi' | \hat{H}' | \Psi' \rangle$ and $E_0 \neq E'_0$.

$$\hat{H} = \hat{T} + \hat{V}_{ee} + \hat{V}_{ext} \quad (2.30)$$

$$\hat{H}' = \hat{T} + \hat{V}_{ee} + \hat{V}'_{ext} \quad (2.31)$$

Because both wave functions produce the same electron density (which is conceivable given that the charge density derived from a wave function by quadrature using Equation 2.22 is not unique), the complete scenario may be depicted graphically as

$$V_{ext} \Rightarrow \hat{H} \Rightarrow \Psi \Rightarrow \rho(\vec{r}) \Leftarrow \Psi' \Leftarrow \hat{H}' \Leftarrow V'_{ext}$$

If we apply the variational principle on the expectation value of energy for the Ψ' with the Hamiltonian \hat{H} ,

$$E_0 < \langle \Psi'_0 | \hat{H} | \Psi'_0 \rangle = \langle \Psi'_0 | \hat{H}' | \Psi'_0 \rangle + \langle \Psi'_0 | \hat{H} - \hat{H}' | \Psi'_0 \rangle \quad (2.32)$$

Putting the values of \hat{H} and \hat{H}' from Equations (2.30) and (2.31) into the Equation (2.32),

$$E_0 < E'_0 + \langle \Psi' | \hat{T} + \hat{V}_{ee} + \hat{V}_{ext} - \hat{T} - \hat{V}_{ee} - \hat{V}'_{ext} | \Psi' \rangle = E'_0 + \int \rho(r) \{ \hat{V}_{ext} - \hat{V}'_{ext} \} dr \quad (2.33)$$

Similarly, applying the variational principle on the expectation value of energy for the Ψ with the Hamiltonian \hat{H}' yields,

$$E'_0 < \langle \Psi | \hat{H}' | \Psi \rangle = \langle \Psi | \hat{H} | \Psi \rangle + \langle \Psi | \hat{H}' - \hat{H} | \Psi \rangle = E_0 - \int \rho(r) \{ \hat{V}_{ext} - \hat{V}'_{ext} \} dr$$

(2.34) Adding Equations (2.33) and (2.34) leads us to a contradictory result,

$$E_0 + E'_0 < E'_0 + E_0 \quad \text{or} \quad 0 < 0 \quad (2.35)$$

It is therefore proved that there cannot be two different \hat{V}_{ext} that give rise to the same ground state density. Thus, the ground state density $\rho(\vec{r})$ uniquely determines the external potential \hat{V}_{ext} . Using again the concept of the variational principle, we can further state that all the properties of the ground state, including the kinetic energy of electrons ($T[\rho]$) and the energy of electron interactions ($E_{ee}[\rho]$) can be uniquely determined by the ground state density. Thus, the total ground state energy of the system can be represented as simply a functional of density alone,

$$E[\rho] = E_n[\rho] + T[\rho] + E_{ee}[\rho] = \int \rho(\vec{r}) \hat{V}_{ne}(\vec{r}) d\vec{r} + T[\rho] + E_{ee}[\rho] \quad (2.36)$$

Here, $E_{ne}[\rho] = \int \rho(\vec{r}) \hat{V}_{ne}(\vec{r}) d\vec{r}$ (the potential energy due to nuclei-electron attraction) is the system dependent term whereas $T[\rho] + E_{ee}[\rho]$ depends only on electron density and is universal, *i.e.*, its mathematical form does not depend on the type of system (*i.e.*, on the n , R and Z of the system). Here, we have retained the subscript

‘ne’ to highlight the fact that the type of external potential in this case is the electron and nuclear attraction. Now, we can further group together the functionals that are just responses (the system independent part) and can be considered secondary as compared to the $E_{ne}[\rho]$,

$$F_{HK}[\rho] = T[\rho] + E_{ee}[\rho] \quad (2.37)$$

The system independent part $F_{HK}[\rho]$ is called the *Hohenberg-Kohn functional*. Now the total energy functional can be written as

$$E[\rho] = \int \rho(\mathbf{r}) \hat{V}_{ne}(\mathbf{r}) d\mathbf{r} + F_{HK}[\rho] \quad (2.38)$$

This, simple-looking (at first glance) $F_{HK}[\rho]$ functional is the most challenging term used in DFT. We could have solved the E perfectly if we knew the explicit form of both of the terms involved. And, because it is totally system agnostic, it may be applied to any system, from the hydrogen atom to massive molecules. The exact forms of these names, however, are uncertain. Further investigation reveals that the electron-electron interaction term's $E_{ee}[\rho]$, second term $F_{HK}[\rho]$ incorporates exchange, Coulomb, and self interaction correction components. Thus, it can be separated into two parts: the classical Coulomb part ($J[\rho]$, the explicit expression for which is known) and the non-classical contribution ($E_{nc}[\rho]$, containing the Coulomb correlation, exchange and self interaction correction terms). Thus,

$$E_{ee}[\rho] = J(\rho) + E_{nc}(\rho) = \frac{1}{2} \iint \frac{\rho(\mathbf{r}_1)\rho(\mathbf{r}_2)}{r_{12}} d\mathbf{r}_1 d\mathbf{r}_2 + E_{nc}(\rho) \quad (2.39)$$

The total energy functional now will be

$$E[\rho] = \int \rho(\mathbf{r}) \hat{V}_{ne}(\mathbf{r}) d\mathbf{r} + \frac{1}{2} \iint \frac{\rho(\mathbf{r}_1)\rho(\mathbf{r}_2)}{r_{12}} d\mathbf{r}_1 d\mathbf{r}_2 + E_{nc}(\rho) + T[\rho] \quad (2.40)$$

There are two terms here whose mathematical forms are unknown: $E_{nc}(\rho)$ and $T[\rho]$. In the next section, we will show how the major part of the $T[\rho]$ can be obtained by the Kohn-Sham (KS) approach.

We have seen that the argument of the first HK theorem demonstrates that the ground state density is adequate to estimate all characteristics of interest in theory. It does not, however, tell us how to know if the density we choose is the proper ground density for the system. In terms of the variational concept described previously in Section 2.2.4 of this chapter, the second HK theorem provides a formal prescription for this.

Theorem 2 $F_{HK}[\rho]$, the functional that delivers the ground state energy of the system delivers the lowest energy if and only if the input density is the true ground state density, ρ .

This theorem can be expressed as,

$$E_0 \leq E[\rho'] = T[\rho'] + E_{ne}[\rho'] + E_{ee}[\rho'] \quad (2.41)$$

Thus, for any chosen trial density ρ' -which satisfies the necessary boundary conditions like, $\rho' \geq 0$ and $\int \rho'(r) dr = n$, and which corresponds to some external potential \hat{V}_{ext} - the obtained energy $E[\rho']$ (from functional given in Equation (2.32)) will be an upper bound to the exact ground state energy $E_0[\rho]$. $E[\rho']$ will only be equal to E_0 if and only if the true ground state density is inserted into Equation (2.35).

The proof of the inequality (2.37) is simple. Since it is known that any trial density ρ' defines its own Hamiltonian $\hat{H}^{\rho'}$ and hence its own wave function $\Psi^{\rho'}$, this wave function can be taken as the trial wave function for the Hamiltonian originated from the true external potential \hat{V}_{ext} . Therefore,

$$\langle \Psi^{\rho'} | \hat{H} | \Psi^{\rho'} \rangle = T[\rho'] + E_{ee}[\rho'] + \int \rho'(r) V_{ext}(r) dr = E[\rho'] \geq E_0[\rho] = \langle \Psi | \hat{H} | \Psi \rangle \quad (2.42)$$

which is what was desired.

Let us knock out a few more formal theoretical difficulties that should be fundamentally addressed in the current setting before moving on. The trial density ρ' must meet some preset parameters in order for the second HK theorem to be true, as we discussed in the preceding paragraph. The representability of density is a term used to describe these criteria. The first is known as the N-representability issue, which asserts that the ρ' entire number of electrons 'n' must be added up.^{4-5,11-13} When stemming from an antisymmetric wave function ρ' , this condition is simple to establish and automatically enforced. Because the wave function is theoretically relevant to practically all practical applications, all densities that occur in these applications essentially meet this criterion. The second condition is known as the \hat{V}_{ext} -representability (or simply as ν -representability) problem, which states that the trial density must be associated with some external potential \hat{V}_{ext} .^{4-5,14} This requirement is more difficult to satisfy than the N-representability one, because many of the available trial densities do not satisfy the HK theorem. Only densities mapped with an antisymmetrized wave function and a Hamilton operator with some form of symmetry are eligible for \hat{V}_{ext} . The difficulty then becomes how such densities can be identified. This is still an open question in DFT since no one knows which constraints a trial density must meet to be ν -representable. Levy (1982) and Lieb (1983) established that some appropriate trial densities cannot be mapped to any other density \hat{V}_{ext} .¹⁵⁻¹⁶ As a result, if one picks any of those densities, variational optimization will not be able to converge to any physically meaningful ground state. It is important to note that the second HK theorem is only true if we limit ourselves to N- and ν -representable trial densities. However, while this is a significant difficulty in theoretical DFT, it has relatively minimal practical implications. Furthermore, these constraints may be simplified to a considerably weaker requirement that the density must come from an antisymmetrized wave function with no explicit external potential (the N-representable condition).

2.3.5 The Kohn-Sham (KS) Approach

The Hohenberg-Kohn theorems allow us to create a rigorous many body theory utilising the electron density as the basic quantity, as explained in the preceding section. The atomic or molecular system's ground state energy may be represented using this paradigm.⁷

$$E_0[\rho] = \min_{\rho \rightarrow n} \left(\int \rho(\mathbf{r}) \hat{V}_{ne}(\mathbf{r}) d\mathbf{r} + F_{HK}[\rho] \right) \quad (2.43)$$

where $F_{HK}[\rho]$ is the universal functional, which is made up of kinetic energy, classical Coulomb, and non-classical contribution components, as illustrated below.,

$$F_{HK}[\rho] = T[\rho] + J(\rho) + E_{nc}(\rho) \quad (2.44)$$

Only is known among them. It is unclear what the exact explicit form of the other two are. Unfortunately, the precise representation of kinetic energy ($T[\rho]$), which is the largest contribution to total energy, is likewise unknown. Even the enlarged Thomas-Fermi model's ultimate formulation is undeveloped and not applicable to molecular systems. Then there is the matter of how to make the Hohenberg-Kohn theorems practical for actual molecular systems. In their second important work on modern DFT, published in 1965, Kohn and Sham suggested an approach to overcome this problem.¹⁷ Their main concept was to concentrate on determining the kinetic energy precisely. To make the problem easier to solve, realise that a system's kinetic energy can be simply estimated from a known wave function (as in the case of the Hartree Fock method). In the Hohenberg-Kohn formalism, Kohn and Sham introduced the concept of the non-interacting reference system (whose electron density is the same as the real interacting system of interest) built from a set of orbitals (one electron functions), which allows the major portion of the kinetic energy to be calculated precisely. A non-interacting system is a hypothetical system in which the electrons behave as uncharged fermions and so do not interact *via* Coulomb repulsion. The non-classical contributions, which are likewise unknown but generally modest, are combined with the remaining kinetic energy. This method computes as much

information as feasible precisely, allowing just a tiny percentage of the total energy to be decided by a functional approximation. Thus,

$$T_S = -\frac{1}{2} \sum_i^n \langle \psi_i | \nabla^2 | \psi_i \rangle \quad (2.45)$$

and

$$\rho_s(\mathbf{r}) = \sum_i^n \sum_s |\psi_i(\mathbf{r}, s)|^2 = \rho(\mathbf{r}) \quad (2.46)$$

where ψ_i and T_S are the reference system's wave function and kinetic energy. It is quite evident that $T_S \neq T$ even if it appears that both the interacting and non-interacting systems have the same electron density. However, it is expected that a major part of $T[\rho]$ is recovered via T_S . Kohn and Sham proposed the following division of the universal functional set to solve this problem $F_{HK}[\rho]$,

$$F_{HK}[\rho] = T_S[\rho] + J[\rho] + E_{XC}[\rho] \quad (2.47)$$

where $E_{XC}[\rho]$ is defined as the *exchange-correlation energy* and is given by

$$E_{XC}[\rho] = (T[\rho] - T_S[\rho]) + (E_{ee}[\rho] - J[\rho]) \quad (2.48)$$

This functional $E_{XC}[\rho]$ contains all the components of energy that are unknown and not accounted for: the electron exchange contribution, the electron correlation contribution (which is a major element of the energy for systems containing interacting electrons), the residual fraction of the kinetic energy (which is not included in the term), and the self-interaction correction (which originated from the classical Coulomb potential). In summary, this functional grouping contains all of the sources to total energy whose explicit forms are unknown and impossible to determine using theoretical approaches. Today, many superior and accurate approximations are available for this functional.

The question that is crucial to be asked at this juncture is how we would find the potential ($V_S(\vec{r})$) for the non-interacting reference system so that it leads to an anti-symmetrized wave function (the Slater determinant) that is associated with the exact same density as our real interacting system. To answer this, we will rewrite the energy of our system of interest in terms of the newly separated $F_{HK}[\rho]$,

$$E[\rho] = T_S[\rho] + J[\rho] + E_{EX}[\rho] + E_{ne}[\rho] \quad (2.49)$$

The further expansion of these terms will lead to

$$\begin{aligned} E[\rho] &= T_S[\rho] + \frac{1}{2} \iint \frac{\rho(\vec{r}_1)\rho(\vec{r}_2)}{r_{12}} d\vec{r}_1 d\vec{r}_2 + E_{EX}[\rho] + \int V_{ne}\rho(\vec{r})d\vec{r} \\ &= -\frac{1}{2} \sum_i^n \langle \psi_i | \nabla^2 | \psi_i \rangle + \frac{1}{2} \sum_i^n \sum_j^n \iint |\psi_i(\vec{r}_1)|^2 \frac{1}{r_{12}} |\psi_j(\vec{r}_2)|^2 d\vec{r}_1 d\vec{r}_2 + E_{EX}[\rho] - \sum_i^n \int \sum_a^m \frac{Z_a}{r_{1a}} |\psi_i(\vec{r}_1)|^2 d\vec{r}_1 \\ &\dots\dots\dots(2.51) \end{aligned}$$

The only unknown variable in Equation (2.45) is $E_{EX}[\rho]$. Now, if we apply the variational principle on Equation (2.45) to minimize the energy under the constraint:

$\langle \psi_i | \psi_j \rangle = \delta_{ij}$, we will obtain the *Kohn-Sham Equation*,

$$\begin{aligned} &\left(-\frac{1}{2} \nabla^2 + \left[\int \frac{\rho(\vec{r}_2)}{r_{12}} d\vec{r}_2 + V_{xc}(\vec{r}_1) - \sum_a^m \frac{Z_a}{r_{1a}} \right] \right) \psi_i \\ &= \left(-\frac{1}{2} \nabla^2 + V_{eff}(\vec{r}_1) \right) \psi_i = \varepsilon_i \psi_i \end{aligned} \quad (2.52)$$

The eigenvalue Equation of the Hartree-Fock (HF) technique is remarkably close to the resultant Equation. The Fock operator of the HF technique, on the other hand, contains the non-local potential that varies for each electron, but the Kohn-Sham operator V_{eff} potential depends only on \vec{r} (and is referred to as the local potential) and not on the index of the electrons, and hence it is equal for all electrons. When we compare this Equation to the non-interacting reference system's one-particle Equations, we get the result for V_S , which is nothing but V_{eff} .

$$V_s(\mathbf{r}) = V_{eff}(\mathbf{r}) = \int \frac{\rho(\mathbf{r}_2)}{r_{12}} d\mathbf{r}_2 + V_{xc}(\mathbf{r}_1) - \sum_a^m \frac{Z_a}{r_{1a}} \quad (2.53)$$

ψ_i in Equation (2.46) is called the *Kohn-Sham orbital* (or briefly *KS orbital*), which can easily be derived from Equation (2.46) and can be used to compute the density (using Equation (2.42)), which can further be utilized for generating a new improved V_{eff} , which will eventually lead to a new self-consistent cycle as shown in the flow chart in Figure 2.1. That is, once we know the various contributions in Equation (2.47), we can get the potential V_{eff} , which we need to insert into the one-particle Equations, which in turn determines the orbitals and consequently the ground state density and the ground state energy by employing the energy expression (2.49). As V_{eff} already depends on the density (and correspondingly on the orbitals) through the classical Coulomb term as shown in Equation (2.45), the Kohn-Sham one-electron Equations (2.46) also have to be solved iteratively until self-consistency is achieved, just like the Hartree-Fock Equations.

V_{xc} in Equation (2.46) is simply defined as the functional derivative of E_{EX} with respect to ρ as its explicit form is also unknown, similar to the E_{XC} ,

$$V_{xc} = \frac{\partial E_{xc}}{\partial \rho} \quad (2.54)$$

It is necessary to realize here that the ψ_i s are not equivalent to the real orbitals of the system and hence they do not connect to any real physically meaningful system. Their exclusive purpose is to provide a theoretical mapping between the kinetic energy and the density. It is also useful to note that the KS wave function is a single determinant approach and it fails where multiple determinants are needed in order to describe the system; for example, the dissociation of a molecule. A general scheme for a KS iteration cycle (during a single point or a geometry optimization process) is illustrated in Figure 2.1 below. Notably, if the exact forms of E_{EX} and V_{XC} are known, the Kohn-Sham strategy would give the exact value of the energy, *i.e.*, the correct

eigenvalue of the Hamilton operator. The formalism that has been illustrated so far in this section does not contain any approximation. Thus, unlike the Hartree-Fock model, where the approximation is introduced right from the beginning, the *Kohn-Sham approach is, in principle, exact!* The approximation enters only when we need to decide on an explicit form of the unknown functional (by any technique) for the exchange-correlation energy E_{EX} and the corresponding potential V_{XC} . The major goal in the development of modern DFT is therefore to find better and better approximations to these two quantities. This has led to a large number of functionals that are available to us for the computation of the energy for a variety of systems. These functionals are found to be highly system specific and require some sort of theoretical understanding, instead of being used blindly.

Over the last few decades, DFT has evolved into a critical computational tool used by a wide spectrum of researchers all over the world. They are made up of both theoretical and experimental chemists and physicists. Many physicists and chemists, on the other hand, see DFT's development from a theoretical notion to its current status as a lucky venture. This might be owing to the ease with which precision, which is frequently seen as a difficult challenge in *ab initio* wave function based approaches, was achieved. A number of theoretical chemists believe that the fundamental ideas are suspect, and that the single-determinant method is a source of further concern. However, the common preference for DFT appears to be a sensible option when considering the accuracy, as well as the reduction in processing cost. Because of the widespread current usage of DFT, it is now possible to do useful calculations for a huge number of real-size systems in a short amount of time. With the use of DFT, confirming experimental data or predicting novel chemistry by theoretical calculations has been reduced to a few days' work. On the other hand, wave function-based approaches are still impractical for use in real-world chemistry, biology, and material science systems. As a result, the widespread availability of DFT software programmes and the ever-expanding DFT-community must be regarded as a normal progression rather than a lucky occurrence.

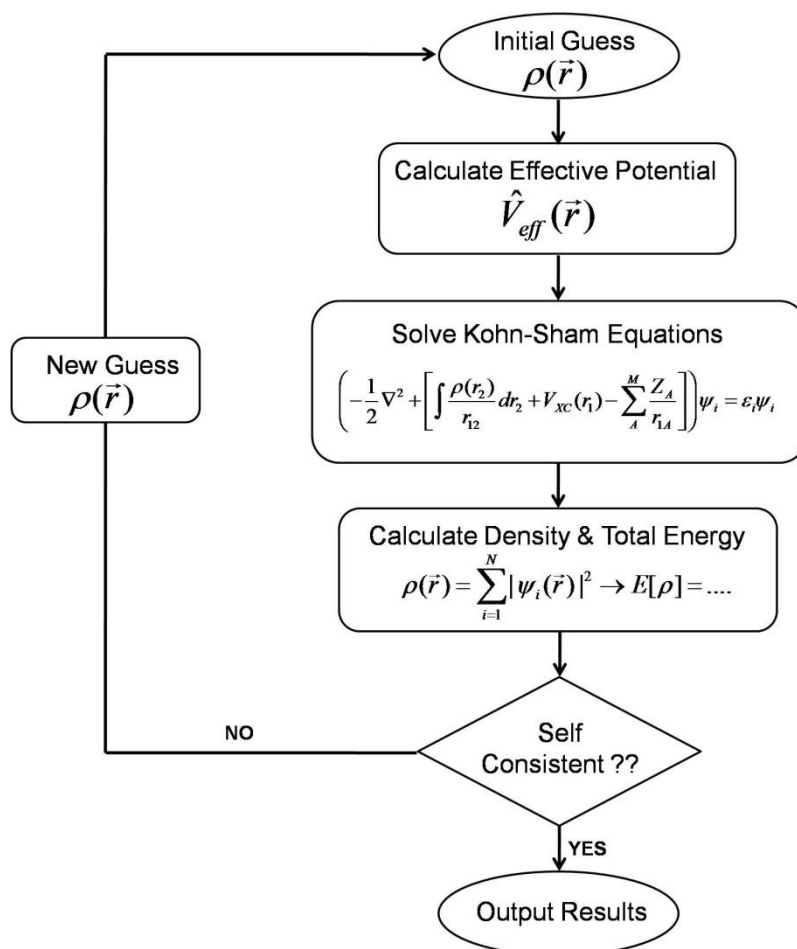


Figure 2.1 The flow chart for Kohn Sham iterations for the single point or the single step during optimization.

2.4 Natural Bond Orbital Analysis (NBO)

Natural bond orbital (NBO) analysis is a technique for converting a wave function into a localised form that corresponds to the one-center ("lone pairs") and two-center ("bonds") parts of a chemist's Lewis structure¹⁸ diagram. The atomic basis set is turned into "natural atomic orbitals" (NAOs), "natural hybrid orbitals" (NHOs), and "natural bonding orbitals" (NBOs) in this study. Per-Olov Löwdin was the first to propose the NBO idea in 1955.¹⁹ The NBO analysis elucidates the molecule's characteristics in greater detail. It reveals how the charges are dispersed across the molecule. Furthermore, it depicts charge transfer in the molecule, both inside atoms and between atoms. It is also possible to calculate the charge transfer between the two

interacting molecules. All conceivable interactions between 'full' (donor) Lewis-type NBOs and 'empty' (acceptor) non-Lewis NBOs are investigated in this study. The second order perturbation theory study of the fock matrix in the NBO basis can yield an energetic estimate of donor (i)-acceptor(j) orbital interactions. The donor-acceptor interaction energy $E(2)$ is given by

$$E(2) = \Delta E_{ij} = q_i \frac{F(i, j)^2}{\varepsilon_i - \varepsilon_j}, \quad (2.55)$$

Where q_i denotes the donor orbital occupancy, ε_i and ε_j denote the diagonal elements (orbital energies), and $F(i, j)$ denotes the off-diagonal NBO fock matrix element. The charge transfer between two interacting molecules was studied using NBO analysis at several points throughout this thesis.

2.5 Free Volume Correction for Translational Entropy

In order to construct the free energy profile diagram, the estimation of entropy is a must-do operation. It should be emphasised that the estimated total entropy is divided into translational, rotational, vibrational, and electronic components:

$$S_{tot} = S_{trans} + S_{rot} + S_{vib} + S_{ele} \quad (2.56)$$

The rotational, vibrational, and electrical components are adequately treated theoretically. The Sackur-Tetrode Equation has typically been used to calculate the translational entropy.²⁰

$$S_{trans} = R \ln \left[\left(\frac{10^{-15/2}}{N_A^4 [X]} \right) \left(\frac{2\pi MRT e^{5/3}}{h^2} \right)^{3/2} \right] \quad (2.57)$$

where T denotes the temperature, M is the mass of the particle, [X] denotes the concentration of the particles, h is the Planck constant, k is the Boltzmann constant, and the Avogadro's number is N_A . The translational entropy estimates with Equation 2.45 for monoatomic gases are shown to be accurate. However, for the molecules in the solution phase, the translational entropy calculated with Equation 2.45 is found to be underestimated. The explanation for this is the Sackur-Tetrode Equation's

assumption concerning the volume. The real space accessible for the solute molecule in the solution is less, as Mammen *et al.* have pointed out²¹ while introducing the concept of the free volume correction to the translation entropy. The free volume model assumes that the volume available to the molecule in solution is less than the total volume, and that the "free volume" is calculated using the following Equation:

$$V_{free} = C_{free} \left(\sqrt[3]{\left(\frac{10^{27}}{[X]N_0} \right)} - \sqrt[3]{V_{molec}} \right)^3 \quad (2.58)$$

Here, C_{free} denotes 8, V_{molec} implies the molecular volume, $[X]$ is the concentration of molecules (mol/L) in solution and N_0 is the Avogadro number. After accounting for the free volume adjustment, the translational entropy obtained is given by

$$S_{trans}^{analyte} = R \ln \left[\left(\frac{10^{-15/2} V_{free}^{solvent}}{N_0^4 [analyte]} \right) \left(\frac{2\pi MRT e^{5/3}}{h^2} \right)^{3/2} \right] \quad (2.59)$$

$$= 11.1 + 12.5 \ln(T) + 12.5 \ln(M) + 8.3 \ln V_{free}^{solvent} \quad (2.60)$$

Here, T is the temperature; M is the molecular weight of the solute and $V_{free}^{solvent}$ is the free volume. As a result, this model defines the translational entropy of molecules in solution ($\Delta S_{trans}(sol)$); as well as providing physically sensible adjustments for translational entropy values based on the Sackur-Tetrode Equation.

2.6 Non-Covalent Interaction Plot

Covalent interactions can be visualised using modern quantum-mechanical bonding models such as the atoms-in-molecule (AIM) theory²² and the electron localization function (ELF).²³ Computational chemists have been able to quantify the role of non-covalent interactions in large organic systems with previously unattainable accuracy, thanks to the concurrent development of density functional theory (DFT) methods capable of capturing dispersion-driven interactions, which are central to many favourable non-covalent interactions.²⁴⁻²⁶ Yang and co-workers have created a new viewpoint based on electron density that may be used to analyse and show a wide spectrum of non-covalent interactions.²⁷ Quantum-mechanical electron density ρ is

the essential quantity in density functional theory (DFT) from which all chemical characteristics may be calculated.²⁸ The first derivative of the decreased density gradient is used to represent the divergence from a homogeneous electron distribution.²⁹ In places distant from the molecule, where density decays to zero rapidly, the lowered gradient will have a substantial positive value. The decreased gradient will have very tiny values approaching zero in the area of both covalent and noncovalent interactions. Noncovalent interactions were discovered as low-density, low-reduced-gradient areas. The second derivative of density is utilised to discriminate between different sorts of interactions in low density or decreased gradient space. The sign of the Laplacian of the density $\Delta^2\rho$ is commonly used to distinguish between different forms of strong interactions.³⁰ The Laplacian is split into three main axes of greatest variation. The three eigenvalues λ_i of the electron-density Hessian (second derivative) matrix are these components such that: $\Delta^2\rho = \lambda_1 + \lambda_2 + \lambda_3$, ($\lambda_1 \leq \lambda_2 \leq \lambda_3$). Chemical bonding has benefited greatly from the analysis of these components.³¹ At nuclei (or non-nuclear attractors), when the density achieves a local maximum, all three eigenvalues are negative. The presence of one positive and two negative eigenvalues distinguishes interatomic areas between bound atoms ($\lambda_1 < 0$, $\lambda_2 < 0$, $\lambda_3 > 0$). In the case of covalent contacts, the negative contributions are prominent, and the resulting Laplacian is negative. The positive contribution for weaker, noncovalent contacts dominates the Laplacian in the interatomic region. The negative sign of λ_2 can be used to identify bonding interactions, such as the hydrogen bond in the water dimer example. In the interatomic area, however, if atoms are in nonbonded contact, $\lambda_2 > 0$ (where $\lambda_3 > 0$ and λ_1 might be positive or negative). As a result, the sign of λ_2 may be utilised to differentiate between bonded ($\lambda_2 < 0$) and non-bonded ($\lambda_2 > 0$) interactions. The sign of λ_2 may thus be used to discriminate between different forms of noncovalent interactions, while the density can be used to determine their intensity. Gradient isosurfaces containing the appropriate areas of real space can be used to find noncovalent interactions. The values of sign (λ_2) might help one understand the different types of interactions in these areas.

2.7 Quantification of Selectivity from Computation

The ideas of transition state (TS), activation barrier, and potential energy surface (PES) were developed by Eyring, Evans, and Polanyi, and were later utilised to account for product distributions in chemical processes under thermodynamic vs kinetic control. The distribution of products in thermodynamically regulated processes is dictated by their respective stabilities. Stereoselectivity is measured in terms of a temperature-dependent equilibrium constant, which is proportional to the reaction's standard-state Gibbs free energy, ΔG° at T , K denotes the equilibrium constant, while R represents the gas constant. R and S are two stereoisomeric products. Because the relative Gibbs energies of enantiomers are identical (i.e. $K = 1$), enantioselectivity is impossible under these conditions. The relative stability of diastereomers R and S determines the amount of diastereoselectivity. The reaction will be kinetically regulated if the activation barriers for converting either stereoisomer R or S back into reactant are substantial enough to prevent the reverse reaction and there is no product interconversion. The stereoselectivity in this scenario will be defined by the relative rates of production of each product.³¹ According to transition state theory, the rate constant for the formation of R and S enantiomeric products can be expressed as k_R and k_S by Equations 2.61 and 2.62

$$k_R = \frac{k_b T}{h} e^{-\frac{\Delta G_R^\ddagger}{RT}} \quad (2.61)$$

$$k_S = \frac{k_b T}{h} e^{-\frac{\Delta G_S^\ddagger}{RT}} \quad (2.62)$$

where ΔG^\ddagger is the free energy of activation for the formation of R or S respectively, k_b is the Boltzmann constant, h is the Planck constant, T is the temperature and R is the universal gas constant.

Stereoselectivity of the chemical reactions can be represented as an enantiomeric ratio (er). The er (for the enantioselective reaction) is directly proportional to the relative rates of formation of the enantiomeric products; that is, the ratio of products depends on the relative free energy barrier ($\Delta\Delta G^\ddagger$), which can be represented by:

$$\frac{R}{S} = \frac{k_R}{k_S} = e^{-\frac{\Delta G_R^\ddagger - \Delta G_S^\ddagger}{RT}} = e^{-\frac{\Delta\Delta G^\ddagger}{RT}} \quad (2.63)$$

The enantioselectivity in a reaction is commonly reported by enantiomeric excess (ee), which can be calculated as

$$ee = \frac{[R]-[S]}{[R]+[S]} \times 100 \quad (2.64)$$

where $[R]$ and $[S]$ represent the mole fraction of the R and S enantiomers. So, ee can be computationally obtained as

$$ee = \frac{1 - e^{-\frac{\Delta\Delta G^\ddagger}{RT}}}{1 + e^{-\frac{\Delta\Delta G^\ddagger}{RT}}} \times 100 \quad (2.65)$$

2.8 References

1. (a) Kümmel, H. G.; *Int. J. Mod. Phys. B*, **2003**, *17*, 5311. (b) In Bishop, R. F.; Brandes, T.; Gernoth, K. A.; Walet, N. R.; Xian, Y.; Kümmel, H. In Proceedings of the 11th International Conference on Recent Progress in many-body theories, Singapore: World Scientific Publishing, 2002, 334–348. (c) Shavitt, I.; Bartlett, R. J. *Many-Body Methods in Chemistry and Physics: MBPT and Coupled-Cluster Theory*, Cambridge University Press. **2009**.
2. (a) C. J. Cramer, *Chichester: John Wiley & Sons, Ltd.* **2002**, 191–232. (b) Sherrill, C. D.; Schaefer III, H. F.; *The Configuration Interaction Method: Advances in Highly Correlated Approaches*, *San Diego: Academic Press*, **1999**, 143–269.
3. (a) Assadi, M. H. N.; Hanao D. A. *H J. Appl. Phys*, **2013**, *113*, 233913. (b) Segall, M. D.; Lindan, P. J. D.; Probert, M. J.; Pickard, C. J.; Hasnip, P. J.; Clark, S. J.; Payne, M. C. *J. Phys: Condens. Matter*, **2002**, *14*, 2717-2743 (c) Somayeh, F. R.; Soleymanabadi, H *J. Mol. Model.*, **2014**, *20*, 2439-2445. (d) Somayeh, F. R.; Soleymanabadi, H *J Mol Model* , **2013**, *19*, 3733-3740 (e) Music, D.; Geyer, R. W.; Schneider, J. M. *Surface & Coatings Technology*, **2016**, *286*, 178.
4. Parr, R. G.; Yang, W. *Density functional theory of atoms and molecules*, *Oxford University Press, New York*: **1989**, pp 1–352.
5. Koch, W.; Holthausen, M. C. *A chemist's guide to density functional theory*; *John Wiley & Sons*: **2015**.
6. Thomas, L. H. *Mathematical Proc. Cambridge Phil. Soc.*, **1927**, *23*, 542-548; E. Fermi, *Rend. Accad. Naz. Lincei*. **1927**, *6*, 602–607.
7. Hohenberg, P.; Kohn, W. *Physical review* **1964**, *136*, B864.
8. Gross, E.; Kurth, S. *Density Functional Theory: The Modern Treatment of Electron Correlations*; Springer US: **1994**, pp 367–409.
9. Gross, E.; Kohn, W. *Advances in quantum chemistry* **1990**, *21*, 255–291.
10. Dreizler, R. M.; Gross, E. *Density Functional Theory: An Approach to the Quantum Many-Body Problem* Springer; Berlin: **1990**.
11. Gilbert, T. *Physical Review B* **1975**, *12*, 2111.
12. Lieb, E. A. H.; Shimony, A.; Feshbach H. (*MIT, Cambridge, MA*) **1982**, pp. 111-149.
13. Harriman, J. E.; *Physical Review A*, **1981**, *24*, 680.

14. W. Kohn, *Physical review letters*, **1983**, *51*, 1596.
15. Levy, M. *Physical Review A*, **1982**, *26*, 1200.
16. Lieb, E. H.; *International Journal of Quantum Chemistry*, **1983**, *24*, 243–277.
17. Kohn, W.; Sham, L. J.; *Physical review*, **1965**, *140*, A1133.
18. Lewis, G. N. J. *Am. Chem. Soc.*, **1916**, *38*, 762–785.
19. Weinhold, Frank; Landis, Clark R. *Chem. Edu. Res. Pract.*, **2001**, *2*, 91–104.
20. Gurney, R. W. *Introduction to statistical mechanics*; 1st ed.; McGraw Hill, **1949**.
21. Mammen, M.; Shakhnovich, E. I.; Deutch, J. M.; Whitesides, G. M. *J. Org. Chem.* **1998**, *63*, 3821-3830.
22. (a) Bader, R. F. W. *Chem. Rev.* **1991**, *91*, 893–928. (b) Bader, R. F. W. *Atoms in Molecules: A Quantum Theory. International Series of Monographs on Chemistry 22*; Oxford Science Publications: Oxford, **1990**. (c) Matta, C. F.; Boyd, R. J. In *The Quantum Theory of Atoms in Molecules*; Matta, C. F., Boyd, R. J., Eds.; Wiley-VCH: New York, **2007**; pp 1–34.
23. (a) Becke, A. D.; Edgecombe, K. E. *J. Chem. Phys.* **1990**, *92*, 5397–5403. (b) Silvi, B.; Savin, A. *Nature* **1994**, *371*, 683–686.
24. Grimme, S. Density Functional Theory with London Dispersion Corrections *WIREs Comp. Mol. Sci.* **2011**, *1*, 211– 228.
25. Ehrlich, S.; Moellmann, J.; Grimme, S. Dispersion-Corrected Density Functional Theory for Aromatic Interactions in Complex Systems *Acc. Chem. Res.* **2013**, *46*, 916– 926.
26. Zhao, Y.; Truhlar, D. G. Density Functionals with Broad Applicability in Chemistry *Acc. Chem. Res.* **2008**, *41*, 157– 167.
27. Johnson, E. R.; Keinan, S.; Mori-Sanchez, P.; Contreras-Garcia, J.; Cohen, A. J.; Yang, W. *J. Am. Chem. Soc.* **2010**, *132*, 6498–6506.
28. Hohenberg, P.; Kohn, W. *Phys. Rev. B* **1964**, *136*, 864–871.

29. (a) Becke, A. D. In *Modern Electronic Structure Theory*; Yarkony, D. R., Ed.; World Scientific: River Edge, NJ, **1995**, pp 1022–1046. (b) Cohen, A. J.; Mori-Sanchez, P.; Yang, W. *Science*. **2008**, *321*, 792–794.

30. Bader, R. F. W.; Essen, H. *J. Chem. Phys.* **1984**, *80*, 1943–1960.

31. Bader, R. F. W. *J. Phys. Chem. A* **1998**, *102*, 7314–7323

Chapter 3
**B(C₆F₅)₃ Catalyst or Initiator? Insights from
Computational Studies**

Chapter 3

B(C₆F₅)₃ Catalyst or Initiator? Insights from Computational Studies

Abstract

One of the most promising recent developments in catalysis has been the use of the metal-free Lewis acid B(C₆F₅)₃ as a catalyst for a range of different chemical transformations. Perhaps the most impressive achievement in this regard is the recently accomplished *in situ* generation of SiH₄ from surrogates (Oestreich and co-workers, *Nature Chemistry*, 2015, 7, 816). However, what the current computational work, with density functional theory (DFT), reveals is that this process, in addition to being catalyzed by B(C₆F₅)₃, is also significantly dominated by a series of autocatalytic reactions. The results are further corroborated by the use of the energetic span model (ESM), which shows that the turnover frequency (TOF) is higher for the newly proposed autocatalytic pathway in comparison to the conventional B(C₆F₅)₃ catalyzed pathway. The current work therefore provides interesting new insights into surrogate silicon chemistry. But, more importantly, the current studies indicate that B(C₆F₅)₃ is likely to function more as an initiator rather than a pure catalyst.

3.1 Introduction

In the two decades since the realization that the Lewis acid, $B(C_6F_5)_3$, is capable of acting as a catalyst, there have been a wide range of chemical transformations where it has been effectively employed,^{1,2} including hydrogenation³ and hydrosilylation,^{4,5,6,7} the transformation of ethers,⁸ the transesterification and deoxygenation of phosphonic and phosphinic esters,⁹ hydrodefluorination with hydrosilanes,¹⁰ dehydrogenative Si–X (X = nitrogen, oxygen, sulphur) coupling^{11,12} and intramolecular sila-Friedel–Crafts-type reactions.^{13,14} Furthermore, $B(C_6F_5)_3$ has also been employed as a catalyst for dihydrogen activation,¹⁵ the deoxygenation of carbohydrates,¹⁶ hydrogermylation,¹⁷ the reduction of amines,¹⁸ as well as allylation.¹⁹ Transfer hydrogenation and transfer hydrosilylation have also been effected with the aid of $B(C_6F_5)_3$.^{20,21,22} There have also been many theoretical studies on the Lewis acidity of fluoroarylboranes.²³ Many mechanistic pathways for $B(C_6F_5)_3$ catalyzed systems have been extensively investigated computationally by Sakata and coworkers.²⁴ What makes this extensive exploration particularly noteworthy, apart from its originality and range, is the fact that it is metal-free catalysis, having the virtues of being both potentially cheap and environmentally friendly.

However, it is also true that there are examples in the literature where $B(C_6F_5)_3$ has been noted to serve only as an initiator of a reaction, extracting a hydride or a methide from a neutral molecule to form a zwitterionic species. In such reactions, $B(C_6F_5)_3$ has been seen to form a counterion in solution that is non-interacting and non-interfering in nature, while the real catalytic active species was the corresponding cation formed. Figure 3.1 shows an example for this, taken from the field of homogeneous olefin polymerization²⁵, but there are also recent examples, such as the Friedel-Crafts C-H borylation of electron rich arenes.²⁶

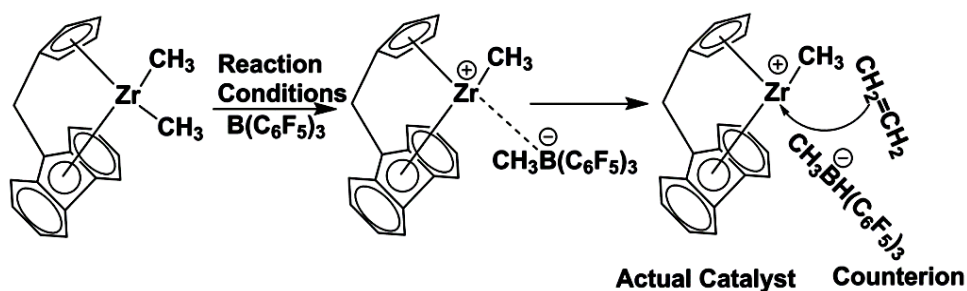


Figure 3.1. The role of $\text{B}(\text{C}_6\text{F}_5)_3$ in homogeneous olefin polymerization has been that of a co-catalyst or initiator, while the cation formed performs as the actual catalyst.²⁵

Now, this gives rise to an interesting question: in all the cases, mentioned in the previous paragraph, where $\text{B}(\text{C}_6\text{F}_5)_3$ has been considered to act as a catalyst,¹⁻²² is there a possibility that in many of them, it is acting more as an initiator, and not as a catalyst? Clearly, for this to be the case, (i) the reaction between the neutral substrate and $\text{B}(\text{C}_6\text{F}_5)_3$ species would have to form a loose, solvent separated ion-pair complex and (ii) the cation part of the ion-pair would then have to be capable of being the active catalytic species. It is the consideration of these possibilities that has led to the current investigation, with a primary focus on the recently reported surrogate chemistry conversion of SiR_3H ($\text{R} = \text{cyclohexa-1,4-diene}$) to SiH_4 ,^{27,28} which is one of the most impressive achievements to date in $\text{B}(\text{C}_6\text{F}_5)_3$ chemistry.

The reason why $\text{B}(\text{C}_6\text{F}_5)_3$ catalysis of SiR_3H to SiH_4 is so important is because it has always been challenging to work with the explosive, pyrophoric and toxic²⁹ SiH_4 directly. However, it is an important source of elemental silicon, which is widely used in the semiconductor industry.³⁰ In addition to this, compounds of silane find use in the hydrosilylation³¹ of alkenes,³² olefins,³³ alcohols³⁴ and carbonyls.³⁵ Hence the significance of the *in situ* generation of SiH_4 with the aid of $\text{B}(\text{C}_6\text{F}_5)_3$ in the reaction pot from cheap, stable surrogates by Simonneau and Oestreich^{27,28} (see Figure 3.2). $\text{B}(\text{C}_6\text{F}_5)_3$, and tri(cyclohexa-2,5-dien-1-yl)silane (SiR_3H) were added in dichloromethane (CH_2Cl_2) under ambient conditions, and this was seen to lead to the rapid generation of SiH_4 .^{27,28}

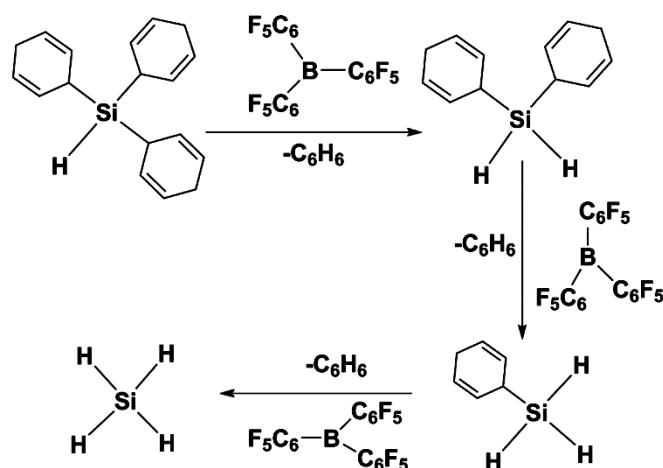


Figure 3.2. The *in situ* generation of SiH₄, as proposed by Simonneau and Oestreich.

The mechanism that has been proposed^{27,28} for this facile transformation involves B(C₆F₅)₃ in the role of catalyst. The first cycle of this process is shown in Figure 3.3 below. A perusal of this mechanism shows that it involves the reorganization of the zwitterionic species, ion-pair **A** (see Figure 3.3).

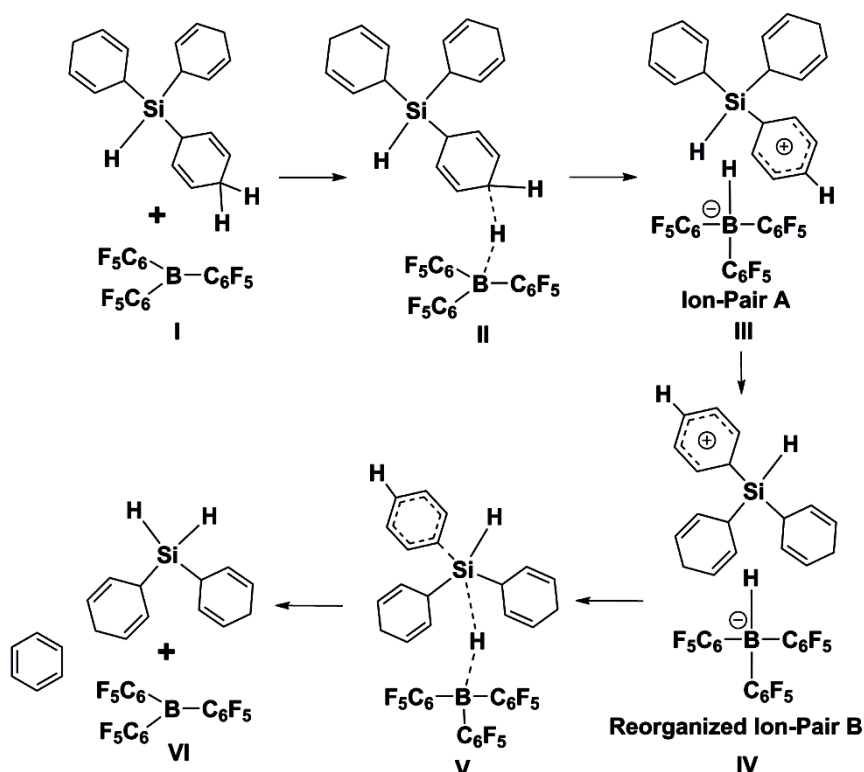


Figure 3.3 The Lewis acid $B(C_6F_5)_3$ catalysed mechanism for the formation of SiH_4 from tri(cyclohexa-2,5-diene-1-yl)silane.

An alternative route after the reorganization of the loosely solvent bound ion-pair would be the interaction of a neutral SiR_3H species with the ion-pair **B**: $[SiR_2R'H]^+[HB(C_6F_5)_3]^-$. I propose an autocatalytic process in this alternative scenario, shown in Figure 3.4 and Figure 3.5, that will allow the formation of new, loosely bound ion-pairs to be generated in each step, along with the expected lower surrogate silicon complex, SiR_2H_2 .

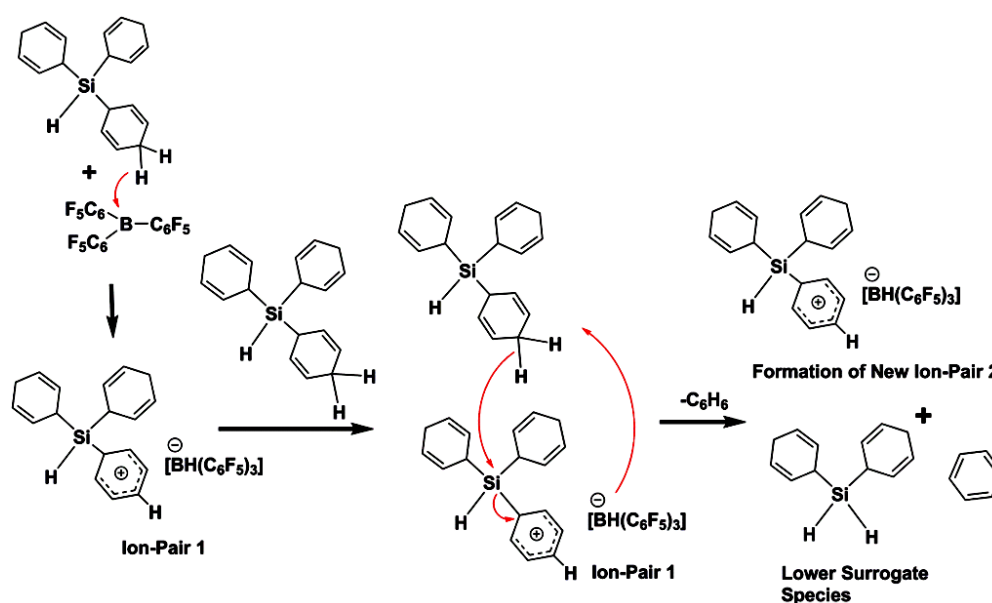
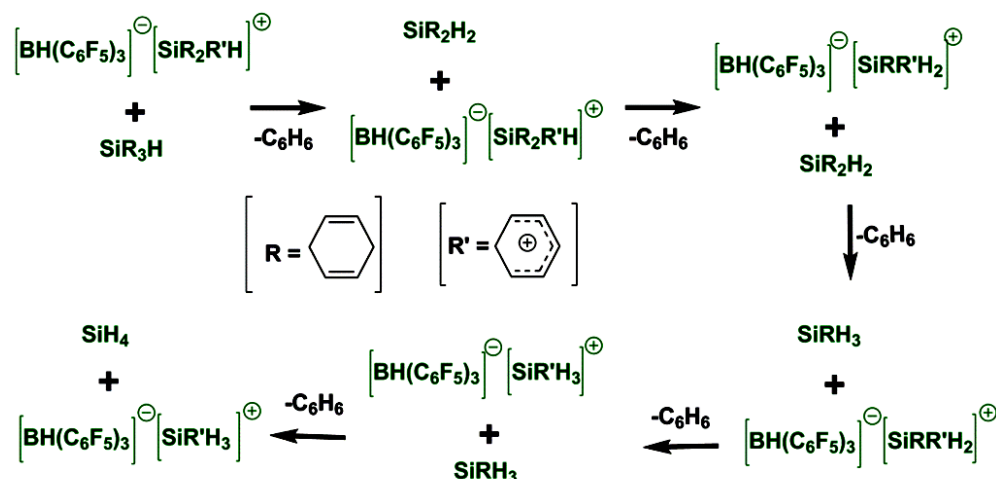


Figure 3.4 The currently proposed autocatalytic mechanism for the formation of di(cyclohexa-2,5-diene-1-yl)silane, which is a lower surrogate of tri(cyclohexa-2,5-diene-1-yl)silane. The $[BH(C_6F_5)_3]^-$ anion remains as a spectator, and shifts to the cation formed to create a new ion-pair.



At Every step, a lower surrogate species is formed.

Figure 3.5. *In situ* generation of SiH₄: the currently proposed autocatalytic approach. The [BH(C₆F₅)₃]⁻ anion remains as a spectator. In each step it forms the ion pair with the new cation which formed from the autocatalytic mechanism. In one step the R' generates and comes out as a cation in the very next step.

This, in turn, can react with the ion-pair species, and thus the sequence of reactions can proceed until SiH₄ is formed. In other words, if conditions (i) and (ii), mentioned earlier, are satisfied for this series of transformations, then the current work will provide insight into the interesting different roles played by B(C₆F₅)₃ during the SiR₃H species to SiH₄ transformation process.

These possibilities, as well as the original proposed mechanism of Simonneau and Oestreich (Figure 3.3), have been carefully investigated in their entirety with density functional theory (DFT). As will be shown in the Results and Discussion Section, I find that the calculations indicate a preference³⁶ for the autocatalytic process, with the B(C₆F₅)₃ seen to be more an initiator and a spectator rather than the pure catalyst. The proton source for the reactions is seen to be the silicon complex, analogous to other experimental cases where species such as substituted cyclohexa-1,4-diene were the hydride source.^{37,38} Furthermore, keeping in mind the implications that these results have for B(C₆F₅)₃ chemistry, I will also discuss the possibility of

$B(C_6F_5)_3$ being more of an initiator in several other reactions where it has, till date, been considered to act as a catalyst.

3.2 Computational Details

All the calculations for the structures reported in this chapter of thesis have been done using density functional theory (DFT).^{39,40} The calculations have been carried out with Turbomole 7.0⁴¹ using the TZVP⁴² basis set. Geometry optimizations were performed using the Perdew, Burke, and Ernzerhof functional (PBE).⁴³ Dispersion corrections (D3)⁴⁴ have been included in all the calculations. Solvent corrections have also been included in all the calculations using the Cosmo model,⁴⁵ with epsilon (ϵ) = 8.93, to model dichloromethane, CH_2Cl_2 , which had been employed as the solvent in the surrogate-to- SiH_4 ^{27,28} experiments. Therefore the level of theory employed is PBE-D3/TZVP+COSMO(CH_2Cl_2).^{42,43,45} The resolution of identity (RI)⁴⁶ along with the multipole accelerated RI (marij)⁴⁷ approximations have been used for an accurate and efficient treatment of the electronic Coulomb term in the DFT calculations. Furthermore, in order to underscore the reliability of the calculations, all the geometry optimizations have also been done at the TPSS-D3/def2-TZVP+COSMO(CH_2Cl_2)^{48,49,45} level of theory. The results from both the levels of theory: PBE-D3/TZVP+COSMO(CH_2Cl_2) and TPSS-D3/def2-TZVP+COSMO(CH_2Cl_2) are shown together with the superscripts “a” and “b” respectively in all the tables in this chapter of thesis. Furthermore, all the figures in this chapter of thesis showing the free energy profiles have two profiles, one each for the PBE-D3/TZVP+COSMO(CH_2Cl_2) and the TPSS-D3/def2-TZVP+COSMO(CH_2Cl_2) levels of theory. In addition to these calculations, single point calculations at the PW6B95-D3/def2-QZVP+COSMO(CH_2Cl_2)^{50,51,45} level of theory have also been done, on the geometries optimized at the TPSS-D3/def2-TZVP+COSMO(CH_2Cl_2) level. In other words, the TPSS-D3/def2-TZVP+COSMO(CH_2Cl_2)/PW6B95-D3/def2-QZVP+COSMO(CH_2Cl_2) level of theory has also been employed to investigate all the catalytic cycles that have been discussed in this chapter of thesis. This is the similar level to that employed by Oestreich and co-workers in their investigations into similar systems.³⁸ All the results

obtained from the calculations at the TPSS-D3/def2-TZVP+COSMO(CH₂Cl₂)/PW6B95-D3/def2-QZVP+COSMO(CH₂Cl₂) level of theory have been provide below. For the purpose of clarity, I will henceforth denote PBE-D3/TZVP+COSMO(CH₂Cl₂) as PTC(DCM) and TPSS-D3/def2-TZVP+COSMO(CH₂Cl₂) as TDC(DCM) in this chapter of thesis. Necessary care was taken to ensure that the obtained transition state structures possessed only one imaginary frequency corresponding to the correct normal mode, in order to obtain more reliable energy values for the investigated potential energy surface. In addition, intrinsic reaction coordinate (IRC)⁵² calculations were done with all the transition states in order to further confirm that they were the correct transition states, yielding the correct reactant and product structures. The values reported in this chapter of thesis are ΔG values, with zero point energy, internal energy, and entropic contributions, with the temperature taken to be 298.15K. The calculation of the translational entropy in standard software involves assumptions about the volume that may be inaccurate. The translational entropy term can be corrected by a free volume correction introduced by Mammen and co-workers.⁵³ Based on the Sackur-Tetrode equation, the free volume model describes the translational entropy of molecules in the solution ($\Delta S_{\text{trans}}(\text{sol})$); and provides physically intuitive corrections for translational entropy values. In the free volume model, it has been assumed that the volume available to the molecule in solution is lower than the total volume, and this “free volume” is determined by the equation (1) below:

$$V_{\text{free}} = C_{\text{free}} \left(\sqrt[3]{\frac{10^{27}}{[X]N_0}} - \sqrt[3]{V_{\text{molecule}}} \right)^3 \quad 3.1$$

Here, V_{molec} is the molecular volume, $[X]$ is the concentration of molecules (mol/L) in solution and N_0 is the Avogadro number. The translational entropy can be obtained after considering the free volume correction, and inserting the value of V_{free} in the Sackur-Tetrode equation. The total entropy is then calculated by adding the corrected translational entropy and the entropic contributions from the rotational and vibrational components. It is to be noted that entropic contributions have been properly handled in every mechanism that has been studied and reported here. For bimolecular

reactions where two species had to come together for the reaction to occur, the barrier for the reactions has always been calculated with the reactants assumed initially to have been at infinite separation, and not from a pre-reactive complex.

3.2.1 The Conformational Exploration

The structures of the reactants and products were first optimized with Gaussian 09⁵⁴ at the B3LYP(PCM)/3-21g^{55,56,57} level of theory. Solvent corrections have been included with PCM,⁵⁶ with the epsilon for dichloromethane, CH₂Cl₂, ($\epsilon = 8.93$) used in all the calculations. For a given structure, a scan to obtain different conformations was done by choosing a dihedral, and different structures were obtained by varying the value of the dihedral. This procedure was repeated with all possible dihedrals for this structure, in order to cover the maximum conformational space. Then the structure with the lowest energy was taken and optimized at the PTC(DCM) level of theory with Turbomole 7.0. This was done with the structures of all the reactants and products. It was seen, in every case, that the geometry obtained by this approach at the PTC(DCM) level of theory with Turbomole 7.0 was lower in energy than other conformations taken and optimized at this level of theory, thereby validating this approach. A similar approach was adopted to scan transition states as well. It is worth mentioning here that, to reduce the computational cost, the transition states involving the autocatalytic pathway were scanned without considering the [HB(C₆F₅)₃]⁻ ion, as it only remains as a spectator in the entire autocatalytic pathway. For the transition state scanning, the atoms involved in the transition state were fixed. Then, the procedure of scanning with the dihedrals was repeated as before, allowing the sampling of the conformational space for the transition states. The lowest energy transition state obtained by this scanning procedure for all the transition states was then optimized at the PTC(DCM) level of theory with Turbomole 7.0. As before, this was seen to be lower in energy than other transition state structures. It is worth mentioning here that I have also followed a similar conformational exploration for the ion-pair structures that I have investigated. Hence, the scanning procedure allowed us to obtain reliable reactant, product and transition state structures for the comparison of

the reaction mechanism proposed in the literature and the new mechanism(s) that I have proposed.

3.2.2 The Energetic Span Model

The efficiency of the catalytic cycle can be analyzed through the Energetic Span Model (ESM), put into practical use by Shaik and coworkers.^{58,59} The ESM provides a straightforward method to calculate the turnover frequencies (TOFs) of catalytic cycles based on their computed energy profiles. In most cases, the TOF is determined by the TOF-determining transition state (TDTS), the TOF-determining intermediate (TDI) and by the reaction energy, ΔG_r . The TOF calculation formula is as below:

$$\text{TOF} = \frac{k_B T}{h} e^{-\delta E/RT} \quad 3.2$$

where δE is the energy span and is defined as the difference in the Gibbs energy between the TDTS and the TDI, with the addition of the ΔG_r when the TDTS appears before the TDI. δE is the effective activation barrier of the global reaction. The TDTS and TDI are the intermediate and the transition states respectively that maximize δE , according to eq 3.

$$\delta E = \begin{cases} \delta_{TDTS} - \delta_{TDI} & \text{if TDTS appears after TDI} \\ \delta_{TDTS} - \delta_{TDI} + \Delta G_r & \text{if TDTS appears before TDI} \end{cases} \quad 3.3$$

This model has been employed to calculate the TOFs (at 298 K). The energetic span model can be applied in a user friendly way with the recently developed AUTOF computer program.^{58,59}

3.3 Results and Discussion

3.3.1 Investigation of $B(C_6F_5)_3$ Involving in Normal Catalytic Pathway

As stated in the Introduction, the possibility of autocatalytic alternatives (see Figure 3.4 and 3.5) to the conventional $B(C_6F_5)_3$ catalyzed pathways (Figure 3.3) for the conversion of SiR_3H to SiH_4 has been considered in our computational studies. Every profile I have shown in this chapter of thesis have been colored with blue for

PTC(DCM) and brown for the TDC(DCM) levels of theory. Figure 3.9 below shows the catalytic cycle proposed by Simonneau and Oestreich,^{27,28} based on a previously proposed mechanism by Sakata and Fujimoto for the formation of the methyl substituted silane (SiHMe_3).⁶⁰ In the first step, the Lewis acid $\text{B}(\text{C}_6\text{F}_5)_3$ extracts a hydride from the bisallylic position^{61,62} of SiR_3H to give rise to the ion-pair $[\text{SiR}_2\text{R}'\text{H}]^+[\text{HB}(\text{C}_6\text{F}_5)_3]^-$ (species 3). The calculations indicate that the hydride *anti* to the silicon is the one preferentially taken by the $\text{B}(\text{C}_6\text{F}_5)_3$, as has also been observed by Sakata and Fujimoto.⁶⁰ Here, it is worth mentioning that Sakata and Fujimoto⁶⁰ have discussed a mechanism where methyl substituted cyclohexene behaves as a hydride source, with the hydride being given to the $[\text{SiMe}_3(\text{C}_6\text{H}_6)]^+$ cation. The barrier for the process was found to be higher than for the conventional $[\text{BH}(\text{C}_6\text{F}_5)_3]^-$ pathway and is different from the newly proposed autocatalytic pathway. Now considering the ion-pair **A**, 3 can rearrange to species 5, with the boron now positioned to deliver the hydride to the silicon. For this, a barrier of 15.1 kcal/mol (blue profile in Figure 3.9) has to be overcome, and yields the lower surrogate species: SiR_2H_2 , the original $\text{B}(\text{C}_6\text{F}_5)_3$ and benzene. However, the alternative route, shown in green in the same figure (see Figure 3.6), would lead to the autocatalytic pathway. Here, it is noted that 5 is a loosely bound ion-pair species. This is because the energy for completely separating 5 into the cation and anion has been calculated to be only 8.5 kcal/mol at the PTC(DCM) level of theory. This would ensure the availability of the cation for participating in the autocatalytic pathway. This cationic species: $[\text{SiR}_2\text{R}'\text{H}]^+$ can be considered a sigma (σ) complex cation.^{63,64} Such silicon-substituted cyclohexadienylcations are low-energy Wheland complexes or, from the perspective of silicon chemistry, arene-stabilized silicon cations.⁶⁵ It has been shown previously⁶⁶ that stabilizing donors are needed in silicon cation generation. Here, cyclohexa-2,5-dien-1-ylsilanes meet this requirement, as they have sufficient hydridic character at the bisallylic position of $\text{C}(\text{sp}^3)\text{-H}$ bond due to hyperconjugation with the $\text{C}(\text{sp}^3)\text{-Si}$ bond. I also note that the fact that the separation of loosely bound ion-pairs involving a cationic silicon species and the $[\text{HB}(\text{C}_6\text{F}_5)_3]^-$ anion in dichloromethane is very facile has also been reported earlier by Sakata and Fujimoto at the M06-2X(PCM)/6-311++g(d,p)//M06-2X(PCM)/6-311g(d,p) level of theory.⁶⁰ It is also

notable that the values obtained at entirely different levels of theory in the current work: the PTC(DCM) and the TDC(DCM) (blue and brown profiles respectively in Figure 3.9) are quite similar in the values obtained, which suggests that the conclusions that have been reached are reliable and robust, and invariant of the level of theory employed.

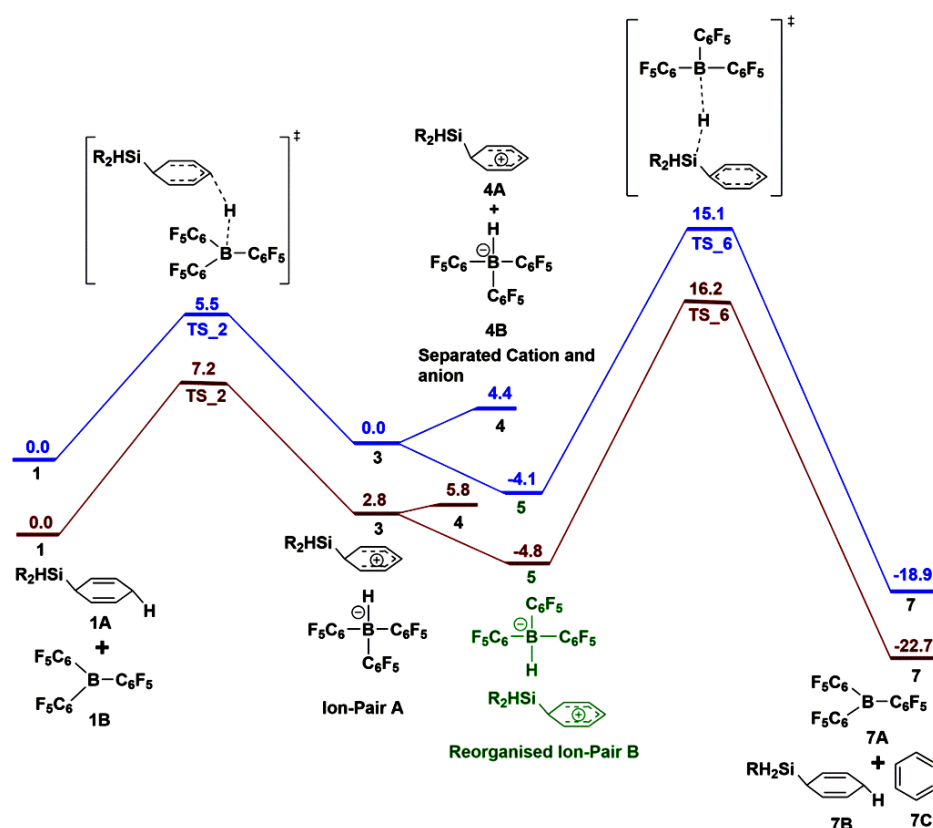


Figure 3.6. The free energy profile (ΔG) in kcal/mol for the proposed mechanism by Simonneau and Oestreich. R=cyclohexa-1,4-diene. The blue profile is for the PTC(DCM) level of theory and the brown profile is for the TDC(DCM) level of theory.

3.3.2. Investigation of $B(C_6F_5)_3$ Involving in Autocatalytic Pathway

Now, the $[SiR_2R'H]^+$ cation, seen to be loosely bound to the anion, can be considered as an independent actor, like in the cases of homogeneous olefin polymerization²⁴ and Friedel-Crafts C-H borylation²⁶ mentioned in the Introduction. The possibility that this species can take part in autocatalytic reactions is explored in Figure 3.10. The

$[\text{SiR}_2\text{R}'\text{H}]^+$ cation can extract a hydride from another SiR_3H substrate molecule to yield SiR_2H_2 , the reaction having a barrier of 10.0 kcal/mol (blue profile in Figure 3.10). This is 5.1 kcal/mol lower than the corresponding step shown in Figure 3.9. Therefore, this newly proposed autocatalytic process is significantly more facile than the conventional pathway.

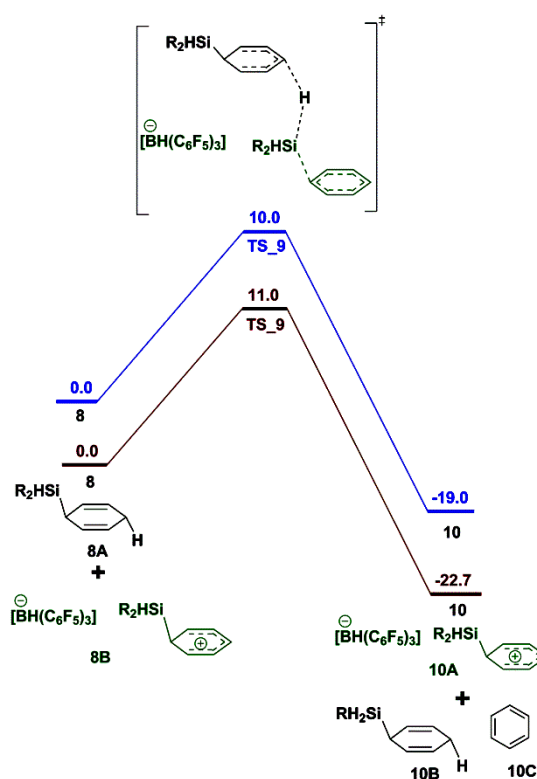


Figure 3.7. The free energy profile (ΔG) in kcal/mol for the autocatalytic mechanism. The $[\text{BH}(\text{C}_6\text{F}_5)_3]^-$ anion remains as a spectator. $\text{R}=\text{cyclohexa-1,4-diene}$. The blue profile is for the PTC(DCM) level of theory and the brown profile is for the TDC(DCM) level of theory.

Now, SiR_2H_2 formed can interact with an $[\text{SiR}_2\text{R}'\text{H}]^+$ cation to convert to $[\text{SiRR}'\text{H}_2]^+$ (with a loosely bound $[\text{HB}(\text{C}_6\text{F}_5)_3]^-$ as a spectator species) to form an SiR_2H_2 species with the release of a benzene molecule. As one can see, there can be several permutations and combinations, where different $\text{Si}(\text{R})_x\text{H}_y$ species can interact with different $[\text{Si}(\text{R})_x(\text{R}')\text{H}_y]^+$ species (with a spectator $[\text{HB}(\text{C}_6\text{F}_5)_3]^-$ always present), to yield the corresponding lower surrogate silicon intermediates. All of these have

been considered in this work, and for each step where the lower surrogate is formed, they have been compared to the $B(C_6F_5)_3$ catalyzed mechanism proposed in the literature. Shown in Table 3.1 are the barriers for the formation of the intermediates by the conventional literature mechanism and the corresponding barriers for the formation of the intermediates by different permutations of the newly proposed pathways, independent of $B(C_6F_5)_3$. As the results indicate, not only are the pathways for forming a given intermediate greater by the routes outlined here, the barriers for forming the intermediates are uniformly lower in each case, in comparison to the $B(C_6F_5)_3$ catalyzed mechanism. While all the cases considered have been comprehensively compared, an illustrative case among the lot is shown below in Figure 3.11, which compares the formation of SiH_4 from $[SiR'H_3]^+[HB(C_6F_5)_3]^-$ from both the conventional and autocatalytic approaches. The profiles show that the barrier for the autocatalytic mechanism is 4.4 kcal/mol lower than the barrier for the conventional pathway for this step (see Figure 3.11).

Table 3.1. The calculated free energy barriers for all possible ways of the lower surrogate SiR_xH_y species formation through the conventional mechanism proposed in the literature and our proposed mechanism.

| Intermediate | Barrier (ΔG^\ddagger kcal/mol) | | | |
|----------------|---|--|--------------------------------------|--------------------------------------|
| | The Literature Mechanism | Our Proposed, Cationic Autocatalytic Mechanism | | |
| | $[HB(C_6F_5)_3]^-$ | SiR_3H | SiR_2H_2 | $SiRH_3$ |
| $[SiR_2R'H]^+$ | 14.9 ^a /16.2 ^b | 10.0 ^a /11.0 ^b | 10.4 ^a /14.5 ^b | 11.2 ^a /11.3 ^b |
| $[SiRR'H_2]^+$ | 14.8 ^a /12.5 ^b | 10.7 ^a /9.0 ^b | 10.3 ^a /10.8 ^b | 12.1 ^a /10.1 ^b |
| $[SiR'H_3]^+$ | 14.5 ^a /14.0 ^b | 8.0 ^a /9.0 ^b | 11.0 ^a /12.0 ^b | 9.2 ^a /9.4 ^b |

^aThe values pertaining to the barriers (ΔG^\ddagger kcal/mol) for the PTC(DCM) calculations.

^bThe values pertaining to the barriers (ΔG^\ddagger kcal/mol) for the TDC(DCM) calculations.

In order to provide a more quantitative estimate of how the newly proposed autocatalytic pathways are more favoured over the $B(C_6F_5)$ catalyzed pathways, I have determined the efficiency for the free energy profiles shown in the Figures 3.9, 3.10, 3.11 and 3.12 (see the flowchart) by employing the “Energetic Span Model” (ESM).^{58,59} In the present case, for the $B(C_6F_5)$ catalyzed pathway (see Figure 3), the TOF-determining transition state, TDTS, appears after the TOF-determining intermediate, TDI. The TDI is determined to be species 5 in the energy profile and the TDTS is species 6 (see Figure 2). The TOF for the autocatalytic pathway is calculated to be $1.0 \times 10^9 \text{ h}^{-1}$ at the PTC(DCM) level of theory. This is obtained by considering that the species involved are (5-8-9-10).⁶⁷ The corresponding value for the conventional pathway is $2.6 \times 10^2 \text{ h}^{-1}$, i.e. the newly proposed pathway is *seven orders of magnitude* superior in efficiency in comparison to the conventional pathway! This is also seen to be true at the TDC(DCM) level of theory. But this is not all. After the reorganized species has been formed in the initiation step (species 5 in Figure 3.9), for subsequent cycles, the TOF calculations would involve only a one step pathway. The calculations indicate that the TOF for this would be several orders of magnitude superior to the conventional pathway, at both levels of theory (see Table 3.2)! Furthermore, in order to make a fairer comparison between the multi-step conventional pathway, and the autocatalytic route, I have also calculated the TOF for the complete catalytic cycle, beginning from SiR_3H and ending finally with the formation of SiH_4 , for both the conventional as well as the autocatalytic routes. This will have several steps in all, the flowchart for which has been provided in Figure 5. The ESM results indicate that the autocatalytic pathway for the complete cycle is 10^3 times superior to the conventional pathway for both the PTC(DCM) and the TDC(DCM) levels of theory (see Table 3.2). Hence, all the ways in which the ESM has been employed to evaluate the conventional and the newly proposed routes for SiH_4 formation all point to significant superiority of the newly proposed pathways over the conventional routes that assume that the $B(C_6F_5)_3$ acts as the catalyst in this process.

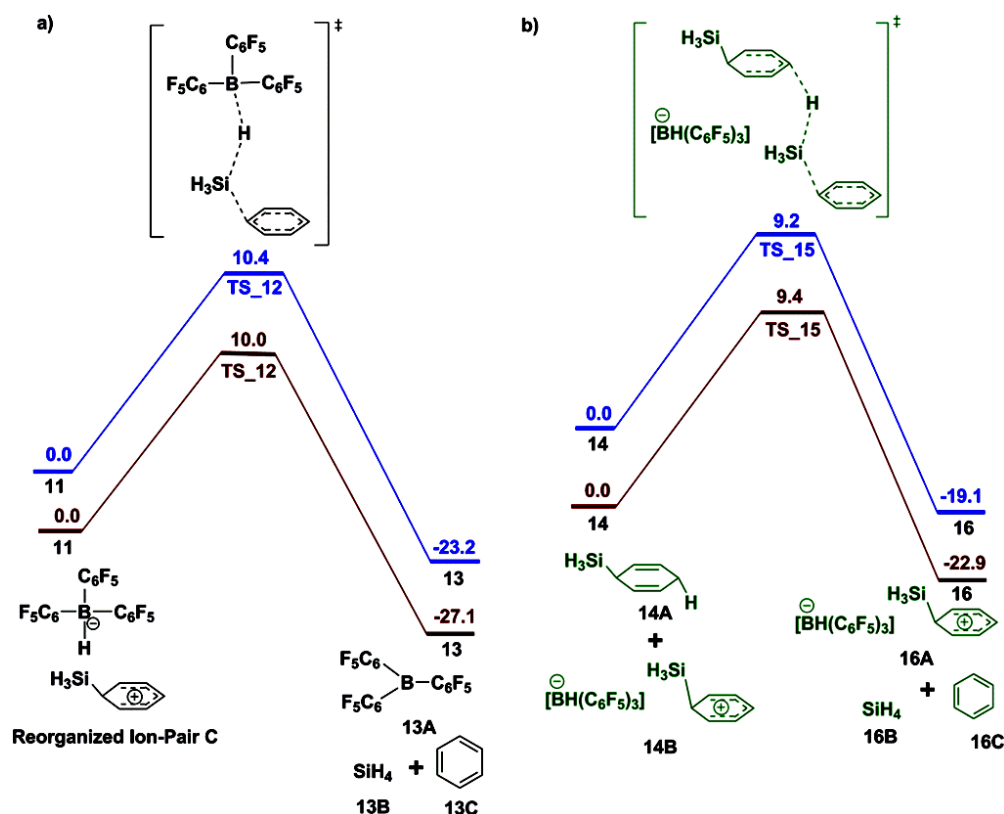


Figure 3.8. The comparison of the free energy profiles (ΔG , kcal/mol) between a) the conventional mechanism with mono(cyclohexa-2,5-dien-1-yl)silane and $B(C_6F_5)_3$, and b) our proposed autocatalytic mechanism. The blue profile is for the PTC(DCM) level of theory and the brown profile is for the TDC(DCM) level of theory for conventional pathway. The deep green species are the ones pertaining to newly proposed autocatalytic pathway.

These results therefore clearly show that the conventional $B(C_6F_5)_3$ catalyzed pathway is only a minor route, while the more significant players in this chemistry are the newly proposed routes involving autocatalytic mechanisms. In order to provide further validation of the results, I have also calculated the barriers with full optimization at the PBE-D3/6-311++G**+COSMO(CH₂Cl₂)⁶⁸ level of theory. The results for this are provided in Table 3.1. Furthermore, single point calculations at PW6B95/def2-QZVP+COSMO(CH₂Cl₂) with the TDC(DCM) optimized structures have been done and the results are provided in the Table 3.2. All these extra

calculations show that the conclusions reached, as well as the trends obtained, remain unaltered, thereby underlining the robustness of the level of theory employed.

Table 3.2. The values for the TOFs obtained for the stepwise and total autocatalytic pathways, as well as with the conventional B(C₆F₅)₃ catalyzed pathway.

| Pathway | TOF (h ⁻¹) | | | |
|---|---|---|---|---|
| | SiR ₃ H→[SiR ₂ H ₂] | SiR ₂ H→[SiRH ₃] | SiRH ₃ →[SiH ₄] | SiR ₃ H→[SiH ₄] |
| B(C ₆ F ₅) ₃ catalyzed | ^a 2.6*10 ² / ^b 8.8*10 ⁰ | ^a 1.7*10 ⁵ / ^b 8.9*10 ⁶ | ^a 1.2*10 ⁶ / ^b 5.2*10 ⁵ | ^a 1.4*10 ⁶ / ^b 9.4*10 ⁷ |
| Autocatalytic | ^a 1.0*10 ⁹ / ^b 1.9*10 ⁸ | ^a 6.3*10 ⁸ / ^b 2.7*10 ⁸ | ^a 8.8*10 ⁸ / ^b 2.0*10 ⁹ | ^a 2.5*10 ⁹ / ^b 2.4*10 ⁹ |

^aThe values pertaining to the TOF (h⁻¹) for the PTC(DCM) calculations.

^bThe values pertaining to the TOF (h⁻¹) for the TDC(DCM) calculations.

Table 3.3. The calculated barriers (single point) for all possible ways of lower surrogate SiR_xH_y species formation through the conventional mechanism proposed in the literature and our proposed mechanism.

| Intermediate | Barrier (ΔE [#] kcal/mol) PW6B95-D3/def2-QZVP+COSMO (CH ₂ Cl ₂) | | | |
|-------------------------------------|---|--|---------------------------------|-------------------|
| | The Literature Mechanism | Our Proposed, Cationic Autocatalytic Mechanism | | |
| | [HB(C ₆ F ₅) ₃] ⁺ | SiR ₃ H | SiR ₂ H ₂ | SiRH ₃ |
| [SiR ₂ R'H] ⁺ | 16.4 | 12.4 | 13.2 | 13.5 |
| [SiRR'H ₂] ⁺ | 9.9 | 10.8 | 10.1 | 11.9 |

| | | | | |
|-----------------------------|-----|------|------|-----|
| $[\text{SiR}'\text{H}_3]^+$ | 5.2 | 11.7 | 10.5 | 9.5 |
|-----------------------------|-----|------|------|-----|

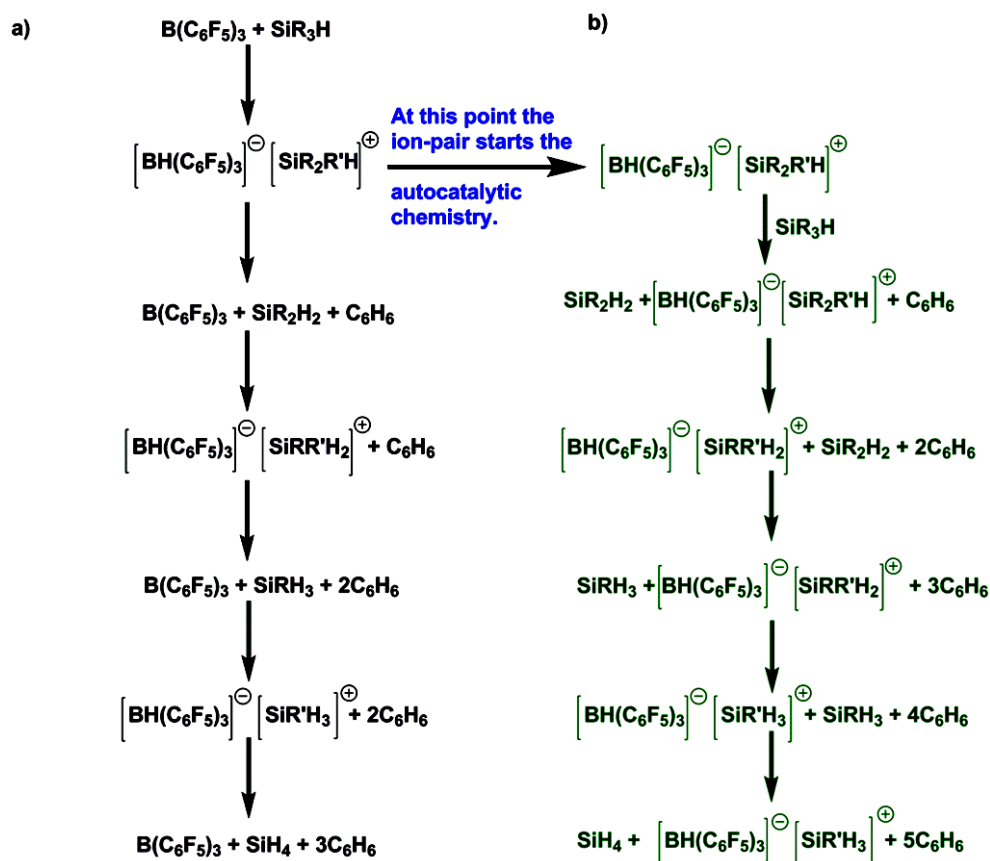


Figure 3.9. Flowchart for the formation of SiH_4 through (a) the conventional $\text{B}(\text{C}_6\text{F}_5)_3$ catalyzed pathway and (b) the newly proposed autocatalytic pathway. The autocatalytic pathway is shown in green.

Furthermore, in order to ensure that there are no other competing pathways, I have also checked another possibility, where the benzene separation from the cationic species of tri(cyclohexa-2,5-dien-1-yl)silane, di(cyclohexa-2,5-dien-1-yl)silane and mono(cyclohexa-2,5-dien-1-yl)silane could take place. The silicon after the benzene dissociation would be stabilized by coordination with the olefinic carbon of the

cyclohexadienyl ring(see Figures 3.10, 3.11 and 3.12 below). Subsequently, the silicon cation could participate in new autocatalytic processes. However, such a possibility was found to be unlikely, because the ΔG for the dissociation of benzene for every case was found to be high (9.0 kcal/mol to greater than 30.0 kcal/mol), at both the PTC(DCM) and the TDC(DCM) levels of theory (see Table 3.4 below). Thus, the overall barrier for such processes would become high, higher than the slowest step for our proposed autocatalytic pathways. Hence this possibility has not been considered further.

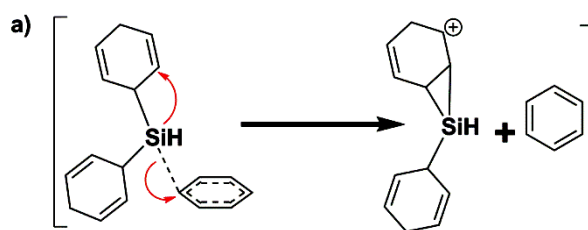


Figure 3.10. a) The dissociation of benzene from the $[\text{SiHR}_2\text{R}']^+$ complex.

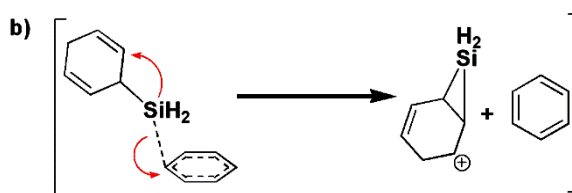


Figure 3.11. b) The dissociation of benzene from the $[\text{SiH}_2\text{RR}']^+$ complex.

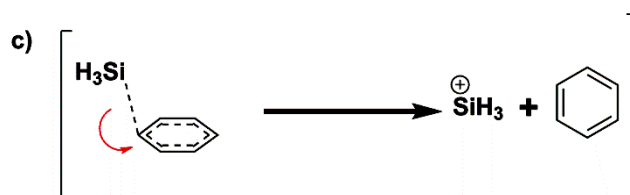


Figure 3.12. c) The dissociation of benzene from the $[\text{SiH}_3\text{R}']^+$ complex.

Table 3.4. The calculated free energies (ΔG , in kcal/mol) for the dissociation of benzene from the respective cations.

| Silyl cations | ΔG (kcal/mol) | |
|--|-----------------------|----------|
| | PTC(DCM) | TDC(DCM) |
| $[\text{SiHR}_3]^+ \longrightarrow [\text{SiHR}_2]^+ \text{C}_6\text{H}_6$ | 8.9 | 10.7 |
| $[\text{SiH}_2\text{R}_2]^+ \longrightarrow [\text{SiH}_2\text{R}]^+ \text{C}_6\text{H}_6$ | 11.6 | 11.9 |
| $[\text{SiH}_3\text{R}]^+ \longrightarrow [\text{SiH}_3]^+ \text{C}_6\text{H}_6$ | 32.7 | 34.3 |

3.4 Conclusion

The current work, with density functional theory (DFT), showcases the elegant and unheralded nature of surrogate silicon chemistry, dependent not on Lewis acid, $\text{B}(\text{C}_6\text{F}_5)_3$, catalysis but on a series of autocatalytic processes. The computational investigations provide important insights that will be helpful for researchers working in the area of silicon chemistry, as well as for those working with surrogates in allied areas. Indeed, recent work reported by Oestreich and coworkers⁷⁷ converting the surrogate GeR_3H to GeR_2H_2 ($\text{R} = \text{cyclohexa-1,4-diene}$) employing $\text{B}(\text{C}_6\text{F}_5)_3$, may also be an example of similar autocatalytic chemistry. Furthermore, the current work shows that cationic autocatalytic processes are not limited to examples in biochemistry⁷⁸ and polymerization,⁷⁹ but are more widespread than had been realized earlier.

3.5 References

- (1) Oestreich, M.; Hermeke, J.; Mohr, J. *Chem. Soc. Rev.* **2015**, *44*, 2202-2220.
- (2) (a) Massey, A. G.; Park, A. J.; Stone, F. G. A., Tris(pentafluorophenyl)boron. *Proc. Chem. Soc.* **1963**, 212. (b) Massey, A. G.; Park, A. J. *J. Organomet. Chem.* **1964**, *2*, 245-250. (c) Massey, A. G.; Park, A. J. *J. Organomet. Chem.* **1966**, *5*, 218-225. (d) Piers, W. E.; Chivers, T. *Chem. Soc. Rev.* **1997**, *26*, 345-354. (e) Jacobsen, H.; Berke, H.; Döring, S.; Kehr, G.; Erker, G.; Fröhlich, R.; Meyer, O. *Organometallics* **1999**, *18*, 1724-1735. (f) Piers, W. E. *Adv. Organomet. Chem.* **2004**, *52*, 1-76. (g) Erker, G. *Dalton Trans.* **2005**, *0*, 1883-1890. (h) Piers, W. E.; Marwitz, A. J. V.; Mercier, L. G. *Inorg. Chem.* **2011**, *50*, 12252-12262.
- (3) (a) Rokob, T. A.; Hamza, A.; Stirling, A.; Pápai, I. *J. Am. Chem. Soc.* **2009**, *131*, 2029-2036. (b) Mahdi, T.; Heiden, Z. M.; Grimme, S.; Stephan, D. W. *J. Am. Chem. Soc.* **2012**, *134*, 4088-4091. (c) Zaher, H.; Ashley, A. E. Irwin, M.; Thompson, A. L.; Gutmann, M. J.; Krämer, T.; O'Hare, D. *Chem. Commun.* **2013**, *49*, 9755-9757. (d) Mahdi, T.; Stephan, D. W. *J. Am. Chem. Soc.* **2014**, *136*, 15809-15812. (e) Scott, D. J.; Fuchter, M. J.; Ashley, A. E. *J. Am. Chem. Soc.* **2014**, *136*, 15813-15816.
- (4) (a) Harrison, D. J.; McDonald, R.; Rosenberg, L. *Organometallics* **2005**, *24*, 1398-1400. (b) Nyhlén, J.; Privalov, T. *Dalton Trans.* **2009**, *0*, 5780-5786. (c) Hounjet, L. J.; Bannwarth, C.; Garon, C. N.; Caputo, C. B.; Grimme, S.; Stephan, D. W. *Angew. Chem., Int. Ed.* **2013**, *52*, 7492-7495.
- (5) For further examples of hydrosilylation of imines catalysed by electron-deficient boranes (a) Hog, D. T.; Oestreich, M. *Eur. J. Org. Chem.* **2009**, *2009*, 5047-5056. (b) Chen, D.; Leich, V.; Pan, F.; Klankermayer, J. *Chem. – Eur. J.* **2012**, *18*, 5184-5187. (c) Zhu, X.; Du, H. *Org. Biomol. Chem.* **2015**, *13*, 1013-1016.
- (6) (a) Chase, P. A.; Jurca, T.; Stephan, D. W. *Chem. Commun.* **2008**, *0*, 1701-1703. (b) Chen, D.; Klankermayer, J. *Chem. Commun.* **2008**, *0*, 2130-2131.

- (7) Hermeke, J.; Mewald, M.; Oestreich, M. *J. Am. Chem. Soc.* **2013**, *135*, 17537-17546.
- (8) (a) Mack, D. J.; Guo, B.; Njardarson, J. T. *Chem. Commun.* **2012**, *48*, 7844-7846. (b) Feghali, E.; Cantat, T. *Chem. Commun.* **2014**, *50*, 862-865. (c) Mohr, J.; Oestreich, M. *Angew. Chem., Int. Ed.* **2014**, *53*, 13278-13281. (d) Hounjet, L. J.; Bannwarth, C.; Garon, C. N.; Caputo, C. B.; Grimme, S.; Stephan, D. W., *Angew. Chem., Int. Ed.* **2013**, *52*, 7492-7495.
- (9) Denis, J. M.; Forintos, H.; Szelke, H.; Keglevich, G. *Tetrahedron Lett.* **2002**, *43*, 5569-5571.
- (10) Caputo, C. B.; Stephan, D. W. *Organometallics* **2012**, *31*, 27-30.
- (11) (a) Shchepin, R.; Xu, C.; Dussault, P. *Org. Lett.* **2010**, *12*, 4772-4775. (b) Strašák, T.; Sýkora, J.; Lamač, M.; Kubišta, J.; Horáček, M.; Gyepes, R.; Pinkas, J. *Organometallics* **2013**, *32*, 4122-4129. (c) Simonneau, A.; Friebe, J.; Oestreich, M. *Eur. J. Org. Chem.* **2014**, *10*, 2077-2083.
- (12) (a) Zhou, D.; Kawakami, Y. *Macromolecules* **2005**, *38*, 6902-6908. (b) Zhang, Z.; Lyons, L. J.; Jin, J. J.; Amine, K.; West, R. *Chem. Mater.* **2005**, *17*, 5646-5650. (c) Hoque, M. A.; Kakihana, Y.; Shinke, S.; Kawakami, Y. *Macromolecules* **2009**, *42*, 3309-3315. (d) Moitra, N.; Ichii, S.; Kamei, T.; Kanamori, K.; Zhu, Y.; Takeda, K.; Nakanishi, K.; Shimada, T. *J. Am. Chem. Soc.* **2014**, *136*, 11570-11573.
- (13) Curless, L. D.; Ingleson, M. J. *Organometallics* **2014**, *33*, 7241-7246.
- (14) (a) Pérez, M.; Hounjet, L. J.; Caputo, C. B.; Dobrovetsky, R.; Stephan, D. W. *J. Am. Chem. Soc.* **2013**, *135*, 18308-18310. (b) Holthausen, M. H.; Mehta, M. Stephan, D. W. *Angew. Chem., Int. Ed.* **2014**, *53*, 6538-6541.
- (15) (a) Welch, G. C.; Stephan, D. W. *J. Am. Chem. Soc.* **2007**, *129*, 1880-1881. (b) Sumerin, V.; Schulz, F.; Nieger, M.; Leskelä, M.; Repo, T.; Rieger, B. *Angew. Chem., Int. Ed.* **2008**, *47*, 6001-6003. (c) Marwitz, A. J. V.; Dutton, J. L.; Mercier, L. G.; Piers, W. E. *J. Am. Chem. Soc.* **2011**, *133*, 10026-10029. (d) Lindqvist, M.; Sarnela,

N.; Sumerin, V.; Chernichenko, K.; Leskelä, M.; Repo, T. *Dalton Trans.* **2012**, *41*, 4310-4312. (e) Zeonjuk, L. L.; Vankova, N.; Mavrandonakis, A.; Heine, T.; Röschenthaler, G. V.; Eicher, J. *Chem. – Eur. J.* **2013**, *19*, 17413-17424.

(16) Adduci, L. L.; McLaughlin, M. P.; Bender, T. A.; Becker, J. J.; Gagné, M. R. *Angew. Chem., Int. Ed.* **2014**, *53*, 1646-1649. (b) Zhang, Z. Y.; Liu, Z. Y.; Guo, R. T.; Zhao, Y. Q. Li, X.; Wang, X. C. *Angew. Chem., Int. Ed.* **2017**, *56*, 4028-4032.

(17) Schwier, T.; Gevorgyan, V. *Org. Lett.* **2005**, *7*, 5191-5194.

(18) (a) Fasano, V.; Radcliffe, J. E.; Ingleson, M. J. *ACS Catal.*, **2016**, *6*, 1793-1798. (b) Gandhamsetty, N.; Joung, S.; Park, S. W.; Park, S.; Chang, S. *J. Am. Chem. Soc.* **2014**, *136*, 16780-16783.

(19) Schwier, T.; Rubin, M.; Gevorgyan, V., B(C₆F₅)₃-Catalyzed Allylation of Propargyl Acetates with Allylsilanes. *Org. Lett.* **2004**, *6*, 1999-2001.

(20) Chatterjee, I.; Qu, Z. W.; Grimme, S.; Oestreich, M. *Angew. Chem., Int. Ed.* **2015**, *54*, 12158-12162.

(21) For a review of transfer hydrosilylation, see: (a) Oestreich, M. *Angew. Chem., Int. Ed.* **2016**, *55*, 494-499. (b) Simonneau, A.; Friebel, J.; Oestreich, M. *Eur. J. Org. Chem.* **2014**, *2014*, 2077-2083.

(22) Keess, S.; Oestreich, M. *Chem. Sci.* **2017**, *8*, 4688-4695.

(23) (a) Timoshkin, A. Y.; Frenking, G. *Organometallics* **2008**, *27*, 371-380. (b) Kim, H. W.; Rhee, Y. M. *Chem.-Eur. J.* **2009**, *15*, 13348-13355. (c) Durfey, B. L.; Gilbert, T. M. *Inorg. Chem.* **2011**, *50*, 7871-7879. (d) Mück, L. A.; Timoshkin, A.Y.; Frenking, G. *Inorg. Chem.* **2012**, *51*, 640-646.

(24) (a) Fujimoto, H.; Sakata, K. *J. Am. Chem. Soc.* **2008**, *130*, 12519-12526. (b) Fujimoto, H.; Sakata, K. *J. Org. Chem.* **2013**, *78*, 3095-3103. (c) Fujimoto, H.; Sakata, K., *Organometallics*, **2015**, *3*, 236-241.

- (25) (a) Chen, Y. X. E.; Marks, T. J. *Chem. Rev.* **2000**, *100*, 1391-1434. (b) Delferro, M.; Marks, T. J. *Chem. Rev.* **2011**, *111*, 2450-2485. (c) Duchateau, R. *Chem. Rev.* **2002**, *102*, 3525-3542. (d) Aoshima, S.; Kanaoka, S. *Chem. Rev.* **2009**, *109*, 5245-5287.
- (26) Yin, Q.; Klare, H. F. T.; Oestreich, M. *Angew. Chem., Int. Ed.* **2017**, *56*, 3712-3717.
- (27) Simonneau, A.; Oestreich, M. *Nature Chemistry* **2015**, *7*, 816-822.
- (28) Simonneau, A.; Oestreich, M., PCT *International Patent Application* WO 2015036309 A1 20150319 (**2015**).
- (29) (a) DHHS. NIOSH Pocket Guide to Chemical Hazards 279 (Department of Health and Human Services, US Government Printing Office, 2007). (b) Chen, J. R. *Process Saf. Prog.* **2002**, *21*, 19-25. (c) Wu, C.C.; Lee, Y.C.; Kuan, C.M.; Shen, C.C.; Hu, S.C.; Pan, H.R.; Chen, S.K.; Tsai, H.Y.; Chen, J. R. *Process Saf. Prog.* **2006**, *25*, 237-244. (d) Chang, Y. Y., Peng, D. J., Wu, H. C., Tsaur, C. C., Shen, C. C., Tsai, H. Y.; Chen, J. R. *Process Saf. Prog.* **2007**, *26*, 155-158.
- (30) (a) Matsumura, H. *Jpn J. Appl. Phys.* **1998**, *37*, 3175-3187. (b) Roca i Cabarrocas, P., *Curr. Opin. Solid State Mater. Sci.* **2002**, *6*, 439-444. (c) Schmidt, V.; Wittemann, J. V.; Senz, S.; Gosele, U. *Adv. Mater.* **2009**, *21*, 2681-2702. (d) Schmidt, V.; Wittemann, J. V.; Gosele, U. *Chem. Rev.* **2010**, *110*, 361-388.
- (31) (a) Ojima, I.; Patai, S.; Rappoport, Z., *The Chemistry of Organic Silicon Compounds*. Eds.; Wiley: New York, **1989**, 1687-1792. (b) Marciniak, B., *Hydrosilylation: A Comprehensive Review on Recent Advances*. Pergamon: New York, **1992**. 1-407.
- (32) (a) Simonneau, A.; Oestreich, M. *Angew. Chem., Int. Ed.* **2013**, *52*, 11905-11907. (b) Keess, S.; Simonneau, A.; Oestreich, M. *Organometallics*, **2015**, *34*, 790-799.
- (33) Rubin, M.; Schwier, T.; Gevorgyan, V., Highly Efficient B(C₆F₅)₃-Catalyzed Hydrosilylation of Olefins. *J. Org. Chem.* **2002**, *67*, 1936-1940.

(34) (a) Blackwell, J. M.; Foster, K. L.; Beck, V. H.; Piers, W. E. *J. Org. Chem.* **1999**, *64*, 4887-4892. (b) Gevorgyan, V.; Liu, J. X.; Rubin, M.; Benson, S.; Yamamoto, Y. *Tetrahedron Lett.* **1999**, *40*, 8919-8922. (c) Gevorgyan, V.; Rubin, M.; Benson, S.; Liu, J. X.; Yamamoto, Y. *J. Org. Chem.* **2000**, *65*, 6179-6186.

(35) (a) Lapkin, I. I.; Povarnitsyna, T. N.; Anvarova, G. Ya. *Zhurnal Obshchei Khimii* **1965**, *35*, 1835-1839. (b) Calas, R. *Pure and Applied Chemistry* **1966**, *13*, 61-79. (c) Lapkin, I. I.; Povarnitsyna, T. N., *Zhurnal Obshchei Khimii* **1968**, *38*, 643-647. (d) Doyle, M. P.; West, C. T.; Donnelly, S. J.; McOsker, C. C. *J. Organomet. Chem.* **1976**, *117*, 129-140. (e) Fry, J. L.; Orfanopoulos, M.; Adlington, M. G.; Dittman Jr., W. R. Silverman, S. B. *J. Org. Chem.* **1978**, *43*, 374-375. (f) Parks, D. J.; Piers, W. E., *J. Am. Chem. Soc.* **1996**, *118*, 9440-9441. (g) Parks, D. J.; Blackwell, J. M.; Piers, W. E. *J. Org. Chem.* **2000**, *65*, 3090-3098. (h) Rendler, S.; Oestreich, M. *Angew. Chem., Int. Ed.* **2008**, *47*, 5997-6000. (i) Fujimoto, H.; Sakata, K. *J. Org. Chem.* **2013**, *78*, 12505-12512.

(36) Ioana, S., Mechanism of Autocatalytic Reactions, ISBN 3659649783, 9783659649783, **2014**, 1-64.

(37) Chatterjee, I.; Oestreich, M. *Org. Lett.* **2016**, *18*, 2463-2466.

(38) Lefranc, I.; Qu, Z.-W.; Grimme, S.; Oestreich, M. *Chem. Eur. J.* **2016**, *22*, 10009-10016.

(39)(a) Hohenberg, P.; Kohn, W. *Phys. Rev.* **1964**, *136*, B864-B871. (b) Kohn, W.; Sham, L. J. *Phys. Rev.* **1965**, *140*, A1133-A1138.

(40) (a) Zhao, Y.; Truhlar, D. G. *Theor. Chem. Acc.* **2008**, *120*, 215-241. (b) Zhao, Y.; Truhlar, D. G. *Acc. Chem. Res.* **2008**, *41*, 157-167.

(41) TURBOMOLE V7.0 2015, a development of University of Karlsruhe an Forschungszentrum Karlsruhe GmbH, 1989-2007, TURBOMOLE GmbH, since 2007; available from <http://www.turbomole.com>.

- (42) Ansgar, S.; Christian, H.; Reinhart, A. *The Journal of Chemical Physics* **1994**, *100*, 5829-5835.
- (43) Perdew, J. P.; Burke, K.; Ernzerhof, M. *Phys. Rev. Lett.* **1996**, *77*, 3865-3868.
- (44) (a) Grimme, S.; Antony, J.; Ehrlich, S.; Krieg, H. *The Journal of Chemical Physics* **2010**, *132*, 154104/1-154104/19. (b) Grimme, S.; Ehrlich, S.; Goerigk, L. *J. Comput. Chem.* **2011**, *32*, 1456-1465.
- (45) Klamt, A.; Schuurmann, G. *J. Chem. Soc. Perkin Trans.* **1993**, *0*, 799-805.
- (46) (a) Eichkorn, K.; Treutler, O.; Öhm, H.; Häser, M.; Ahlrichs, R. *Chem. Phys. Lett.* **1995**, *240*, 283-290. (b) Eichkorn, K.; Weigend, F.; Treutler, O.; Ahlrichs, R. *Theor. Chem. Acc.* **1997**, *97*, 119-124.
- (47) (a) Sierka, M.; Hogeckamp, A.; Ahlrichs, R. *The Journal of Chemical Physics* **2003**, *118*, 9136-9148. (b) Deglmann, P.; May, K.; Furche, F.; Ahlrichs, R. *Chem. Phys. Lett.* **2004**, *384*, 103-107.
- (48) Tao, J.; Perdew, J. P.; Staroverov, V. N.; Scuseria, G. E. *Phys. Rev. Lett.* **2003**, *91*, 146401/1-146401/4.
- (49) (a) Weigend, F.; Häser, M.; Patzelt, H.; Ahlrichs, R. *Chem. Phys. Lett.* **1998**, *294*, 143-152. (b) Weigend, F.; Ahlrichs, R. *Phys. Chem. Chem. Phys.* **2005**, *7*, 3297-3305.
- (50) Zhao, Y.; Truhlar, D. G. *J. Phys. Chem. A.* **2005**, *109*, 5656-5667.
- (51) Weigend, F.; Furche, F.; Ahlrichs, R. *The Journal of Chem. Phys.* **2003**, *119*, 12753-12762.
- (52) Fukui, K. *Acc. Chem. Res.* **1981**, *14*, 363-368.
- (53) Mammen, M.; Shakhnovich, E. I.; Deutch, J. M.; Whitesides, G. M. *J. Org. Chem.* **1998**, *63*, 3821-3830.

(54) Frisch, M. J.; Trucks, G. W.; Schlegel, H. B.; Scuseria, G. E.; Robb, M. A.; Cheeseman, J. R.; Scalmani, G.; Barone, V.; Mennucci, B.; Petersson, G. A.; Nakatsuji, H.; Caricato, M.; Li, X.; Hratchian, H. P.; Izmaylov, A. F.; Bloino, J.; Zheng, G.; Sonnenberg, J. L.; Hada, M.; Ehara, M.; Toyota, K.; Fukuda, R.; Hasegawa, J.; Ishida, M.; Nakajima, T.; Honda, Y.; Kitao, O.; Nakai, H.; Vreven, T.; Montgomery, Jr., J. A.; Peralta, J. E.; Ogliaro, F.; Bearpark, M.; Heyd, J. J.; Brothers, E.; Kudin, K. N.; Staroverov, V. N.; Kobayashi, R.; Normand, J.; Raghavachari, K.; Rendell, A.; Burant, J. C.; Iyengar, S. S.; Tomasi, J.; Cossi, M.; Rega, N.; Millam, J. M.; Klene, M.; Knox, J. E.; Cross, J. B.; Bakken, V.; Adamo, C.; Jaramillo, J.; Gomperts, R.; Stratmann, R. E.; Yazyev, O.; Austin, A. J.; Cammi, R.; Pomelli, C.; Ochterski, J. W.; Martin, R. L.; Morokuma, K.; Zakrzewski, V. G.; Voth, G. A.; Salvador, P.; Dannenberg, J. J.; Dapprich, S.; Daniels, A. D.; Farkas, Ö.; Foresman, J. B.; Ortiz, J. V.; Cioslowski, J.; Fox, D. J., Gaussian, Inc., Wallingford CT, 2009.

(55) Binkley, J. S.; Pople, J. A.; Hehre, W. J. *J. Am. Chem. Soc.* **1980**, *102*, 939-947.

(56) Tomasi, J.; Mennucci, B.; Cammi, R. *Chem. Rev.* **2005**, *105*, 2999-3094.

(57) Becke, A. D. *The Journal of Chemical Physics* **1993**, *98*, 5648-5652.

(58) (a) Kozuch, S.; Shaik, S. *J. Am. Chem. Soc.* **2006**, *128*, 3355-3365. (b) Kozuch, S.; Shaik, S. *J. Phys. Chem. A* **2008**, *112*, 6032-6041.

(59) Uhe, A.; Kozuch, S.; Shaik, S. *J. Comput. Chem.* **2011**, *32*, 978-985.

(60) Sakata, K.; Fujimoto, H. *Organometallics* **2015**, *34*, 236-241.

(61) Webb, J. D.; Laberge, V. S.; Geier, S. J.; Stephan, D. W.; Crudden, C. M. *Chem. Eur. J.* **2010**, *16*, 4895-4902.

(62) Gutsulyak, D. V.; van der Est, A.; Nikonov, G. I. *Angew. Chem., Int. Ed.* **2011**, *50*, 1384-1387.

(63) For the crystal structure of the $\text{Et}_3\text{Si}(\text{toluene})^+$ cation, see: (a) Lambert, J. B.; Zhao, Y., *Angew. Chem., Int. Ed.* **1997**, *36*, 400-401. (b) Reed, C. A. *Acc. Chem. Res.* **1998**, *31*, 325-332.

(64) For theoretical studies of the σ complex: (a) Schleyer, P. v. R.; Buzek, P.; Müller, T.; Apeloig, Y.; Siehl, H. U. *Angew. Chem., Int. Ed.* **1993**, *32*, 1471-1473. (b) Olsson, L.; Cremer, D. *Chem. Phys. Lett.* **1993**, *215*, 433-443. (c) Olah, G. A.; Rasul, G.; Li, X.-Y.; Buchholz, H. A. Sandford, G.; Prakash, G. K. S., *Science* **1994**, *263*, 983-984.

(65) (a) Lambert, J. B.; Zhang, S.; Stern, C. L.; Huffman, J. C., *Science* **1993**, *260*, 1917-1918.

(66) For the preparation of donor-stabilised silylium ions from cyclohexa-2,5-dien-1-yl-substituted silanes, see: Simonneau, A.; Biberger, T.; Oestreich, M. *Organometallics*, **2015**, *34*, 3927-3929.

(67) As suggested by Professor Sebastian Kozuch, during discussions of the energy profiles shown in Figures 3.2 and 3.3.

(68) Hehre, W. J.; Radom, L.; Schleyer, P. v. R.; Pople, J., A. *Ab Initio Molecular Orbital Theory* Wiley: New York, **1986**.

(69) Heiden, Z. M.; Lathem, A. P. *Organometallics*, **2015**, *34*, 1818-1827.

(70) (a) Houghton, A. Y.; Hurmalainen, J.; Mansikkamäki, A.; Piers, W. E.; Tuononen, H. M. *Nature Chem.* **2014**, *6*, 983-988. (b) Houghton, A. Y.; Karttunen, V. A.; Piers, W. E.; Tuononen, H. M. *Chem. Commun.*, **2014**, *50*, 1295-1298.

(71) Ma, Y.; Wang, B.; Zhang, L.; Hou, Z. *J. Am. Chem. Soc.* **2016**, *138*, 3663-3666.

(72) Kim, D. W.; Joung, S.; Kim, J. G. Chang, S. *Angew. Chem., Int. Ed.* **2015**, *54*, 14805-14809.

(73) Farrell, J. M.; Heiden, Z. M.; Stephan, D. W. *Organometallics* **2011**, *30*, 4497-4500.

(74) Blackwell, J. M.; Sonmor, E. R.; Scoccitti, T.; Piers, W. E. *Org. Lett.* **2000**, *2*, 3921-3923.

(75) Chatterjee, I.; Oestreich, M. *Angew. Chem., Int. Ed.* **2015**, *54*, 1965-1968.

- (76) Geier, S. J.; Stephan, D. W. *J. Am. Chem. Soc.* **2009**, *131*, 3476-3477.
- (77) Keess, S.; Oestreich, M. *Org. Lett.* **2017**, *19*, 1898-1901.
- (78) (a) Kamioka, S.; Ajami, D.; Jr. Rebek, J. *Chem. Commun.* **2009**, 7324-7326. (b) Kamioka, S.; Ajami, D.; Jr. Rebek, J. *PNAS*, **2010**, *107*, 541-544. (c) Brook, M. A.; Grand, J. B.; Ganachaud, F. *Silicone Polymers* **2010**, *235*, 161-183. (d) Bisette, A. J.; Fletcher, S. P., *Angew. Chem., Int. Ed.* **2013**, *52*, 12800-12826. (e) Plasson, R.; Brandenburg, A.; Jullien, L.; Bersini, H. *J. Phys. Chem. A* **2011**, *115*, 8073-8085.
- (79) (a) Valente, A.; Mortreux, A.; Visseaux, M.; Zinck, P. *Chem. Rev.* **2013**, *113*, 3836-3857. (b) Jr. Starnes, W. H.; Ge, X., *Macromolecules* **2004**, *37*, 352-359. (c) Thompson, D. B.; Brook, M. A. *J. Am. Chem. Soc.* **2008**, *130*, 32-33. (d) Moitra, N.; Ichii, S.; Kamei, T.; Kanamori, K.; Zhu, Y.; Takeda, K.; Nakanishi, K.; Shimada, T. *J. Am. Chem. Soc.* **2014**, *136*, 11570-11573.

Chapter 4
**The Role of Ion-pair in $B(C_6F_5)_3$ Catalyzed
Zwitterionic Chemistry**

Chapter 4

The Role of Ion-pair in $B(C_6F_5)_3$ Catalyzed Zwitterionic Chemistry

Abstract

In homogeneous Ziegler–Natta chemistry, tris(pentafluorophenyl)borane ($B(C_6F_5)_3$) is well recognised for its role as a good activator component. However, due to its unique features, $B(C_6F_5)_3$ is becoming a more often employed catalyst or stoichiometric reagent in organic and organometallic chemistry. However, what the current computational work, with density functional theory (DFT), reveals that what could be the benchmark for the ion-pair to be considered as separated or non-separated species in all the $B(C_6F_5)_3$ induced reactions. The simple free energy calculations show the way how to predict whether the ion-pairs are separated or not. The results are further corroborated by the use of the energetic span model (ESM), which shows that the turnover frequency (TOF) is higher for the reaction when it goes through a separated species. The current work therefore provides interesting new insights into the $B(C_6F_5)_3$ induced reactions.

4.1 Introduction

Bjerrum¹ proposed the ion-pair concept²⁻⁵ in 1926 to explain the behaviour of ionophores (species that are ionic in the crystalline form but exist as ions in the fused state and in dilute solutions) in solvents with low relative permittivity. Generally ion pairs in solvent are described as pair of oppositely charged ions with a shared solvation shell that are bound together primarily by Coulombic interactions and have (a) lives sufficiently longer than Brownian motion's correlation time (kinetic stability) and (b) a binding energy greater than kT (thermodynamic stability). A contact (or intimate or tight) ion pair is one in which there is no solvent molecule between the two ions (Figure 4.1). It's also known as the (partial) association of oppositely charged ions in electrolyte solutions, which results in the formation of separate chemical species. The most logical explanation for some sorts of direct experimental evidence or discrepancies found at intermediate concentrations from predictions of electrolyte theories that precisely explain the features of very dilute electrolyte solutions is ion pair creation. If the ion association is strong enough (the value varies depending on the charges on the ions and the relative permittivity of the solvent, but it roughly corresponds to an association constant, of 1000 M^{-1} in water, where $\text{M}=\text{mol}/\text{dm}^3$), separating the properties of the ion pair from the long-range nonspecific ion-ion interactions that exist in all electrolyte solutions is usually not difficult. When the ion connection is weak, however, there is a substantial link between nonspecific ion-ion interactions (as measured by activity coefficients) and the creation of ion pairs (characterized in terms of an association constant). The often quoted saying of Onsager⁶ is appropriate here: “The distinction between free ions and associated pairs depends on an arbitrary convention.... In a complete theory this does not matter; what we remove from one page of the ledger would be entered elsewhere with the same effect.” From a more practical standpoint, Robinson and Stokes⁷ comment: “The chief criterion for [classifying] an electrolyte [as non-associated] is the absence of valid evidence for any form of association. Since the validity of such evidence can be a matter of personal opinion...there can be no general agreement.”

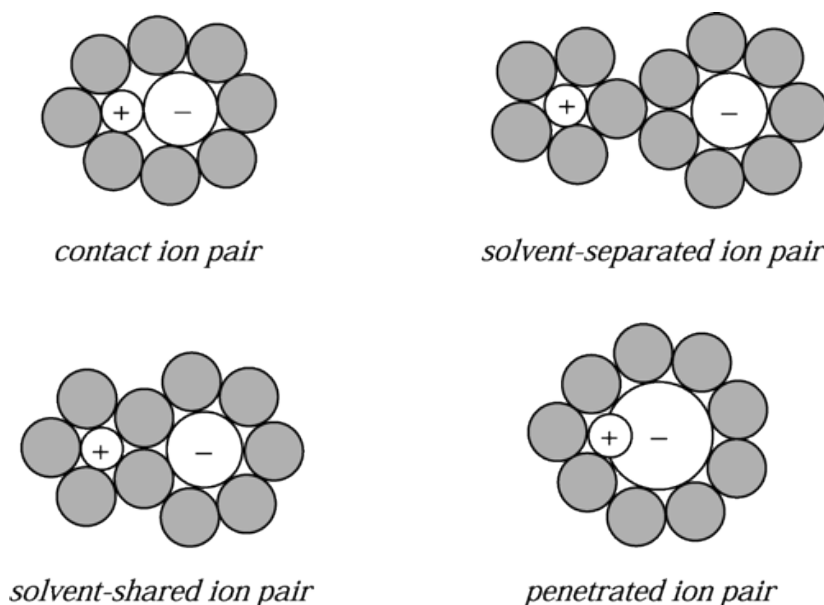


Figure 4.1 Showing possibilities of ion-pair in solvent bounded systems.

The significance of ion pairing in organic chemistry has long been acknowledged.⁸⁻¹⁰ Only in the last few decades, $B(C_6F_5)_3$ catalysed complex ion-pair been thoroughly researched. The electronic properties of $B(C_6F_5)_3$'s three C_6F_5 rings give it a high Lewis acidity, making it a useful reagent for a wide range of reactions.¹¹ Furthermore, the steric bulk of these rings allows it to act as the Lewis acid in an FLP, giving this reagent still another synthetic use. However, as main-group chemistry develops as a science, additional reagents beyond BCF are needed, expanding not just the variety of reactions but also the range of compounds that may be synthesised. Great efforts have already been achieved in this direction on recent boron chemistry advancements related to borylation processes. $B(C_6F_5)_3$ (often known as BCF) has been shown to be useful in a range of processes, including borylation,¹² hydrogenation,¹³ hydrosilylation,¹⁴ frustrated Lewis pair (FLP) chemistry,¹⁵ and more.¹⁶ It has always been observed that all the reactions involved *via* $B(C_6F_5)_3$ pathway goes through hydride abstraction. Once the hydride abstraction takes place the hydride donor and hydride acceptor (here $B(C_6F_5)_3$) species forms the ion-pair complex. In this chapter I focus what is the fate of these ion-pair forms in the reaction medium. There could be two possibilities a) The ion-pair can be a non-separable zwitterionic species which can further proceed into the reaction generating product and regenerate the catalyst

and b) The ion-pair can be loosely bound to each other which can create a possibility of separated cation and anion. If the second process happens then the reaction goes through an autocatalytic way. But what will be the benchmark to decide whether the ion-pairs will separate or not? This is the question addressed in this chapter.

4.2 Computational Details

All the calculations for the structures reported in this chapter of thesis have been done using density functional theory (DFT).^{17,18} The calculations have been carried out with Turbomole 7.0¹⁹ using the TZVP²⁰ basis set. Geometry optimizations were performed using the Perdew, Burke, and Ernzerhof functional (PBE).²¹ Dispersion corrections (D3)²² have been included in all the calculations. Solvent corrections have also been included in all the calculations using the Cosmo model,²³ Therefore the level of theory employed is PBE-D3/TZVP+COSMO(CH₂Cl₂).^{20,21,23} The resolution of identity (RI)²⁴ along with the multipole accelerated RI (marij)²⁵ approximations have been used for an accurate and efficient treatment of the electronic Coulomb term in the DFT calculations. Furthermore, in order to underscore the reliability of the calculations, all the geometry optimizations have also been done at the TPSS-D3/def2-TZVP+COSMO(CH₂Cl₂)^{26,27,23} level of theory. The results from both the levels of theory: PBE-D3/TZVP+COSMO(CH₂Cl₂) and TPSS-D3/def2-TZVP+COSMO(CH₂Cl₂) are shown together with the superscripts “a” and “b” respectively in all the tables in this chapter of thesis. Furthermore, all the figures in this chapter of thesis showing the free energy profiles have two profiles, one each for the PBE-D3/TZVP+COSMO(CH₂Cl₂) and the TPSS-D3/def2-TZVP+COSMO(CH₂Cl₂) levels of theory. In addition to these calculations, single point calculations at the PW6B95-D3/def2-QZVP+COSMO(CH₂Cl₂)^{28,29,23} level of theory have also been done, on the geometries optimized at the TPSS-D3/def2-TZVP+COSMO(CH₂Cl₂) level. In other words, the TPSS-D3/def2-TZVP+COSMO(CH₂Cl₂)/PW6B95-D3/def2-QZVP+COSMO(CH₂Cl₂) level of theory has also been employed to investigate all the catalytic cycles that have been discussed in this chapter of thesis. This is the similar level to that employed by Oestreich and co-workers in their investigations into similar systems.³⁰ For the

purpose of clarity, we will henceforth denote PBE-D3/TZVP+COSMO(CH₂Cl₂) as PTC(DCM) and TPSS-D3/def2-TZVP+COSMO(CH₂Cl₂) as TDC(DCM) in the thesis. Necessary care was taken to ensure that the obtained transition state structures possessed only one imaginary frequency corresponding to the correct normal mode, in order to obtain more reliable energy values for the investigated potential energy surface. In addition, intrinsic reaction coordinate (IRC)³¹ calculations were done with all the transition states in order to further confirm that they were the correct transition states, yielding the correct reactant and product structures. The values reported in this chapter of thesis are ΔG values, with zero point energy, internal energy, and entropic contributions, with the temperature taken to be 298.15K. The calculation of the translational entropy in standard software involves assumptions about the volume that may be inaccurate. The translational entropy term can be corrected by a free volume correction introduced by Mammen and co-workers.³² Based on the Sackur-Tetrode equation, the free volume model describes the translational entropy of molecules in the solution ($\Delta S_{\text{trans}}(\text{sol})$); and provides physically intuitive corrections for translational entropy values. In the free volume model, it has been assumed that the volume available to the molecule in solution is lower than the total volume, and this “free volume” is determined by the equation (1) below:

$$V_{\text{free}} = C_{\text{free}} \left(\sqrt[3]{\frac{10^{27}}{[X]N_0}} - \sqrt[3]{V_{\text{molecule}}} \right)^3 \quad 4.1$$

Here, V_{molec} is the molecular volume, $[X]$ is the concentration of molecules (mol/L) in solution and N_0 is the Avogadro number. The translational entropy can be obtained after considering the free volume correction, and inserting the value of V_{free} in the Sackur-Tetrode equation. The total entropy is then calculated by adding the corrected translational entropy and the entropic contributions from the rotational and vibrational components. It is to be noted that entropic contributions have been properly handled in every mechanism that has been studied and reported here. For bimolecular reactions where two species had to come together for the reaction to occur, the barrier for the reactions has always been calculated with the reactants assumed initially to have been at infinite separation, and not from a pre-reactive complex.

4.2.1 The Energetic Span Model

The efficiency of the catalytic cycle can be analyzed through the Energetic Span Model (ESM), put into practical use by Shaik and coworkers.^{33,34} The ESM provides a straightforward method to calculate the turnover frequencies (TOFs) of catalytic cycles based on their computed energy profiles. In most cases, the TOF is determined by the TOF-determining transition state (TDTS), the TOF-determining intermediate (TDI) and by the reaction energy, ΔG_r . The TOF calculation formula is as below:

$$\text{TOF} = \frac{k_B T}{h} e^{-\delta E/RT} \quad 4.2$$

where δE is the energy span and is defined as the difference in the Gibbs energy between the TDTS and the TDI, with the addition of the ΔG_r when the TDTS appears before the TDI. δE is the effective activation barrier of the global reaction. The TDTS and TDI are the intermediate and the transition states respectively that maximize δE , according to equation 4.2.

$$\delta E = \begin{cases} \delta_{TDTS} - \delta_{TDI} & \text{if TDTS appears after TDI} \\ \delta_{TDTS} - \delta_{TDI} + \Delta G_r & \text{if TDTS appears before TDI} \end{cases} \quad 4.3$$

This model has been employed to calculate the TOFs (at 298 K). The energetic span model can be applied in a user friendly way with the recently developed AUTOF computer program.^{33,34}

4.3 Results and Discussion

What the previous chapter made clear is the significant difference between the perceived role of $B(C_6F_5)_3$ in the formation of SiH_4 from SiR_3H , and the reality, which is that $B(C_6F_5)_3$ acts less as a pure catalyst, and more as an initiator and then a spectator in the entire, multi-step process. This leads to a much larger, and very interesting question: since there are many metal-free chemical transformations that have emerged in recent years where $B(C_6F_5)_3$ has been considered to act as a catalyst,⁸⁻¹⁶ in how many of them is $B(C_6F_5)_3$ really the catalyst, and in how many is it acting more as an initiator? One means of answering the question is by investigating the hydricities of borohydrides,³⁵ but a potentially simpler solution lies in looking at

the ease of separation of the cation from the ion-pair created when $B(C_6F_5)_3$ reacts with the substrate. In the case of the surrogate silicon chemistry, for instance, once the zwitterionic complex (ion-pair B), was formed, the total separation of the cation from the ion-pair required only 8.5 kcal/mol additional energy, at the PTC(DCM) level of theory (see Figure 4.1).

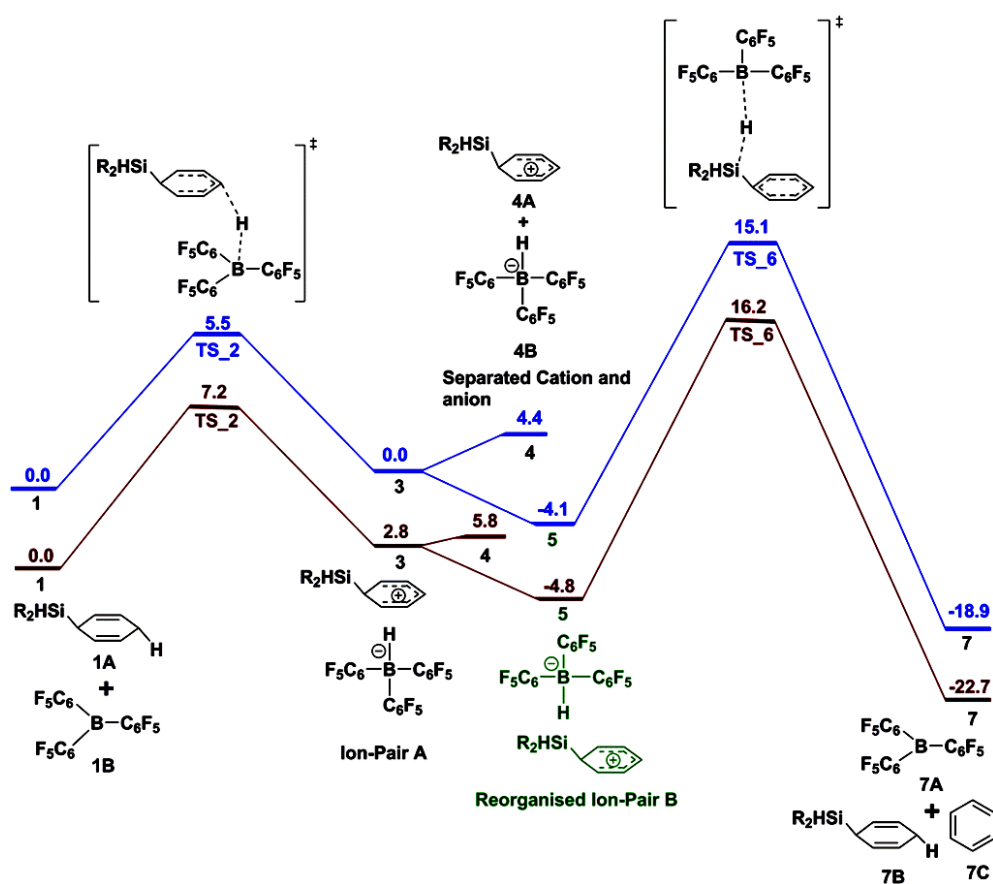


Figure 4.2 The free energy profile (ΔG) in kcal/mol for the proposed mechanism by Simonneau and Oestreich. R=cyclohexa-1,4-diene. The blue profile is for the PTC(DCM) level of theory and the brown profile is for the TDC(DCM) level of theory.

Thus, the cation would exist as a loosely bound ion-pair in solution, and the subsequent autocatalytic processes could thus emerge as an alternative. Hence, the ΔG of total separation of the cation from the ion-pair can provide a reliable parameter for how loosely bound the cation would be in solution to the ion-pair. But, what value of

the ΔG of total separation can be considered facile? A good indicator for this would be the initiator chemistry for the electrophilic C–H borylation of electron-rich (hetero)arenes done at room temperature by Oestreich and co-workers³⁶ that had been mentioned earlier in the Introduction. Here, the $B(C_6F_5)_3$ had been clearly noted by Oestreich *et al.* to act as the initiator, and therefore the determination of the ΔG of separation of the ion-pairs for these cases can serve as an upper bound for deciding the ΔG for the facile separation of ions in other reactions. We have therefore calculated the ease of separation of the ion-pairs formed in this case and found them to be 25.2 kcal/mol, 28.3 kcal/mol and 30.8 kcal/mol for the ΔG of separation of the ion-pairs $[CatB-(NMe_2Ph)_2]^+[HB(C_6F_5)_3]^-$, $[CatB-NMe_2Ph]^+[HB(C_6F_5)_3]^-$ and $[CatB-PhNMe_2]^+[HB(C_6F_5)_3]^-$ respectively at the PTC(DCM) level of theory (see Figure 4.3-4.5 below).

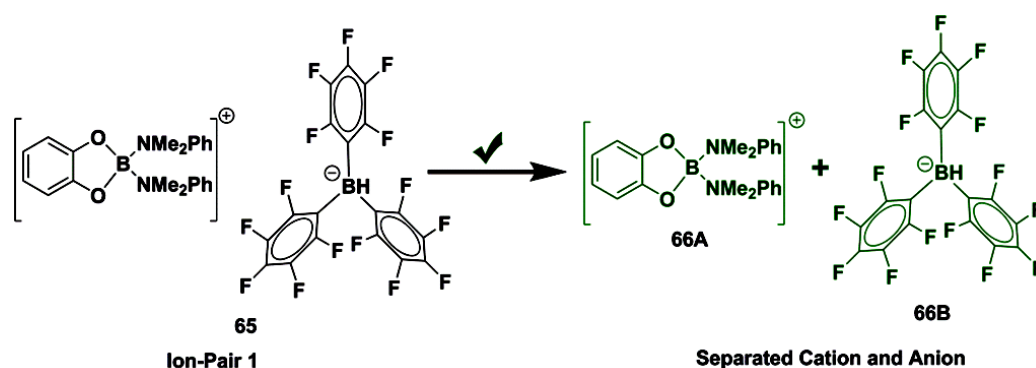


Figure 4.3 The separation of the ion-pair is favorable for the borane-silane zwitterionic complex shown in this figures (experimentally studied by Oestreich *et al.* *Angew. Chem., Int. Ed.* 2017, 56, 3712): the ΔG for this has been calculated to be 25.2 kcal/mol for the PTC(toluene) level of theory and 28.5 kcal/mol for the TDC(toluene) level of theory.

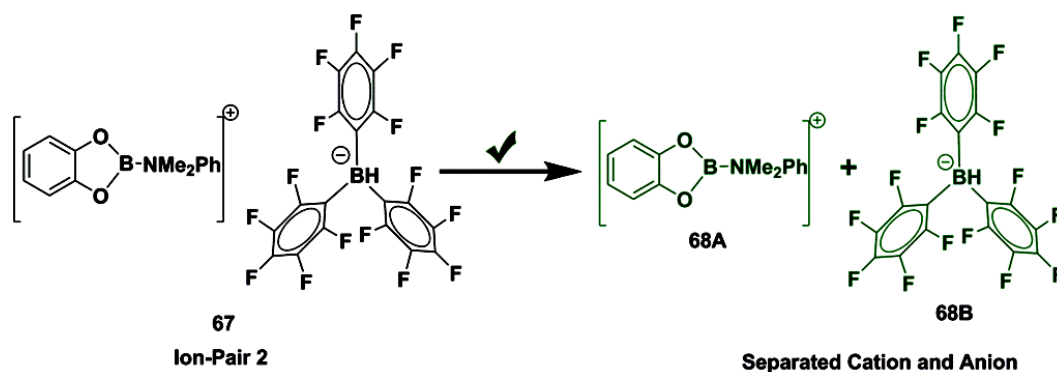


Figure 4.4 The separation of the ion-pair is favorable for the borane-silane zwitterionic complex shown in this figures (experimentally studied by Oestreich *et al.* *Angew. Chem., Int. Ed.* 2017, 56, 3712): the ΔG for this has been calculated to be 28.3 kcal/mol for the PTC(toluene) level of theory and 30.8 kcal/mol for the TDC(toluene) level of theory.

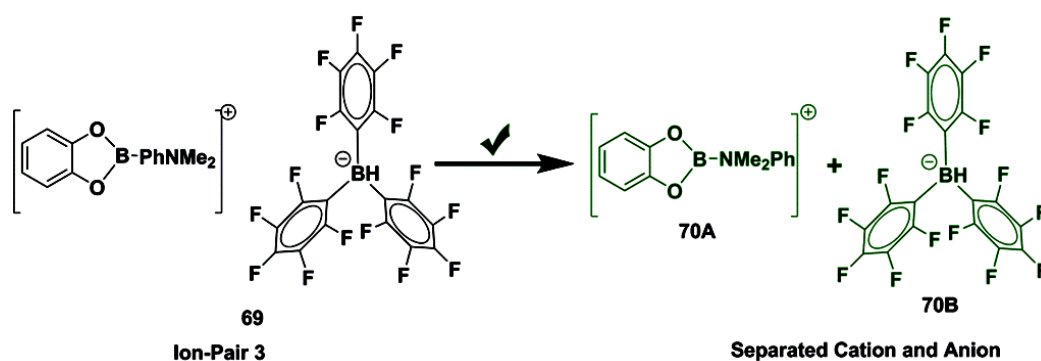


Figure 4.5 The separation of the ion-pair is favorable for the borane-silane zwitterionic complex shown in this figures (experimentally studied by Oestreich *et al.* *Angew. Chem., Int. Ed.* 2017, 56, 3712): the ΔG for this has been calculated to be 30.8 kcal/mol for the PTC(toluene) level of theory and 22.3 kcal/mol for the TDC(toluene) level of theory.

These values, then, can serve as a benchmark for determining the possibility of ion-pair dissociation at room temperature for other cases. One could also consider slightly higher ΔG values, of up to 35.0 kcal/mol using the PTC(DCM) level of theory, for experiments done at higher temperatures (100 °C to 120 °C). One should note that these values provide an *upper bound* to the energy required to separate the ion-pairs in

solution. In other words, what these values represent is the complete separation and isolation of the ions by the solvent in question. In reality, what is more likely is that the solvent would only serve to separate the ions and that they would remain in the same vicinity. However, the ions thus separated would be independent actors, each doing chemistry without interference (or assistance) from the other. In other words, the more likely scenario is that of solvent *separated* ions than solvent *isolated* ions. However, the values shown in Table 4.1, which represent the latter case, are still of significance, because they serve to provide the relative trend in the ease of ion-pair separation. That is, if an ion-pair in one case separates with ease to completely to form solvent isolated ions, this also indicates that it would show ease in forming solvent separated ions, in comparison to another case where the complete separation of the ions is less favored.

Now, considering the values of about 25.0-30.0 kcal/mol for room temperature dissociation of ions, and about 35.0 kcal/mol for dissociation at higher temperatures, as discussed above, admittedly, a perusal of the literature shows that there are cases in $B(C_6F_5)_3$ chemistry where the values for the separation of the cation from the ion-pair fall do not fall within this range. These include the formation of the zwitterionic species $[Et_3Si]^+[X]^-$ {X = 1,2,3-Tris(pentafluorophenyl)-4,5,6,7-tetrafluoro-1-boraindene anion: see structure provided below in Table 4.1} studied by Piers, Tuononen and co-workers,³⁷ (see Figure 4.6 below) where the ΔG is found to be 63.5 kcal/mol (see Table 4.1).

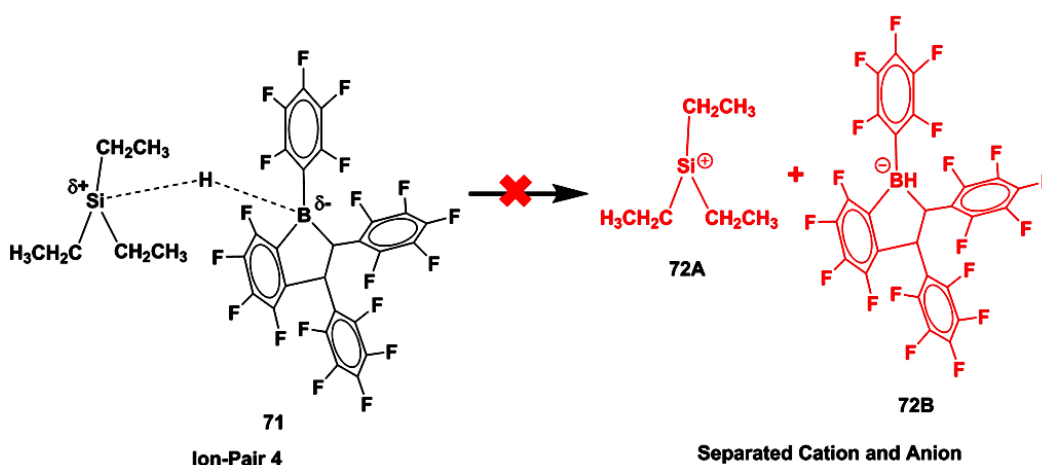


Figure 4.6 The separation of the ion-pair is unfavorable for the borane-silane zwitterionic complex shown in this figures (experimentally studied by Piers *et al. Nature Chem.* 2014, 6, 983): the ΔG for this has been calculated to be 63.5 kcal/mol for the PTC(toluene) level of theory and 68.8 kcal/mol for the TDC(toluene) level of theory.

In this case, it would be most likely that the ion-pair would not separate, and this is borne out by the experimental isolation of the $[\text{Et}_3\text{Si}]^+[\text{X}]^-$ crystal structure.³⁷ Therefore, $[\text{Et}_3\text{Si}]^+[\text{X}]^-$ would act as a frustrated Lewis pair (FLP), as believed(see Figure 4.6 above). This fact is further buttressed by the calculations that we have done (at the PTC(DCM) level of theory) that show the energy required to separate the $[\text{Et}_3\text{Si}]^+[\text{X}]^-$ ion-pair by 1.0 angstrom is as high as 25.3 kcal/mol. This is in contrast to : $[\text{SiR}_2\text{R}'\text{H}]^+[\text{HB}(\text{C}_6\text{F}_5)_3]^-$, and $[\text{PhSiMe}_2\text{-Olefin}]^+[\text{HB}(\text{C}_6\text{F}_5)_3]^-$ (see Figure 4.7) where the energy required to separate the two ions by 1.0 angstrom was only 0.7 and 1.2 kcal/mol respectively (the values for other ion-pairs are collected in Table 4.2 below).

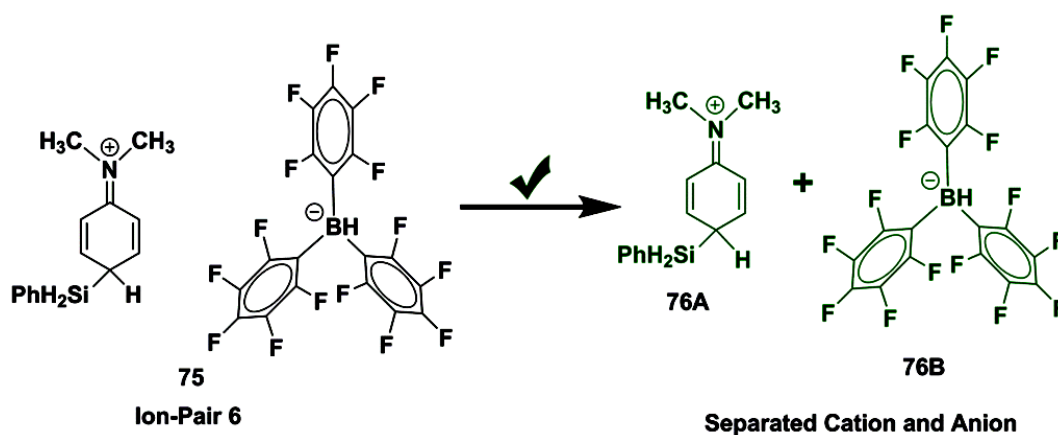


Figure 4.7 The separation of the ion-pair is favorable for the borane-silane zwitterionic complex shown in this figures (experimentally studied by Hou *et al. J. Am. Chem. Soc.* 2016, 138, 3663): the ΔG for this has been calculated to be 14.2 kcal/mol for the PTC(cholorobenzene) level of theory and 4.8 kcal/mol for the TDC(cholorobenzene) level of theory.

However, there are several other cases, which are also reported in Table 4.1 below, where the ΔG values do fall in the range where separation would be expected. Among these, there are some, like entry 6, where the formation of only a single ion-pair, $[(\text{PhCH})(\text{Ph})\text{N}(\text{SiHMe}_2\text{Ph})]^+[\text{HB}(\text{C}_6\text{F}_5)_3]^-$ is involved, which would yield the $[(\text{PhCH})(\text{Ph})\text{N}(\text{SiHMe}_2\text{Ph})]^+$ cation in a facile manner ($\Delta G = 24.8$ kcal/mol at room temperature(RT)) (see Table 4.1).

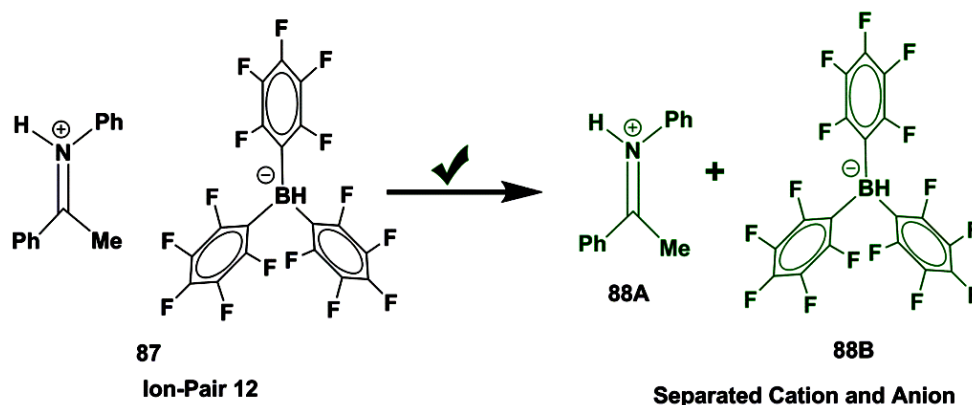


Figure 4.8 The separation of the ion-pair is favorable for the borane-silane zwitterionic complex shown in this figures (experimentally studied by Oestreich *et al. Angew. Chem., Int. Ed.* 2015, 54, 1965): the ΔG for this has been calculated to be 34.7 kcal/mol for the PTC(toluene) level of theory and 36.0 kcal/mol for the TDC(toluene) level of theory.

For such a case, it is highly likely that the cation would be taking part in autocatalytic processes similar to the ones that have been described in the previous section. It is easy to envisage an alternative pathway not involving $\text{B}(\text{C}_6\text{F}_5)_3$ as the catalyst that would yield the same products ($[(\text{PhCH})(\text{Ph})\text{NH}(\text{SiHMe}_2\text{Ph})]$, from toluene) as experimentally observed.³⁸ There are other cases, however, where two ion-pair species would be formed during the reaction, such as in the case of entry 4 in Table 4.1, which involves the formation of the $[\text{PhSi-Olefin}]^+[\text{HB}(\text{C}_6\text{F}_5)_3]^-$ and the $[\text{PhSiMe}_2\text{-Olefin}]^+[\text{HB}(\text{C}_6\text{F}_5)_3]^-$ ion-pairs (Olefin=1,4-diisopropenylbenzene). Here, while the separation of the cation from $[\text{PhSiMe}_2\text{-Olefin}]^+[\text{HB}(\text{C}_6\text{F}_5)_3]^-$ is seen to be very facile ($\Delta G = 14.2$ kcal/mol), the corresponding reaction for $[\text{PhSi-}$

Olefin]⁺[HB(C₆F₅)₃]⁻ is seen to be unfavorable ($\Delta G = 40.6$ kcal/mol) at the PTC(DCM) level of theory.

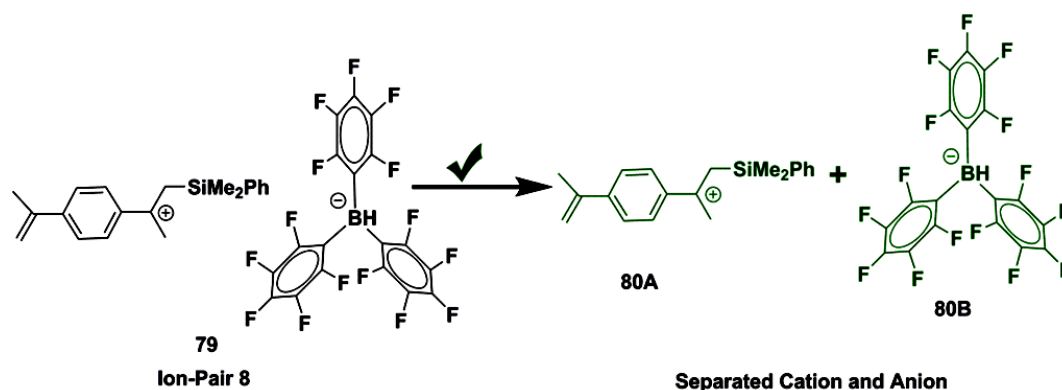


Figure 4.9 The separation of the ion-pair is favorable for the borane-silane zwitterionic complex shown in this figures (experimentally studied by Chang *et al.* *Angew. Chem., Int. Ed.* 2015, 54, 14805): the ΔG for this has been calculated to be 14.2 kcal/mol for the PTC(choloroform) level of theory and 13.3 kcal/mol for the TDC(choloroform) level of theory.

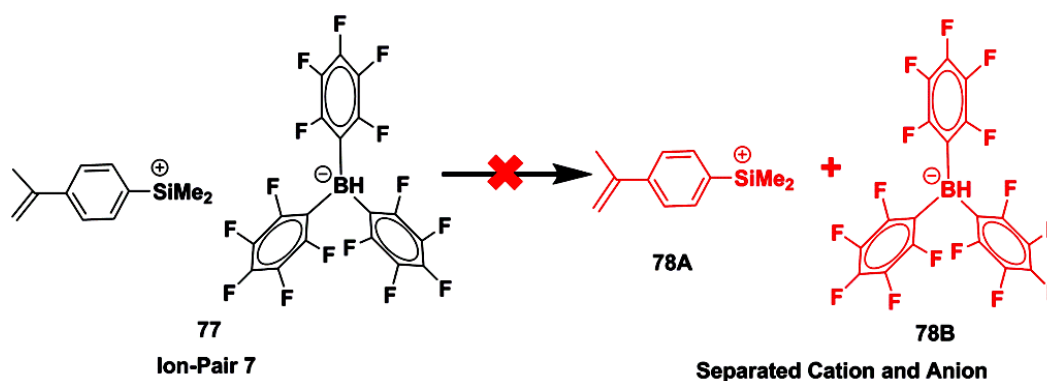


Figure 4.10 The separation of the ion-pair is unfavorable for the borane-silane zwitterionic complex shown in this figures (experimentally studied by Chang *et al.* *Angew. Chem., Int. Ed.* 2015, 54, 14805): the ΔG for this has been calculated to be 40.6 kcal/mol for the PTC(choloroform) level of theory and 42.3 kcal/mol for the TDC(choloroform) level of theory.

It is worth mentioning here that Chatterjee and Oestreich have discussed the possibility of Brønsted acid-catalyzed transfer hydrogenation of imines in a separate (experimental) investigation.³⁹ They have proposed a catalytic cycle based on $B(C_6F_5)_3$ and Brønsted acid catalysis. Earlier Grimme, Oestreich and co-workers had proposed transfer hydrogenation promoted by Ru-S complexes⁴⁰ based on experimental work supported by computation. It is, thus, important to note that Oestreich and co-workers had laid a path that researchers could follow, pertaining to mechanisms other than the $B(C_6F_5)_3$ Lewis acid catalyzed pathway.

Table 4.1 The calculated free energies, (ΔG , in kcal/mol) for the separation of the ion-pairs formed in the different experimentally studied reactions (references provided after the ion-pair formulae for each case) where $B(C_6F_5)_3$ has previously been considered to act as a catalyst. Cases where the separation is energetically non-feasible have been shown in shaded columns.

| Ion-pair | Temperature | Energy for the Separation of the Ion-Pair (ΔG^b , kcal/mol) |
|---|-----------------|--|
| 1. (a) $[CatB^a-(NMe_2Ph)_2]^+[HB(C_6F_5)_3]^{-41}$ | RT ^c | 25.2 ^a /28.5 ^b |
| (b) $[CatB-NMe_2Ph]^+[HB(C_6F_5)_3]^{-41}$ | RT | 28.3 ^a /30.8 ^b |
| (c) $[CatB-PhNMe_2]^+[HB(C_6F_5)_3]^{-41}$ | RT | 30.8 ^a /22.3 ^b |
| 2. $[Et_3Si]^+[X^d]^{-37}$ | RT | 63.5 ^a /68.8 ^b |
| 3. (a) $[PhSiH_2]^+[HB(C_6F_5)_3]^{-38}$ | 120°C | 48.7 ^a /52.2 ^b |
| (b) $[Me_2N(Ph-SiH_2Ph)]^+[HB(C_6F_5)_3]^{-38}$ | 120°C | 14.2 ^a /4.8 ^b |
| 4. (a) $[PhSi-Olefin^e]^+[HB(C_6F_5)_3]^{-42}$ | RT | 40.6 ^a /42.3 ^b |

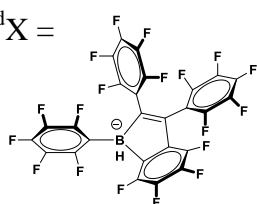
| | | |
|---|--------|--------------------------------------|
| (b) [PhSiMe ₂ -Olefin] ⁺ [HB(C ₆ F ₅) ₃] ⁻⁴² | RT | 14.2 ^a /13.3 ^b |
| 5. [NH ₂ (CHMePh) ₂] ⁺ [HB(C ₆ F ₅) ₃] ⁻⁴³ | 100 °C | 31.4 ^a /16.1 ^b |
| 6. [(PhCH)(Ph)N(SiHMe ₂ Ph)] ⁺ [HB(C ₆ F ₅) ₃] ⁻⁴⁴ | RT | 24.8 ^a /29.1 ^b |
| 7. (a) [1,3-dimethyl-2,4-cyclohexadiene] ⁺ [HB(C ₆ F ₅) ₃] ⁻⁴⁵ | 120 °C | 40.8 ^a /49.7 ^b |
| (b) [NH(Ph)(CMePh)] ⁺ [HB(C ₆ F ₅) ₃] ⁻⁴⁵ | 120 °C | 34.7 ^a /36.0 ^b |
| 8. [2,6-Me ₂ C ₅ H ₃ N] ⁺ [HB(C ₆ F ₅) ₃] ⁻⁴⁶ | RT | 31.9 ^a /28.0 ^b |

^aThe values pertaining to the barriers (ΔG kcal/mol) for the PTC(DCM) calculations.

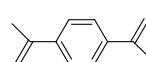
^bThe values pertaining to the barriers (ΔG kcal/mol) for the TDC(DCM) calculations.

^aCatB: Catecholborane; ^b $\Delta G = \{G_{[A^+]} + G_{[HB(C_6F_5)_3]^-}\} - \{G_{[A^+][HB(C_6F_5)_3]^-}\}$; ^cRT: Room

Temperature; ^dX =



^eOlefin =



4.3.1 The Formation of Different Favorable and Unfavorable Ion-Pairs as mentioned in the Table 4.1

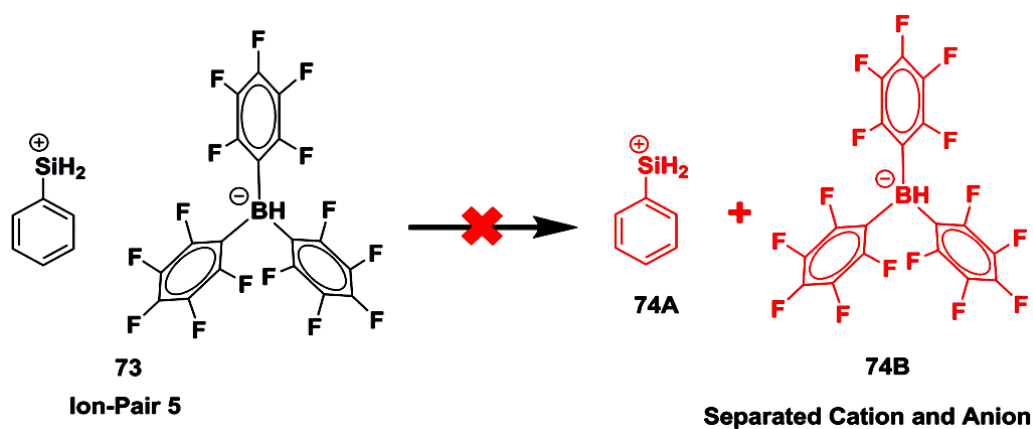


Figure 4.11 The separation of the ion-pair is unfavorable for the borane-silane zwitterionic complex shown in this figures (experimentally studied by Hou *et al.* *J. Am. Chem. Soc.* 2016, 138, 3663): the ΔG for this has been calculated to be 48.7 kcal/mol for the PTC(cholorobenzene) level of theory and 52.2 kcal/mol for the TDC(cholorobenzene) level of theory.

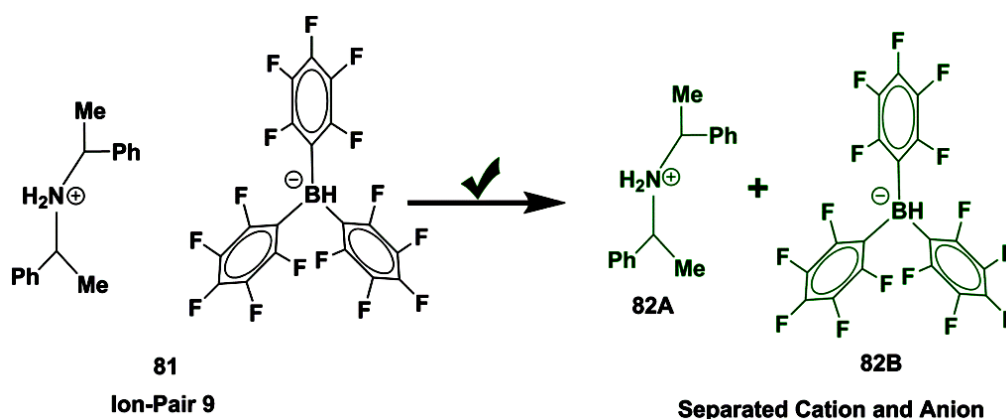


Figure 4.12 The separation of the ion-pair is favorable for the borane-silane zwitterionic complex shown in this figures (experimentally studied by Stephan *et al.* *Organometallics* 2011, 30, 4497): the ΔG for this has been calculated to be 31.4 kcal/mol for the PTC(toluene) level of theory and 16.1 kcal/mol for the TDC(toluene) level of theory.

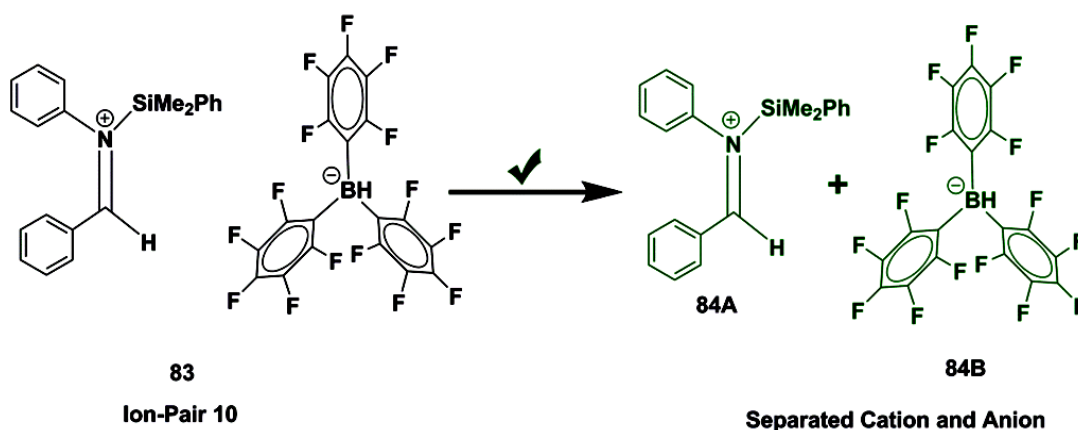


Figure 4.13 The separation of the ion-pair is favorable for the borane-silane zwitterionic complex shown in this figures (experimentally studied by Piers *et al.* *Org. Lett.* 2000, 2, 3921): the ΔG for this has been calculated to be 24.8 kcal/mol for

the PTC(toluene) level of theory and 29.1 kcal/mol for the TDC(toluene) level of theory.

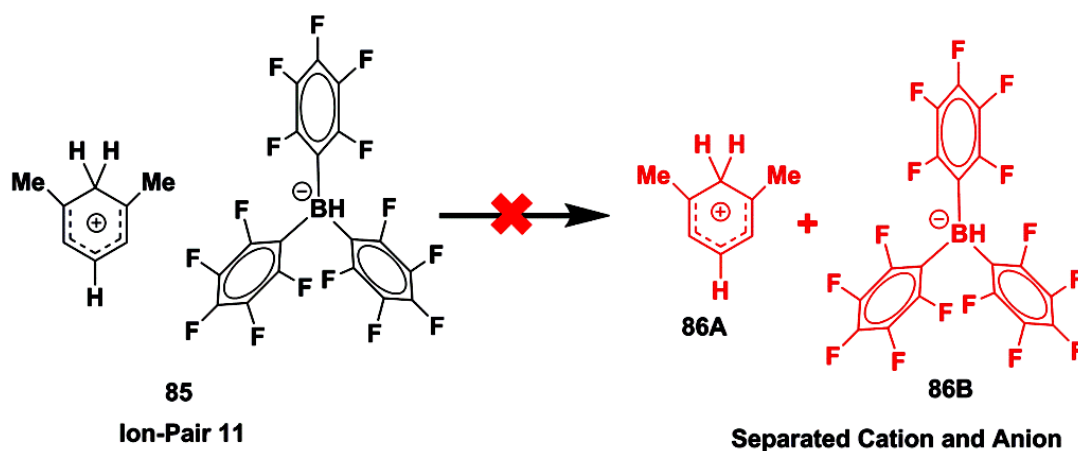


Figure 4.14 The separation of the ion-pair is unfavorable for the borane-silane zwitterionic complex shown in this figures (experimentally studied by Oestreich *et al.* *Angew. Chem., Int. Ed.* 2015,54, 1965): the ΔG for this has been calculated to be 40.8 kcal/mol for the PTC(toluene) level of theory and 49.7 kcal/mol for the TDC(toluene) level of theory.

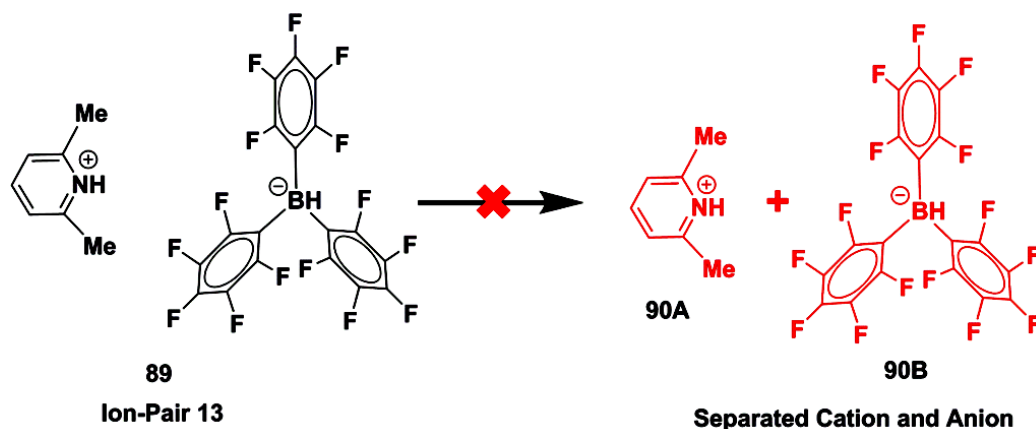


Figure 4.15 The separation of the ion-pair is unfavorable for the borane-silane zwitterionic complex shown in this figures (experimentally studied by Stephan *et al.* *J. Am. Chem. Soc.* 2009, 131, 3476): the ΔG for this has been calculated to be 31.9 kcal/mol for the PTC(toluene) level of theory and 28.0 kcal/mol for the TDC(toluene) level of theory.

In order to further verify whether the easily separated ion-pair would follow the autocatalytic mechanism or the $B(C_6F_5)_3$ catalyzed pathway, we have investigated one such system that was experimentally investigated by Oestreich and co-workers.⁴⁵ They proposed the reaction, the hydrogenation of imine, to be a $B(C_6F_5)_3$ catalyzed process. This is shown in Figure 4.16 below. However, it is easy to envisage a mechanism where the cation $[(PhMeC)NH(Ph)]^+$ formed would take over and lead to autocatalytic pathways independent of $B(C_6F_5)_3$ (see Figure 4.17 below).

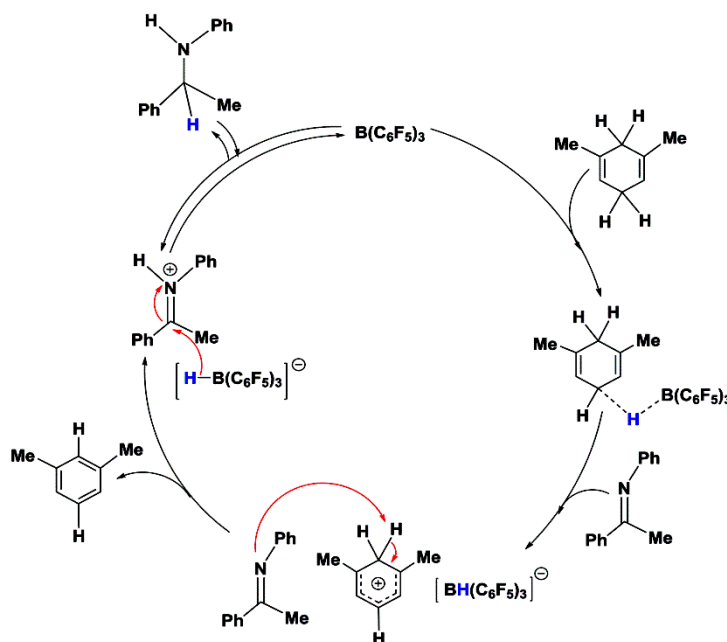


Figure 4.16 The proposed mechanism by Oestreich and co-workers⁴⁵ for the hydrogenation of imine by $B(C_6F_5)_3$.

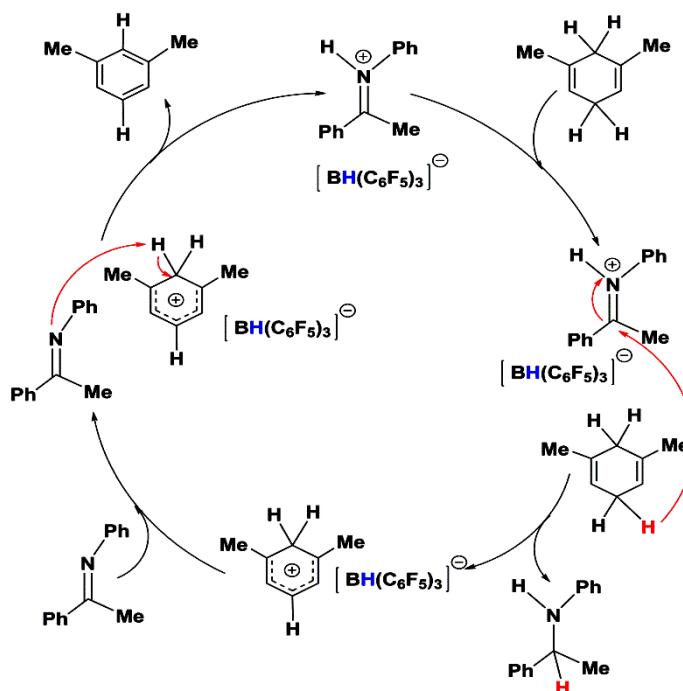


Figure 4.17 The mechanism that I propose, for the same reaction: hydrogenation of imine by $B(C_6F_5)_3$,⁴⁵ based on the facile separation of the cation from the ion-pair.

Calculations have been done to investigate this possibility. As the free energy profiles shown below in Figure 4.18 indicate, the $B(C_6F_5)_3$ -free pathway is more favorable by 3.6 kcal/mol at the PTC(DCM) level of theory for this case. We have also calculated the barriers at the TDC(DCM) levels of theory. The results are provided Table 4.3, and show the same trend.

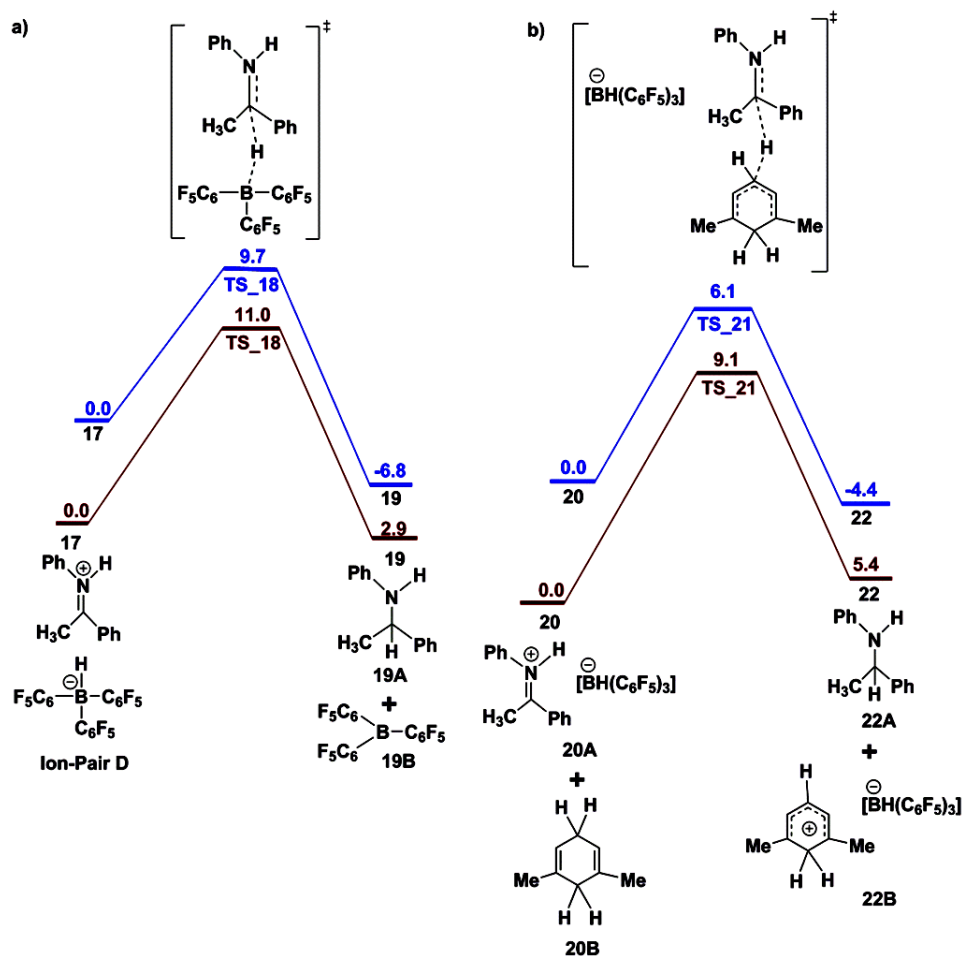


Figure 4.18 The comparison of the free energy profiles (ΔG , kcal/mol) for the formation of [PhNH(HC(CH₃)(Ph))] between a) the conventional mechanism with [PhNH(C(CH₃)(Ph))]⁺ cation and [BH(C₆F₅)₃]⁻ anion, and b) our proposed autocatalytic mechanism. The blue profile is for the PTC(DCM) level of theory and the brown profile is for the TDC(DCM) level of theory. The autocatalytic mechanism is more favourable than the conventional mechanism.

Table 4.2 The calculated free energy barriers for the formation of PhNH(HC)(CH₃)(Ph) through the conventional mechanism proposed in the literature, and our proposed mechanism.

| Intermediate | Barrier (ΔG^\ddagger kcal/mol) | |
|---|---|------------------------------------|
| | The Literature Mechanism | Our Proposed, Cationic Mechanism |
| | $[\text{HB}(\text{C}_6\text{F}_5)_3]^-$ | 1,5-dimethyl-1,4-Cyclohexadiene |
| $[\text{PhNH}(\text{C}(\text{CH}_3)(\text{Ph}))^+]$ | 9.7 ^a /11.0 ^b | 6.1 ^a /9.1 ^b |

^aThe values pertaining to the barriers (ΔG^\ddagger kcal/mol) for the PTC(DCM) calculations.

^bThe values pertaining to the barriers (ΔG^\ddagger kcal/mol) for the TDC(DCM) calculations.

Therefore, a simple means of determining when $\text{B}(\text{C}_6\text{F}_5)_3$ acts as a catalyst and when it may perform only as an initiator becomes clear: if the formed cation, A^+ , can separate in a facile manner from $[\text{A}]^+[\text{HB}(\text{C}_6\text{F}_5)_3]^-$, then catalytic pathways not involving $\text{B}(\text{C}_6\text{F}_5)_3$ can become competitive in the reaction. Hence, the implications of the current investigations extend well beyond the unravelling of the elegant autocatalytic mechanisms in surrogate silicon chemistry.

4.4 Conclusion

There is a deeper realization inherent in the findings reported here. This pertains to the exciting and rapidly developing field of Lewis acid mediated metal free catalytic processes. It becomes clear that there are several recently reported chemical transformations^{37,38,41-46} where the real mechanism may be significantly different from what is believed, with the $\text{B}(\text{C}_6\text{F}_5)_3$ possibly acting more as the initiator and not the catalyst in these cases. The current work provides a simple means of determining computationally when $\text{B}(\text{C}_6\text{F}_5)_3$ is the former and when it is the latter: by a calculation of the ease of separation of the cation, A^+ and anion $[\text{HB}(\text{C}_6\text{F}_5)_3]^-$, from the $[\text{A}]^+[\text{HB}(\text{C}_6\text{F}_5)_3]^-$ ion-pair. In all the cases where A^+ can separate easily, it is possible that alternative mechanisms would become dominant in the reaction medium. The findings are therefore also likely to provide considerable guidance to experimentalists

working in this important area of research. For instance, for cases where the real role of $\text{B}(\text{C}_6\text{F}_5)_3$ is to act more as an initiator, it should be possible to substitute it with another Lewis acid, without loss of efficiency in the system. Furthermore, if it is the cationic species, created during the reaction of the pre-catalyst with $\text{B}(\text{C}_6\text{F}_5)_3$, that is the actual catalyst, then attention can also be focused on investigating means of modifying the pre-catalyst so that the catalytic process can be made more efficient for analogous systems. Therefore, the current findings represent an important advance in metal-free Lewis acid chemistry.

I would also like to note that the current work, revealing the competition between the initiator and catalytic mechanisms, can also provide impetus for kinetic experiments that would yield insights into which mechanism predominates for a given system. For instance, the conventional mechanism emphasizes the role of $\text{B}(\text{C}_6\text{F}_5)_3$, and involves the formation and breaking of a B-H bond, while the newly proposed mechanism focuses on the formation and breaking of the Si-H bond, with the $\text{B}(\text{C}_6\text{F}_5)_3$ converted to an anion and present more as a spectator. Thus, kinetic isotope effects would be different for the different mechanistic scenarios. Likewise, other kinetic experiments can also be designed in order to test the nature of the reactions in these interesting systems.

4.5 References

1. (a) Bjerrum, N. K. *Dan. Vldensk. Selesk. Math. Phys. Medd.* **1926**, 7, 3. (b) Bjerrum, N. *Chem. Zentralbl.***1926**, II, 1378. (c) Bjerrum, N. *Svensk Kem. Tidskr.* **1926**, 38, 2–18. (b) Bjerrum, N. *Chem. Zentralbl.***1926**, I, 2174.
2. Swarc, M. *Ions and Ion Pairs in Organic Reactions*; Wiley-Interscience: New York, 1972; Vol. 1.
3. Reichardt, C. *Solvents and Solvent Effect in Organic Chemistry*; Wiley-VCH: Weinheim, 2003.
4. Swarc, M. *Acc. Chem. Res.***1969**, 2, 87.
5. Kraus, C. A. *J. Phys. Chem.***1956**, 60, 129.
6. Onsager, L. *J. Chim. Phys.* **1968**, 86.
7. Robinson, R. A.; Stokes, R. H. *Electrolyte Solutions*, 2nd ed., revised; Butterworth: London, 1965.
8. Hayes, P. G.; Piers, W. E.; Parvez, M. *J. Am. Chem. Soc.***2003**, 125, 5622.
9. Doerrer, L. H.; Green, M. L. H.; Häussinger, D.; Sassmannshausen, J. *Chem. Soc., Dalton Trans.* **1999**, 2111.
10. Fusco, R.; Longo, L.; Proto, A.; Masi, F.; Garbassi, F. *Macromol. Rapid Commun.* **1998**, 19, 257.
11. Laszlo, P.; Teston, M. *J. Am. Chem. Soc.* **1990**, 112, 8750– 8754.
12. Sutaο Zhang, Yuxi Han, Jianghua He, and Yuetao Zhang, *J. Org. Chem.* **2018**, 83, 1377–1386.
13. Rokob, T. A.; Hamza, A.; Stirling, A.; Pápai, I. *J. Am. Chem. Soc.* **2009**, 131, 2029– 2036. (b) Mahdi, T.; Heiden, Z. M.; Grimme, S.; Stephan, D. *W. J. Am. Chem. Soc.* **2012**, 134, 4088– 4091. (c) Zaher, H.; Ashley, A. E.; Irwin, M.; Thompson, A. L.; Gutmann, M. J.; Krämer, T.; O’Hare, D. *Chem. Commun.*,

- 2013**, *49*, 9755-9757. (d) Mahdi, T.; Stephan, D. *W. J. Am. Chem. Soc.* **2014**, *136*, 15809–15812. (e) Scott, D. J.; Fuchter, M. J.; Ashley, A. E. *J. Am. Chem. Soc.* **2014**, *136*, 15813–15816.
14. Harrison, D. J.; McDonald, R.; Rosenberg, L. *Organometallics* **2005**, *24*, 1398–1400. (b) Hounjet, L. J.; Bannwarth, C.; Garon, C. N.; Caputo, C. B.; Grimme, S.; Stephan, D. W. *Angew. Chem., Int. Ed.* **2013**, *52*, 7492–7495. (c) Hermeke, J.; Mewald, M.; Oestreich, M. *J. Am. Chem. Soc.* **2013**, *135*, 17537–17546.
15. Houghton, A. Y.; Hurmalainen, J.; Mansikkamäki, A.; Piers, W. E.; Tuononen, H. M. *Nat. Chem.* **2014**, *6*, 983–988. (b) Houghton, A. Y.; Karttunen, V. A.; Piers, W. E.; Tuononen, H. M. *Chem. Commun.* **2014**, *50*, 1295–1298.
16. Oestreich, M.; Hermeke, J.; Mohr, J. *Chem. Soc. Rev.* **2015**, *44*, 2202–2220. (b) Massey, A. G.; Park, A. J.; Stone, F. G. A. *J. Am. Chem. Soc.* **1963**, *85*, 2021. (c) Piers, W. E.; Chivers, T. *Chem. Soc. Rev.* **1997**, *26*, 345–354. (d) Jacobsen, H.; Berke, H.; Döring, S.; Kehr, G.; Erker, G.; Fröhlich, R.; Meyer, O. *Organometallics* **1999**, *18*, 1724–1735. (e) Erker, G. *Dalton Trans.* **2005**, 1883–1890.
17. (a) Hohenberg, P.; Kohn, W. *Phys. Rev.* **1964**, *136*, B864-B871. (b) Kohn, W.; Sham, L. J. *Phys. Rev.* **1965**, *140*, A1133-A1138.
18. (a) Zhao, Y.; Truhlar, D. G. *Theor. Chem. Acc.* **2008**, *120*, 215-241. (b) Zhao, Y.; Truhlar, D. G. *Acc. Chem. Res.* **2008**, *41*, 157-167.
19. TURBOMOLE V7.0 2015, a development of University of Karlsruhe an Forschungszentrum Karlsruhe GmbH, 1989-2007, TURBOMOLE GmbH, since 2007; available from <http://www.turbomole.com>.
20. Ansgar, S.; Christian, H.; Reinhart, A. *The Journal of Chemical Physics* **1994**, *100*, 5829-5835.
21. Perdew, J. P.; Burke, K.; Ernzerhof, M. *Phys. Rev. Lett.* **1996**, *77*, 3865-3868.

22. (a) Grimme, S.; Antony, J.; Ehrlich, S.; Krieg, H. *The Journal of Chemical Physics* **2010**, *132*, 154104/1-154104/19. (b) Grimme, S.; Ehrlich, S.; Goerigk, L. *J. Comput. Chem.* **2011**, *32*, 1456-1465.
23. Klamt, A.; Schuurmann, G. *J. Chem. Soc. Perkin Trans.* **1993**, *0*, 799-805.
24. (a) Eichkorn, K.; Treutler, O.; Öhm, H.; Häser, M.; Ahlrichs, R. *Chem. Phys. Lett.* **1995**, *240*, 283-290. (b) Eichkorn, K.; Weigend, F.; Treutler, O.; Ahlrichs, F. *Theor. Chem. Acc.* **1997**, *97*, 119-124.
25. (a) Sierka, M.; Hogeckamp, A.; Ahlrichs, R. *The Journal of Chemical Physics* **2003**, *118*, 9136-9148. (b) Deglmann, P.; May, K.; Furche, F.; Ahlrichs, R. *Chem. Phys. Lett.* **2004**, *384*, 103-107.
26. Tao, J.; Perdew, J. P.; Staroverov, V. N.; Scuseria, G. E. *Phys. Rev. Lett.* **2003**, *91*, 146401/1-146401/4.
27. (a) Weigend, F.; Häser, M.; Patzelt, H.; Ahlrichs, R. *Chem. Phys. Lett.* **1998**, *294*, 143-152. (b) Weigend, F.; Ahlrichs, R. *Phys. Chem. Chem. Phys.* **2005**, *7*, 3297-3305.
28. Zhao, Y.; Truhlar, D. G. *J. Phys. Chem. A* **2005**, *109*, 5656-5667.
29. Weigend, F.; Furche, F.; Ahlrichs, R. *The J. of Chem. Phys.* **2003**, *119*, 12753-12762.
30. Fukui, K. *Acc. Chem. Res.* **1981**, *14*, 363-368.
31. Mammen, M.; Shakhnovich, E. I.; Deutch, J. M.; Whitesides, G. M. *J. Org. Chem.* **1998**, *63*, 3821-3830.
32. Lefranc, I.; Qu, Z.-W.; Grimme, S.; Oestreich, M. *Chem. Eur. J.* **2016**, *22*, 10009-10016.
33. (a) Kozuch, S.; Shaik, S. *J. Am. Chem. Soc.* **2006**, *128*, 3355-3365. (b) Kozuch, S.; Shaik, S. *J. Phys. Chem. A* **2008**, *112*, 6032-6041.
34. Uhe, A.; Kozuch, S.; Shaik, S. *J. Comput. Chem.* **2011**, *32*, 978-985.

35. Heiden, Z. M.; Lathem, A. P. *Organometallics* **2015**, *34*, 1818– 1827.
36. (a) Chen, Y. X. E.; Marks, T. J. *Chem. Rev.* **2000**, *100*, 1391– 1434. (b) Delferro, M.; Marks, T. J. *Chem. Rev.* **2011**, *111*, 2450– 2485. (c) Duchateau, R. *Chem. Rev.* **2002**, *102*, 3525– 3542. (d) Aoshima, S.; Kanaoka, S. *Chem. Rev.* **2009**, *109*, 5245– 5287.
37. (a) Houghton, A. Y.; Hurmalainen, J.; Mansikkamäki, A.; Piers, W. E.; Tuononen, H. M. *Nat. Chem.* **2014**, *6*, 983– 988. (b) Houghton, A. Y.; Karttunen, V. A.; Piers, W. E.; Tuononen, H. M. *Chem. Commun.* **2014**, *50*, 1295– 1298.
38. Ma, Y.; Wang, B.; Zhang, L.; Hou, Z. *J. Am. Chem. Soc.* **2016**, *138*, 3663– 3666.
39. Chatterjee, I.; Oestreich, M. *Org. Lett.* **2016**, *18*, 2463– 2466.
40. Lefranc, I.; Qu, Z.-W.; Grimme, S.; Oestreich, M. *Chem. - Eur. J.* **2016**, *22*, 10009– 10016.
41. Yin, Q.; Klare, H. F. T.; Oestreich, M. *Angew. Chem., Int. Ed.* **2017**, *56*, 3712– 3717.
42. Kim, D. W.; Joung, S.; Kim, J. G.; Chang, S. *Angew. Chem., Int. Ed.* **2015**, *54*, 14805– 14809.
43. Farrell, J. M.; Heiden, Z. M.; Stephan, D. W. *Organometallics* **2011**, *30*, 4497– 4500.
44. Blackwell, J. M.; Sonmor, E. R.; Scoccitti, T.; Piers, W. E. *Org. Lett.* **2000**, *2*, 3921– 392.
45. Chatterjee, I.; Oestreich, M. *Angew. Chem., Int. Ed.* **2015**, *54*, 1965– 1968.
46. Geier, S. J.; Stephan, D. W. *J. Am. Chem. Soc.* **2009**, *131*, 3476– 3477.

Chapter 5

**The Role of Hydride Transfer in Stannylenes and
Germylenes Initiated Catalysis**

Chapter 5

The Role of Hydride Transfer in Stannylenes and Germylenes Initiated Catalysis

Abstract

The chemistry of low valent main group compounds has grown as an alternative to the chemistry of less abundant and less green transition metal complexes. It has been found that low valent compounds such as carbenes, silylenes, stannylenes and germylenes are efficient for activating small molecules and for catalysis. However, the reaction mechanism and the factors that affect the rate of reaction are not completely understood. In this computational investigation with density functional theory (DFT), I have investigated and demonstrated the efficiency of a new mechanism for the hydroboration of aldehydes by germylenes and stannylenes, in the presence of the common hydroborating agent, pinacolborane, HBpin. This mechanism involves an HBpin molecule as an additional catalyst that cooperates with the germylene or stannylene catalyst to efficiently carry out the hydroboration. This mechanism is first demonstrated to work for experimentally reported systems, and then shown to be efficient for newly proposed germylene and stannylene systems. These new systems are α -Borylamido-germylene ((2,6-*i*Pr₂C₆H₃NBCy₂)₂Ge(II)) and α -Borylamido-stannylene((2,6-*i*Pr₂C₆H₃NBCy₂)₂Sn(II)). These new insights will help researchers look into low valent germylene and stannylene chemistry from a new perspective.

5.1 Introduction

In recent years, the chemistry of low valent main group compounds has become a topic of great interest in the field of catalysis, with main group based catalysts sometimes showing comparable or greater efficiency than transition metal catalysts.¹⁻¹⁷ The central atom of these compounds has a lone pair of electrons, as well as unoccupied orbitals, giving them the ability to be both nucleophilic as well as electrophilic, leading to interesting chemical properties.¹⁸ Generally, carbenes,¹⁹⁻²⁵ silylenes,²⁶⁻³⁰ germylenes,³¹⁻³⁷ stannylene,³⁸⁻⁴¹ and borylenes⁴²⁻⁴⁸ have been employed. In these compounds, the central carbon, silicon, germanium or tin atom is stable in a lower oxidation state(II), than the usual (IV), while the boron atom is stable in the (I) oxidation state rather than in (III) (see Figure 5.1). Moreover, low valent main group compounds also include compounds in zero oxidation states, such as carbones,^{49,50} silylones⁵¹ and germylones.⁵² The addition of bulky ligands prevent these low valent main group compounds from oligomerizing and polymerizing, thereby allowing them to act as stable catalysts.

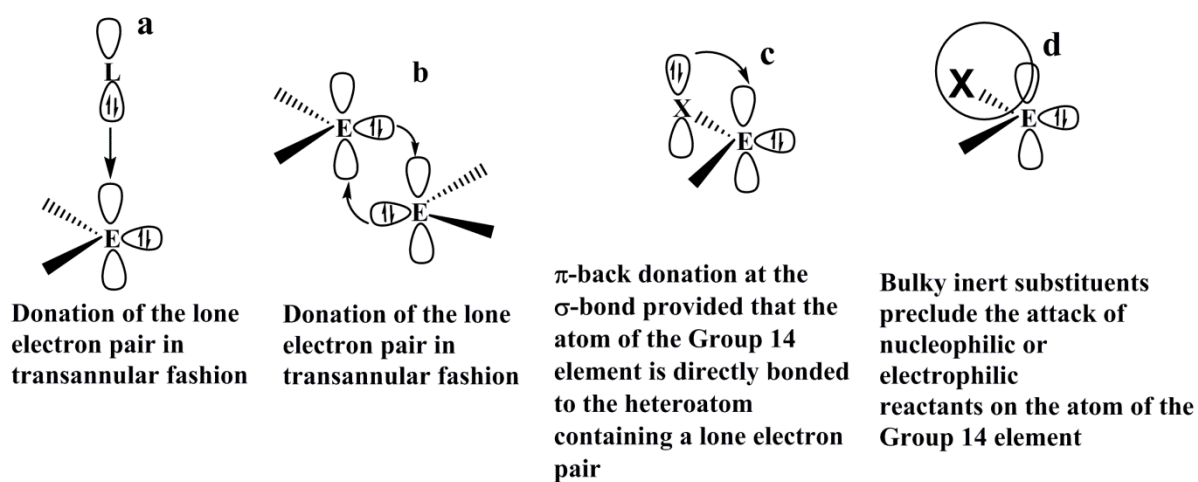


Figure 5.1 The ability of low valent main group compounds to act as both electrophiles and nucleophiles.

In addition to their catalytic abilities, discussed above, low valent carbenes have also emerged as essential synthetic intermediates for a wide range of organic transformations in recent years.¹⁹⁻²⁵ This has led to the synthesis of different metal

carbene complexes to explore their potential applications in chemistry.²⁶⁻⁴⁸ The pioneering work of Lappert in the 1970s led to the development of persistent group 14 tetrylenes compounds of the type EX_2 .⁵³⁻⁵⁷ In contrast to carbenes, the ground electronic state of their heavier congeners X_2E (with $E=Si, Ge$ and Sn) is usually a singlet state, which gives rise to a high energy lone pair (HOMO) and an energetically accessible vacant p-orbital (LUMO).⁵⁸ This orbital configuration resembles transition metal frontier d-orbitals and contributes to the dual donor and acceptor character required for bond activation.⁵⁹ The reactivity of tetrylenes towards small molecules and strong bonds is largely determined by the nature of the many X substituents that govern the energy of the frontier orbitals. Thus, many different substituents with varying steric and electronic properties have been employed to date to tune the ability of tetrylenes to engage in bond activation reactions.⁶⁰⁻⁷² In general, small HOMO-LUMO gaps lead to higher activity of tetrylenes towards small molecules, as has been demonstrated by Bertrand and coworkers, by means of the different behavior of N-heterocyclic carbenes (NHCs) compared to cyclic alkyl (amino) carbenes (CAACs) towards dihydrogen.²¹ Two key factors influence this energy separation: the angle created by the substituents at the central group 14 element and the donor/acceptor properties of the substituents.⁷³⁻⁷⁴ It has generally been observed that the acyclic tetrylenes are usually more reactive than their cyclic derivatives. Likewise, bulky groups are beneficial for small molecule activation, since they, too, increase the X-E-X angle. A wide range of substituents have been used for electronic manipulation, notably for the heavier group 14 analogues of carbenes.⁶⁵⁻⁷² While amino groups are favoured substituents for stabilising tetrylenes due to their $-I$ and $+M$ donor characteristics, they frequently generate a substantial HOMO-LUMO separation. More reactive species suitable for small molecule activation are thus generated with strongly σ -donating (that is, more electropositive) groups, which leave the empty p-orbital unpopulated. This lowers the energy of the LUMO and makes it available for interactions with the bonding orbitals of further substrates. Thus, besides alkyl moieties, silyl or, more lately, boryl groups have also been employed in this chemistry.⁶⁵⁻⁷² These bond activation mechanisms for group 14 tetrylenes have been studied in depth,⁷⁵⁻⁷⁸ with the silyl-substituted germylene and the boryl-functionalized

silylene described by Aldridge and associates serving as examples. Aside from single-site reactivity, E-H bond activation mechanisms have also been reported, including the active engagement of the α -substituent.⁷⁹

After the landmark discovery of the hydroboration reaction by H. C. Brown,⁸⁰ organoboranes have been used extensively for different hydroboration reactions.⁸¹⁻⁸⁵ The hydroboration of C=O bonds has been significant, solidifying its reputation as one of the most beneficial and commonly utilised reactions in the pharmaceutical industry.⁸⁶ There are a lot of examples of carbonyl hydroboration catalysts, including alkaline earthmetals,⁸⁷⁻⁹⁵ transition metals,⁹⁶⁻¹⁰³ group 13 metal catalysts,¹⁰⁴⁻¹⁰⁷ lanthanides,¹⁰⁸⁻¹¹² actinides¹¹³ and other unique and sophisticated systems.¹¹⁴⁻¹¹⁸ It has always been challenging to develop cost effective and non-toxic p-block based catalysts for the catalytic hydroboration reactions. There are only a few reports on germylenes and stannylenes as catalysts for the hydroboration of unsaturated substrates, and the most noteworthy examples are the bulky amine substituted germylene hydrides and stannylene hydrides reported by Jones and coworkers.¹¹⁹ Zhao and coworkers have investigated the hydroboration of aldehydes and ketones with the ylide type N-heterocyclic germylene reported by Driess and coworkers.^{120,121} Later, Wesemann and coworkers reported the hydroboration of aldehydes and ketones using intramolecular heavier tetrellylenes and phosphine based Lewis pairs.^{122,123} Recently, Khan and coworkers have shown the hydroboration of aldehydes using N-heterocyclic germylenes and stannylenes.¹²⁴ However, there have been very few computational studies identifying the role(s) of germylenes and stannylenes in such reactions.¹²⁵⁻¹²⁹ Computational investigations on hydroboration reactions with germylene and stannylene catalysts are even fewer.^{119,121,124} This has inspired us to model new catalysts and investigate the hydroboration reaction computationally in order to find an efficient mechanistic pathway for the same.

It has always been a challenge to model a catalyst and find an efficient mechanistic pathway using computational tools. In the current work, I have first investigated a catalytic system that has already been proposed in the literature. Our investigations reveal a new mechanistic pathway that can be achieved by changing the concentration

of the reacting species: the hydroborating agent pinacolborane (HBpin). Then, I have modelled new germylene and stannylene catalyst systems, shown in Figure 5.2 below, which have been designed by taking into consideration the HOMO-LUMO energy gap. I have then investigated our newly proposed mechanism for the aldehyde hydroboration reaction with the modelled α -Borylamido-germylene ((2,6-*iPr*₂C₆H₃NBCy₂)₂Ge(II)) (Catalyst 3) and α -Borylamido-stannylene ((2,6-*iPr*₂C₆H₃NBCy₂)₂Sn(II)) (Catalyst 4) systems, in the presence of the common hydroborating agent, HBpin.



Figure 5.2 The germylene and stannylene systems considered in this work.

To date, it has been believed that these families of stannylene and germylene systems proceed in the hydroboration reaction with HBpin *via* a four membered cyclic transition state. The current investigation shows that the hydroboration reaction proceeds *via* a six membered cyclic transition state. Along with the external catalyst, a molecule of HBpin assists in facilitating the reaction effectively. The current computational investigation thus finds new insights into the hydroboration reaction with low valent main group catalysts.

5.2 Computational Details

All the calculations for the structures reported herein have been done using DFT.¹²⁹⁻¹³² The calculations have been carried out with Turbomole 7.4¹³³ using the TZVP¹³⁴ basis set. Geometry optimizations were performed using the Perdew, Burke, and Ernzerhof (PBE) functional.¹³⁵ Dispersion corrections (D3)^{136,137} have been

included in all the calculations. Solvent corrections have also been included in the calculations using the COSMO model,¹³⁸ with $\epsilon=2.38$ to model toluene, PhCH₃. Therefore, the level of theory employed is PBE-D3/TZVP+COSMO(PhCH₃).¹³⁴⁻¹³⁸ The resolution of identity (RI)^{139,140} along with the multipole accelerated RI (marij)^{141,142} approximations have been used for an accurate and efficient treatment of the electronic Coulomb term in the DFT calculations. Necessary care was taken to ensure that the obtained transition state structures possessed only one imaginary frequency corresponding to the correct normal mode, in order to obtain more reliable energy values for the investigated potential energy surface. In addition, intrinsic reaction coordinate (IRC)¹⁴³ calculations were done with all the transition states in order to further confirm that they were the correct transition states, yielding the correct reactant and product structures. The values reported herein are ΔG values, with zero point energy, internal energy, and entropic contributions, with the temperature taken to be 298.15 K. The calculation of the translational entropy in standard software involves assumptions about the volume that may be inaccurate. The translational entropy term can be corrected by a free volume correction introduced by Mammen and co-workers.¹⁴⁴ Based on the Sackur–Tetrode equation, the free volume model describes the translational entropy of molecules in solution ($\Delta S_{\text{trans(sol)}}$); and provides physically intuitive corrections for translational entropy values. In the free volume model, it has been assumed that the volume available to the molecule in solution is lower than the total volume, and this “free volume” is determined by the equation below:

$$V_{\text{free}} = C_{\text{free}} \left(\sqrt[3]{\frac{10^{27}}{[X]N_0}} - \sqrt[3]{V_{\text{molecule}}} \right)^3 \quad 5.1$$

Here, V_{molecule} is the molecular volume, $[X]$ is the concentration of molecules (mol/L) in solution and N_0 is the Avogadro number. The translational entropy can be obtained after considering the free volume correction, and inserting the value of V_{free} in the Sackur-Tetrode equation. The total entropy is then calculated by adding the corrected translational entropy and the entropic contributions from the rotational and vibrational components.

5.3 Results and Discussion

At first, I have calculated the barrier for the proton relay mechanism without the stabilizing role of the catalysts. The barrier for this process was found to be 31.7 kcal/mol (see Figure 3 below). The barrier would have to reduce below 31.7 kcal/mol when catalysts were considered. This was the case when I further investigated the mechanism with the involvement of the catalyst included.

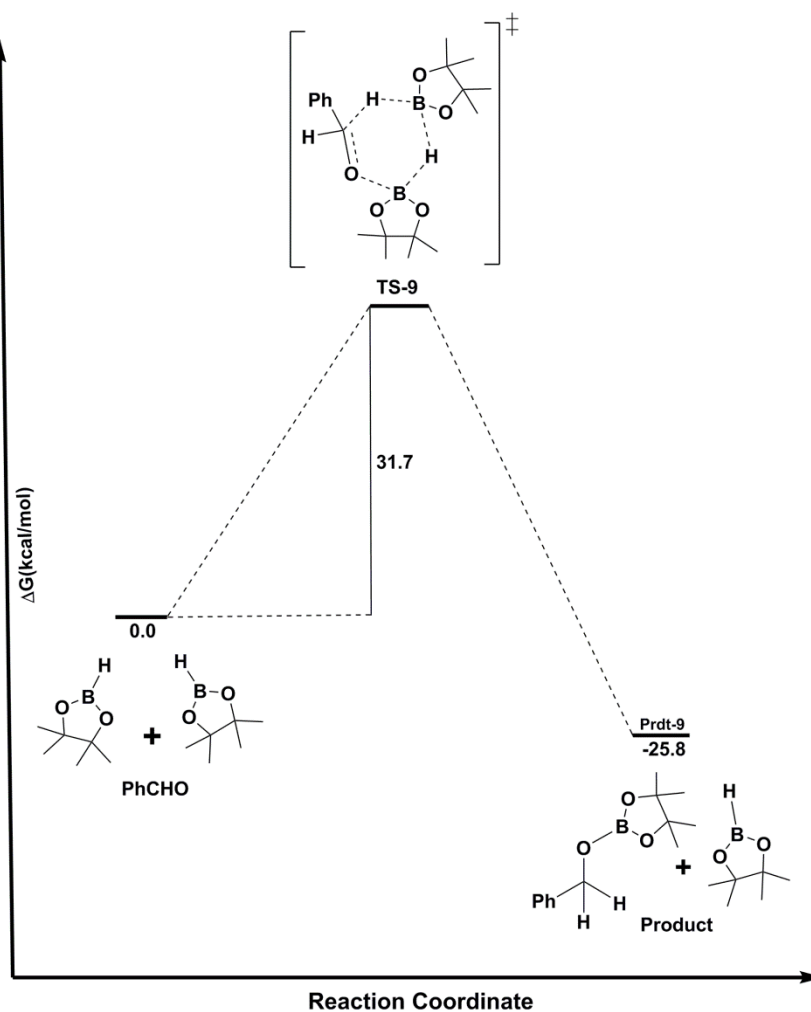


Figure 5.3 The free energy profile for the catalytic aldehyde hydroboration without any catalyst through a six-membered cyclic transition state. The values (in kcal/mol) have been calculated at the PBE/TZVP level of theory.

Then I investigated the mechanism proposed by Khan and co-workers for the hydroboration reaction with N-heterocyclic germylene.¹²⁴ Initially, two N-heterocyclic germylene molecules interact with two oxygens of HBpin and form a stable intermediate. In the next step, the aldehyde reacts with this intermediate to form a borate adduct *via* a four membered cyclic transition state. This mechanism has been investigated computationally by Khan and coworkers,¹²⁴ along with a competing mechanism where only one germylene molecule is involved as a catalyst with the HBpin and aldehyde reactants. The resultant barrier for the mechanism with one catalyst molecule was found by them to be higher than the barrier for the two catalyst case. It is worth mentioning here that they employed a 2:1 catalyst to HBpin ratio in the experiments. The intermediate was also confirmed *via* NMR.

I began by investigating the mechanism where two catalysts were involved in the four membered cyclic transition state as proposed by Khan and coworkers. In the first step of this mechanism, two catalyst molecules react with two oxygen atoms of HBpin. This forms an intermediate (**Int-1**) that is stable by 5.0 kcal/mol. After this, the aldehyde approaches and forms a four membered cyclic transition state. The barrier for the transition state (**TS-1**) was calculated to be 26.8 kcal/mol (see Figure 5.4 below).

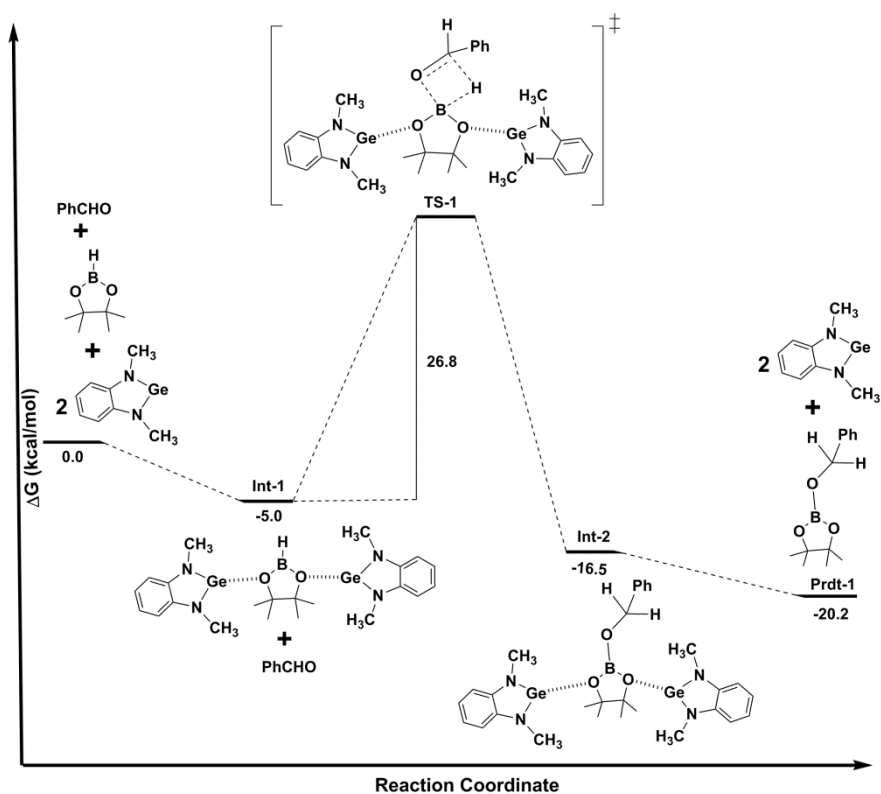


Figure 5.4 The free energy profile for the hydroboration reaction with germylene catalyst: mechanism proposed in the literature by Khan and coworkers.¹²⁴

I have then investigated the mechanism for the hydroboration reaction with the N-heterocyclic stannylene catalyst. The intermediate (**Int-3**), at which the two molecules of stannylene and one molecule of HBpin form a complex, is stable by 7.0 kcal/mol. The barrier for the transition state (**TS-2**) is 24.2 kcal/mol (see Figure 5.5 below).

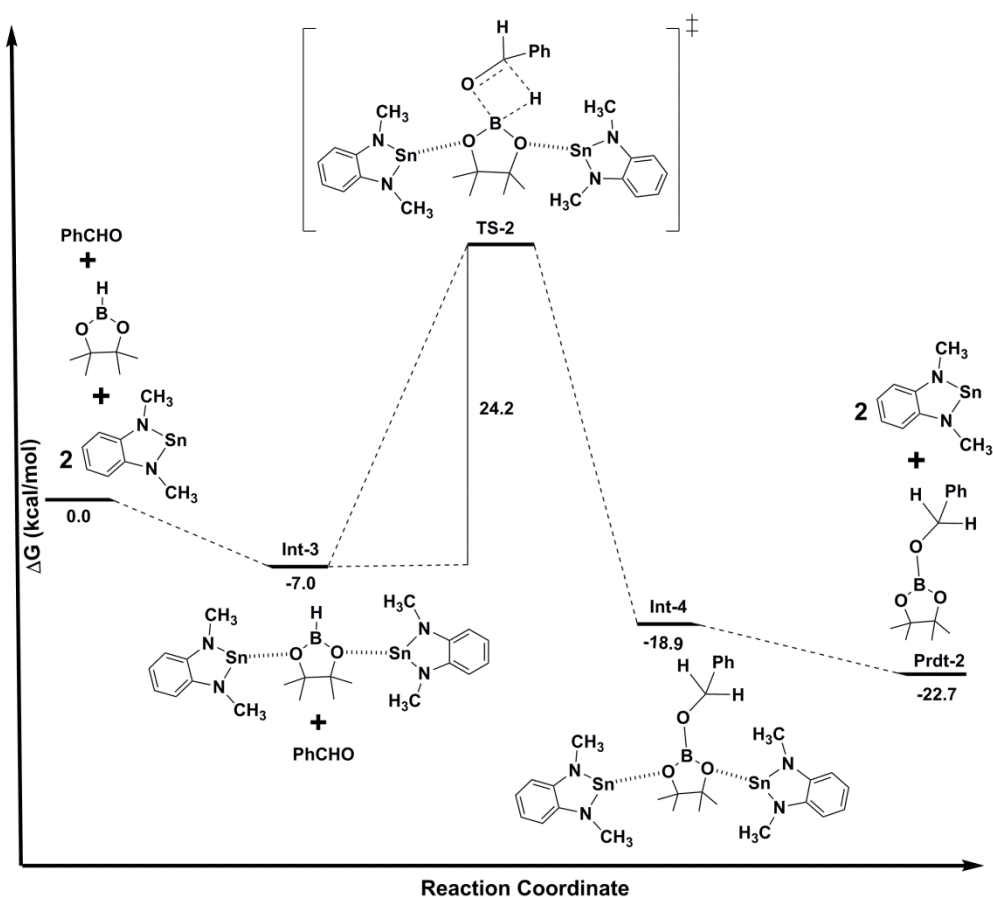


Figure 5.5 The free energy profile for the hydroboration reaction with the stannylene catalyst: mechanism proposed in the literature by Khan and coworkers.¹²⁴

I have then proceeded to reinvestigate the mechanism for this conversion. Instead of two germylene molecules acting as catalysts, I propose a system containing one germylene molecule, along with two HBpin and one aldehyde molecules. This is shown in Figure 5.6 below. The two HBpin molecules form an intermediate with one N-heterocyclic germylene molecule. The intermediate (**Int-5**) is stable by 2.0 kcal/mol. Then, the aldehyde reacts with the intermediate (**Int-5**) via a six membered cyclic transition state. The barrier for this transition state (**TS-3**) is 22.4 kcal/mol. This indicates that the six membered transition state is favourable by 4.4 kcal/mol over the four membered cyclic transition state. This suggests that if HBpin is used in excess amount, the catalytic pathway may vary for the hydroboration reaction.

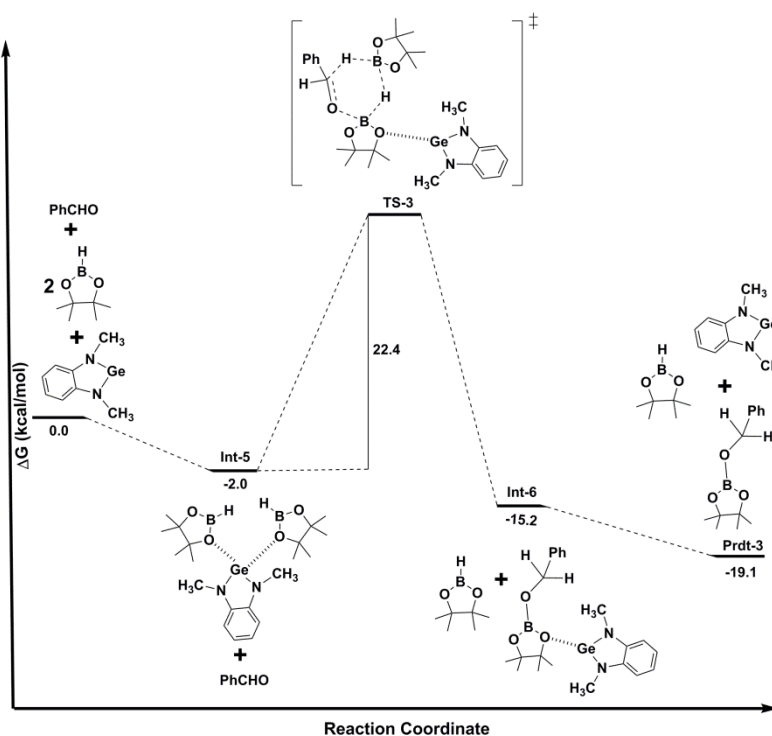


Figure 5.6 The free energy profile for a new mechanism that I have propose for the hydroboration of benzaldehyde by HBpin, in the presence of the germylene catalyst.

I have also investigated the same mechanism with the stannylene catalyst. The catalyst forms a stable product *via* a six membered cyclic transition state. The barrier for the transition state (TS-4) is 19.8 kcal/mol (see Figure 5.7 below).

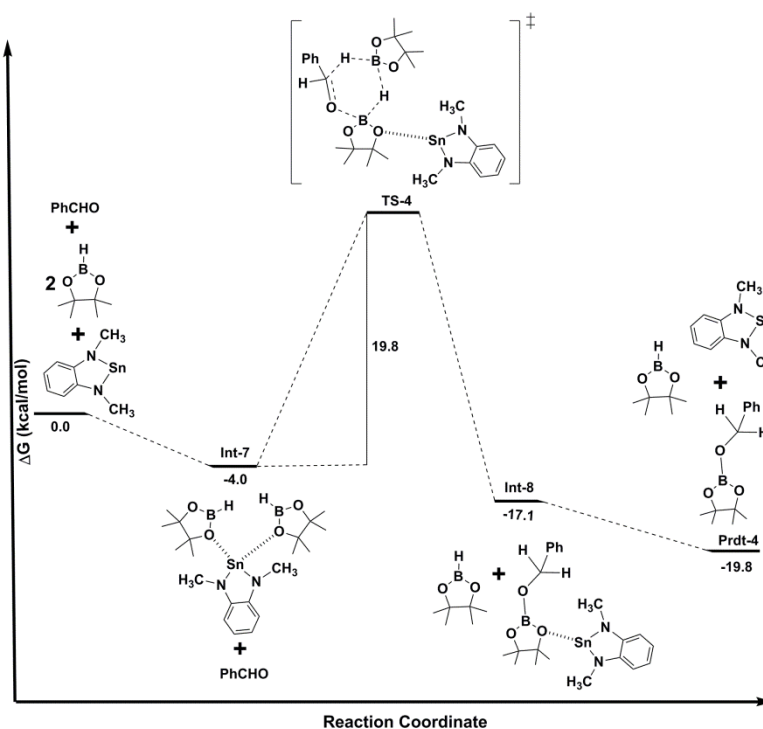


Figure 5.7 The free energy profile for a new mechanism that I propose for the hydroboration of benzaldehyde by HBpin, in the presence of the stannylene catalyst.

Then, I have calculated the HOMO-LUMO energy gap for the germylene catalysts that have experimentally been employed for the hydroboration reaction, and discussed above.

Table 5.1. HOMO-LUMO energy gap by using the TDDFT approach for the X_2E type germylene catalyst. For the first three cases, the hydroboration reaction has been investigated experimentally and for the last case, the hydroboration reaction has been investigated computationally in this current work, with a designed catalyst system.

| Catalyst | ΔE (TDDFT) (First Excitation Energy) (ev) |
|--|---|
| 1. Zhao and coworkers germylene ¹³⁹ | 1.92 |
| 2. Wesemann and coworkers germylene ¹⁴⁰ | 2.15 |
| 3. Khan, Pati and coworkers germylene ¹⁴¹ | 2.88 |

| | |
|--|------|
| 4. Modeled germylene system in this work | 2.42 |
|--|------|

The calculated HOMO-LUMO energy gap in the above table shows that the more bulky the catalyst, the lesser is the HOMO-LUMO energy gap. In the introduction, I have already mentioned that the lesser the HOMO-LUMO gap, the more is the reactivity of tetrylenes towards small molecules. The HOMO-LUMO energy gap for the first catalyst is 63.1 kcal/mol. Now, it has been found experimentally as well as computationally that the first catalyst can facilitate hydroboration reaction effectively. Therefore, it stands to reason that systems having a HOMO-LUMO gap below 63.1 kcal/mol can also catalyse hydroboration effectively, which is actually the case with the second and the third catalyst. Considering 63.1 kcal/mol as the benchmark for the germylene systems to undergo hydroboration reaction I have proceeded further. Recently, Khan and coworkers experimentally obtained a bulky acyclic α -phosphinoamido-germylene $(2,6\text{-}i\text{Pr}_2\text{C}_6\text{H}_3\text{NPPH}_2)_2\text{Ge}$, which can be a potential catalyst for the hydroboration reaction.¹⁴⁵ The HOMO-LUMO gap for this catalyst was found to be 52.4 kcal/mol. Inspired by this work and keeping the criterion of the HOMO-LUMO gap in mind, I propose new catalysts for the hydroboration reaction: α -Borylamido-germylene $((2,6\text{-}i\text{Pr}_2\text{C}_6\text{H}_3\text{NBCy}_2)_2\text{Ge(II)})$ (Catalyst-3) and α -Borylamido-stannylene $((2,6\text{-}i\text{Pr}_2\text{C}_6\text{H}_3\text{NBCy}_2)_2\text{Sn(II)})$ (Catalyst-4). The HOMO-LUMO energy gap for the modeled germylene system is 51.1 kcal/mol. The replacement of the phosphorous atom by boron and also the replacement of the phenyl group with a cyclohexyl group leads to the decrease in HOMO-LUMO gap by 1.3 kcal/mol, in comparison to the α -phosphinoamido-germylene $(2,6\text{-}i\text{Pr}_2\text{C}_6\text{H}_3\text{NPPH}_2)_2\text{Ge}$ catalyst mentioned above. Based on the HOMO-LUMO energy gap I have considered that the modeled germylene and stannylene catalyst could further undergo hydroboration reaction.

In order to get insights into the hydroboration reaction with the newly designed systems, I have investigated the traditional mechanism of the hydroboration of benzaldehyde with Catalyst-3. As shown in Figure 5.8, in the first step, a weakly

bound complex (**Int-9**) between Catalyst-3 and HBpin would be formed, with one of the oxygen atoms of HBpin approaching the germanium atom of Catalyst-3.

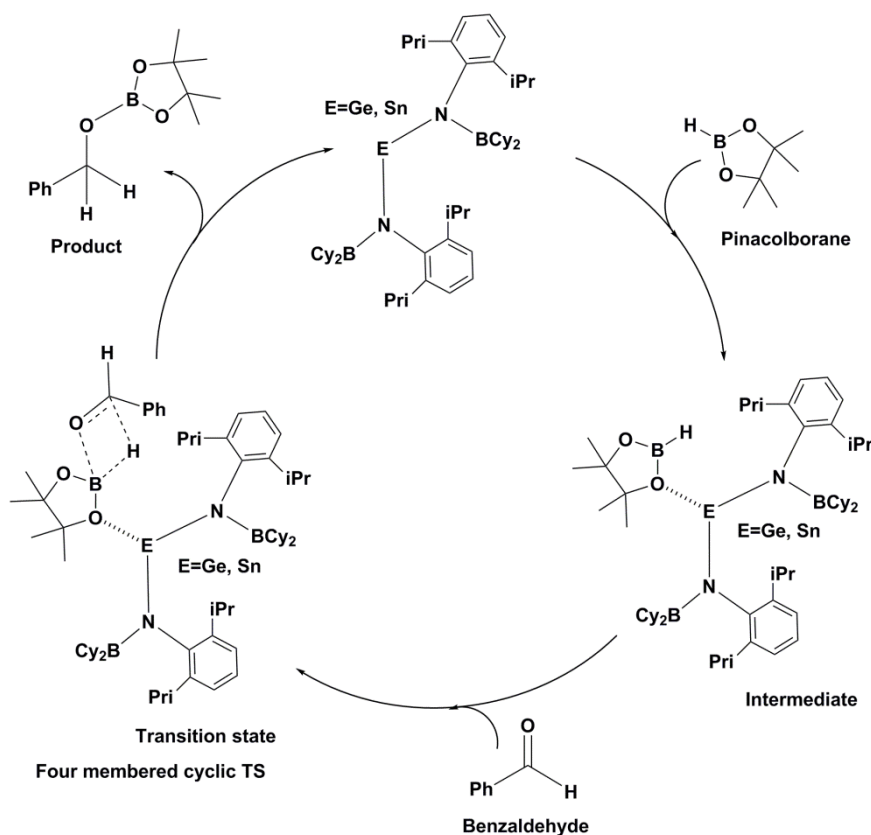


Figure 5.8 The catalytic cycle and reaction mechanism for the aldehyde hydroboration by Catalyst-3 ($E=Ge$) and Catalyst 4 ($E=Sn$), *via* a four membered cyclic transition state.

Figure 5.8 below shows the free energy profile for the proposed reaction. The DFT calculations show that the Ge-O distance (Ge from Catalyst-3 and oxygen from HBpin) is 3.73 \AA , and the intermediate (**Int-9**) is unfavourable by 1.7 kcal/mol (ΔG) in comparison to the separated reactant species, Catalyst-3 and HBpin. Now, the benzaldehyde approaches the B-H bond of **Int-9**. This leads to nucleophilic attack by the carbonyl oxygen of benzaldehyde to the boron centre of HBpin, with the hydride being transferred from the boron centre to the electrophilic carbonyl carbon of the

benzaldehyde. This occurs *via* a four membered cyclic transition state (**TS-5**) in the traditional mechanism reported in the literature, and leads to the formation of the hydroboration product along with the regeneration of the catalyst (see Figure 5.8 and Figure 5.9). The barrier (ΔG^\ddagger) corresponding to the transition state is 35.6 kcal/mol, which is high for a reaction that should take place at room temperature.

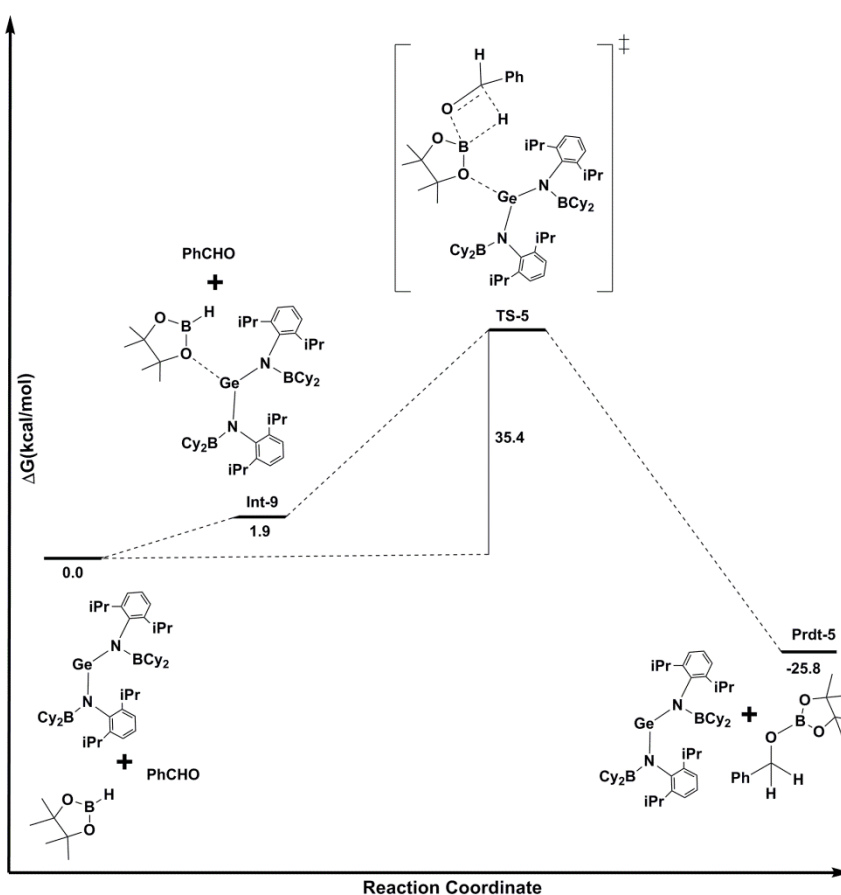


Figure 5.9 The free energy profile for the catalytic aldehyde hydroboration by Catalyst-3 with a four-membered cyclic transition state. The values (in kcal/mol) have been calculated at the PBE/TZVP level of theory.

I have also investigated the same pathway with Catalyst-4. The barrier for the four membered cyclic transitions state is 32.1 kcal/mol (see Figure 5.10 below)

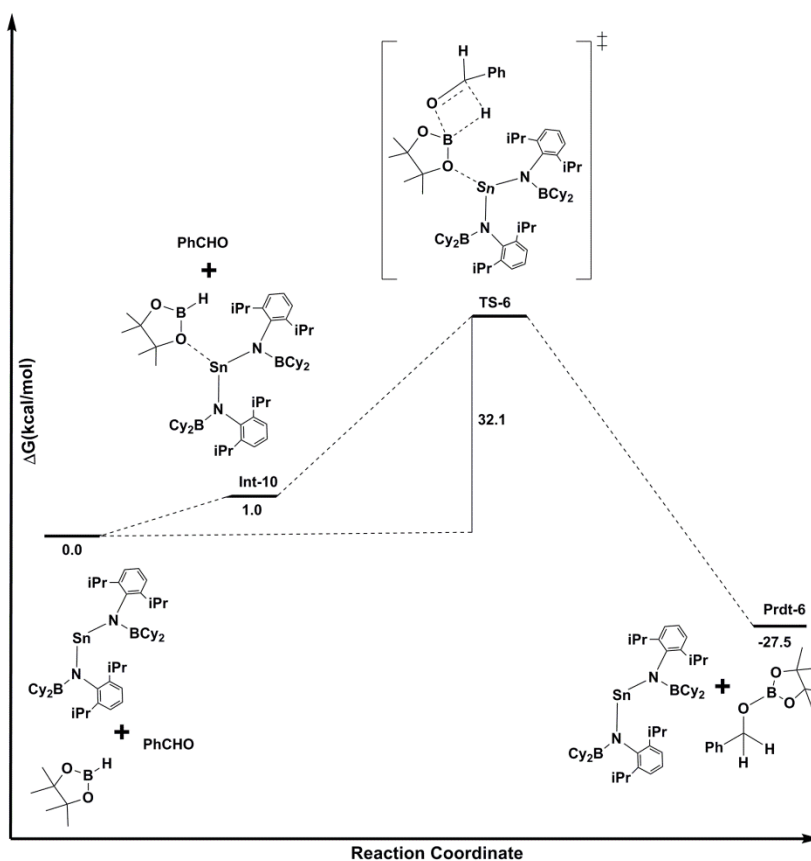


Figure 5.10 The free energy profile for the catalytic aldehyde hydroboration by Catalyst-4 with a four-membered cyclic transition state. The values (in kcal/mol) have been calculated at the PBE/TZVP level of theory.

5.3.1. Calculations According to the Newly Proposed Mechanism

Since the slowest step of the mechanism discussed above appears to be too high for a room temperature reaction, I have attempted to explore other mechanisms. For this, I have investigated the different possible interactions between the metal centre (Ge) of the catalyst and pinacolborane. There are no interactions that were found that could stabilise the intermediate more than the Ge-O interaction (between the catalyst and pinacolborane) that I already studied. Therefore, I have considered this interaction to be the most favourable. I thus proceeded to investigate a six membered cyclic transition state, with two pinacolboranes and one aldehyde taking part: the mechanism that I have investigated and discussed above for the reported germylene system (see Figure 5.11 and Figure 5.12 below).

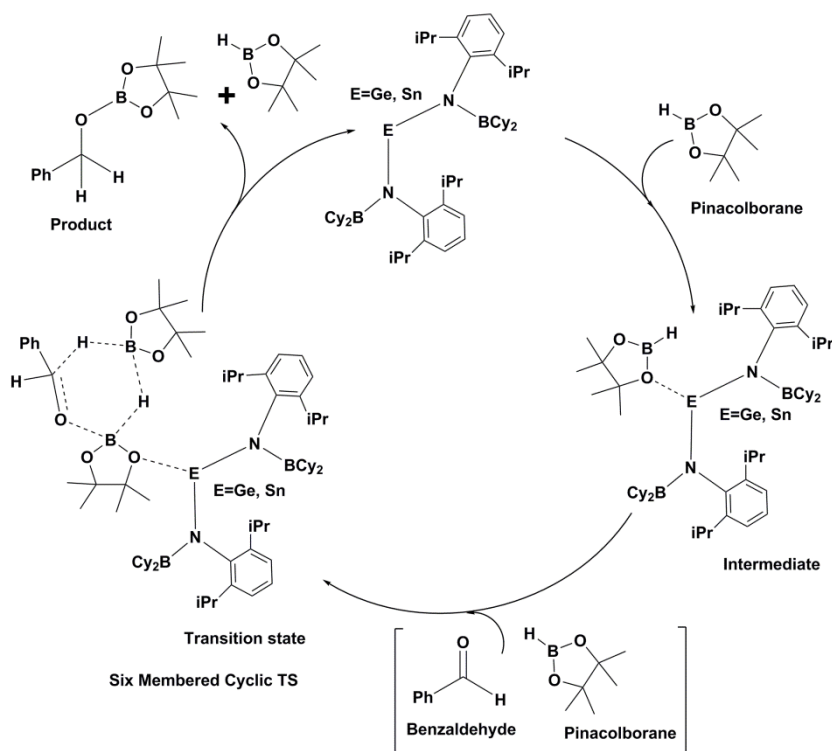


Figure 5.11 The catalytic cycle and reaction mechanism for aldehyde hydroboration by Catalyst-3 and Catalyst-4, *via* a six-membered cyclic transition state.

The transition state (**TS-6**) involves an HBpin molecule as the catalytic agent for a proton relay mechanism, while the Ge centre of the catalyst employed acts to stabilize the other HBpin molecule in the system. The activation energy (ΔG^\ddagger) barrier corresponding to this transition state is 25.7 kcal/mol, which is significantly lower than the corresponding barrier for the previously proposed mechanism (see Figure 5.9 above) and explains why the reaction is feasible at room temperature.

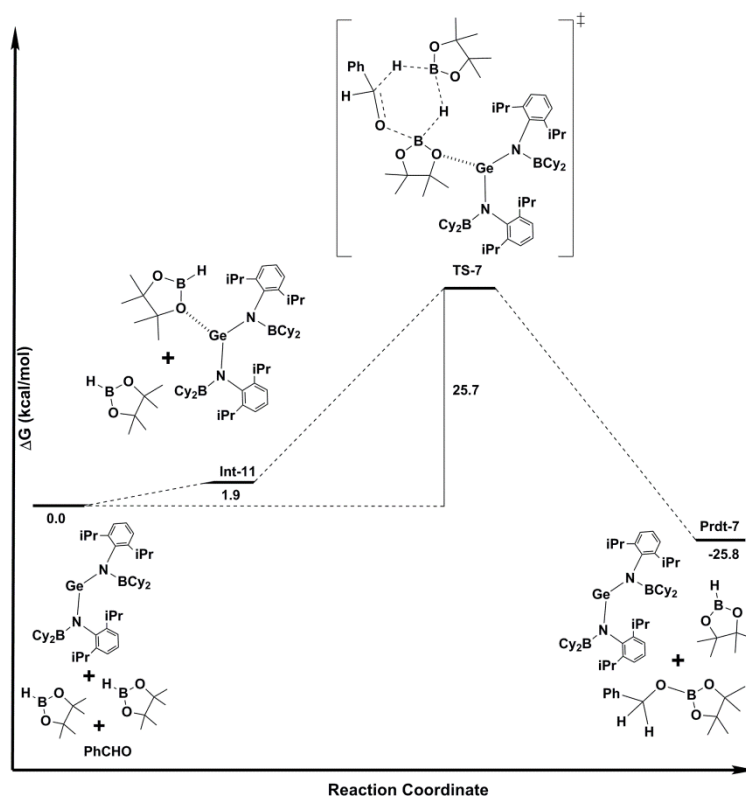


Figure 5.12 The free energy profile for the catalytic aldehyde hydroboration by Catalyst-3 passing through a six membered cyclic transition state. The values (in kcal/mol) have been calculated at the PBE/TZVP level of theory.

I note that the corresponding reaction using the stannylene catalyst also yielded a favourable reaction pathway. The barrier for this process was found to be 23.3 kcal/mol (see Figure 5.11 and Figure 5.13).

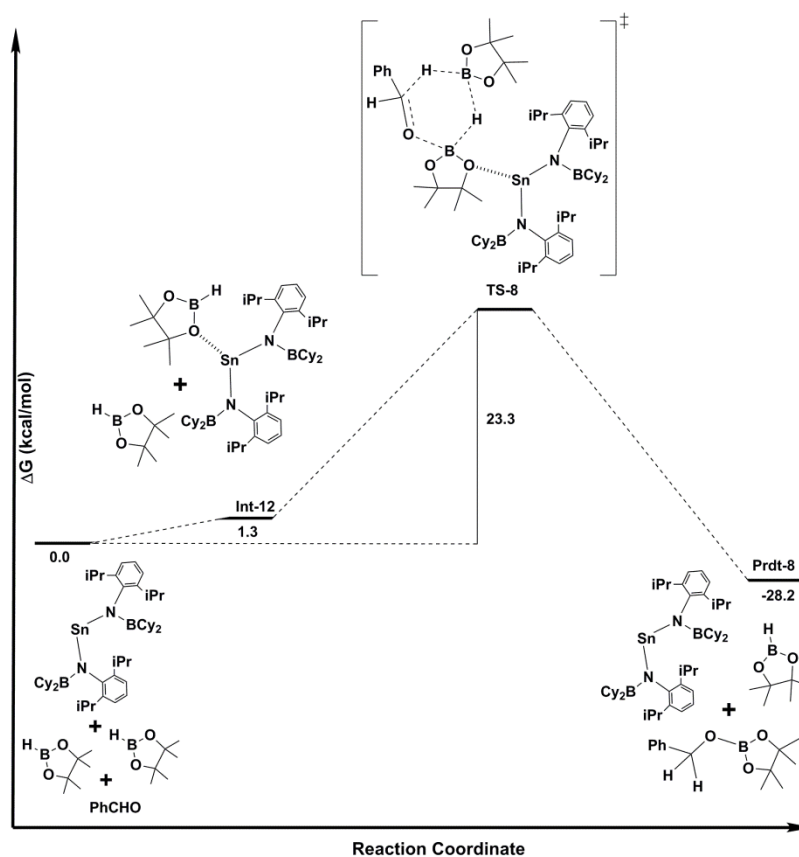


Figure 5.13 The free energy profile for the catalytic aldehyde hydroboration by Catalyst-4 passing through a six-membered cyclic transition state. The values (in kcal/mol) have been calculated at the PBE/TZVP level of theory.

Therefore, the germylene and stannylene catalysts, with the aid of an additional HBpin molecule, allow the reaction to proceed in a facile manner under mild conditions. The current report thus reveals an interesting example of “dual” catalysis, where low valent main group compounds, as well as a substrate, both act as catalysts.

5.4 Conclusion

The current study, employing density functional theory (DFT), sheds light on the mechanism of the hydroboration reaction with low valent main group catalysts: germynes and stannylens, with the aid of the hydroborating agent, pinacolborane, HBpin. I have computationally investigated a previously proposed mechanism for a germylene catalyst system that has been experimentally reported. Then, I have

compared the free energy profile of this reported mechanism with a newly proposed mechanism, which incorporates an additional HBpin molecule as a second catalyst. Subsequent to this, I have proposed two new catalysts, keeping in mind the electronic structure of previously reported germylenes and stannylenes. Since the HOMO-LUMO energy gap calculations indicate that the more bulky the catalyst, the lower is the energy gap, I have computationally designed a new acyclic α -borylamido-germylene, and a stannylene catalyst having an electron deficient boron atom. I have investigated our newly proposed mechanism for the hydroboration reaction with these newly designed catalyst systems, and demonstrated that such a mechanism would be effective in making these systems good catalysts for the hydroboration of aldehydes in the presence of HBpin as the hydroborating agent. The newly proposed mechanism thus provides new insights for the hydroboration reactions with germylene and stannylene catalysts.

5.5 References

1. Power, P. P. *Nature*, **2010**, *463*, 171–177.
2. Braunschweig, H.; Dewhurst, R. D.; Hupp, F.; Nutz, M.; Radacki, K.; Tate, C. W.; Vargas, A.; Ye, Q. *Nature*, **2015**, *522*, 327–330.
3. Vasko, P.; Wang, S.; Tuononen, H. M.; Power, P. P. *Angew. Chem. Int. Ed.*, **2015**, *54*, 3802–3805.
4. Peng, Y.; Guo, J.-D.; Ellis, B. D.; Zhu, Z.; Fettinger, J. C.; Nagase, S.; Power, P. P. *J. Am. Chem. Soc.*, **2009**, *131*, 16272 – 16282.
5. Peng, Y.; Ellis, B. D.; Wang, X.; Fettinger, J. C.; Power, P. P. *Science*, **2009**, *325*, 1668 – 1670.
6. Martin, D.; Soleilhavoup, M.; Bertrand, G. *Chem. Sci.*, **2011**, *2*, 389 – 399.
7. Asay, M.; Jones, C.; Driess, M. *Chem. Rev.*, **2010**, *110*, 354 – 396.
8. Xiong, Y.; Szilvsi, T.; Yao, S.; Tan, G.; Driess, M. *J. Am. Chem. Soc.*, **2014**, *136*, 11300 – 11303.
9. Protchenko, A. V.; Bates, J. I.; Saleh, L. M. A.; Blake, M. P.; Schwarz, A. D.; Kolychev, E. L.; Thompson, A. L.; Jones, C.; Mountford, P.; Aldridge, S. *J. Am. Chem. Soc.*, **2016**, *138*, 4555 – 4564.
10. Hermann, M.; Jones, C.; Frenking, G.; *Inorg. Chem.*, **2014**, *53*, 6482–6490.
11. Li, J.; Hermann, M.; Frenking, G.; Jones, C. *Angew. Chem. Int. Ed.* **2012**, *51*, 8611 – 8614.
12. Usher, M.; Protchenko, A. V.; Rit, A.; Campos, J.; Kolychev, E. L.; Tirfoin, R.; Aldridge, S. *Chem. Eur. J.*, **2016**, *22*, 11685 – 11698.
13. Yang, Z.; Zhong, M.; Ma, X.; Nijesh, K.; De, S.; Parameswaran, P.; Roesky, H.W. *J. Am. Chem. Soc.*, **2016**, *138*, 2548 – 2551.
14. Mandal, S. K.; Roesky, H.W. *Acc. Chem. Res.*, **2012**, *45*, 298 – 307.

15. Jana, A.; Roesky, H.W.; Schulzke, C.; Döring, A.; *Angew. Chem. Int. Ed.*, **2009**, *48*, 1106 – 1109.
16. Reißmann, M.; Schfer, A.; Jung, S.; Müller, T.; *Organometallics*, **2013**, *32*, 6736–6744.
17. Rivard, E. *Chem. Soc. Rev.* **2016**, *45*, 989 – 1003.
18. Nesterov, V.; Reiter, D.; Bag, P.; Frisch, P.; Holzner, R.; Porzelt, A.; Inoue, S. *Chem. Rev.*, **2018**, *118*, 9678–9842.
19. Arduengo III, A. J.; Harlow, R. L.; Kline, M. *J. Am. Chem. Soc.*, **1991**, *113*, 361–363.
20. Arduengo III, A. J.; Goerlich, J. R.; Marshall, W. J. *J. Am. Chem. Soc.*, **1995**, *117*, 11027–11028.
21. Frey, G. D.; Lavallo, V.; Donnadiou, B.; Schoeller, W. W.; Bertrand, G.; *Science*, **2007**, *316*, 439-441.
22. Nelsona, D. J.; Nolan, S. P.; *Chem. Soc. Rev.*, **2013**, *42*, 6723-6753.
23. Sau, S. C.; Hota, P. K.; Mandal, S. K.; Soleilhavoup, M.; Bertrand, G. *Chem. Soc. Rev.*, **2020**, *49*, 1233-1252.
24. Vivancos, Á.; Segarra, C.; Albrecht, M. *Chem. Rev.*, **2018**, *118*, 9493–9586.
25. Peris, E. *Chem. Rev.*, **2018**, *118*, 9988–10031.
26. Becerra, R.; Goldberg, N.; Cannady, J. P.; Almond, M. J.; Ogden, J. S.; Walsh, R. *J. Am. Chem. Soc.*, **2004**, *126*, 6816-6824.
27. Jana, A.; Schulzke, C.; Roesky, H. W.; *J. Am. Chem. Soc.*, **2009**, *131*, 4600-4601.
28. Kuriakose, N.; Vanka, K.; *Dal. Trans.*, **2014**, *43*, 2194-2201.
29. Chu, T.; Nikonov, G. I. *Chem. Rev.*, **2018**, *118*, 3608–3680.

30. Roy, M. M. D.; Omaña, A. A.; Wilson, A. S. S.; Hill, M. S.; Aldridge, S.; Rivard, E. *Chem. Rev.*, **2021**, *121*, 12784–12965.
31. Jutzi, P.; Burford, N.; *Chem. Rev.*, **1999**, *99*, 969–990.
32. Kira, M.; Ishida, S.; Iwamoto, T. *Chem. Rec.*, **2004**, *4*, 243–253.
33. Kira, M.; *J. Organomet. Chem.*, **2004**, *689*, 4475–4488.
34. Jana, A.; Objartel, I.; Roesky, H. W.; Stalke, D. *Inorg. Chem.*, **2009**, *48*, 798–800.
35. Wang, W.; Inoue, S.; Yao, S.; Driess, M. *Chem. Commun.*, **2009**, 2661–2663.
36. Wang, W.; Inoue, S.; Yao, S.; Driess, M. *Organometallics*, **2011**, *30*, 6490–6494.
37. Wang, W.; Inoue, S.; Enthaler, S.; Driess, M. *Angew. Chem., Int. Ed.*, **2012**, *51*, 6167–6171.
38. Mizuhata, Y.; Sasamori, T.; Tokitoh, N.; *Chem. Rev.*, **2009**, *109*, 3479–3511.
39. Hadlington, T. J.; Driess, M.; Jones, C. *Chem. Soc. Rev.*, **2018**, *47*, 4176–4197.
40. Kaysa, D. L. *Chem. Soc. Rev.*, **2016**, *45*, 1004–1018.
41. Ota, K.; Kinjo, R. *Chem. Soc. Rev.*, **2021**, *50*, 10594–10673.
42. Braunschweig, H.; Dewhurst, R. D.; Schneider, A. *Chem. Rev.*, **2010**, *110*, 3924–3957.
43. E. C. Neeve, S. J. Geier, I. A. I. Mkhaliid, S. A. Westcott, T. B. Marder, *Chem. Rev.*, **2016**, *116*, 9091–9161.
44. Légaré, M.-A.; Pranckevicius, C.; Braunschweig, H. *Chem. Rev.*, **2019**, *119*, 8231–8261.
45. Braunschweig, H.; Dewhurst, R. D.; Gessner, V. H. *Chem. Soc. Rev.*, **2013**, *42*, 3197–3208.

46. Frenking, G.; Hermann, M.; Andradaa, D. M.; Holzmann, N. *Chem. Soc. Rev.*, **2016**, *45*, 1129-1144.
47. Sua, Y.; Kinjo, R. *Chem. Soc. Rev.*, **2019**, *48*, 3613-3659.
48. Taniguchi, T.; *Chem. Soc. Rev.*, **2021**, *50*, 8995-9021.
49. Tonner, R.; Frenking, G. *Pure Appl. Chem.*, **2009**, *81*, 597-614.
50. Frenking, G.; *Angew. Chem. Int. Ed.*, **2014**, *53*, 6040-6046.
51. Mondal, K. C.; Roesky, H. W.; Klinke, F.; Schwarzer, M. C.; Frenking, G.; Niepçtter, B.; Wolf, H.; Herbst-Irmer, R.; Stalke, D. *Angew. Chem. Int. Ed.*, **2013**, *52*, 2963-2967.
52. Xiong, Y.; Yao, S.; Tan, G., Inoue, S.; Driess, M. *J. Am. Chem. Soc.*, **2013**, *135*, 5004-5007.
53. Davidson, P.J.; Lappert, M.F.; *J. Chem. Soc., Chem. Commun.*, **1973**, 317a-317a.
54. Harris, D. H.; Lappert, M. F.; *J. Chem. Soc., Chem. Commun.*, **1974**, 895-896.
55. Gynane, M. J. S.; Lappert, S. M. F.; Miles, J.; Power, P. P. *J. Chem. Soc., Chem. Commun.*, **1976**, 256-257.
56. Goldberg, D. E.; Harris, D. H.; Lappert, M. F.; Thomas, K. M. *J. Chem. Soc., Chem. Commun.*, **1976**, 261-262.
57. M. F. Lappert, *J. Organomet. Chem.*, **1975**, *100*, 139-159.
58. Apeloig, Y.; Pauncz, R.; Karni, M.; West, R.; Steiner, W.; Chapman, D.; *Organometallics*, **2003**, *22*, 3250-3256.
59. Weetman, C.; Inoue, S. *ChemCatChem*, **2018**, *10*, 4213-4228.
60. Haaf, M.; Schmedake, T. A.; West, R. *Acc. Chem. Res.*, **2000**, *33*, 704-714.
61. Roy, M. D.; Rivard, E.; *Acc. Chem. Res.*, **2017**, *50*, 2017-2025.

62. Fujimori, S.; Inoue, S.; *Eur. J. Inorg. Chem.*, **2020**, 2020, 3131-3142.
63. Melen, R. L. *Science*, **2019**, 363, 479-484.
64. Yadav, S.; Saha, S.; Sen, S. S. *ChemCatChem*, **2016**, 8, 486-501.
65. Protchenko, A. V.; Birjkumar, K. H.; Dange, D.; Schwarz, A. D.; Vidovic, D.; Jones, C.; Kaltsoyannis, N.; Mountford, P.; Aldridge, S. *J. Am. Chem. Soc.*, **2012**, 134, 6500-6503.
66. Kira, M.; Ishida, S.; Iwamoto, T.; Kabuto, C. *J. Am. Chem. Soc.*, **1999**, 121, 9722-9723.
67. Rekker, B. D.; Brown, T. M.; Fettingner, J. C.; Tuononen, H. M.; Power, P. P. *J. Am. Chem. Soc.*, **2012**, 134, 6504-6507.
68. Hering- Junghans, C.; Andreiuk, P.; Ferguson, M. J.; McDonald, R.; Rivard, E. *Angew. Chem. Int. Ed.*, **2017**, 56, 6272-6275.
69. Ochiai, T.; Szilvási, T.; Franz, D.; Irran, E.; Inoue, S.; *Angew. Chem. Int. Ed.*, **2016**, 55, 11619-11624.
70. Protchenko, A. V.; Schwarz, A. D.; Blake, M. P.; Jones, C.; Kaltsoyannis, N.; Mountford, P.; Aldridge, S. *Angew. Chem. Int. Ed.*, **2013**, 52, 568-571.
71. Wendel, D.; Porzelt, A.; Herz, F. A. D.; Sarkar, D.; Jandl, C.; Inoue, S.; Rieger, B. *J. Am. Chem. Soc.*, **2017**, 139, 8134-8137.
72. Kristinsdóttir, L.; Oldroyd, N. L.; Grabiner, R.; Knights, A. W.; Heilmann, A.; Protchenko, A. V.; Niu, H.; Kolychev, E. L.; Campos, J.; Hicks, J.; Christensena, K. E.; Aldridge, S. *Dalton Trans.*, **2019**, 48, 11951-11960.
73. Munz, D. *Organometallics*, **2018**, 37, 275-289.
74. Andrada, D. M.; Holzmann, N.; Hamadi, T.; Frenking, G. *Beilstein J. Org. Chem.*, **2015**, 11, 2727-2736.
75. Wang, Y.; Ma, J.; *J. Organomet. Chem.*, **2009**, 694, 2567-2575.

76. Denk, M.; Lennon, R.; Hayashi, R.; West, R.; Belyakov, A. V.; Verne, H. P.; Haaland, A.; Wagner, M.; Metzler, N. *J. Am. Chem. Soc.*, **1994**, *116*, 2691-2692.
77. Becerra, R.; Boganov, S. E.; Egorov, M. P.; Faustov, V. I.; Nefedov, O. M.; Walsh, R. *Can. J. Chem.*, **2000**, *78*, 1428-1433.
78. Dasgupta, R.; Khan, S. *Advances in Organometallic Chemistry*, **2020**, *74*, 105-152.
79. Greb, L.; Ebner, F.; Ginzburg, Y.; Sigmund, L. M. *Eur. J. Inorg. Chem.*, **2020**, *2020*, 3030-3047.
80. Brown, H. C.; Rao, B. C. S. *J. Am. Chem. Soc.*, **1959**, *81*, 6423-6428.
81. Suzuki, A. *Proc. Japan Acad. Ser. B Phys. Biol. Sci.*, **2004**, *80*, 359-371.
82. King, R. B.; *Chem. Rev.*, **2001**, *101*, 1119-1152.
83. Piers, W. E. *Adv. Organomet. Chem.*, **2004**, *52*, 1-77.
84. Staubitz, A.; Robertson, A. P. M.; Sloan, M. E.; Manners, I. *Chem. Rev.*, **2010**, *110*, 4023-4078.
85. Curran, D. P.; Solovyev, A.; Makhlof Brahmi, M.; Fensterbank, L.; Malacria, M.; Lacôte, E. *Angew. Chem. Int. Ed.*, **2011**, *50*, 10294-10317.
86. Arrowsmith, M.; Hadlington, T. J.; Hill, M. S.; Kociok-Köhn, G.; *Chem. Commun.*, **2012**, *48*, 4567-4569.
87. Zhang, G.; Zeng, H.; Wu, J.; Yin, Z.; Zheng, S.; Fettinger, J. C. *Angew. Chemie Int. Ed.*, **2016**, *55*, 14369-14372.
88. Kuciński, K.; Hreczycho, G. *Green Chem.*, **2019**, *21*, 1912-1915.
89. Kim, J. H.; Jaladi, A. K.; Kim, H. T.; An, D. K. *Bull. Korean Chem. Soc.*, **2019**, *40*, 971-975.

90. Yang, S. J.; Jaladi, A. K.; Kim, J. H.; Gundeti, S.; An, D. K. *Bull. Korean Chem. Soc.*, **2019**, *40*, 34–38.
91. Harinath, A.; Bhattacharjee, J.; Nayek, H. P.; Panda, T. K. *Dalt. Trans.*, **2018**, *47*, 12613–12622.
92. Ma, D. H.; Jaladi, A. K.; Lee, J. H.; Kim, T. S.; Shin, W. K.; Hwang, H.; An, D. K. *ACS Omega*, **2019**, *4*, 15893–15903.
93. Yadav, S.; Pahar, S.; Sen, S. S. *Chem. Commun.*, **2017**, *53*, 4562–4564.
94. Wu, Y.; Shan, C.; Ying, J.; Su, J.; Zhu, J.; Liu, L. L.; Zhao, Y. *Green Chem.*, **2017**, *19*, 4169–4175.
95. McLellan, R.; Kennedy, A. R.; Mulvey, R. E.; Orr, S. A.; Robertson, S. D. *Chem.-A Eur. J.*, **2017**, *23*, 16853–16861.
96. Gunanathan, C.; Hölscher, M.; Pan, F.; Leitner, W.; *J. Am. Chem. Soc.*, **2012**, *134*, 14349–14352.
97. Liu, Y. N.; Su, H. F.; Li, Y. W.; Liu, Q. Y.; Jagličić, Z.; Wang, W. G.; Tung, C. H.; Sun, D. *Inorg. Chem.*, **2019**, *58*, 4574–4582.
98. Zeng, H.; Wu, J.; Li, S.; Hui, C.; Ta, A.; Cheng, S. Y.; Zheng, S.; Zhang, G. *Org. Lett.*, **2019**, *21*, 401–406.
99. Zhang, G.; Cheng, J.; Davis, K.; Bonifacio, M. G.; Zajaczkowski, C. *Green Chem.*, **2019**, *21*, 1114–1121.
100. Copéret, C.; Ghaffari, B.; Mendes Burak, J.; Chan, K. W.; *Chem.-A Eur. J.*, **2019**, *25*, 13869–13873.
101. Gudun, K. A.; Segizbayev, M.; Adamov, A.; Plessow, P. N.; Lyssenko, K. A.; Balanay, M. P.; Khalimon, A. Y. *Dalt. Trans.* **2019**, *48*, 1732–1746.
102. Arévalo, R.; Vogels, C. M.; Macneil, G. A.; Riera, L.; Pérez, J.; Westcott, S. A. *Dalt. Trans.*, **2017**, *46*, 7750–7757.

103. Bai, T.; Janes, T.; Song, D. *Dalt. Trans.*, **2017**, *46*, 12408–12412.
104. Z. Yang, M. Zhong, X. Ma, K. Nijesh, S. De, P. Parameswaran, H. W. Roesky, *J. Am. Chem. Soc.*, **2016**, *138*, 2548–2551.
105. Ding, Y.; Ma, X.; Liu, Y.; Liu, W.; Ni, C.; Yan, B.; Yan, L.; Yang, Z. *Inorganica Chim. Acta*, **2019**, *497*, 119091.
106. Jin, D.; Ma, X.; Liu, Y.; Peng, J.; Yang, Z. *Appl. Organomet. Chem.*, **2019**, *33*, e4637.
107. Woodside, A. J.; Smith, M. A.; Herb, T. M.; Manor, B. C.; Carroll, P. J.; Rablen, P. R.; Graves, C. R. *Organometallics*, **2019**, *38*, 1017–1020.
108. Weidner, V. L.; Barger, C. J.; Delferro, M.; Lohr, T. L.; Marks, T. J.; *ACS Catal.*, **2017**, *7*, 1244–1247.
109. Wang, W.; Shen, X.; Zhao, F.; Jiang, H.; Yao, W.; Pullarkat, S. A.; Xu, L.; Ma, M. *J. Org. Chem.*, **2018**, *83*, 69–74.
110. Chen, S.; Yan, D.; Xue, M.; Hong, Y.; Yao, Y.; Shen, Q. *Org. Lett.*, **2017**, *19*, 3382–3385.
111. Yan, D.; Dai, P.; Chen, S.; Xue, M.; Yao, Y.; Shen, Q.; Bao, X. *Org. Biomol. Chem.*, **2018**, *16*, 2787–2791.
112. Zhu, Z.; Dai, P.; Wu, Z.; Xue, M.; Yao, Y.; Shen, Q.; Bao, X. *Catal. Commun.*, **2018**, *112*, 26–30.
113. Ghatak, T.; Makarov, K.; Fridman, N.; Eisen, M. S. *Chem. Commun.*, **2018**, *54*, 11001–11004.
114. Mukherjee, D.; Osseili, H.; Spaniol, T. P.; Okuda, J.; *J. Am. Chem. Soc.*, **2016**, *138*, 10790–10793.
115. Phillips, N. A.; O’Hanlon, J.; Hooper, T. N.; White, A. J. P.; Crimmin, M. R. *Org. Lett.*, **2019**, *21*, 7289–7293.

116. J. L. Carden, L. J. Gierlichs, D. F. Wass, D. L. Browne, R. L. Melen, *Chem. Commun.*, **2019**, 55, 318–321.
117. W. Wang, M. Luo, W. Yao, M. Ma, S. A. Pullarkat, L. Xu, P. H. Leung, *New J. Chem.*, **2019**, 43, 10744–10749.
118. Li, T.; Zhang, J.; Cui, C. *Chinese J. Chem.*, **2019**, 37, 679–683.
119. Hadlington, T. J.; Hermann, M.; Frenking, G.; Jones, C. *J. Am. Chem. Soc.*, **2014**, 136, 3028–3031.
120. Driess, M.; Yao, S.; Brym, M.; Wllen, C. V. *Angew. Chem. Int. Ed.*, **2006**, 45, 4349–4352.
121. Wu, Y.; Shan, C.; Sun, Y.; Chen, P.; Ying, J.; Zhu, J.; Liu, L.; Zhao, Y. *Chem. Commun.*, **2016**, 52, 13799–13802.
122. Schneider, J.; Sindlinger, C. P.; Freitag, S. M.; Schubert, H.; Wesemann, L. *Angew. Chem. Int. Ed.*, **2017**, 56, 333–337.
123. Schneider, J.; Sindlinger, C. P.; Freitag, S. M.; Schubert, H.; Wesemann, L. *Angew. Chem. Int. Ed.*, **2017**, 129, 339–343.
124. Dasgupta, R.; Das, S.; Hiwase, S.; Pati, S. K.; Khan, S.; *Organometallics*, **2019**, 38, 1429–1435.
125. Zhong-yang, L.; Long-qiang, H.; Ahmadi, S. *J. Phys Org Chem.*, **2021**, 34, e4266.
126. Abedini, N.; Kassae, MZ. *J. Phys Org Chem.*, **2021**, 34, e4208.
127. Iversen, K. J.; Dutton, J. L.; Wilson, D. J. D. *Chem. Asian J.*, **2017**, 12, 1499–1508.
128. Elveny, M.; Alrazzak, N. A.; Aljeboree, A. M.; Alkaim, A. F.; Ebadi, A. G. *J. Phys Org Chem.*, **2021**, 34, e4262.

129. Steinert, H.; Löffler, J.; Gessner, V. H.; *Eur. J. Inorg. Chem.*, **2021**, 2021, 5004-5013.
130. Hohenberg, P.; Kohn, W. *Phys. Rev.*, **1964**, 136, B864-B871.
131. Kohn, W.; Sham, L.; *J. Phys. Rev.*, **1965**, 140, A1133-A1138.
132. Zhao, Y.; Truhlar, D. G. *Theor. Chem. Acc.*, **2008**, 120, 215-241.
133. Zhao, Y.; Truhlar, D. G.; *Acc. Chem. Res.*, **2008**, 41, 157-167.
134. TURBOMOLE V7.4 2019, a development of University of Karlsruhe and Forschungszentrum Karlsruhe GmbH, 1989-2007, TURBOMOLE GmbH, since 2007; available from <http://www.turbomole.com>.
135. Ansgar, S.; Christian, H.; Reinhart, A. *The Journal of Chemical Physics*, **1994**, 100, 5829-5835.
136. Perdew, J. P.; Burke, K.; Ernzerhof, M. *Phys. Rev. Lett.*, **1996**, 77, 3865-3868.
137. Grimme, S.; Antony, J.; Ehrlich, S.; Krieg, H.; *The Journal of Chemical Physics*, **2010**, 132, 154104/1-154104/19.
138. Grimme, S.; Ehrlich, S.; Goerigk, L.; *J. Comput. Chem.*, **2011**, 32, 1456-1465.
139. Klamt, A.; Schuurmann, G. *J. Chem. Soc. Perkin Trans.*, **1993**, 799-805.
140. Eichkorn, K.; Treutler, O.; Öhm, H.; Häser, M.; Ahlrichs, R. *Chem. Phys. Lett.*, **1995**, 240, 283-290.
141. Eichkorn, K.; Weigend, F.; Treutler, O.; Ahlrichs, F. *Theor. Chem. Acc.*, **1997**, 97, 119-124.
142. Sierka, M.; Hogeckamp, A. Ahlrichs, R. *The Journal of Chemical Physics*, **2003**, 118, 9136-9148.
143. Deglmann, P.; May, K.; Furche, F.; Ahlrichs, R.; *Chem. Phys. Lett.*, **2004**, 384, 103-107.

144. Fukui, K. *Acc. Chem. Res.*, **1981**, *14*, 363-368.
145. Mammen, M.; Shakhnovich, E. I.; Deutch, J. M.; Whitesides, G. M. *J. Org. Chem.*, **1998**, *63*, 3821-3830.
146. Pal, S.; Dasgupta, R.; Khan, S. *Organometallics*, **2016**, *35*, 3635–3640.

Chapter 6

**Unraveling the Role of Organocatalysis in
Modified Cinchona Alkaloid Catalyst via Proton
Transfer**

Chapter 6

Unraveling the Role of Organocatalysis in Modified Cinchona Alkaloid Catalyst via Proton Transfer

Abstract

An important aspect of asymmetric organocatalysis is the role of aromatic additives in enhancing the yield and enantioselectivity of the desired product. The primary explanation given for their effectiveness is that their presence promotes proton release because of their high pKa values. However, in the current computational work with density functional theory (DFT), focusing on a *cinchona* alkaloid C9 O-benzyl substituted cupreidine (BzCPD) catalyst system, it is shown that presence of the aromatic additive, 2-naphthol, modifies the transition state in the thiocyanation reaction of oxindole and N-thiocyanatophthalimide. This finding unveils a new Wynberg model for asymmetric catalysis, and shows that the aromatic additive acts as a second catalyst in the reaction, stabilizing both the electrophile and the nucleophile through non-covalent interactions: $\pi \cdots \pi$ stacking with the electrophile and hydrogen bonding with the nucleophile. Given the large number of different organocatalyst systems where an analogous additive has been employed, the work indicates a general principle by which such additives operate. Furthermore, the current study also sheds light on the interesting experimental finding of the reversal of enantioselectivity of the BzCPD catalysed thiocyanation reaction upon changing the nucleophile from oxindole to β -keto ester. It is seen that the predominant stabilizing influence is the C–H \cdots S non-covalent interaction, which is present only in the major transition state obtained for each of the two cases. This interesting observation showcases the subtle, hitherto unknown role of the sulphur heteroatom in the asymmetric catalysed thiocyanation reaction, and has implications for the large number of asymmetric organocatalytic reactions involving the sulphur heteroatom.

6.1 Introduction

Two decades after the seminal publications of List¹ and Macmillan,² it is now universally acknowledged that organocatalysts form the third pillar of asymmetric catalysis,³ along with enzymes and chiral organometallic complexes. Along with the tremendous spurt in the application of organocatalysts to a wide range of different transformations, there has also been a concerted effort to understand the mechanism(s) by which such asymmetric catalytic processes take place, both through experimental,⁴⁻⁶ as well as computational⁷⁻¹¹ studies. This has helped develop greater mechanistic understanding, and thereby improved the efficiency of the systems. Nevertheless, there are still some interesting aspects of organocatalytic systems that are yet to be completely understood. One such aspect is the use of additives: it has been observed that the presence of an additive leads to improvement in the yield, enantioselectivity, or both, in a wide variety of organocatalytic systems.¹² Such additives include organic acids,¹³ chiral phosphoric acids,¹⁴ alcohols,¹⁵ water,¹⁶ amines,¹⁷ molecular sieves¹⁸ and salts.¹⁹ Of these, the most common are acids and alcohols. It has been hypothesized that their role in such systems is to increase the pK_a of the reaction medium through their acidic nature. In some cases, they have been seen as proton shuttles.²⁰ However, researchers have wondered whether additives could have a more active, defined role in increasing the efficiency of organocatalytic systems.²¹

Such a possibility seems particularly pertinent when one considers the salutary effect aromatic additives have played in organocatalytic systems. C-H activation *via* cross coupling between aryl iodides/bromides and the C-H bonds of arenes, mediated solely by the presence of 1,10-phenanthroline as catalyst in the presence of potassium tert-butoxide as a base, studied by Shi and coworkers^{21a} for instance, was seen to benefit from the presence 1,10-phenanthroline. Curran and Studer, commenting on this work, pointed out that the role played by 1,10-phenanthroline as additive was unclear.^{21b} There are several interesting reports where aromatic alcohols such as phenol (substituted and unsubstituted) and naphthol, have been employed as additives, leading to improved yield and enantioselectivity.¹⁵ Ooi and co-workers have reported

a supramolecular assembly system for the conjugate addition of azalactones to unsaturated acyl benzotriazoles, where three molecules of phenol were envisaged to participate through a hydrogen bonding network,²² which led to an increase in the enantioselectivity. Fu and co-workers used 2-chloro-6-methylphenol as an additive in the phosphine-catalyzed double γ -addition of racemic heterocycles to racemic allenates.^{20a,23} Zhu *et al.* found that the addition of a small amount of β -naphthol in the aza-Morita–Baylis–Hillman reaction of imine and β -naphthyl acrylate led to improved yield and enantiomeric excess (ee).²⁴ Chen and co-workers studied phenol-additive effects on the aza-MBH reaction of ketimines and acrolein: the addition of (*R*)- or (*S*)-BINOL to the system as additive was found to dramatically improve the enantioselectivity.²⁵ Rovis and co-workers investigated the asymmetric intermolecular Stetter reaction of enals with nitroalkenes using catechol as the additive.²⁶ This was found to increase the yield quite significantly. The same group also found that bisphenol additives improved product enantioselectivities in the Stetter reaction of intermediate aldehydes.²⁷ These specific instances mentioned here are taken out of a range of other examples of effective aromatic alcohol additives, and highlight an interesting point: both the substrates involved in each case could display non-covalent interactions with the additive: through $\pi \cdots \pi$ stacking or through hydrogen bonding. This potential of the aromatic alcohols to stabilize both substrates leads to an important question: is it possible that the additive plays a previously unsuspected role in such systems, by explicitly participating in the reaction as a second catalyst? This is the question that has motivated the current investigation.

In order to explore this possibility, I have focused on a recent experimental report by Chen and co-workers, on the alpha thiocyanation of oxindole (see Figure 6.1), using the BzCPD *cinchona* alkaloid catalyst, and employing 2-naphthol as the additive.²⁸ Bronsted base *cinchona* alkaloid catalysts are a very successful family of organocatalysts²⁹ that have been employed for a variety of different transformations. These molecules demonstrate both conformational flexibility and multi-site interactions with different substrates, leading to cooperative interplay between substrate and catalyst in the transition states, which forms the basis of the observed enantioselectivity. They have found extensive use in medicinal chemistry,³⁰ and

chemical industries,³¹ and more than four dozen diverse chemical transformations have been successfully catalyzed by various *cinchona* alkaloid derivatives.^{32,33} In particular, *cinchona* alkaloids with a free C6'-OH functionality (the structure, BzCPD, in Figure 6.1 below, is an example of the same) have been found to be very effective in asymmetric organocatalysis.³⁴ These systems are known to work through the stabilization of the electrophile and nucleophile through non-covalent interactions, which is the basis of the two standard mechanisms: a) the Wynberg ion-pair hydrogen bonding model³⁵ and b) the Houk-Grayson hydrogen bonding model,³⁶ which have been invoked to explain their activity. The BzCPD *cinchona* alkaloid catalyst, therefore, is a good candidate for exploring the question that was raised in the previous paragraph: is the aromatic additive, 2-naphthol, employed by Chen and co-workers,²⁸ functioning as a second catalyst in the thiocyanation reaction that they had studied?

Our computational studies with density functional theory (DFT) indeed indicate this to be the case. The *cinchona* alkaloid is seen to stabilize the substrates in the fashion of the Wynberg model, but what is also observed is that an explicit 2-naphthol molecule is present in the transition state, stabilizing the electrophile by $\pi \cdots \pi$ stacking and the nucleophile by hydrogen bonding (see Figure 6.1 below). This new finding elevates the role of the aromatic additive beyond merely increasing the pKa of the system, and, furthermore, reveals a new Wynberg model, modifying the standard Wynberg that has existed for 45 years. The favourability of the enantioselectivity calculated on the basis of this new Wynberg model in comparison to the competing Houk-Grayson model is seen to be in good agreement with experimental observations. The general implications of the results obtained for asymmetric organocatalysis become clear when one considers the many known examples in literature where aromatic additives have been seen to enhance yield and enantioselectivity in systems where they could stabilize both the electrophile and the nucleophile.

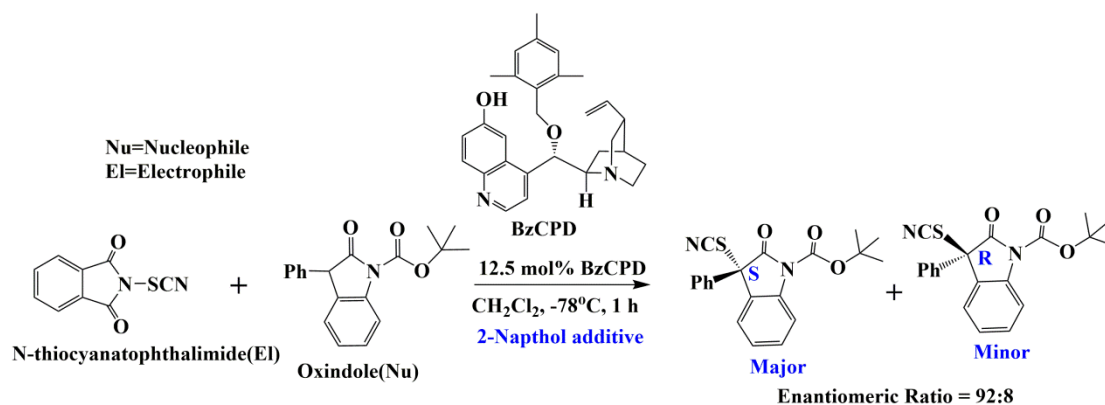


Figure 6.1 Alpha thiocyanation of oxindole using N-thiocyanatophthalimide. The BzCPD catalyst, with 2-naphthol employed as additive, works to provide the S-enantiomer as the major product.

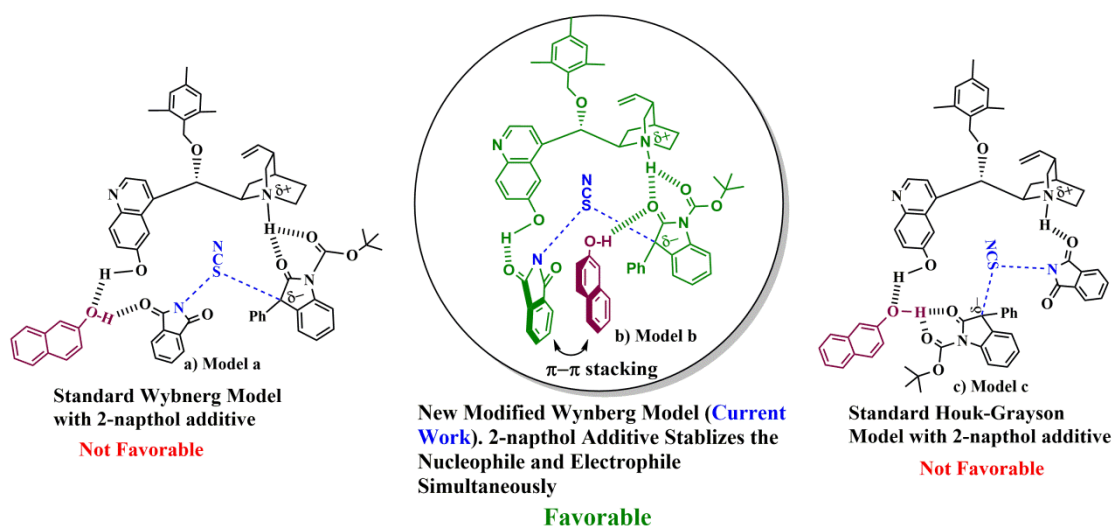


Figure 6.2. The three models shown above describe how the 2-naphthol additive participates in the reaction. The model in green (Model b) is the most correct mode of activation, where the additive serves to stabilize both the electrophile and nucleophile, along with the C6'-OH *cinchona* alkaloid catalyst. This is based on insights gained from the current work.

Another reason for choosing the *cinchona* alkaloid system studied by Chen and co-workers is the interesting fact that the enantioselectivity of the thiocyanation reaction was seen to be reversed upon going from the oxindole to β -keto ester nucleophile, for the same catalyst and electrophile: BzCPD and N-

thiocyanatophthalimide respectively³⁷ in the absence of any additive (Scheme 2). The reasons for this reversal have also been uncovered in this work. It is seen that the *cinchona* alkaloid catalyst employs a combination of multiple weak non-covalent interactions, including O–H···O, N–H···O, C–H···O, C–H···S, C–H···N, C–H··· π , and π ··· π , and what stands out is the C–H···S interaction, which preferentially stabilizes only the transition state corresponding to the major product formed in the case of each nucleophile (see Figure 6.4 below). This result puts the spotlight on the sulphur heteroatom, revealing how it is a prominent contributing factor in determining the enantioselectivity in the BzCPD catalyzed thiocyanation reaction. These results, too, have general implications, since there are a large number of asymmetric organocatalysis reactions involving the sulphur heteroatom.

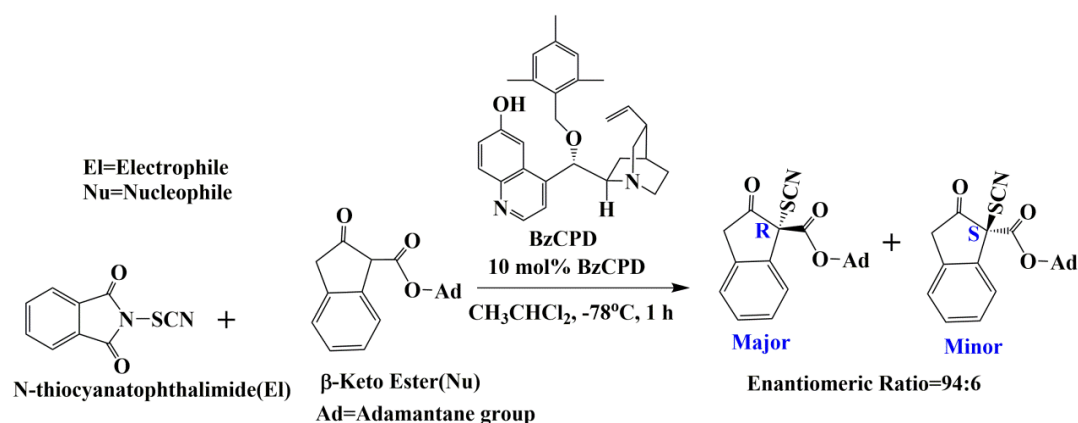


Figure 6.3 Alpha thiocyanation of β -keto ester (nucleophile) using N-thiocyanatophthalimide (electrophile). BzCPD works as catalyst and the R-enantiomer is the major product.

Therefore, the current work has significant relevance, bringing to light the elegant interplay of different complementary factors that make the *cinchona* alkaloid catalysts so effective in asymmetric organocatalysis, and providing general insights into the potential catalytic role of aromatic additives in enhancing yield and enantioselectivity for a vast number of chemical transformations, as well as into the unsung role of the supposedly weak C–H···S interaction in determining the enantioselectivity of reactions.

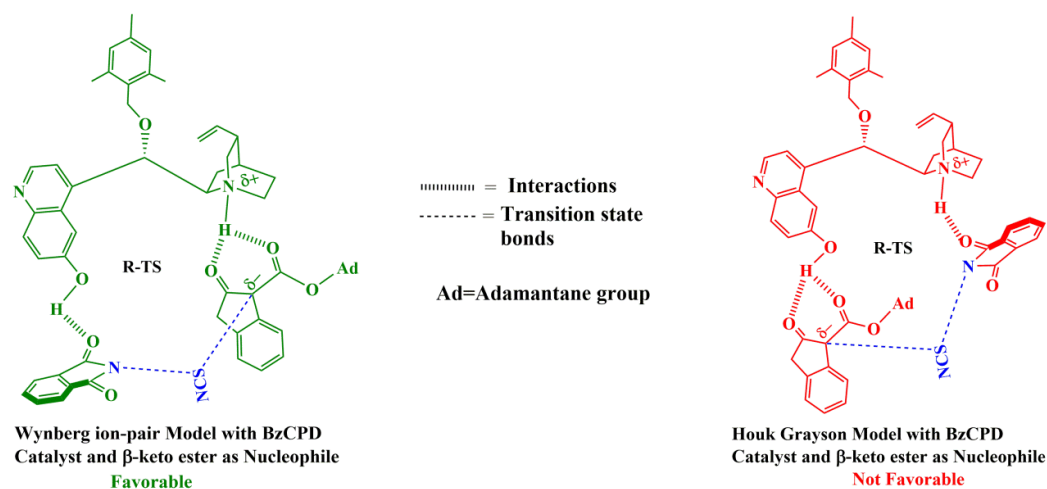


Figure 6.4 Transition state (TS) models show the TS from the favourable Wynberg ion-pair hydrogen bonding mechanism and from the unfavourable Houk-Grayson bifunctional Brønsted acid-hydrogen bonding mechanism, with the β -keto ester nucleophile. The reactions occur in the absence of additive. The catalyst and electrophile are BzCPD and N-thiocyanatophthalimide respectively.

6.2 Computational Details

All the calculations for the structures reported in this work have been done using density functional theory (DFT).^{38,39} The calculations have been carried out with Turbomole 7.4⁴⁰ using the TZVP⁴¹ basis set. Geometry optimizations were performed using the Perdew, Burke, and Ernzerhof (PBE) functional.⁴² Dispersion corrections (D3)⁴³ have been included in all the calculations. Solvent corrections have also been included using the COSMO model,⁴⁴ with $\epsilon=8.93$ and $\epsilon=10.90$ employed to model dichloromethane, CH_2Cl_2 , when the nucleophile is oxindole and dichloroethane, $\text{CH}_3\text{CH}_2\text{Cl}_2$, when the nucleophile is the β -keto ester. Therefore, the level of theory employed is PBE-D3/TZVP+COSMO(CH_2Cl_2) and PBE-D3/TZVP+COSMO($\text{CH}_3\text{CH}_2\text{Cl}_2$) respectively.⁴¹⁻⁴⁴ Furthermore, in order to underscore the reliability of the enantiomeric calculations, all the enantioselective transition states have also been further optimized at the M06-2X/TZVP+COSMO(CH_2Cl_2)^{45,41,44} level of theory for the case when the nucleophile

is oxindole, and at the M06-2X/TZVP+COSMO(CH₃CH₂Cl₂) level of theory when the nucleophile is the β-keto ester. The results ($\Delta\Delta G^\ddagger$ values) show that the trends obtained with the PBE functional are replicated with the M06-2X functional.

The resolution of identity (RI)⁴⁶ along with the multipole accelerated RI (marij)⁴⁷ approximations have been employed for an accurate and efficient treatment of the electronic Coulomb term in the DFT calculations. Necessary care was taken to ensure that the obtained transition state structures possessed only one imaginary frequency corresponding to the correct normal mode, in order to obtain more reliable energy values for the investigated potential energy surface. In addition, intrinsic reaction coordinate (IRC)⁴⁸ calculations were done with all the transition states in order to further confirm that they were the correct transition states, yielding the correct reactant and product structures. The values reported herein are ΔG values, with zero point energy, internal energy, and entropic contributions, with the temperature taken to be 195.15 K. The calculation of the translational entropy in standard software involves assumptions about the volume that may be inaccurate. The translational entropy term can be corrected by a free volume correction introduced by Mammen and co-workers.⁴⁹ Based on the Sackur–Tetrode equation, the free volume model describes the translational entropy of molecules in the solution ($\Delta S_{\text{trans}}(\text{sol})$); and provides physically intuitive corrections for translational entropy values. In the free volume model, it has been assumed that the volume available to the molecule in solution is lower than the total volume, and this “free volume” is determined by the equation below:

$$V_{\text{free}} = C_{\text{free}} \left(\sqrt[3]{\frac{10^{27}}{[X]N_0}} - \sqrt[3]{V_{\text{molecule}}} \right)^3 \quad 6.1$$

Here, V_{molec} is the molecular volume, $[X]$ is the concentration of molecules (mol/L) in solution and N_0 is the Avogadro number. The translational entropy can be obtained after considering the free volume correction, and after inserting the value of V_{free} in the Sackur-Tetrode equation. The total entropy is then calculated by adding the corrected translational entropy and the entropic contributions from the rotational and

vibrational components. Multiwfn were employed for topology analysis.⁵⁰ Structures with NCI plots were generated using VMD.⁵¹

6.2.1. Enantiomeric Ratio (er) Calculations

According to transition state theory, the rate constant for the formation of *R* and *S* enantiomeric products can be expressed as k_R and k_S by Equations 2 and 3

$$k_R = \frac{k_b T}{h} e^{-\frac{\Delta G_R^\ddagger}{RT}} \quad 6.2$$

$$k_S = \frac{k_b T}{h} e^{-\frac{\Delta G_S^\ddagger}{RT}} \quad 6.3$$

where ΔG^\ddagger is the free energy of activation for the formation of *R* or *S* respectively, k_b is the Boltzmann constant, h is the Planck constant, T is the temperature and R is the universal gas constant. Stereoselectivity of the chemical reactions can be represented as an enantiomeric ratio (er). The er (for the enantioselective reaction) is directly proportional to the relative rates of formation of the enantiomeric products; that is, the ratio of products depends on the relative free energy barrier ($\Delta\Delta G^\ddagger$), which can be represented by:

$$\frac{R}{S} = \frac{k_R}{k_S} = e^{-\frac{\Delta G_R^\ddagger - \Delta G_S^\ddagger}{RT}} = e^{-\frac{\Delta\Delta G^\ddagger}{RT}} \quad 6.4$$

The enantioselectivity in a reaction is commonly reported by enantiomeric excess (ee), which can be calculated as

$$ee = \frac{[R] - [S]}{[R] + [S]} \times 100 \quad 6.5$$

where $[R]$ and $[S]$ represent the mole fraction of the *R* and *S* enantiomers. ee can be computationally obtained as

$$ee = \frac{1 - e^{-\frac{\Delta\Delta G^\ddagger}{RT}}}{1 + e^{-\frac{\Delta\Delta G^\ddagger}{RT}}} \times 100 \quad 6.6$$

6.2.2 Non-Covalent Interaction (NCI) Plot Analysis

The analysis of NCIs in the stereo-controlling transition states has been carried out by employing the NCI plot developed by Yang *et al.*⁵² The NCI plot is a program that shows the graphical representation of inter- and intramolecular NCIs based on the electron density and its derivatives.

6.3 Results and Discussion

6.3.1 Conformational Analysis of BzCPD

One of the most influential characteristics of *cinchona*-based catalyst systems is their active conformation, because this decides the nature and extent of the stereoselectivity. The conformational space is rather small due to the rigidity and bulk of the substituents and gives rise to a restricted number of conformer populations.⁵³ Wynberg and co-workers have done a substantial amount of work to come up with four major conformations: a) *anti* open, b) *syn* open, c) *anti* closed and d) *syn* closed (see Figure 6.5).⁵⁴

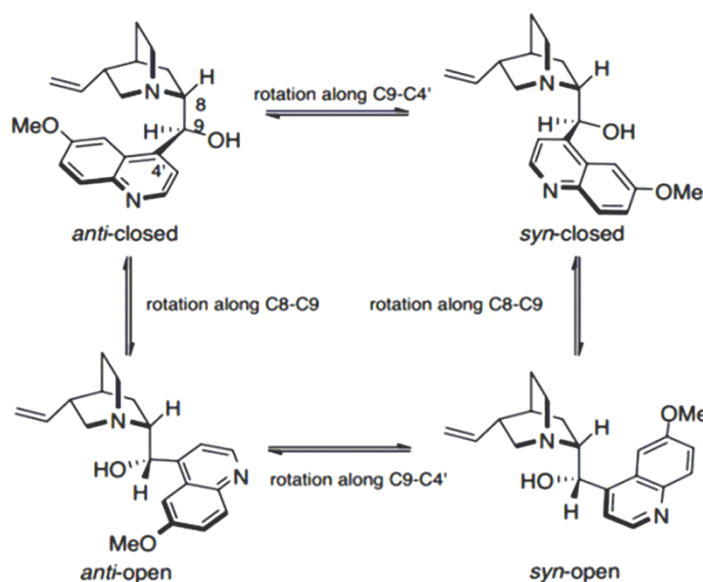


Figure 6.5. Different conformations (*anti* open, *anti* closed, *syn* open, *syn* closed) of the *Cinchona* alkaloid proposed by Wynberg and co-workers.^{35a,35b}

Later, Bürgi and Baiker, through combined NMR experiments and *ab initio* calculations, revealed that the *anti* open conformation of the catalyst is the most stable in aprotic solvents.⁵⁵ They also observed that in polar solvents, the *syn* closed and *anti* closed conformations were preferred over the *anti* open conformation. As the implicit solvents employed in the current computational study are dichloromethane and dichloroethane, a systematic conformational analysis was required at the outset in order to identify the most stable conformer. In order to carry out such an analysis, it was necessary to identify the principal torsional angles that distinguish the conformers from each other. *Cinchona* catalysts are rigid molecules containing relatively few rotatable bonds, and torsional angles around rotatable single bonds in the vicinity of the two chiral carbon atoms, namely C8 and C9 (see Figure 6.6), are crucial structural parameters of the conformational space. Four torsional angles, modelled as α (N1–C8–C9–C4'), β (\angle C8–C9–C4'–C3'), γ (\angle C8–C9–O10–C9''), and δ (\angle C9–O10–C9''–C10'') were seen to be the most relevant in determining the four different conformations that were possible for the rigid structure, and altering them gave rise to the four conformers. All the four conformers were investigated to find the most stable structure. A similar approach has been followed by Wong and co-workers in their computational study of the asymmetric methanolysis of meso-cyclic anhydrides through oxyanion hole stabilization.⁵⁶ It is also worth mentioning that BzCPD has a flexible benzyl moiety at C9-O. It was, therefore, necessary to obtain a potential energy surface scan along the dihedral (C8-C9-O10-C11) to find the most stable orientation of the C9-O-benzyl group in BzCPD.

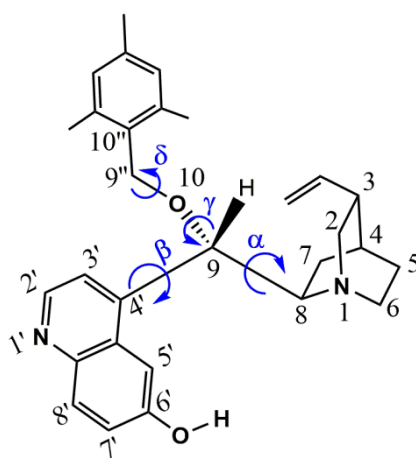


Figure 6.6 The relevant angles and dihedrals in the BZCPD catalyst structure.

Table 6.1. Energy values of the calculated conformations. The first and second values are calculated at the M06-2X/TZVP+COSMO(CH₂Cl₂) and M06-2X/TZVP+COSMO(CH₃CH₂Cl₂) level of theory respectively.

| BzCPD conformers | $\Delta\Delta G(\text{kcal/mol})$ |
|--------------------|-----------------------------------|
| <i>anti</i> open | 0.0/0.0 |
| <i>anti</i> closed | 1.7/1.8 |
| <i>syn</i> open | 2.2/2.1 |
| <i>syn</i> closed | 2.5/2.7 |

Based on the results of the conformational analysis, the most stable structure was seen to be *anti* open (see Table 6.1). Since the relative population of the different conformers in solution is dependent on the exponent of the difference of their free energies divided by RT, it is thus clear that the *anti* open conformer would be the dominant one in solution for BzCPD. This conformer has therefore been chosen as the active catalyst in all of the calculations mentioned in the thesis.

6.3.2. Mechanistic study of the BzCPD Catalyzed Thiocyanation Reaction with Oxindole as Nucleophile, N-Thiocyanatophthalimide as Electrophile and 2-naphthol as Additive

In order to investigate the mechanism of Chen's thiocyanation reaction with 2-naphthol as additive, I have considered the system comprising of the catalyst, BzCPD, the electrophile, N-thiocyanatophthalimide, the nucleophile, oxindole, and the additive, 2-naphthol, and explored the pathway for the reaction shown in Scheme 1.

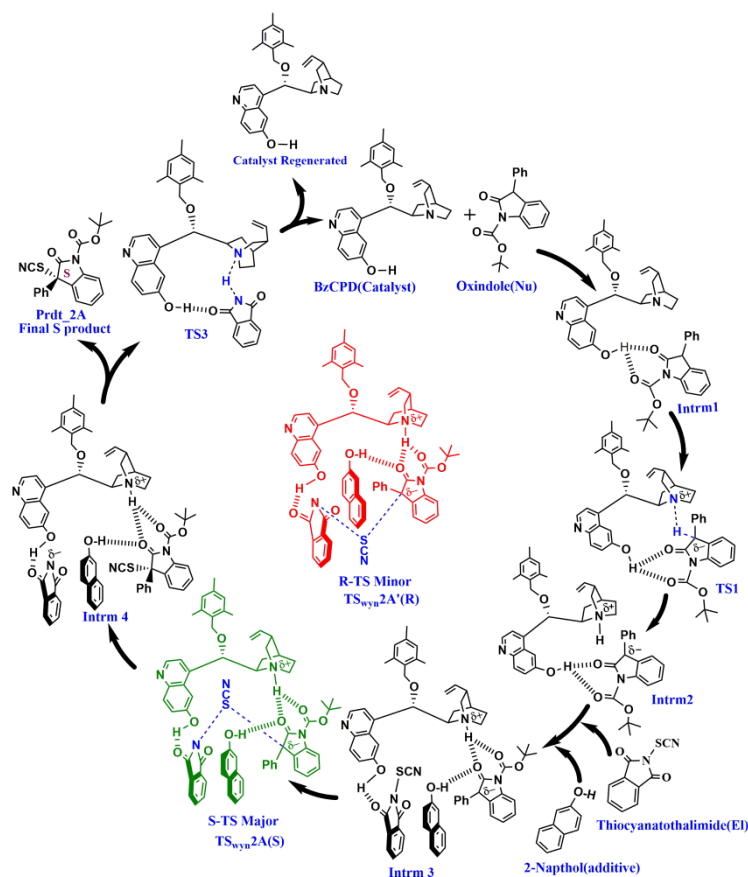


Figure 6.7 The scheme for the new model where a molecule of the additive 2-naphthol plays an explicit role in the thiocyanation reaction along with the quinuclidine nitrogen of the catalyst. The blue coloured atoms are those participating in the transition states (TSs). The green coloured species is the major TS and the red coloured species is the minor TS.

As discussed in the Introduction, there are primarily two mechanisms that have been proposed in the literature to account for the manner by which the enantioselective products are formed with the aid of the catalyst. One is a) the Wynberg ion-pair hydrogen bonding model³⁵ and the other is b) the Houk-Grayson bifunctional Brønsted acid-hydrogen bonding model.³⁶ However, the inclusion of an additive (2-naphthol) necessitates the study of new possible pathways, because of the possibilities of different interactions of the O-H group in 2-naphthol with the different oxygen atoms of the electrophile and nucleophile. What is discussed here is the comparison of the lowest energy pathways that have been obtained for the new Wynberg ion-pair

mechanism and the Houk-Grayson bifunctional mechanism compared to the proposed mechanism by Chen and co-workers in their experimental work²⁸ (see Models a, b and c shown in Figure 6.2). The new pathway that I propose with the Wynberg ion-pair-hydrogen bonding mechanism (Model b in Figure 6.2) features dual activation of the electrophilic thiocyanato reagent (electrophile **EI**) by the catalyst's hydroxyl group and of the oxindole (nucleophile **Nu**) by the protonated quinuclidine nitrogen. The 2-naphthol activates the nucleophile and electrophile by hydrogen bonding and $\pi\cdots\pi$ stacking respectively. In the Houk-Grayson new bifunctional Brønsted acid-hydrogen bonding mechanism (Model c in Figure 6.2), the electrophilic thiocyanato reagent is activated by the protonated quinuclidine nitrogen and the oxindole by the catalyst's C6'-OH and 2-naphthol respectively. I have also investigated the activation of 2-naphthol with different oxygens of the electrophile and the nucleophile for the Houk-Grayson pathway. In other words, the best pathway for the Wynberg model has been compared with the best pathway of the Houk-Grayson model. There have been many mechanistic investigations of the transfer cyanation reactions,⁵⁷ but the transfer thiocyanation,⁵⁸ i.e., the -SCN group transfer from N-thiocyanatophthalimide to the quinuclidine nitrogen of the *cinchona* alkaloid catalyst, has not yet been investigated. It is worth mentioning here that Xue and co-workers have investigated the pathway for the transfer trifluoromethylthiolation and have obtained a very high barrier for the $^+\text{SCF}_3$ transfer process, as compared to the Wynberg ion-pair hydrogen bonding pathway.⁵⁹ Therefore, such a transfer thiocyanation pathway has not been studied in the current work. It is also to be noted that, due to the available conformational space between the C6'-OH and the quinuclidine NH of the catalyst, the nucleophile can approach in both the *syn* or *anti* fashions to give different *syn*-S, *syn*-R and *anti*-S, *anti*-R products (see Figure 6.8 below). I have considered all the approaches to find the best approach. It was seen the *syn* approach was favoured over the *anti* by 6.3 kcal/mol. Therefore the complete pathway for the thiocyanation was then studied for the *syn* approach pathway. The energy profile for the Wynberg ion-pair hydrogen bonding model, which is the most favorable pathway for the thiocyanation reaction with the 2-naphthol additive, is presented in Figure 6.9.

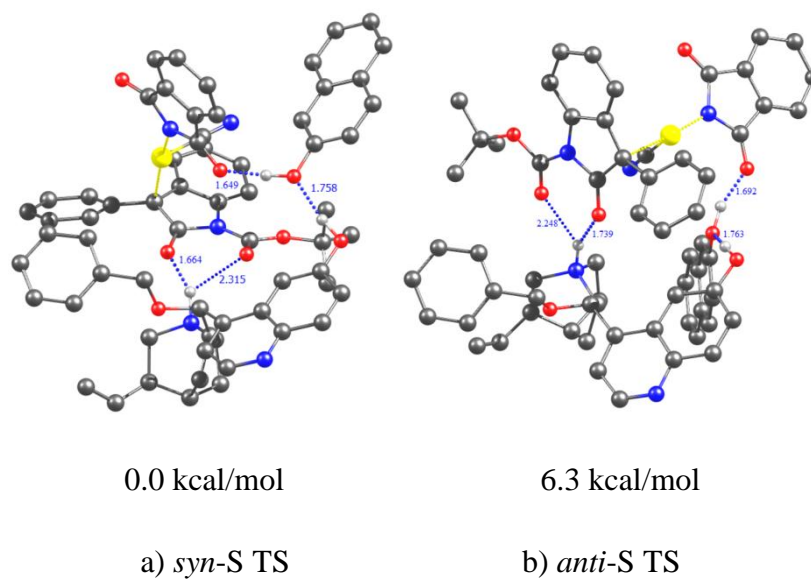


Figure 6.8 The optimized transition state structures for the *syn*-S and *anti*-S approach cases.

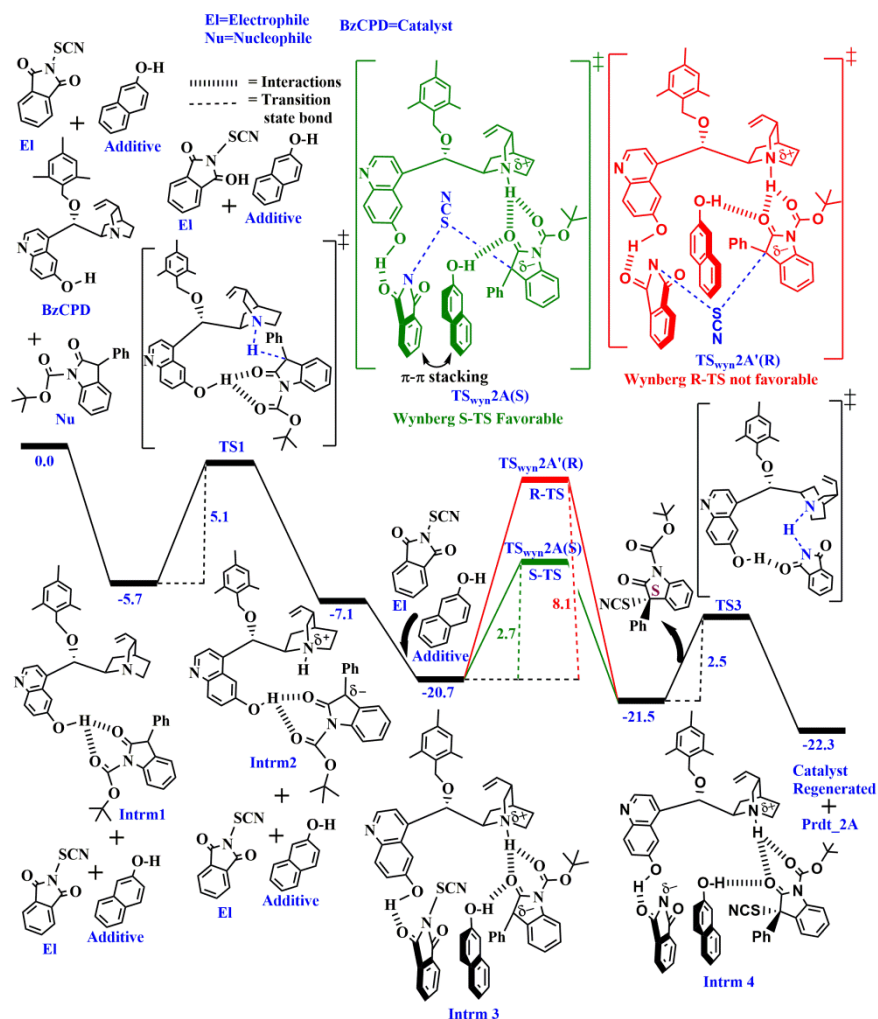


Figure 6.9 Energy profile for the BzCPD catalyzed thiocyanation of oxindole. 2-naphthol acts as an additive, activating both the nucleophile as well as the electrophile. The free energy (ΔG) values are in kcal/mol, at the PBE-D3/TZVP+COSMO($\text{CH}_3\text{CH}_2\text{Cl}_2$) level of theory.

In the dual activation mechanism shown in Figure 6.9 above, the formation of the hydrogen-bonded complex **Intrm1** between the oxindole and catalyst OH is energetically favoured by 5.7 kcal/mol. The proton transfer from the oxindole carbon to the quinuclidine nitrogen takes place after surmounting a barrier of 5.1 kcal/mol. This leads to the ion-pair complex **Intrm2**, which is 7.1 kcal/mol more stable than the totally separated reactant species. I, note that the 2-naphthol and the thiocyanating reagent have not been considered from the starting point of the calculation, i.e., from

Intrm1, as the enantioselective step in the complete cycle is the formation of **TS_{wyn}2A**. This reduces the computational cost without hampering the reliability. After the formation of **Intrm2**, the 2-naphthol(**Ad**) additive and N-thiocyanatophthalimide (**El**) begin to participate in the mechanistic cycle. The coordination of **El** and **Ad** through O–H···O and N–H···O hydrogen-bonding interactions yields **Intrm3**, which is located 20.7 kcal/mol below the separated reactants and 13.6 kcal/mol below **Intrm2**. After this step, the stereoselective thiocyanation takes place. The overall activation free energy (ΔG^\ddagger) for the Wynberg ion-pair-hydrogen bonding model is calculated to be only 2.7 kcal/mol. The corresponding Houk-Grayson Model has a barrier of 10.3 kcal/mol. Thus, the free energy of activation required for the Wynberg pathway is 7.6 kcal/mol lower than that for the Houk-Grayson pathway, indicating that the most likely pathway is the Wynberg ion-pair-hydrogen bonding model. The enantioselective S-product is stable by 21.5 kcal/mol. After this, the regeneration of the catalyst takes place with a barrier of 1.5 kcal/mol, thereby completing the catalytic cycle. The energy differences between the enantiocontrolling TSs are somewhat overestimated by the DFT calculations. This is not an uncommon situation in quantum mechanical investigations of catalysis, as has been pointed out earlier, for instance, by Houk and co-workers.⁶⁰ I have also investigated the mechanism where the reaction happens without the influence of the 2-naphthol additive. The mechanistic pathway and energy profile is shown below (see Figures 6.10 and 6.11 below).

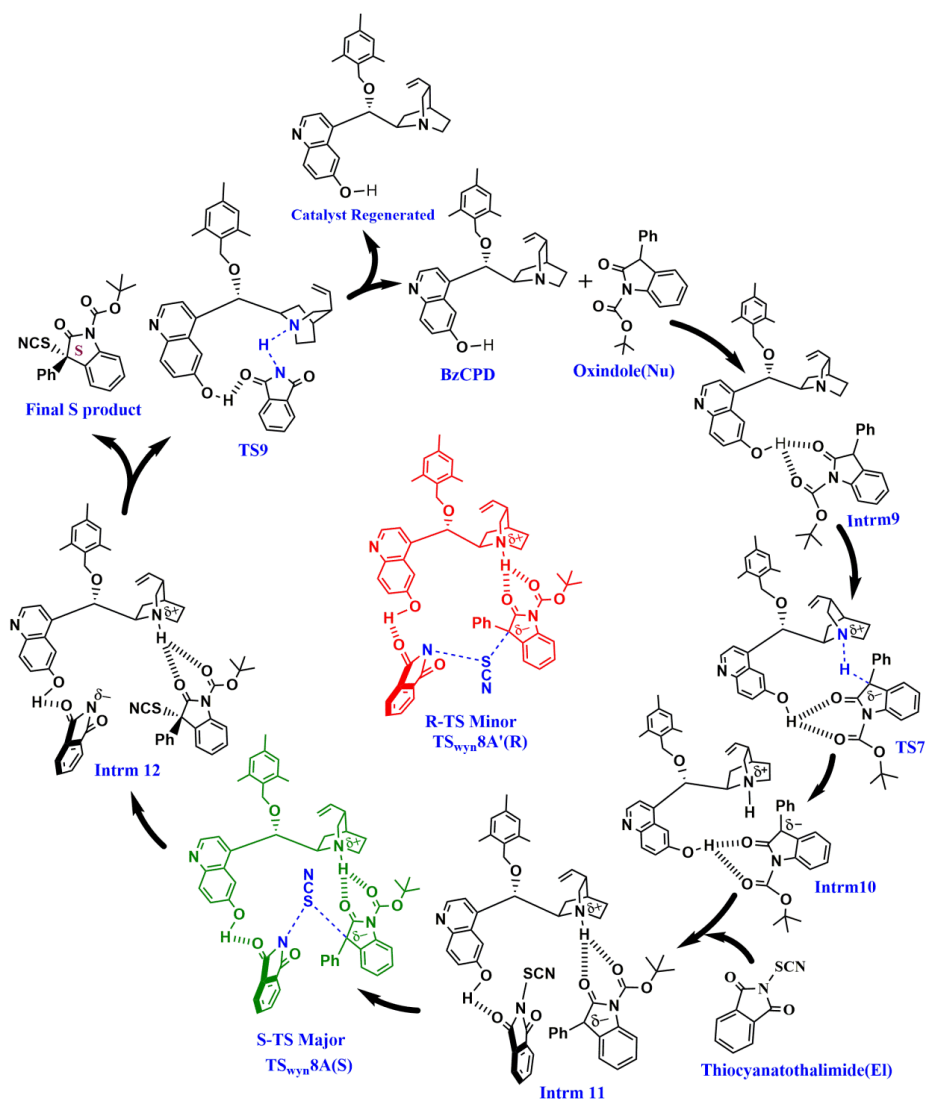


Figure 6.10 Alpha thiocyanation of oxindole(nucleophile) using thiocyanatophthalimide (electrophile). No additive plays a role. BzCPD works as catalyst to give S-enantiomer as the major product.

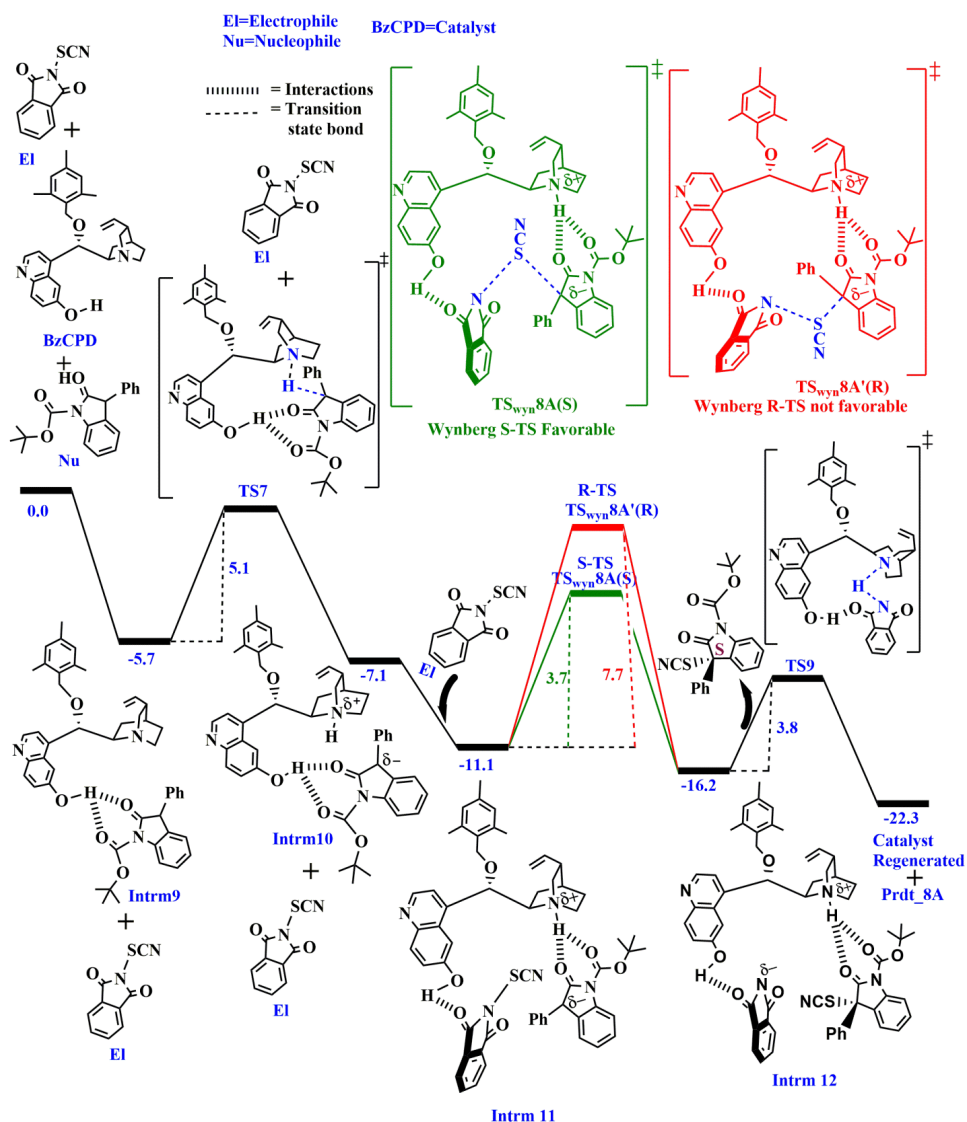


Figure 6.11 Energy profile for the BzCPD catalyzed thiocyanation of oxindole. The free energy (ΔG) values are in kcal/mol, at the PBE-D3/TZVP+COSMO(CH_2Cl_2) level of theory.

The calculations show that, for this case, the Wynberg ion-pair-hydrogen bonding model is favoured by 8.3 kcal/mol over the Houk-Grayson bifunctional hydrogen bonding model. Furthermore, the difference in the energies of the major and minor transition states was seen to be 4.0 kcal/mol, which is 1.4 kcal/mol smaller than the corresponding difference with the additive, thereby indicating the favourable effect of the 2-naphthol on the enantioselectivity of the reaction.

6.3.3. Origin of Enantioselectivity for Reaction with Additive and Oxindole

After establishing the preferred dual activation mode (i.e., the new Wynberg ion-pair-hydrogen bonding model with 2-naphthol as additive), I have subsequently explored the origin of stereoinduction in this reaction. In order to shed light on the source of energy differences between $\text{TS}_{\text{wyn}}2\text{A}(\text{S})$ and $\text{TS}_{\text{wyn}}2\text{A}'(\text{R})$, I have performed a form of energy decomposition analysis (EDA)⁶¹⁻⁶³ for the two transition state (TS) structures (see Figure 6.12). I note here that this same approach for EDA analysis has recently been adopted for the electrophilic trifluoromethylthiolation of β -keto ester with N-Trifluoromethylthiophthalimide by Xue and coworkers.⁵⁹ The activation energy ΔE^\ddagger of the TSs can be written as $\Delta E^\ddagger = \Delta E_{\text{def}} + \Delta E_{\text{int}}$, where the terms ΔE_{def} and ΔE_{int} are the deformation and interaction energies, respectively. The deformation energy ΔE_{def} is the energy difference that arises from structural changes toward the TS formation. The interaction energy ΔE_{int} corresponds to the energy difference between the sum of the cationic catalyst, the anionic oxindole substrate, the neutral N-thiocyanatophthalimide substrate and the 2-naphthol additive, minus the complex at the TS structure. The results are presented in Table 6.2.

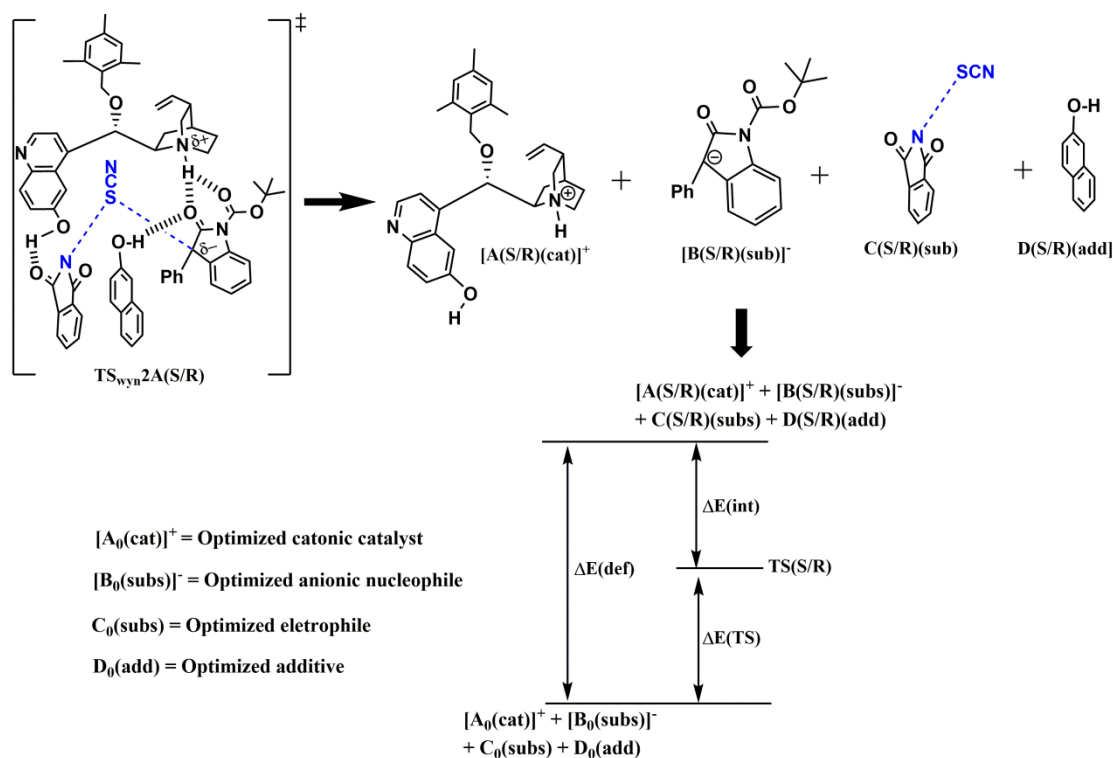


Figure 6.12 Energy decomposition analysis (EDA) for the newly proposed Wynberg ion-pair transition state model.

The results obtained make it clear that the large energy separation between $\text{TS}_{\text{wyn}}2\text{A}(\text{S})$ and $\text{TS}_{\text{wyn}}2\text{A}'(\text{R})$ mainly arises from differences in the interaction energy ($\Delta\Delta E_{\text{int}} = 5.0$ kcal/mol). Both $\Delta\Delta E_{\text{int}}$ and $\Delta\Delta E_{\text{def}}$ are positive, meaning that the two components contribute synergistically to the overall energy difference between $\text{TS}_{\text{wyn}}2\text{A}(\text{S})$ and $\text{TS}_{\text{wyn}}2\text{A}'(\text{R})$. In other words, the substrates in $\text{TS}_{\text{wyn}}2\text{A}(\text{S})$ are not only more stable but also interact more favorably with the catalyst, than do those in $\text{TS}_{\text{wyn}}2\text{A}'(\text{R})$.

Table 6.2 An energy decomposition analysis(EDA) approach adopted for $\text{TS}_{\text{wyn}}2\text{A}(\text{S})$ and $\text{TS}_{\text{wyn}}2\text{A}'(\text{R})$.

| Transition state | $\Delta E(\text{def})$ kcal/mol | $\Delta E(\text{int})$ kcal/mol | $\Delta E(\text{TS})$ kcal/mol |
|--|---------------------------------|---------------------------------|--------------------------------|
| $\text{TS}_{\text{wyn}}2\text{A}(\text{S})$ | 29.2 | -97.3 | -68.8 |
| $\text{TS}_{\text{wyn}}2\text{A}'(\text{R})$ | 29.8 | -92.3 | -62.5 |

In order to reveal the difference in interaction energies between the substrates and the catalyst ($\Delta\Delta E_{\text{int}}$), the non-covalent interaction (NCI) analysis of the TS structures was conducted, which enabled the visualization of the non-covalent interactions.⁶⁴ The results are shown in Figure 6.13. The NCI analyses of $\text{TS}_{\text{wyn}}2\text{A}(\text{S})$ and $\text{TS}_{\text{wyn}}2\text{A}'(\text{R})$ reveal that, in addition to the strong conventional $\text{N}^+-\text{H}\cdots\text{O}$ and $\text{O}-\text{H}\cdots\text{O}$ hydrogen bonding interactions, several weak non-conventional $\text{C}-\text{H}\cdots\text{O}$,⁶⁵ $\text{C}-\text{H}\cdots\text{S}$,^{36b} and $\text{C}-\text{H}\cdots\pi$ ⁶⁶ interactions are present. Most interestingly, there is a favorable $\pi\cdots\pi$ stacking^{65a,67} interaction between the additive and the electrophile, which also contributes to the stabilization of both $\text{TS}_{\text{wyn}}2\text{A}(\text{S})$ and $\text{TS}_{\text{wyn}}2\text{A}'(\text{R})$ (see Figure 6.15).⁶⁸ As the substrates and additive interact with the catalyst through a network of hydrogen bonding interactions, as well as through a $\pi\cdots\pi$ stacking interaction, it is still not easy to figure out which factors are the major ones contributing to the $\Delta\Delta E_{\text{int}}$. In order to understand the factors

involved, it is therefore also necessary to quantify the weak interactions in the transition state structures.

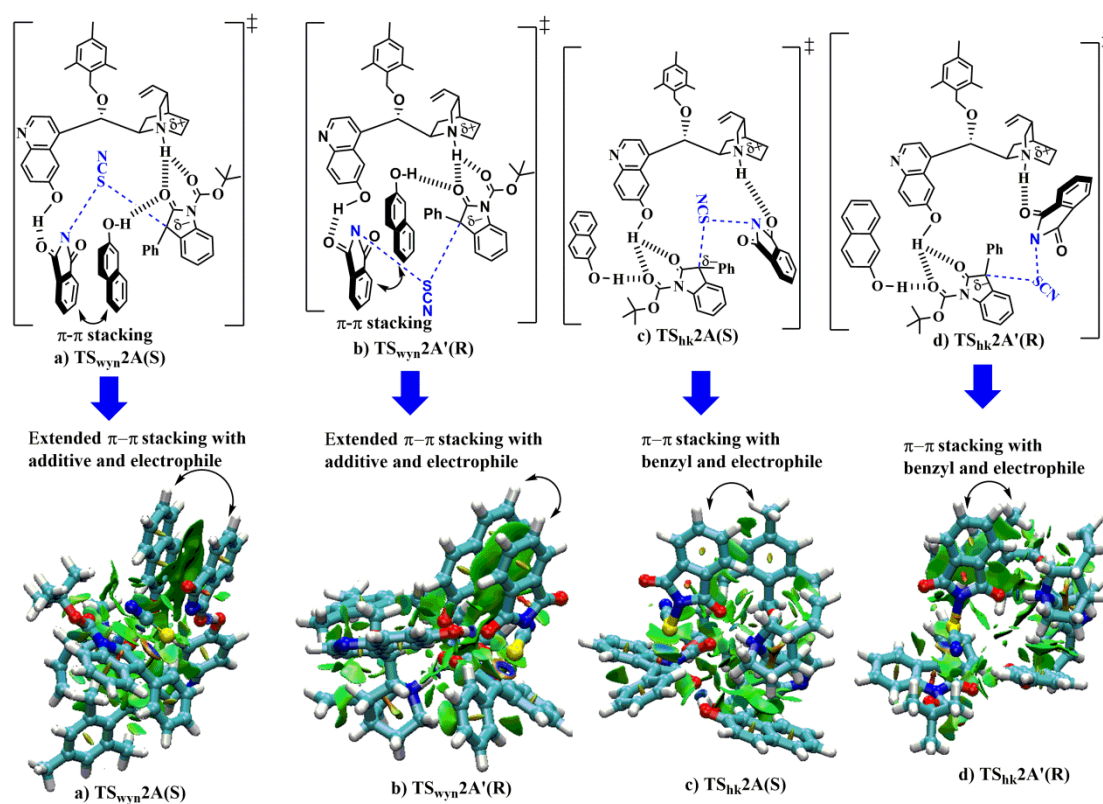


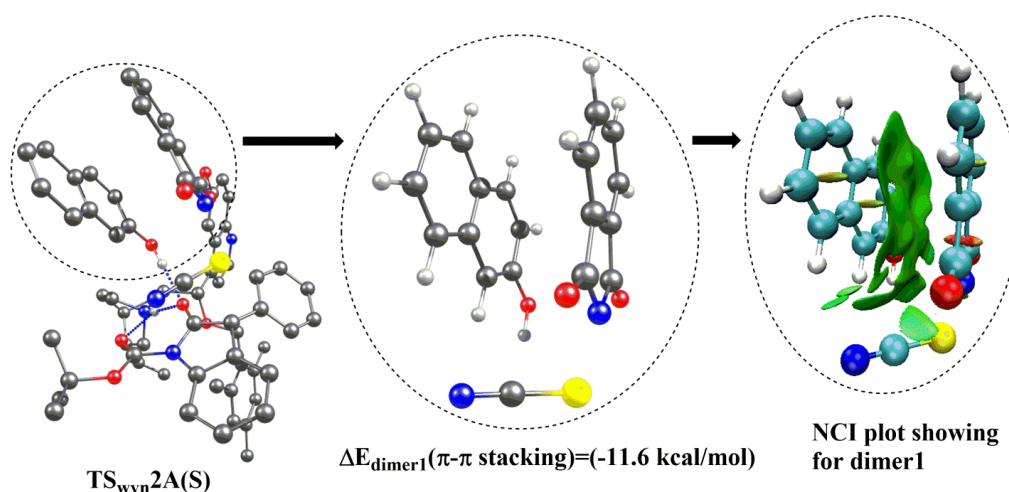
Figure 6.13. The non-covalent interaction (NCI) plot showing extended $\pi \cdots \pi$ stacking interactions between 2-naphthol and the electrophile for the Wynberg ion-pair transition states (**a** and **b**). The Houk-Grayson model transition states (**c** and **d**) show no extended $\pi \cdots \pi$ stacking between 2-naphthol and the electrophile. $\pi \cdots \pi$ stacking between the electrophile and the benzyl group of the catalyst is not so predominant.

For a better understanding of the contributions of individual non-covalent interactions to the $\Delta\Delta E_{int}$, I have applied Espinosa's equation⁶⁹ (Eq. 6.7) to quantify the strength of hydrogen bonds in the hydrogen-bond network. The equation implies the correlation of the hydrogen bond energy (E_{HB}) to the pressure exerted on the electrons around the critical point ($V(r_{cp})$), both related to the strength of the hydrogen bonding (HB) interaction.

$$E_{\text{HB}}=(1/2)*V*(r_{\text{cp}})$$

6.7

The estimated energies for the HB interactions, E_{HB} , and the $\Delta\Delta E$ π -stacking values, are summarized in Figures 6.15 and 6.16 (various interactions are denoted using the labels **a-u**). It is seen that the strong conventional O-H \cdots O hydrogen-bonds (**a**) contribute identically to the stabilization of the two TS structures. On the other hand, the N⁺-H \cdots O hydrogen-bonds (**c** and **d**) contribute 18.0 kcal/mol (4.9+13.1 = 18.0 kcal/mol) to the stabilization of **TS_{wyn}2A(S)**, but only 14.9 kcal/mol (5.7+9.2 = 14.9 kcal/mol) to the stabilization of **TS_{wyn}2A'(R)**. Moreover, the sum total of the weak non-conventional C-H \cdots S, C-H \cdots O, C-H \cdots N and C-H \cdots π interactions contribute (2.2+2.7+1.3+1.9+2.0+1.2+2.0+1.5+1.9+0.8+2.0+0.3+0.5+0.8+0.2+0.4+0.2+0.9)=22.8 kcal/mol to the stabilization of **TS_{wyn}2A(S)**, but only 20.8 kcal/mol (2.2+2.0+1.9+0.3+1.3+1.8+0.3+0.3+0.8+3.0+0.2+1.0+1.5+0.3+2.5+0.1+1.3) to the stabilization of **TS_{wyn}2A'(R)**. The $\pi\cdots\pi$ stacking energy has been calculated considering the truncated model of **TS_{wyn}2A(S)** and **TS_{wyn}2A'(R)** employing Wheeler's strategy (see Figure 6.14 below).⁷⁰ The $\pi\cdots\pi$ stacking energy for the **TS_{wyn}2A(S)**, which is the major transition state, is -11.6 kcal/mol, whereas the $\pi\cdots\pi$ stacking energy for the minor transition state **TS_{wyn}2A'(R)** is -9.9 kcal/mol (see Figure 6.14 below). Therefore, the $\pi\cdots\pi$ interaction is seen to be 1.7 kcal/mol stronger in **TS_{wyn}2A(S)** than in **TS_{wyn}2A'(R)** (see Figure 6.14 below).



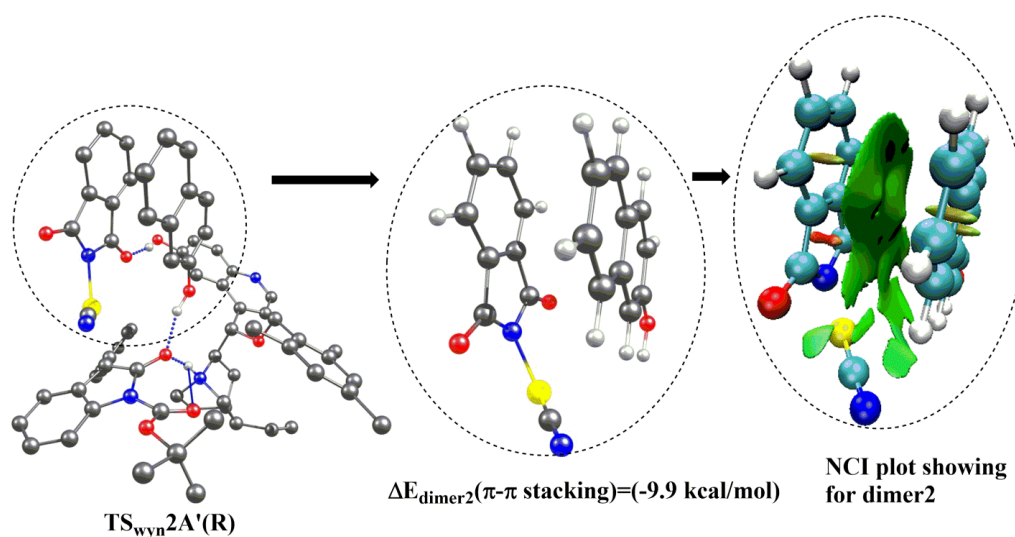


Figure 6.14 Truncated model showing $\pi\text{-}\pi$ stacking interactions for the transition states TS_{wyn2A(S)} and TS_{wyn2A'(R)}. The $\Delta\Delta E$ ($\pi\cdots\pi$ stacking) is 1.7 kcal/mol favorable for TS_{wyn2A(S)} over TS_{wyn2A'(R)}.

Adding all the non-covalent interactions for the major TS, i.e. TS_{wyn2A(S)}, yields the value -70.0 kcal/mol, while the corresponding value for the minor TS, i.e. TS_{wyn2A'(R)}, is -63.6 kcal/mol, i.e., unfavourable by 6.4 kcal/mol. This gives us a clear idea as to why one enantioselective product is favoured over the other.

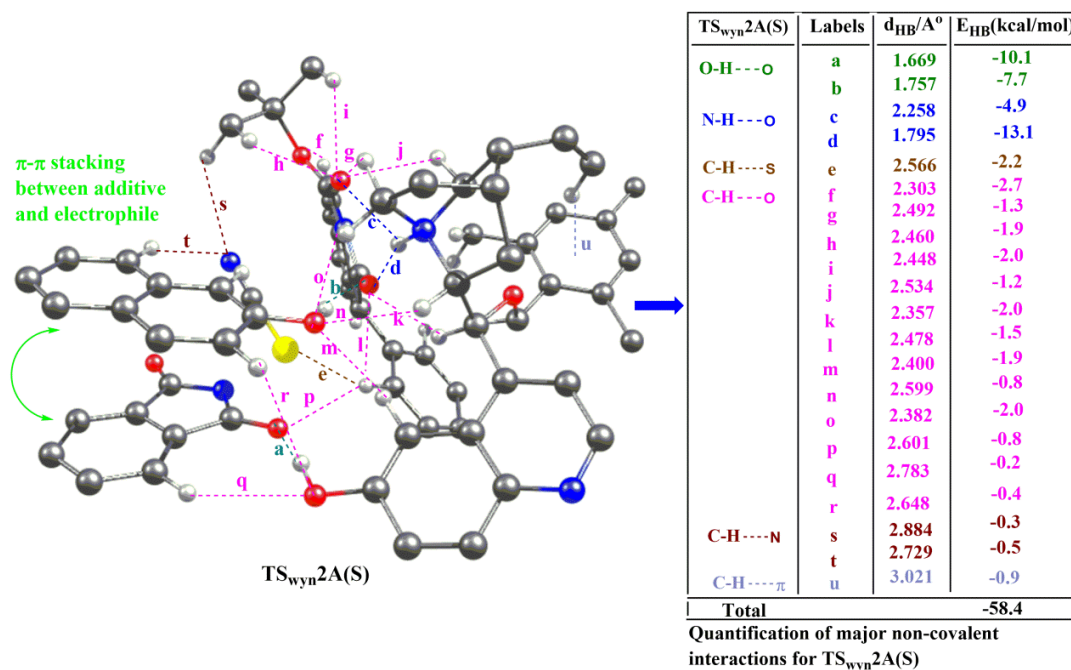


Figure 6.15 The quantification of the different non-covalent interactions in the transition state leading to the major S product.

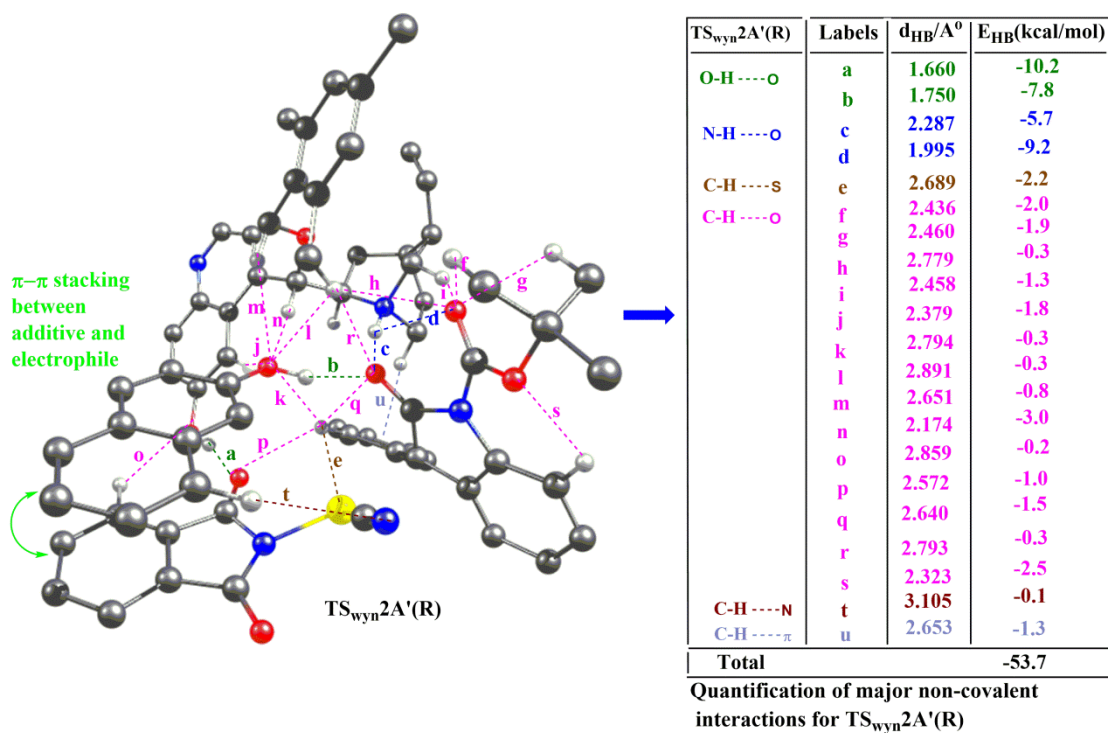


Figure 6.16 The quantification of the different non-covalent interactions in the transition state leading to the minor R product.

6.3.4. Mechanistic study of the thiocyanation reaction with BzCPD as catalyst, β -keto ester as nucleophile, and N-thiocyanatophthalimide as electrophile.

In order to gain more insights into the thiocyanation reaction, I have investigated the mechanism of another thiocyanation reaction reported by Chen and co-workers³⁷ with the same electrophile: N-thiocyanatophthalimide (thiocyanating agent) and the same catalyst, BzCPD, but with β -keto ester employed as the nucleophile instead of the oxindole. What is interesting about this reaction is that the reaction yields the R enantiomer as the major product, i.e., it displays enantioselectivity that is the reverse of the case with the oxindole as nucleophile. The purpose of the computational investigations discussed in this section was to investigate why this switch takes place.

The reaction pathway of Chen's thiocyanation reaction was studied (see Figure 6.3). Here, note that the nucleophile for the reaction employed experimentally had an adamantyl group. Since carrying out calculations with such a large group is highly expensive computationally, the nucleophile was modeled with a tertiary butoxide group instead of the adamantyl group. Chen and co-workers in their experimental work of the enantioselective thiocyanation reaction with the BzCPD catalyst had employed β -keto ester with the tertiary butoxide group and obtained fairly good enantioselectivity.³⁷ The enantiomeric ratio they reported with tertiary butoxide was 93:7 in favour of the R enantiomer.

As in the previous section, I have investigated two mechanistic pathways: a) the Wynberg ion pair hydrogen bonding model³⁵ and b) the Houk-Grayson bifunctional Brønsted acid-hydrogen bonding model³⁶ (see Figure 6.17). The energy profile for the Wynberg ion-pair hydrogen bonding mechanism, which is the more favorable pathway for the thiocyanation reaction with the BzCPD catalyst, is presented in Figure 6.17. The less favoured Houk-Grayson pathway would take place with a enantioselectivity determining transition state that is 4.7 kcal/mol less stable than the corresponding transition state for the more favoured Wynberg pathway.

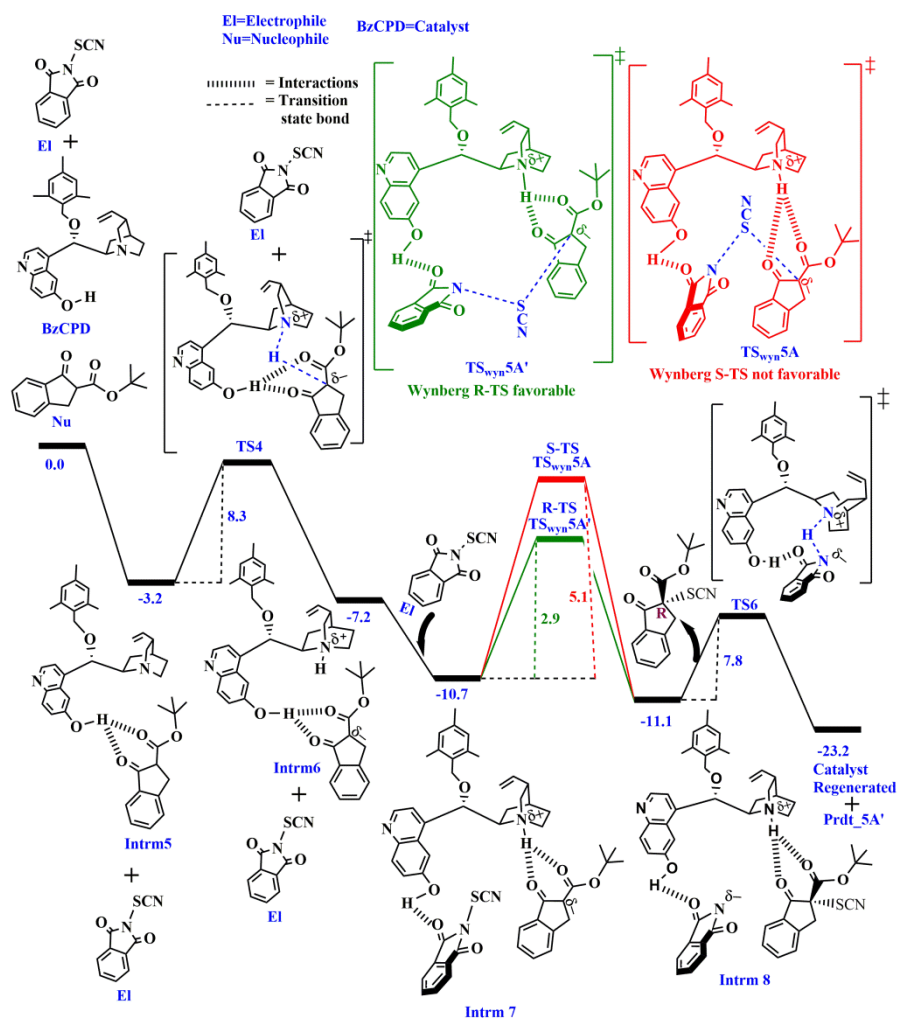


Figure 6.17 The free energy profile for the BzCPD catalyzed thiocyanation of the β -keto ester. The free energy (ΔG) values are in kcal/mol, at the PBE-D3/TZVP+COSMO($\text{CH}_3\text{CH}_2\text{Cl}_2$) level of theory.

6.3.5. Origin of Enantioselectivity for reaction without Additive and β -keto ester

After having established that the Wynberg ion-pair hydrogen bonding model was preferred, I subsequently explored the origin of stereoselection in Chen's asymmetric electrophilic thiocyanation reaction with the β -keto ester nucleophile. I have performed one form of the energy decomposition analysis (EDA)⁶¹⁻⁶³ for the two transition states $\text{TS}_{\text{wyn}5\text{A}'(\text{R})}$ and $\text{TS}_{\text{wyn}5\text{A}(\text{S})}$, structures (see Figure 6.18 below). It

is important to note here that this same approach for EDA analysis has been used in the previous section where I have investigated the origin of enantioselectivity for the thiocyanation reaction with additive and the oxindole nucleophile. Here, the interaction energy, ΔE_{int} , corresponds to the energy difference between the sum of the cationic catalyst, the anionic β -keto ester substrate and the neutral N-thiocyanatophthalimide substrate, minus the complex at the TS structure. The results are presented in Table 6.3.

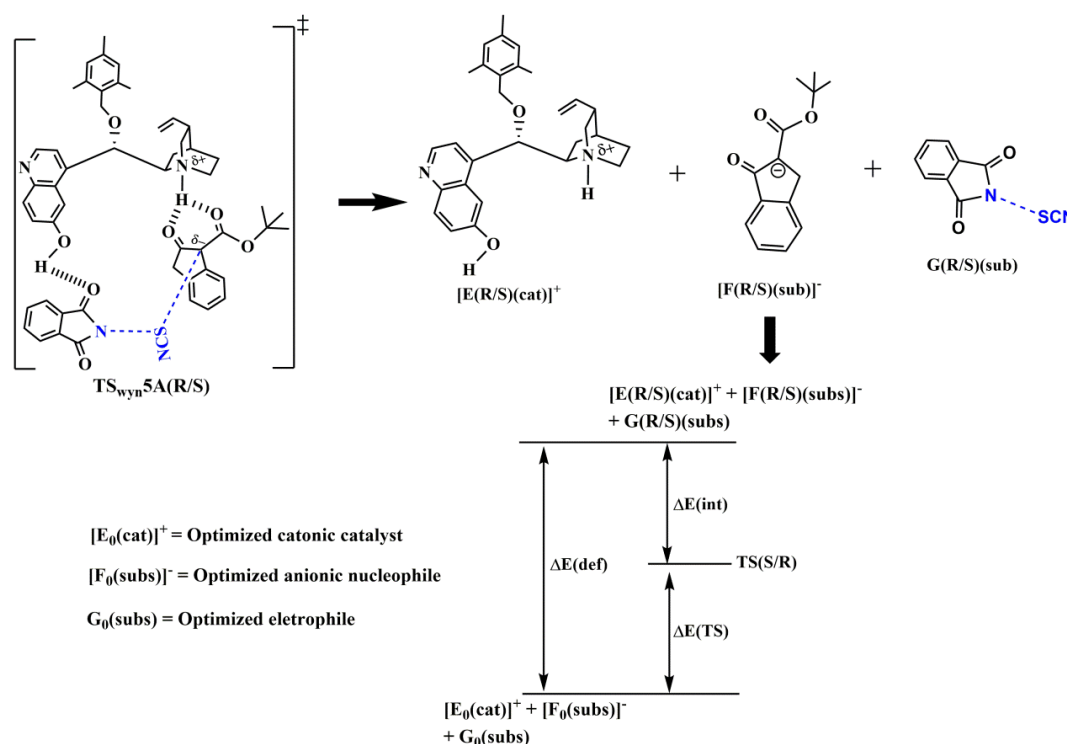


Figure 6.18 Energy decomposition analysis for the Wynberg ion-pair transition state model.

Table 6.3: Energy decomposition analysis (EDA) for $\text{TS}_{\text{wyn}5\text{A}'(\text{R})}$ and $\text{TS}_{\text{wyn}5\text{A}(\text{S})}$.

| Transition state | $\Delta E(\text{def})$ kcal/mol | $\Delta E(\text{int})$ kcal/mol | $\Delta E(\text{TS})$ kcal/mol |
|--|------------------------------------|---------------------------------|-----------------------------------|
| $\text{TS}_{\text{wyn}5\text{A}(\text{S})}$ | 20.3 | -63.6 | -44.4 |
| $\text{TS}_{\text{wyn}5\text{A}'(\text{R})}$ | 17.3 | -66.0 | -46.3 |

6.3.6. Determining why there is change in enantioselectivity when the nucleophile is changed

In order to gain insights into why the enantioselectivity changes from S to R for the thiocyanation reaction when the nucleophile is changed from oxindole to β -keto ester, I have investigated the different hydrogen bonds and other non-covalent interactions present in the S and R transition states for the two different nucleophiles. O-H \cdots O, N-H \cdots O, C-H \cdots O, C-H \cdots S and C-H $\cdots\pi$ interactions were observed for the transition state which produced the R enantiomer as the major product with the β -keto ester as nucleophile. The minor product S enantiomer had all the interactions present for the case of the R enantiomer, except the C-H \cdots S interaction (see Figure 6.19). For the case when the nucleophile was oxindole, the transition state that produced the S enantiomer as the major product showed O-H \cdots O, N-H \cdots O, C-H \cdots O, C-H \cdots S and C-H $\cdots\pi$ non-covalent interactions. The minor product R enantiomer for the same oxindole had all the interactions as the S enantiomer except for the C-H \cdots S interaction (see Figure 6.19). Therefore, the C-H \cdots S interaction present in the major enantiomer for the two cases considered was seen to be the influential factor that changed the enantioselectivity when the nucleophile was changed from oxindole to β -keto ester.

I have also applied Espinosa's equation (Eq. 6.7)⁷⁰ to quantify the strength of the non-covalent interactions present in the transition state conformations. This analysis further confirms the fact that the factor that determines the enantioselectivity is the C-H \cdots S interaction, which is seen to be present only in the transition states of the eventual major products formed, and, despite being a weak non-covalent interaction, contributing substantially (1.4-2.2 kcal/mol) – in a relative sense - to the stabilization of the major transition state. This result thus puts a spotlight on the unsuspected importance of the sulphur heteroatom in determining the outcome of the enantioselectivity, and on the significance of C-H \cdots S interaction, which has only very recently being recognized as having the same properties as a hydrogen bond.⁷¹

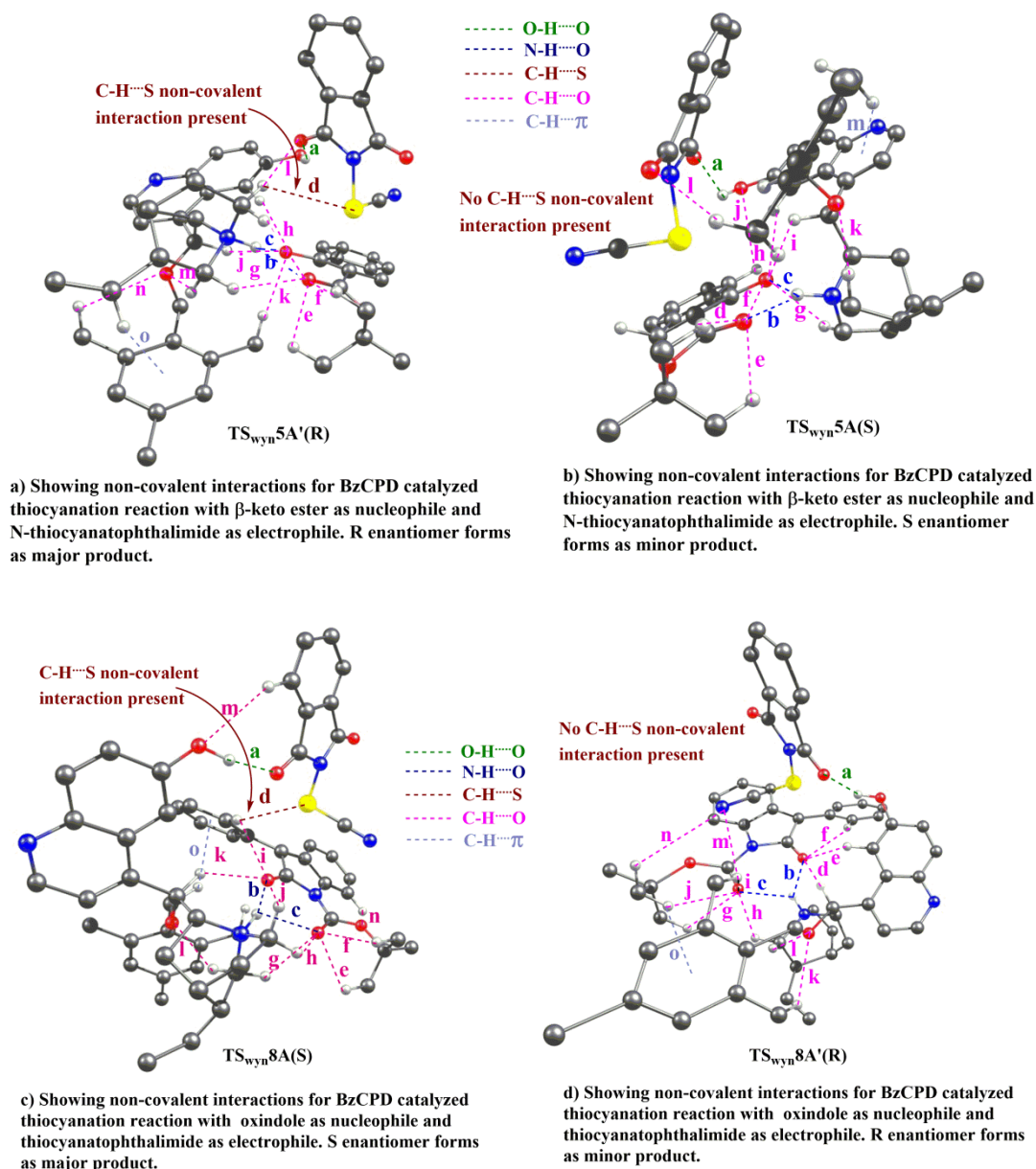


Figure 6.19 The optimized transition state structures showing different non-covalent interactions for the major and minor transition states. a) The R enantiomer as the major product with BzCPD as catalyst, β -keto ester as nucleophile, and N-thiocyanatophthalimide as electrophile. b) S enantiomer as minor product with BzCPD as catalyst, β -keto ester as nucleophile, and N-thiocyanatophthalimide as electrophile. c) S enantiomer as major product with BzCPD as catalyst, oxindole as nucleophile, and thiocyanatophthalimide as electrophile. d) R enantiomer as minor

product with BzCPD as catalyst, oxindole as nucleophile, and N-thiocyanatophthalimide as electrophile.

6.4 Conclusion

There have been a vast number of organocatalytic reactions where the addition of aromatic additives such as acids or alcohols, has been seen to have a beneficial effect on the yield and the enantioselectivity. The conventional explanation for this has been their ability to increase the pKa, or in some cases, create a proton shuttle mechanism. However, what the current study, focusing on the aromatic additive 2-naphthol, demonstrates is that aromatic additives can perform the role of a second catalyst, stabilizing both the electrophile and the nucleophile through non-covalent interactions. This has been shown for the C6'-OH *cinchona* alkaloid catalyzed electrophilic thiocyanation of oxindole, with N-thiocyanatophthalimide as the electrophilic SCN source. Two mechanistic possibilities: the a) Wynberg ion-pair-hydrogen bonding model, and b) the Houk-Grayson bifunctional Brønsted acid-hydrogen bonding model, which are the primary, well studied and well accepted mechanisms for such transformations, have been evaluated. The preferred model of catalysis was seen to be through the Wynberg ion-pair-hydrogen bonding model, in which the SCN transfer from the thiocyanating reagent to oxindole would proceed *via* an SN₂-like mechanism. The predicted enantioselectivities were found to be in good agreement with experimental data, lending strong support to the plausibility of this pathway. The non-covalent interaction (NCI) analysis of the stereocontrolling transition state structures revealed that the enantioselectivity was mainly induced by the concerted action of multiple non-covalent substrate-catalyst-additive interactions, such as C-H...O, C-H...S, C-H... π , and π ... π interactions. Of special interest was the observation of a favorable π ... π stacking interaction between the electrophile and additive that preferentially stabilized the transition state (TS) leading to the observed major product. It should be noted that, although the π ... π stacking interaction has been recognized as an important design element for enantioselective catalysis, an additive such as 2-naphthol acting as a stereocontrolling agent through non-covalent interactions has been ignored in mechanistic studies of reactions catalyzed by natural

cinchona alkaloids. Furthermore, since there are a significant number of literature reports⁴⁻⁶ pertaining to a range of electrophiles that can likewise do $\pi\cdots\pi$ stacking interactions with aromatic additives (employed in these reported reactions), while the nucleophile could be stabilized by hydrogen bonding interactions in the same systems, the current work indicates a general principle by which such aromatic additives function. As such, the insights gained about the role of additives from the current work can help in the design of more efficient organocatalytic systems in the near future.

The current work also sheds light on why there is a reversal of enantioselectivity for the thiocyanation reaction from S to R when the nucleophile is changed from oxindole to β -keto ester (in the absence of additives). This was seen to be primarily due to the C-H \cdots S non-covalent interaction, which was only seen to be present in the major transition states for the two nucleophiles considered. The fact that C-H \cdots S interactions display characteristics of a hydrogen bond has been discovered only recently,⁷¹ and the fact that this is a major contributor to the enantioselectivity is not only relevant and interesting, but also highlights the underappreciated role of the sulphur heteroatom in determining the enantioselectivity of the thiocyanation reaction. More importantly there are several cases reported in the literature, involving the transfer of the sulphur moiety during asymmetric catalysis,⁷² which suggests that C-H \cdots S non-covalent interactions are likely to be more significant in enantioselective transformations than previously suspected. As such, the current work provides important and interesting insights into asymmetric organocatalysis.

6.5 References

- (1) (a) List, B. *J. Am. Chem. Soc.* **2000**, *122*, 9336–9337. (b) List, B. *J. Am. Chem. Soc.* **2002**, *124*, 5656–5657. (c) Bahmanyar, S.; Houk, K. N.; Martin, H. J.; List, B. *J. Am. Chem. Soc.* **2003**, *125*, 2475–2479. (d) List, B. *Acc. Chem. Res.* **2004**, *37*, 548–557. (e) List, B. *Wiley-VCH Verlag GmbH: Weinheim*, **2004**, 1021–1021.
- (2) (a) Ahrendt, K. A.; Borths, C. J.; MacMillan, D. W. C. *J. Am. Chem. Soc.* **2000**, *122*, 4243–4244. (b) Paras, N. A.; MacMillan, D. W. C. *J. Am. Chem. Soc.* **2001**, *123*, 4370–4371. (c) Austin, F. J.; MacMillan, D. W. C. *J. Am. Chem. Soc.* **2002**, *124*, 1172–1173. (d) Brown, S. P.; Goodwin, N. C.; MacMillan, D. W. C. *J. Am. Chem. Soc.* **2003**, *125*, 1192–1194.
- (3) (a) Xiang, SH.; Tan, B. *Nat Commun.* **2020**, *11*, 1–4. (b) Parella, R., Jakkampudi, S.; Zhao, J. C.-G. *Recent ChemistrySelect* **2021**, *6*, 2252–2280. (c) Giacalone, F.; Gruttadauria, M.; Agrigento P.; Noto, R. *Chem. Soc. Rev.* **2012**, *41*, 2406–2447. (d) Seayad, J.; List, B. *Org. Biomol. Chem.* **2005**, *3*, 719–724. (d) Asymmetric Organocatalysis. (2009). Germany: Springer Berlin Heidelberg. Benjamin List (e) Cinchona Alkaloids in Synthesis and Catalysis: Ligands, Immobilization and Organocatalysis. (2009). Germany: Wiley. Choong Eui Song
- (4) (a) Ye, J.; Dixon, D. J.; Hynes, P. S. *Chem. Commun.* **2005**, 4481–4483. (b) Dixon, D. J.; Tillman, A. L. *Synlett*, **2005**, *17*, 2635–2638. (c) Tillman, L.; Ye, J.; Dixon, D. J. *Chem. Commun.* **2006**, 1191–1193. (d) Tillman, A. L.; Dixon, D. J. *Org. Biomol. Chem.* **2007**, *5*, 606–609.
- (5) (a) Li, H.; Wang, Y.; Tang, L.; Deng, L. *J. Am. Chem. Soc.* **2004**, *126*, 9906–9907. (b) Li, H.; Wang, Y.; Tang, L.; Wu, F.; Liu, X.; Guo, C.; Foxman, B.M.; Deng, L. *Angew. Chem., Int. Ed.* **2005**, *44*, 105–108
- (6) (a) Bogle, K. M.; Hirst, D. J.; Dixon, D. J. *Org. Lett.* **2007**, *9*, 4901–4904. (b) Bandini, M.; Sinisi, R.; Umani-Ronchi, A. *Chem. Commun.* **2008**, 4360–4362. (c) Guo, C.; Xue, M.-X.; Zhu, M.-K.; Gong, L.-Z. *Angew. Chem. Int. Ed.* **2008**, *47*, 3414–3417.
- (7) (a) Vayner, G.; Houk, K. N.; Sun, Y. K. *J. Am. Chem. Soc.* **2004**, *126*, 199–203. (b) Hammar, P.; Marcelli, T.; Hiemstra, H.; Himo, F. *Adv. Synth. Catal.* **2007**, *349*, 2537–2548. (c) Çelebi-Ölçü m, N.; Aviyente, V.; Houk, K. N. *J. Org. Chem.* **2009**, *74*, 6944–6952. (d) Cucinotta, C. S.; Kosa, M.; Melchiorre, P.; Cavalli, A.; Gervasio, F. L. *Chem.-Eur. J.* **2009**, *15*, 7913–7921.

- (8) (a) Michigami, K.; Murakami, H.; Nakamura, T.; Hayama, N.; Takemoto, Y. *Org. Biomol. Chem.* **2019**, *17*, 2331-2335. (b) Okino, T.; Hoashi, Y.; Furukawa, T.; Xu, X.; Takemoto, Y. *J. Am. Chem. Soc.* **2005**, *127*, 119-125. (c) Tokuhiko, Y.; Hayama, N.; Kobayashi, Y.; Takemoto, Y. *Heterocycles*, **2021**, *103*, 484-493.
- (9) (a) Zhu, L.; Yang, H.; Wong, M. W. *J. Org. Chem.* **2021**, *86*, 8414-8424. (b) Kee, C. W.; Wong, M. W. *J. Org. Chem.* **2020**, *85*, 15139-15153. (c) Lu, S.; Ong, J-Y.; Yang, H.; Poh, S. B.; Liew, X.; Seow, C. S. D.; Wong, M. W.; Zhao, Y. *J. Am. Chem. Soc.* **2019**, *141*, 17062-17067
- (10) (a) Sim, F.; Amant, A. S.; Pápai, I.; Salahub, D. R. *J. Am. Chem. Soc.* **1992**, *114*, 4391-4400. (b) Hamza, A.; Schubert, G.; Soós, T.; Pápai, I. *J. Am. Chem. Soc.* **2006**, *128*, 13151-13160. (c) Kótai, B.; Kardos, G.; Hamza, A.; Farkas, V.; Pápai, I.; Soós, T. *Chem. Eur. J.* **2014**, *20*, 5631-5639. (d) Neuvonen, A. J.; Földes, T.; Madarász, A.; Pápai, I. Pihko, P. M. *ACS Catal.* **2017**, *7*, 3284-3294.
- (11) (a) Lindqvist, M.; Borre, K.; Axenov, K.; Kótai, B.; Nieger, M.; Leskelä, M.; Pápai, I.; Repo, T.; *J. Am. Chem. Soc.* **2015**, *137*, 4038-4041. (b) Rahaman, H.; Madarász, Á.; Pápai, I.; Pihko, P.M. *Angew. Chem. Int. Ed.* **2011**, *50*, 6123-6127. (c) Probst, N.; Madarász, Á.; Valkonen, A.; Pápai, I.; Rissanen, K.; Neuvonen, A.; Pihko, P.M. *Angew. Chem. Int. Ed.* **2012**, *51*, 8495-8499.
- (12) (a) Patil, M.; Sunoj, R. *Chem. Eur. J.* **2008**, *14*, 10472-10485. (b) Patil, M.; Sunoj, R. *Chem. Asian J.* **2009**, *4*, 714-724. (c) Hein, J. E.; Burés, J.; Lam, Y-h.; Hughes, M.; Houk, K. N.; Armstrong, A.; Blackmond, D. G. *Org. Lett.* **2011**, *13*, 5644-5647.
- (13) (a) Jen, W. S.; Wiener, J. J. M.; MacMillan, D. W. C. *J. Am. Chem. Soc.* **2000**, *122*, 9874-9875. (b) Sparr, C.; Gilmour, R. *Angew. Chem., Int. Ed.* **2010**, *49*, 6520-6523 (c) Cozzi, P. G.; Benfatti, F.; Zoli, L. *Angew. Chem., Int. Ed.* **2009**, *48*, 1313-1316.
- (14) (a) Lifchits, O.; Reisinger, C. M.; List, B. *J. Am. Chem. Soc.* **2010**, *132*, 10227-10229. (b) Wang, X.; Reisinger, C. M.; List, B. *J. Am. Chem. Soc.* **2008**, *130*, 6070-6071. (c) Bergonzini, G.; Vera, S.; Melchiorre, P. *Angew. Chem., Int. Ed.* **2010**, *49*, 9685-9688. (d) Tian, X.; Cassani, C.; Liu, Y.; Moran, A.; Urakawa, A.; Galzerano, P.; Arceo, E.; Melchiorre, P. *J. Am. Chem. Soc.* **2011**, *133*, 17934-17941.

- (15) (a) Ogura, Y.; Akakura, M.; Sakakura, A.; Ishihara, K. *Angew. Chem., Int. Ed.* **2013**, *52*, 8299–8303 (b) Cheng, Y. A.; Yu, W. Z.; Yeung, Y.-Y. *Angew. Chem., Int. Ed.* **2015**, *54*, 12102–12106. (c) Silverio, D. L.; Torker, S.; Pilyugina, T.; Vieira, E. M.; Snapper, M. L.; Haeffner, F.; Hoveyda, A. H. *Nature* **2013**, *494*, 216–221.
- (16) (a) Aratake, S.; Itoh, T.; Okano, T.; Nagae, N.; Sumiya, T.; Shoji, M.; Hayashi, Y. *Chem. Eur. J.* **2007**, *13*, 10246–10256. (b) Hayashi, Y.; Aratake, S.; Itoh, T.; Okano, T.; Sumiya, T.; Shoji, M. *Chem. Commun.* **2007**, 957–959. (c) Córdova, A.; Zou, W.; Dziejczak, P.; Ibrahim, I.; Reyes, E.; Xu, Y. *Chem. Eur. J.* **2006**, *12*, 5383–5397. (d) Ibrahim, I.; Zou, W.; Xu, Y.; Córdova, A. *Adv. Synth. Catal.* **2006**, *348*, 211–222.
- (17) (a) Dell’Amico, L.; Albrecht, L.; Naicker, T.; Poulsen, P. H.; Jørgensen, K. A. *J. Am. Chem. Soc.* **2013**, *135*, 8063–8070. (b) Brindani, N.; Rassu, G.; Dell’Amico, L.; Zambrano, V.; Pinna, L.; Curti, C.; Sartori, A.; Battistini, L.; Casiraghi, G.; Pelosi, G.; Greco, D.; Zanardi, F. *Angew. Chem., Int. Ed.* **2015**, *54*, 7386–7390. (c) Raja, A.; Hong, B.-C.; Lee, G.-H. *Org. Lett.* **2014**, *16*, 5756–5759. (d) Yoon, T. P.; Jacobsen, E. N. *Angew. Chem., Int. Ed.* **2005**, *44*, 466–468.
- (18) (a) Itoh, J.; Fuchibe, K.; Akiyama, T. *Angew. Chem., Int. Ed.* **2008**, *47*, 4016–4018. (b) Sakamoto, T.; Itoh, J.; Mori, K.; Akiyama, T. *Org. Biomol. Chem.* **2010**, *8*, 5448–5454. (c) Lou, S.; Moquist, P. N.; Schaus, S. E. *J. Am. Chem. Soc.* **2007**, *129*, 15398–15404.
- (19) (a) Phillips, E. M.; Riedrich, M.; Scheidt, K. A. *J. Am. Chem. Soc.* **2010**, *132*, 13179–13181. (b) Dugal-Tessier, J.; O’Byrne, E. A.; Schroeder, T. B. H.; Cohen, D. T.; Scheidt, K. A. *Angew. Chem., Int. Ed.* **2012**, *51*, 4963–4967. (c) White, N. A.; Rovis, T. *J. Am. Chem. Soc.* **2015**, *137*, 10112–10115.
- (20) (a) Kalek, M.; Fu, G. C. *J. Am. Chem. Soc.* **2015**, *137*, 9438–9442. (b) Yuan, B.; He, R.; Shen, W.; Xu, Y.; Liu, X.; Li, M. *ChemistrySelect* **2016**, *1*, 2971–2978. (c) Eger, W.A.; Genest, A.; Rieger, B.; Rösch, N. *ChemSusChem* **2012**, *5*, 1967–1973.
- (21) (a) Sun, C.-L.; Li, H.; Yu, D.-G.; Yu, M.; Zhou, X.; Lu, X.-Y.; Huang, K.; Zheng, S.-F.; Li, B.-J.; Shi, Z.-J. *Nat. Chem.* **2010**, *2*, 1044–1049. (b) Studer, A.; Curran, D.P. *Angew. Chem. Int. Ed.* **2011**, *50*, 5018–5022. (c) Chen, M.; Sun, J. *Angew. Chem. Int. Ed.* **2017**, *56*, 11966–11970.
- (22) Uruguchi, D.; Ueki, Y.; Ooi, T. *Science* **2009**, *326*, 120–123.

- (23) Smith, S. W.; Fu, G. C. *J. Am. Chem. Soc.* **2009**, *131*, 14231–14233.
- (24) (a) Abermil, N.; Masson, G.; Zhu, J. *J. Am. Chem. Soc.* **2008**, *130*, 12596–12597. (b) Abermil, N.; Masson, G.; Zhu, J. *Org. Lett.* **2009**, *11*, 4648–4651.
- (25) Yao, Y.; Li, J.-L.; Zhou, Q.-Q.; Dong, L.; Chen, Y.-C. *Chem. - Eur. J.* **2013**, *19*, 9447–9451.
- (26) DiRocco, D. A.; Rovis, T. *J. Am. Chem. Soc.* **2011**, *133*, 10402–10405.
- (27) Filloux, C. M.; Lathrop, S. P.; Rovis, T. *Proc. Natl. Acad. Sci.* **2010**, *107*, 20666–20671.
- (28) Qiu, J.; Wu, D.; Yuan, L.; Long, P.; Yin, H.; Chen, F.-X. *J. Org. Chem.* **2019**, *84*, 7917–7926.
- (29) (a) Shibasaki, M.; Kanai, M. Chiral Bifunctional Acid/Base Catalysts. *New Frontiers in Asymmetric Catalysis* (eds K. Mikami and M. Lautens). **2007**, 383–410. (b) Akalay, D.; Dürner, G.; Bats, J. W.; Göbel, M. W. *Beilstein J. Org. Chem.* **2008**, *4*, 1–6. (c) Palomo, C.; Oiarbidea, M.; López, R. *Chem. Soc. Rev.* **2009**, *38*, 632–653. (d) Ting A., Goss J., McDougal N., Schaus S. Brønsted Base Catalysts. In: List B. (eds) *Asymmetric Organocatalysis. Topics in Current Chemistry* **2010**, 291, 201–232.
- For computational studies with C6'-OH *cinchona* alkaloid catalyst see:
- (d) Xue, X.-S.; Li, X.; Yu, A.; Yang, C.; Song, C.; Cheng, J.-P. *J. Am. Chem. Soc.* **2013**, *135*, 7462–7473. (e) Jiang, H., Sun, Y., Liu, H., Huang, X. *Int. J. Quantum Chem.* **2014**, *114*, 642–651. (f) Jiang, H., Zhang, G., Liu, Y.; Guo, X.; Liu, Z.; Yan, H.; Liu, H.; Huang, X. *Struct Chem.* **2015**, *26*, 951–959.
- (30) (a) Thompson, J. S. *C. Nature* **1940**, *145*. (c) Russell, F. P. *Bull N Y Acad Med.* **1943**, *19*, 599–630.
- (31) (a) Jacobsen, E. N.; Pfaltz, A.; Yamamoto, H. *Comprehensive Asymmetric Catalysis Supplement 1*, Eds.; Springer: Berlin, **2003**; 1–254. (b) Jacobsen, E. N.; Pfaltz, A.; Yamamoto, H. *Comprehensive Asymmetric Catalysis Supplement 2* Eds.; Springer: Berlin, **2010**, 1–153. (c) Jacobsen, E. N.; Pfaltz, A.; Yamamoto, H. *Comprehensive Asymmetric Catalysis*. Eds.; Springer: Berlin, **2000**, 1–1381.

- (32) (a) Stork, G. In *Classics in Total Synthesis II: More Targets, Strategies, Methods*; Nicolaou, K. C.; Snyder, S. A. Eds.; Wiley-VCH: Weinheim, **2003**, 443–464. (b) Kaufman, T. S.; Ru'veda, E. A. *Angew. Chem., Int. Ed.* **2005**, *44*, 854–885. (c) Seeman, J. I. *Angew. Chem., Int. Ed.* **2007**, *46*, 1378–1413. (d) Cheong, P. H.; Legault, C. Y.; Um, J. M.; Celebi-Olcum, N.; Houk, K. N. *Chem. Rev.* **2011**, *111*, 5042–5137.
- (33) (a) Verpoorte, R.; Schripsema, J.; Van der Leer, T. Cinchona alkaloids. In: Brossi A (ed) *The alkaloids*. Academic Press: New York, **1988**, *34*, 331. (b) Dalko, P. I.; Moisan, L. Enantioselective Organocatalysis. *Angew. Chem. Int. Ed.* **2001**, *40*, 3726–3748, (c) Kacprzak, S.; Gawronski, J. Cinchona Alkaloids and Their Derivatives: Versatile Catalysts and Ligands in Asymmetric Synthesis. *Synthesis* **2001**, *7*, 961–998.
- (34) (a) Marcelli, T.; van Maarseveen, J. H.; Hiemstra, H. *Angew. Chem., Int. Ed.* **2006**, *45*, 7496–7504. (b) Bryant, L. A.; Fanelli, R.; Cobb, A. J. A.; Beilstein. *J. Org. Chem.* **2016**, *12*, 429–443.
- (35) (a) Helder, R.; Arends, R.; Bolt, W.; Hiemstra, H.; Wynberg, H. *Tetrahedron Lett.* **1977**, *18*, 2181–2182. (b) Hiemstra, H.; Wynberg, H. *J. Am. Chem. Soc.* **1981**, *103*, 417–430 (c) Dijkstra, G. D. H.; Kellogg, R. M.; Wynberg, H. *Recl. Trav. Chim. Pays-Bas.* **1989**, *108*, 195–204.
- (36) (a) Lam, Y. H.; Grayson, M. N.; Holland, M. C.; Simon, A.; Houk, K. N. *Acc. Chem. Res.* **2016**, *49*, 750–762. (b) Grayson, M. N.; Houk, K. N. *J. Am. Chem. Soc.* **2016**, *138*, 1170–1173.
- (37) Qiu, J.; Wu, D.; Karmaker, P.G.; Yin, H.; Chen, F-X. *Org. Lett.* **2018**, *20*, 1600–1603.
- (38) (a) Hohenberg, P.; Kohn, W. *Phys. Rev.* **1964**, *136*, B864–B871. (b) Kohn, W.; Sham, L. *J. Phys. Rev.* **1965**, *140*, A1133–A1138.
- (39) Zhao, Y.; Truhlar, D. G., *Acc. Chem. Res.* **2008**, *41*, 157–167.
- (40) TURBOMOLE V7.4 2019, a development of University of Karlsruhe and Forschungszentrum Karlsruhe GmbH, 1989–2007, TURBOMOLE GmbH, since 2007; available from <http://www.turbomole.com>.
- (41) Ansgar, S.; Christian, H.; Reinhart, A. *J. Chem. Phys.* **1994**, *100*, 5829–5835.
- (42) Perdew, J. P.; Burke, K.; Ernzerhof, M. *Phys. Rev. Lett.* **1996**, *77*, 3865–3868.

- (43) (a) Grimme, S.; Antony, J.; Ehrlich, S.; Krieg, H. *J. Chem. Phys.* **2010**, *132*, 154104/1-154104/19. (b) Grimme, S.; Ehrlich, S.; Goerigk, L. *J. Comput. Chem.* **2011**, *32*, 1456-1465.
- (44) Klamt, A.; Schuurmann, G., *J. Chem. Soc. Perkin Trans.* 1993, *0*, 799-805.
- (45) (a) Zhao, Y.; Truhlar, D. G. *Theor. Chem. Acc.* **2008**, *120*, 215-241. (b) Walker, M.; Harvey, A. J. A.; Sen, A.; Dessent, C. H. E. *J. Phys. Chem. A* **2013**, *117*, 12590-12600.
- (46) (a) Eichkorn, K.; Treutler, O.; Öhm, H.; Häser, M.; Ahlrichs, R. *Chem. Phys. Lett.* **1995**, *240*, 283-290. (b) Eichkorn, K.; Weigend, F.; Treutler, O.; Ahlrichs, F. *Theor. Chem. Acc.* **1997**, *97*, 119-124.
- (47) (a) Sierka, M.; Hogekamp, A.; Ahlrichs, R. *J. Chem. Phys.* **2003**, *118*, 9136-9148. (b) Deglmann, P.; May, K.; Furche, F.; Ahlrichs, R. *Chem. Phys. Lett.* **2004**, *384*, 103-107.
- (48) Fukui, K. *Acc. Chem. Res.* **1981**, *14*, 363-368.
- (49) Mammen, M.; Shakhnovich, E. I.; Deutch, J. M.; Whitesides, G. M. *J. Org. Chem.* **1998**, *63*, 3821-3830.
- (50) Lu, T.; Chen, F. *J. Comput. Chem.* **2012**, *33*, 580-592.
- (51) Humphrey, W.; Dalke, A.; Schulten, K. *J. Mol. Graphics* **1996**, *14*, 33-38.
- (52) (a) Johnson, E. R.; Keinan, S.; Sanchez, P. M.; Garcia, J. C.; Cohen, A. J.; Yang, W. *J. Am. Chem. Soc.* **2010**, *132*, 6498-6506. (b) Garcia, J. C.; Johnson, E. R.; Keinan, S.; Chaudret, R.; Piquemal, J.-P.; Beratan, D. N.; Yang, W. *J. Chem. Theory Comput.* **2011**, *7*, 625-632.
- (53) (a) Tan, S.-K.; Chen, Y.; Hang, J.; Tang, L.; McDaid, P.; Deng, L. *Acc. Chem. Res.* **2004**, *37*, 621-631. (b) Hoffmann, H. M. R.; Frackenhohl, J. *Eur. J. Org. Chem.* **2004**, *2004*, 4293-4312. (c) Szöllösi, G.; Chatterjee, A.; Forgó, P.; Bartók, M.; Mizukami, F. *J. Phys. Chem A* **2005**, *109*, 860-868. (d) Olsen, R. A.; Borchardt, D.; Mink, L.; Agarwal, A.; Mueller, L. J.; Zaera, F. *J. Am. Chem. Soc.* **2006**, *128*, 15594-15595. (e) Zhu, J.-L.; Zhang, Y.; Liu, C.; Zheng, A.-M.; Wang, W. *J. Org. Chem.* **2012**, *77*, 9813-9825.
- (54) (a) Dijkstra, G. D. H.; Kellogg, R. M.; Wynberg, H.; Svendsen, J. S.; Marko, I.; Sharpless, K. B. *J. Am. Chem. Soc.* **1989**, *111*, 8069-8076. (b) Dijkstra, G. D. H.; Kellogg, R. M.; Wynberg, H. *J. Org. Chem.* **1990**, *55*, 6121-6131.

(55) (a) Burgi, T.; Baiker, A. *J. Am. Chem. Soc.* **1998**, *120*, 12920-12926. (b) Vargas, A.; Bonalumi, N.; Ferri, D.; Baiker, A. *J. Phys. Chem. A* **2006**, *110*, 1118-1127. (c) Urakawa, A.; Meier, D. M.; Rügger, H.; Baiker, A. *J. Phys. Chem. A* **2008**, *112*, 7250-7255.

(56) Yang, H.; Wong, M. W. *J. Am. Chem. Soc.* **2013**, *135*, 5808-5818.

(57) (a) Wang, M.- X. *Acc. Chem. Res.* **2015**, *48*, 602-611. (b) Chowdhury, R.; Schörghumer, J.; Novacek, J.; Waser, M. *Tetrahedron Letters* **2015**, *56*, 1911-1914. (c) Liu, Y.; Shirakawa, S.; Maruoka, K. *Org. Lett.* **2013**, *15*, 1230-1233. (d) Khan, N.H.; Kureshy, R.I.; Abdi, S.H.R.; Bajaj, H.C.; Sadhukhan, A. Asymmetric Cyanation Reactions, Editor(s): Jan Reedijk, Kenneth Poepelmeier, *Comprehensive Inorganic Chemistry II*, **2013**, pp:413-456.

(58) (a) Castanheiro, T.; Suffert, J.; Donnard, M.; Gulea, M. *Chem. Soc. Rev.*, **2016**, *45*, 494-505. (b) Schörghumer, J.; Waser, M. *Org. Chem. Front.*, **2016**, *3*, 1535-1540 (b) Li, C.; Long, P.; Wu, H.; Yin, H.; Chen, F. *Org. Biomol. Chem.*, **2019**, *17*, 7131-7134.

(59) Li, M.; Xue, X-S.; Cheng, J-P. *ACS Catal.* **2017**, *7*, 7977-7986.

(60) (a) Lam, Y.-h.; Houk, K. N.; Scheffler, U.; Mahrwald, R. *J. Am. Chem. Soc.* **2012**, *134*, 6286-6295. (b) Hong, X.; Kucuk, H. B.; Maji, M. S.; Yang, Y. F.; Rueping, M.; Houk, K. N. *J. Am. Chem. Soc.* **2014**, *136*, 13769-13780. (c) Holland, M. C.; Gilmour, R.; Houk, K. N. *Angew. Chem. Int. Ed.* **2016**, *55*, 2022-2027.

(61) Kitaura, K.; Morokuma, K. *Int. J. Quantum Chem.* **1976**, *10*, 325-340. (b) Ziegler, T.; Rauk, A. *Theor. Chim. Acta.* **1977**, *46*, 1-10. (c) Ziegler, T.; Rauk, A. *Inorg. Chem.* **1979**, *18*, 1558-1565.

(62) For the usage of the term “distortion/interaction analysis”: (a) Ess, D. H.; Houk, K. N. *J. Am. Chem. Soc.* **2007**, *129*, 10646-10647. (b) Legault, C. Y.; Garcia, Y.; Merlic, C. A.; Houk, K. N. *J. Am. Chem. Soc.* **2007**, *129*, 12664-12665. (c) Ess, D. H.; Houk, K. N. *J. Am. Chem. Soc.* **2008**, *130*, 10187-10198. (d) Lu, T.; Zhu, R.; An, Y.; Wheeler, S. E. *J. Am. Chem. Soc.* **2012**, *134*, 3095-3102.

(63) For the usage of the term “activation strain analysis”, see the following: (a) Diefenbach, A.; Bickelhaupt, F. M. *J. Phys. Chem. A* **2004**, *108*, 8460-8466. (b) van Zeist, W.-J.; Bickelhaupt, F. M. *Org. Biomol. Chem.* **2010**, *8*, 3118-3127.

(64) (a) Johnson, E. R.; Keinan, S.; Mori-Sánchez, P.; Contreras-García, J.; Cohen, A. J.; Yang, W. *J. Am. Chem. Soc.* **2010**, *132*, 6498-6506. (b) Contreras-García, J.; Johnson, E. R.; Keinan, S.; Chaudret, R.; Piquemal, J.-P.; Beratan, D. N.; Yang, W. *J. Chem. Theory Comput.* **2011**, *7*, 625-632.

(65) For a recent review of transition state stabilization by C–H···O interactions, see: (a) Johnston, R. C.; Cheong, P. H.-Y. *Org. Biomol. Chem.* **2013**, *11*, 5057-5064. (b) Washington, I.; Houk, K. N. CH···O *Angew. Chem. Int. Ed.* **2001**, *40*, 4485-4488. (c) Cannizzaro, C. E.; Houk, K. N. *J. Am. Chem. Soc.* **2002**, *124*, 7163-7169. (d) Maity, P.; Pemberton, R. P.; Tantillo, D. J.; Tambar, U. K. *J. Am. Chem. Soc.* **2013**, *135*, 16380-16383.

(66) For a recent review of transition state stabilization by C–H··· π interactions, see: (a) Krenske, E. H.; Houk, K. N. *Acc. Chem. Res.* **2013**, *46*, 979-989. (b) Antoline, J. E.; Krenske, E. H.; Lohse, A. G.; Houk, K. N.; Hsung, R. P. *J. Am. Chem. Soc.* **2011**, *133*, 14443-14451. (c) Dang, Y.; Qu, S.; Wang, Z.-X.; Wang, X. *J. Am. Chem. Soc.* **2014**, *136*, 986-998. (d) Jindal, G.; Sunoj, R. B. *Angew. Chem. Int. Ed.* **2014**, *53*, 4432-4436.

(67) For recent reviews on π ··· π interactions, see: (a) Wheeler, S. E. *Acc. Chem. Res.* **2013**, *46*, 1029-1038. (b) Wheeler, S. E.; Bloom, J. W. G. *J. Phys. Chem. A* **2014**, *118*, 6133-6147. (c) Wheeler, S. E.; McNeil, A. J.; Müller, P.; Swager, T. M.; Houk, K. N. *J. Am. Chem. Soc.* **2010**, *132*, 3304-3311. (d) Zhang, Z.; Lippert, K. M.; Hausmann, H.; Kotke, M.; Schreiner, P. R. *J. Org. Chem.* **2011**, *76*, 9764-9776.

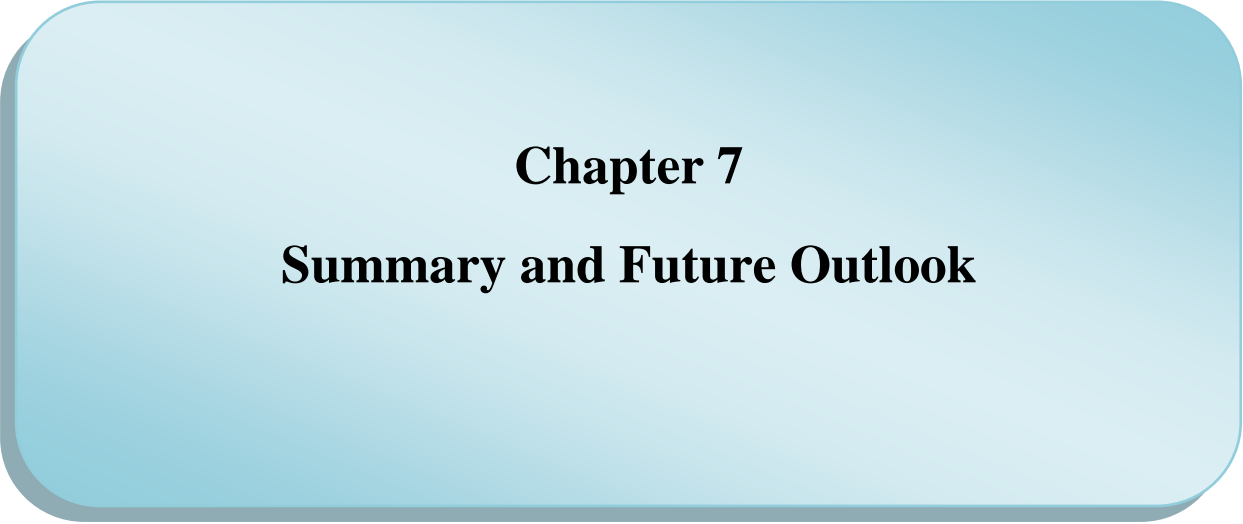
(68) For examples of π -stacking involved in stereocontrol in Cinchona alkaloid derived phase transfer catalyst promoted reactions, see: (a) Kawai, H.; Kusuda, A.; Nakamura, S.; Shiro, M.; Shibata, N. *Angew. Chem. Int. Ed.* **2009**, *48*, 6324-6327. (b) Cook, T. C.; Andrus, M. B.; Ess, D. H. *Org. Lett.* **2012**, *14*, 5836-5839. (c) Kawai, H.; Yuan, Z.; Kitayama, T.; Tokunaga, E.; Shibata, N. *Angew. Chem. Int. Ed.* **2013**, *52*, 5575-5579 (d) de Freitas Martins, E.; Pliego Jr, J. R. *ACS Catal.* **2013**, *3*, 613-616.

(69) Espinosa, E.; Molins, E.; Lecomte, C. *Chem. Phys. Lett.* **1998**, *285*, 170-173.

(70) Seguin, T. J.; Lu, T.; Wheeler, S. E. *Org. Lett.* **2015**, *17*, 3066-3069.

(71) Ghosh, S.; Chopra, P.; Wategaonkar, S. *Phys. Chem. Chem. Phys.* **2020**, *22*, 17482-17493.

(72) (a) Hilby, K. M.; Denmark, S. E. *J. Org. Chem.* **2021**, *86*, 14250-14289. (b) Panger, J. L.; Denmark, S. E. *Org. Lett.* **2020**, *22*, 2501-2505. (c) Roth, A.; Denmark, S. E. *J. Am. Chem. Soc.* **2019**, *141*, 13767-13771. (d) Matviitsuk, A.; Denmark, S. E. *Angew. Chem. Int. Ed.* **2019**, *58*, 12486-12490.



Chapter 7
Summary and Future Outlook

Chapter 7

Summary and Future Outlook

7.1 Focus of the Thesis

As mentioned in Chapter 1 and in Chapters 3-6, the focus of the thesis work presented here is twofold. In the first part of the thesis, I have focused on the important aspects of homogeneous catalysis where hydride transfer plays an important role. Two important reactions have been investigated in this part: a) hydrosilylation of silicone surrogates using tris(pentafluorophenyl)borane ($B(C_6F_5)_3$) as an initiator and b) hydroboration using N-heterocyclic stannylene and germylene catalysts. In order to employ DFT to shed light on the activity difference in the catalysis, an important homogeneous catalysis reaction, hydrosilylation, has been chosen. The reaction was chosen to explore the effect of hydride transfer on the hydrosilylation reaction, which has been experimentally studied by Oestreich and co-workers.¹ The *in situ* generation of SiH_4 was the major point of interest in their work.¹ The myth behind $B(C_6F_5)_3$ acting as a catalyst in the entire catalytic pathway involving multiple transition states has been reconsidered. The conditions under which tris(pentafluorophenyl)borane ($B(C_6F_5)_3$) can act as initiator or catalyst has also been revealed in this work.² The investigation of the hydroboration of aldehyde using N-heterocyclic stannylene and germylene provides a new mechanistic pathway. Here, I have modeled new stannylene and germylene catalysts considering the HOMO-LUMO energy gap. The hydroboration reaction has been investigated with the new modeled catalyst. The new pathway has been compared with the earlier proposed pathway. Further, computational investigations have been carried out to show how easily one can decide which pathway the reaction mechanism will follow between two comparable pathways using turn over frequency (TOF) calculations. In the second part of the thesis, I have focused on reaction mechanisms involving proton transfer. In this part, I have mainly investigated the asymmetric organocatalysis of the thiocyanation reaction with and without the involvement of an additive.^{3,4} There are many experimental observations in asymmetric organocatalysis where aromatic additives like phenol and benzoic acid play a crucial role in increasing yield and enantioselectivity.^{5,6} The

commonly held belief about the role of the additive is that it increases the pK_a of the system. It has also been observed that in some cases the additive aids in proton transfer.⁷ In order to understand clearly what the real role of the additive could be, I have investigated whether there is an explicit role played by such additive involved in asymmetric transformations. The outcome of the investigations clearly show that the additive play a crucial role in activating both the electrophile and the nucleophile simultaneously. This essentially suggests that the additive plays the role of a second catalyst in asymmetric organocatalytic reactions.

7.2 Methodology Employed

All the DFT calculations were performed using the Turbomole suites of programs. Turbomole 7.0,⁸ Turbomole 7.2⁹ and Turbomole 7.4¹⁰ have been used. The geometry optimizations have been done with the Perdew, Burke, and Erzenhof density functional (PBE).¹¹ Along with the PBE, in some cases, the TPSS¹² and the M06-2X¹³ functional have also been used to validate the results obtained from PBE. The electronic configuration of the atoms was described by a triple- ζ basis set augmented by a polarization function (Turbomole basis set TZVP).¹⁴ The resolution of identity (ri),¹⁵ along with the multipole accelerated resolution of identity (marij)¹⁶ approximations, were employed for an accurate and efficient treatment of the electronic Coulomb term in the density functional calculations. Solvent effects and dispersion corrections have been incorporated as well. Solvent effects were incorporated using the COSMO model.¹⁷ The contributions of internal energy and entropy were obtained from frequency calculations done on the DFT structures at 298.15 K; thus, the energies reported are the ΔG values. The calculations discussed in Chapter 6 were done at 195.15 K. Care was taken to ensure that the obtained transition state structures possessed only one imaginary frequency corresponding to the correct normal mode.

7.3 Summary of results

The outcomes of the investigations done in this thesis work have been summarized below.

1) My work has served to highlight the elegant and underappreciated nature of surrogate silicon chemistry, which is based on a sequence of autocatalytic processes rather than Lewis acid, $B(C_6F_5)_3$, catalysis. Researchers working in the field of silicon chemistry, as well as those working with surrogates in related fields, will benefit from the findings of the computational investigations. The computational investigation of the hydrosilylation reaction using $B(C_6F_5)_3$ shows that the actual pathway is the autocatalytic pathway involving $B(C_6F_5)_3$ as an initiator. One of the significant outcomes of this investigation is that for the first time, the autocatalytic mechanistic pathway is shown when $B(C_6F_5)_3$ acts as a hydride acceptor. More importantly, a very experimentally challenging reaction, which is the conversion of SiR_3H to SiH_4 , has been investigated computationally. The reaction itself has huge industrial relevance, because it is a major source of elemental silicon, which is utilised extensively in the semiconductor industry. Several surrogates of silicone species have been investigated to get a clear idea about the mechanistic pathway. The silicon complex appears to be the hydride source for the reactions, similar to prior experimental situations where the hydride source was substituted cyclohexa-1,4-diene. The results from the energetic span model clearly show that the autocatalytic pathway is much better than the normal catalytic pathway. These interesting results will help experimentalists to choose an efficient initiator instead of considering $B(C_6F_5)_3$ as the catalyst. This study demonstrates that cationic autocatalytic activities are more prevalent than previously thought, including instances in biochemistry¹⁸ and polymerization.¹⁹ The outcome of the investigation has been experimentally proven by many researchers.

2) The current investigation clearly shows two important outcomes: (i) the reaction between boron catalyst and the neutral substrate would have to form a solvent-separated ion-pair complex that is very loosely bound and secondly, (ii) The active catalytic species would thus have to be the cation component of the ion pair. The interaction of a neutral species with the loosely solvent bound ion-pair is an alternate

pathway following the reorganisation of the loosely solvent bound ion-pair. This section demonstrates that $B(C_6F_5)_3$ is more of an initiator and subsequently a spectator in the multistep process than a pure catalyst in most of the transformations that have been investigated. The outcome of the investigation on several ion-pair species gives us a benchmark as to when the ion-pair will easily separate. Ion-pair separation energy is the main criteria for the deciding which pathway between autocatalytic and catalytic the $B(C_6F_5)_3$ will follow.²

3) The chemistry of low valent main group compounds has grown as an alternative to the chemistry of less abundant and less green transition metal complexes. It has been found that low valent compounds such as carbenes, silylenes, stannylenes and germylenes are efficient for activating small molecules and for catalysis. However, the reaction mechanism and the factors that affect the rate of the reaction are not completely understood. I investigate and demonstrate the efficiency of a new mechanism for the hydroboration of aldehydes by germylenes and stannylenes, in the presence of the common hydroborating agent, pinacolborane, HBpin. The outcome of this work shows that the mechanism involves an HBpin molecule as an additional catalyst that cooperates with the germylene or stannylene catalyst to efficiently carry out the hydroboration. The mechanism is first demonstrated to work for experimentally reported systems, and then shown to be efficient for newly proposed germylene and stannylene systems. The current investigation also shows that finding the HOMO-LUMO energy gap can be good criterion for choosing tetrylene catalysts. The outcome of the new insights will help researchers to look into low valent germylene and stannylene systems from a new perspective.

4) There have been several organocatalytic processes where aromatic additives, such as acids or alcohols, have been shown to improve yield and enantioselectivity. The outcome of the new work, which focuses on aromatic additives, shows that they can operate as a second catalyst, stabilising both the electrophile and the nucleophile through non-covalent interactions. The thiocyanation of oxindole and β -keto ester using an electrophilic SCN source shows that the mechanism proceeds *via* an S_N2 pathway. The principal, well-studied, and well-accepted mechanisms for such

transformations, the Wynberg ion-pair-hydrogen bonding model and the Houk-Grayson bifunctional Brnsted acid-hydrogen bonding model, have been assessed. The Wynberg ion-pair-hydrogen bonding model was shown to be the preferred model of catalysis. The calculated enantioselectivities were found to be very close to experimental data, indicating that this approach is quite plausible. The enantioselectivity was predominantly produced by the concerted action of several non-covalent substrate-catalyst-additive interactions, such as C-H \cdots O, C-H \cdots S, C-H \cdots π , and $\pi\cdots\pi$ interactions, according to the non-covalent interaction (NCI) analysis of the stereocontrolling transition state structures. The finding of a favourable $\pi\cdots\pi$ stacking interaction between the electrophile and additive that preferentially stabilised the transition state (TS) and led to the observed main product was of particular interest. This work also explains why the enantioselectivity of the thiocyanation reaction shifts from S to R when the nucleophile is changed from oxindole to β -keto ester. This was attributed to the non-covalent C-H \cdots S interaction, which was only observed in the main transition states for the two nucleophiles studied.

7.4 Future Outlook

Insights gained from of the work presented in this thesis shed light on critical areas of research and are also likely to help experimentalists design systems by simple computational calculations. In this thesis, new and efficient pathways have been proposed. These suggest that the new systems could be designed based on the criteria proposed in the work. For the hydride transfer reactions with B(C₆F₅)₃, the experimentalists can easily choose a new initiator. The HOMO-LUMO gap could be a simple but interesting criteria for catalyst design for tetrylenes systems. Studies on asymmetric organocatalysis systems show how important is the use of aromatic additives in achieving higher yield and enantioselectivity. Researchers can now modify the systems accordingly to achieve higher yield and enantioselectivity. In this thesis work, several noncovalent interactions have been found to be useful in deciding enantioselectivity. This suggests that new systems could be designed where such interactions would be strengthened, which would lead to the higher efficiency of the activation reactions and to controlling the stereoselectivity of the reactions. Therefore,

this work is an interesting forward step in the area of low valent main group chemistry, small molecule activation, catalysis, asymmetric organocatalysis, noncovalent interactions and stereoselectivity.

7.5 References

1. Simonneau, A.; Oestreich, M. *Nat. Chem.* **2015**, *7*, 816-822.
2. Banerjee S.; Vanka, K. *ACS Catal.* **2018**, *8*, 6163–6176.
3. Qiu, J.; Wu, D.; Yuan, L.; Long, P.; Yin, H.; Chen, F-X. *J. Org. Chem.* **2019**, *84*, 7917-7926.
4. Qiu, J.; Wu, D.; Karmaker, P.G.; Yin, H.; Chen, F-X. *Org. Lett.* **2018**, *20*, 1600-1603.
5. (a) Ogura, Y.; Akakura, M.; Sakakura, A.; Ishihara, K. *Angew. Chem., Int. Ed.* **2013**, *52*, 8299– 8303 (b) Cheng, Y. A.; Yu, W. Z.; Yeung, Y.-Y. *Angew. Chem., Int. Ed.* **2015**, *54*, 12102-12106. (c) Silverio, D. L.; Torker, S.; Pilyugina, T.; Vieira, E. M.; Snapper, M. L.; Haeffner, F.; Hoveyda, A. H. *Nature* **2013**, *494*, 216–221. (d) Wu, H.; Haeffner, F.; Hoveyda, A. H. *J. Am. Chem. Soc.* **2014**, *136*, 3780–3783. (e) Fuerst, D. E.; Jacobsen, E. N. *J. Am. Chem. Soc.* **2005**, *127*, 8964– 8965. (f) Zuend, S. J.; Jacobsen, E. N. *J. Am. Chem. Soc.* **2007**, *129*, 15872–15883. (g) Zuend, S. J.; Jacobsen, E. N. *J. Am. Chem. Soc.* **2009**, *131*, 15358–15374. (h) Guin, J.; Varseev, G.; List, B. *J. Am. Chem. Soc.* **2013**, *135*, 2100–2103. (i) Uraguchi, D.; Kinoshita, N.; Ooi, T. *J. Am. Chem. Soc.* **2010**, *132*, 12240–12242. (k) Cheon, C. H.; Yamamoto, H. *J. Am. Chem. Soc.* **2008**, *130*, 9246– 9247. (l) Kawahara, S.; Nakano, A.; Esumi, T.; Iwabuchi, Y.; Hatakeyama, S. *Org. Lett.* **2003**, *5*, 3103–3105. (m) Nakano, A.; Takahashi, K.; Ishihara, J.; Hatakeyama, S. β -Isocupreidine-catalyzed Baylis - Hillman Reaction of Chiral N-boc- α -Amino Aldehydes. *Org. Lett.* **2006**, *8*, 5357–5360. (n) Shi, M.; Xu, Y.-M.; Shi, Y.-L. *Chem.-Eur. J.* **2005**, *11*, 1794–1802. (o) Abermil, N.; Masson, G.; Zhu, J. *Adv. Synth. Catal.* **2010**, *352*, 656-660. (p) Takizawa, S.; Inoue, N.; Hirata, S.; Sasai, H. *Angew. Chem. Int. Ed.* **2010**, *49*, 9725-9729.
6. (a) Sun, C-L.; Li, H.; Yu, D-G.; Yu, M.; Zhou, X.; Lu, X-Y.; Huang, K.; Zheng, S-F.; Li, B-J.; Shi, Z-J. *Nat. Chem.* **2010**, *2*, 1044-1049. (b) Studer, A.; Curran, D.P.

Angew. Chem. Int. Ed. **2011**, *50*, 5018-5022. (c) Chen, M.; Sun, J.; *Angew. Chem. Int. Ed.* **2017**, *56*, 11966-11970.

7. (a) Kalek, M.; Fu, G. C. *J. Am. Chem. Soc.* **2015**, *137*, 9438–9442. (b) Yuan, B.; He, R.; Shen, W.; Xu, Y.; Liu, X.; Li, M. *ChemistrySelect* **2016**, *1*, 2971-2978. (c) Eger, W.A.; Genest, A.; Rieger, B.; Rösch, N. *ChemSusChem* **2012**, *5*, 1967-1973.

8. TURBOMOLE V7.0 2015, a development of University of Karlsruhe and Forschungszentrum Karlsruhe GmbH, 1989-2007, TURBOMOLE GmbH, since 2007; available from <http://www.turbomole.com>.

9. TURBOMOLE V7.2 2017, a development of University of Karlsruhe and Forschungszentrum Karlsruhe GmbH, 1989-2007, TURBOMOLE GmbH, since 2007; available from <http://www.turbomole.com>.

10. TURBOMOLE V7.4 2019, a development of University of Karlsruhe and Forschungszentrum Karlsruhe GmbH, 1989-2007, TURBOMOLE GmbH, since 2007; available from <http://www.turbomole.com>.

11. Perdew, J. P.; Burke, K.; Ernzerhof, M., Generalized Gradient Approximation Made Simple. *Phys. Rev. Lett.* **1996**, *77*, 3865-3868.

12. Tao, J.; Perdew, J. P.; Staroverov, V. N.; Scuseria, G. E. *Phys. Rev. Lett.* **2003**, *91*, 146401-1-146401-4.

13. Zhao, Y.; Truhlar, D. G. *Theor. Chem. Acc.* **2008**, *120*, 215-241.

14. Schafer, A.; Huber, C. *J. Chem. Phys.* **1994**, *100*, 5829–5835.

15. (a) Eichkorn, K.; Treutler, O.; Öhm, H.; Häser, M.; Ahlrichs, R. *Chem. Phys. Lett.* **1995**, *240*, 283–290. (b) Eichkorn, K.; Weigend, F.; Treutler, O.; Ahlrichs, R. *Theor. Chem. Acc.* **1997**, *97*, 119–124.

16. (a) Sierka, M.; Hoge Kamp, A.; Ahlrichs, R. *J. Chem. Phys.* **2003**, *118*, 9136–9148. (b) Deglmann, P.; May, K.; Furche, F.; Ahlrichs, R. *Chem. Phys. Lett.* **2004**, *384*, 103–107.

17. Klamt, A.; Schuurmann, G. *J. Chem. Soc., Perkin Trans. 2* **1993**, 799–805.
18. (a) Kamioka, S.; Ajami, D.; Jr. Rebek, J. *Chem. Commun.* **2009**, 7324-7326. (b) Kamioka, S.; Ajami, D.; Jr. Rebek, J. *PNAS*, **2010**, *107*, 541-544. (c) Brook, M. A.; Grand, J. B.; Ganachaud, F. *Silicone Polymers* **2010**, *235*, 161-183. (d) Bissette, A. J.; Fletcher, S. P. *Angew. Chem., Int. Ed.* **2013**, *52*, 12800-12826. (e) Plasson, R.; Brandenburg, A.; Jullien, L.; Bersini, H. *J. Phys. Chem. A* **2011**, *115*, 8073-8085.
- (19) (a) Valente, A.; Mortreux, A.; Visseaux, M.; Zinck, P., *Chem. Rev.* **2013**, *113*, 3836-3857. (b) Jr. Starnes, W. H.; Ge, X. *Macromolecules* **2004**, *37*, 352-359. (c) Thompson, D. B.; Brook, M. A. *J. Am. Chem. Soc.* **2008**, *130*, 32-33. (d) Moitra, N.; Ichii, S.; Kamei, T.; Kanamori, K.; Zhu, Y.; Takeda, K.; Nakanishi, K.; Shimada, T. *J. Am. Chem. Soc.* **2014**, *136*, 11570-11573.

Abstract

Name of the Student: Subhrashis Banerjee

Registration No.: 10CC18A26012

Faculty of Study: Chemical Science

Year of Submission: 2022

CSIR Lab: NCL, Pune

Name of the Supervisor: Dr. Kumar Vanka

Title of the thesis: Computational Insights into Proton and Hydride Transfer Chemistry

Hydride and proton transfer is one of the very basic reaction happens in chemistry and biology. This has been an effective means of initiating chemical reactions in many important chemical and biological processes. The knowledge of the role of the hydride and proton transfer reactions and its effect on the rate of the reaction can be of great value to chemists. However, there is still a need to study the influence of hydride transfer in important areas of research in main group chemistry such as hydrosilylation and hydroboration. Also, there is also need to study how proton transfer can initiate the asymmetric organocatalysis. Density functional theory (DFT) could be employed to provide insight into the role that the hydride and proton transfer plays in those very important reactions.

The aim of this thesis is to study hydride transfer chemistry in main group catalysis and proton transfer chemistry in asymmetric organocatalysis. Main group reactions is a genuine alternative to transition metals. Thus, due to aforementioned reasons, coupled with a scarcity of computational investigations on these environmentally benign compounds, I have these investigations. I have studied the hydrosilylation reaction with tris(pentafluorophenyl)borane $B(C_6F_5)_3$ as initiator proposing the new autocatalytic pathway. It was also necessary to predict the role of $B(C_6F_5)_3$ in different chemical transformations. It can easily be decided whether $B(C_6F_5)_3$ will act as catalyst or initiator based on the ion-pair separation energy. In further investigations, I have modeled stannylene and germylene catalysts for the hydroboration reaction. Using the new modeled catalyst a new improved mechanistic pathway has been investigated. Lastly, how proton transfer helps the asymmetric organocatalysis has been investigated. A new modeled has been proposed, based on the interaction of additive, catalysts, electrophile and nucleophile. Furthermore, TOF calculations, volume correction in the entropy, and NCI plot analyses have been employed in our investigations into the role of hydride and proton transfer in chemistry.

Details of the publications emanating from the thesis work

1) List of publication(s) in SCI Journal(s) (published & accepted) emanating from the thesis work

(1) **Subhrashis Banerjee**, Kumar Vanka.

B(C₆F₅)₃: Catalyst or Initiator? Insights from Computational Studies into Surrogate Silicon Chemistry, *ACS Catalysis*, **2018**, 8 (7), 6163-6176.

DOI: 10.1021/acscatal.7b04489

(2) **Subhrashis Banerjee**, Kumar Vanka.

Computational Insights into Hydroboration with Acyclic α -Borylamido-Germylene and Stannylyene Catalysts: Cooperative Dual Catalysis the Key to Systems Efficiency, *Polyhedron*, **2022**, 222, 115907.

2) List of papers with abstract presented (oral/poster) at national/international conferences/seminars with complete details.

(i) Presented a poster entitled “Unraveling the Importance and the Actual Role of Lewis Acid B(C₆F₅)₃: Catalyst or Initiator? A Computational Investigation” at Modern Trends in Inorganic Chemistry(MTIC-XVII), IISER Pune/CSIR-NCL/UOP, Maharashtra, 11th-14th December 2017.

Abstract

There are few areas in chemistry that are generating as much excitement as the field of Lewis acid catalysis. One of the most promising recent developments has been the use of the metal-free Lewis acid B(C₆F₅)₃, to aid in effecting different chemical transformations. However, it has always been challenging for experimentalists to predict its exact role. Does B(C₆F₅)₃ behave as a catalyst, or is its role limited to merely being an initiator? An important recent work in this context is the recently accomplished, experimental *in situ* generation of SiH₄ from surrogates with the aid of B(C₆F₅)₃. The current computational investigation, with density functional theory (DFT), reveals that this process is not, in fact, catalyzed by B(C₆F₅)₃ at all, but is dominated instead by a series of cationic autocatalytic reactions, where the role of B(C₆F₅)₃ is to function more as an initiator. Now, given the ambivalence in the behaviour of B(C₆F₅)₃, the obvious question that comes to mind is: can it made possible for an experimentalist to determine easily whether B(C₆F₅)₃ is acting as a catalyst or initiator in a given reaction? We have employed some

very simple computational calculations to provide insight in this regard. Depending on the ease of separation of ion-pairs, we have come to a generalized conclusion for evaluating and separating reactions where $B(C_6F_5)_3$ can act as a catalyst or co-catalyst or initiator.

(ii) Presented a poster entitled “Unraveling the Importance and the Actual Role of Lewis Acid $B(C_6F_5)_3$: Catalyst or Initiator? A Computational Investigation” at Theoretical Chemistry Symposium, BITS-Pilani, Rajasthan, 13th -16th February, 2019.

Abstract

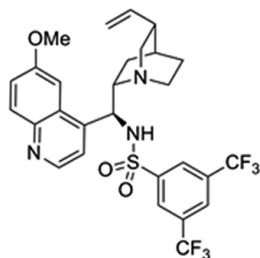
There are few areas in chemistry that are generating as much excitement as the field of Lewis acid catalysis. One of the most promising recent developments has been the use of the metal-free Lewis acid $B(C_6F_5)_3$, to aid in effecting different chemical transformations. However, it has always been challenging for experimentalists to predict its exact role. Does $B(C_6F_5)_3$ behave as a catalyst, or is its role limited to merely being an initiator? An important recent work in this context is the recently accomplished, experimental *in situ* generation of SiH_4 from surrogates with the aid of $B(C_6F_5)_3$. The current computational investigation, with density functional theory (DFT), reveals that this process is not, in fact, catalyzed by $B(C_6F_5)_3$ at all, but is dominated instead by a series of cationic autocatalytic reactions, where the role of $B(C_6F_5)_3$ is to function more as an initiator. Now, given the ambivalence in the behaviour of $B(C_6F_5)_3$, the obvious question that comes to mind is: can it made possible for an experimentalist to determine easily whether $B(C_6F_5)_3$ is acting as a catalyst or initiator in a given reaction? We have employed some very simple computational calculations to provide insight in this regard. Depending on the ease of separation of ion-pairs, we have come to a generalized conclusion for evaluating and separating reactions where $B(C_6F_5)_3$ can act as a catalyst or co-catalyst or initiator.[5]

(iii) Presented a poster entitled “Hidden Role of Intramolecular Non-covalent Interactions in Cinchona Alkaloid Catalysts for Asymmetric Organocatalysis” at Science day, CSIR-NCL, Pune, 26th -27th February 2020.

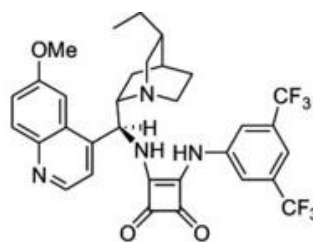
The history of cinchona is very much well known to us for the use of medicine in treatment of malaria. Cinchona alkaloids isolated from the bark of several species of cinchona trees, are the organic molecules having its wide use in organic chemistry. The different forms of cinchona alkaloid includes 1) cinchonine 2) cinchonidine 3) quinine 4) quinidine.

The role of cinchona in organic chemistry was confirmed by Pasteur in 1853. The most interesting application of cinchona alkaloids in chemistry is to catalyze in enantioselective transformations in both homogeneous and heterogeneous reactions.

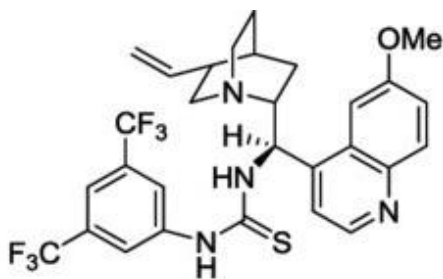
In this study we mainly focus into the modified cinchona alkaloid as organocatalysts. In our study modified cinchona alkaloid includes mainly 1) Cinchona sulfonamide catalyst 2) Cinchona squaramide catalyst 3) Cinchona thiourea catalyst and 4) Cinchona amide urea catalyst.



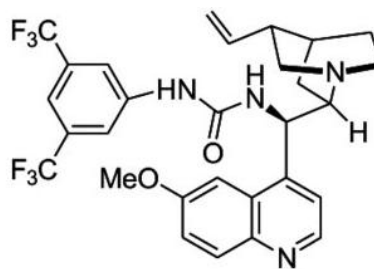
Cinchona sulfonamide catalyst



Cinchona squaramide catalyst



Cinchona thiourea catalyst



Cinchona amide-urea catalyst

The main goal of this study is to find how non-covalent interactions mainly intramolecular pi-pi stacking and NH-pi interaction play an important role in this wide range of organocatalysis. In order to search for the answer we modeled different modified cinchona alkaloid mentioned above. Those molecules have been optimized computationally at the density functional(DFT) level of theory. We found there are several cases where the stable confirmation of the catalysts have either intramolecular NH-pi or pi-pi stacking or NH-pi and pi-pi both interaction exist simultaneously.

B(C₆F₅)₃: Catalyst or Initiator? Insights from Computational Studies into Surrogate Silicon Chemistry

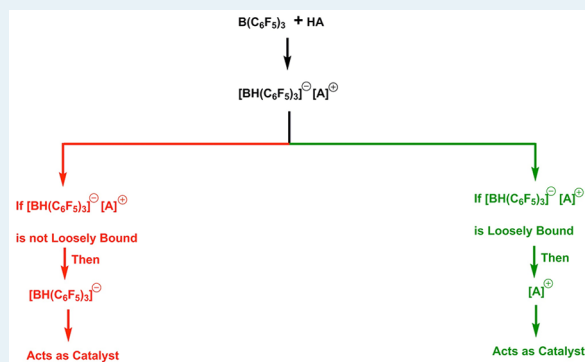
Subhrashis Banerjee and Kumar Vanka*¹

Physical and Material Chemistry Division, CSIR-National Chemical Laboratory, Dr. Homi Bhabha Road, Pune 411008, Maharashtra, India

Supporting Information

ABSTRACT: One of the most promising recent developments in catalysis has been the use of the metal-free Lewis acid B(C₆F₅)₃ as a catalyst for a range of different chemical transformations. Perhaps the most impressive achievement in this regard is the recently accomplished *in situ* generation of SiH₄ from surrogates (Simonneau and Oestreich, *Nat. Chem.*, 2015, 7, 816). However, what the current computational work, with density functional theory, reveals is that this process, in addition to being catalyzed by B(C₆F₅)₃, is also significantly dominated by a series of autocatalytic reactions. The results are further corroborated by the use of the energetic span model, which shows that the turnover frequency is higher for the newly proposed autocatalytic pathway in comparison to the conventional B(C₆F₅)₃-catalyzed pathway. The current work therefore provides interesting new insights into surrogate silicon chemistry. But, more importantly, the current studies indicate that B(C₆F₅)₃ is likely to function more as an initiator rather than a pure catalyst in many metal-free transformations that have been reported to date.

KEYWORDS: tris(pentafluorophenyl)borane, surrogate silicone chemistry, ion-pair, Lewis acid catalysis, autocatalysis, reaction mechanism, density functional theory



INTRODUCTION

In the two decades since the realization that the Lewis acid, B(C₆F₅)₃, is capable of acting as a catalyst, there have been a wide range of chemical transformations where it has been effectively employed,^{1,2} including hydrogenation³ and hydrosilylation,^{4–7} the transformation of ethers,⁸ the transesterification and deoxygenation of phosphonic and phosphinic esters,⁹ hydrodefluorination with hydrosilanes,¹⁰ dehydrogenative Si–X (X = nitrogen, oxygen, sulfur) coupling,^{11,12} and intramolecular silyl-Friedel–Crafts-type reactions.^{13,14} Furthermore, B(C₆F₅)₃ has also been employed as a catalyst for dihydrogen activation,¹⁵ the deoxygenation of carbohydrates,¹⁶ hydrogermylation,¹⁷ and the reduction of amines,¹⁸ as well as allylation.¹⁹ Transfer hydrogenation and transfer hydrosilylation have also been effected with the aid of B(C₆F₅)₃.^{20–22} There have also been many theoretical studies on the Lewis acidity of fluoroarylboranes.²³ Many mechanistic pathways for B(C₆F₅)₃-catalyzed systems have been extensively investigated computationally by Sakata and co-workers.²⁴ What makes this extensive exploration particularly noteworthy, apart from its originality and range, is the fact that it is metal-free catalysis, having the virtues of being both potentially cheap and environmentally friendly.

However, it is also true that there are examples in the literature where B(C₆F₅)₃ has been noted to serve only as an initiator of a reaction, extracting a hydride or a methide from a

neutral molecule to form a zwitterionic species. In such reactions, B(C₆F₅)₃ has been seen to form a counterion in solution that is non-interacting and non-interfering in nature, while the real catalytic active species was the corresponding cation formed. Figure 1 shows an example for this, taken from the field of homogeneous olefin polymerization,²⁵ but there are also recent examples, such as the Friedel–Crafts C–H borylation of electron-rich arenes.²⁶

Now, this gives rise to an interesting question: in all the cases mentioned in the previous paragraph, where B(C₆F₅)₃ has been

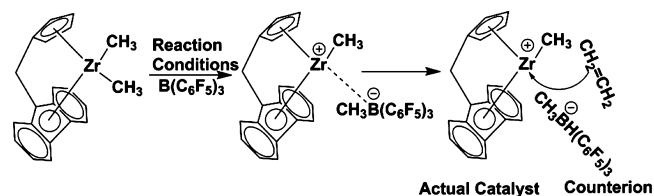


Figure 1. Role of B(C₆F₅)₃ in homogeneous olefin polymerization has been that of a co-catalyst or initiator, while the cation formed performs as the actual catalyst. The specific example shown here has been demonstrated by Marks and co-workers.²⁵

Received: December 29, 2017

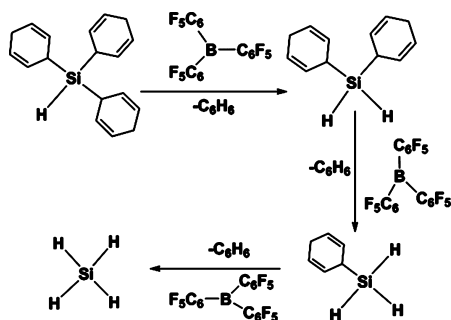
Revised: April 22, 2018

Published: May 22, 2018

considered to act as a catalyst,^{1–22} is there a possibility that in many of them it is acting more as an initiator, and not as a catalyst? Clearly, for this to be the case, (i) the reaction between the neutral substrate and $B(C_6F_5)_3$ species would have to form a loose, solvent-separated ion-pair complex and (ii) the cation part of the ion-pair would then have to be capable of being the active catalytic species. It is the consideration of these possibilities that has led to the current investigation, with a primary focus on the recently reported surrogate chemistry conversion of SiR_3H ($R = \text{cyclohexa-1,4-diene}$) to SiH_4 ,^{27,28} which is one of the most impressive achievements to date in $B(C_6F_5)_3$ chemistry.

The reason why $B(C_6F_5)_3$ catalysis of SiR_3H to SiH_4 is so important is because it has always been challenging to work with the explosive, pyrophoric and toxic²⁹ SiH_4 directly. However, it is an important source of elemental silicon, which is widely used in the semiconductor industry.³⁰ In addition to this, compounds of silane find use in the hydrosilylation³¹ of alkenes,³² olefins,³³ alcohols³⁴ and carbonyls.³⁵ Hence the significance of the *in situ* generation of SiH_4 with the aid of $B(C_6F_5)_3$ in the reaction pot from cheap, stable surrogates by Simonneau and Oestreich^{27,28} (see Scheme 1).

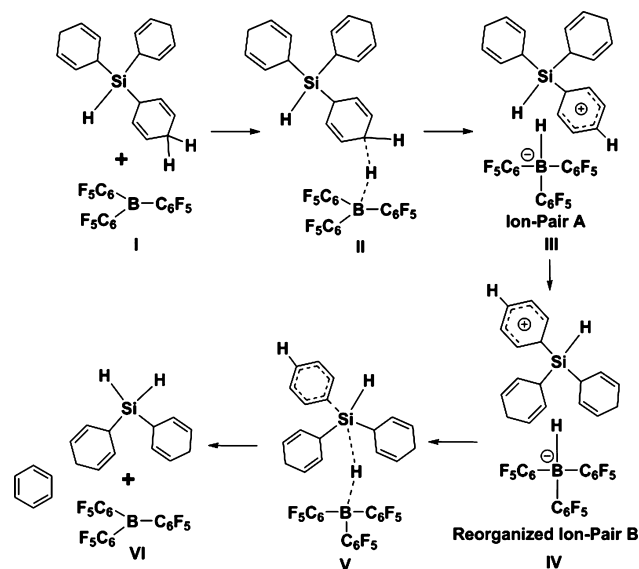
Scheme 1. *In Situ* Generation of SiH_4 , As Proposed by Simonneau and Oestreich^{27,28}



$B(C_6F_5)_3$, and tri(cyclohexa-2,5-dien-1-yl)silane (SiR_3H) were added in dichloromethane (CH_2Cl_2) under ambient conditions, and this was seen to lead to the rapid generation of SiH_4 .^{27,28}

The mechanism that has been proposed^{27,28} for this facile transformation involves $B(C_6F_5)_3$ in the role of catalyst. The first cycle of this process is shown in Scheme 2, and similar cycles have been proposed for the lower surrogates, leading finally to SiH_4 (Supporting Information (SI), Figures S1 and S2). A perusal of this mechanism shows that it involves the reorganization of the zwitterionic species, ion-pair A (see Scheme 2). An alternative route after the reorganization of the loosely solvent bound ion-pair would be the interaction of a neutral SiR_3H species with the ion-pair B: $[SiR_2R'H]^+[HB(C_6F_5)_3]^-$. We propose an autocatalytic process in this alternative scenario, shown in Scheme 3 and Scheme 4, that will allow the formation of new, loosely bound ion-pairs to be generated in each step, along with the expected lower surrogate silicon complex, SiR_2H_2 . This, in turn, can react with the ion-pair species, and thus the sequence of reactions can proceed until SiH_4 is formed (see SI, Figures S4–S6). In other words, if conditions (i) and (ii), mentioned earlier, are satisfied for this series of transformations, then the current work will provide insight into the interesting different roles played by $B(C_6F_5)_3$ during the SiR_3H species to SiH_4 transformation process.

Scheme 2. Lewis Acid $B(C_6F_5)_3$ -Catalyzed Mechanism for the Formation of SiH_4 from Tri(cyclohexa-2,5-diene-1-yl)silane

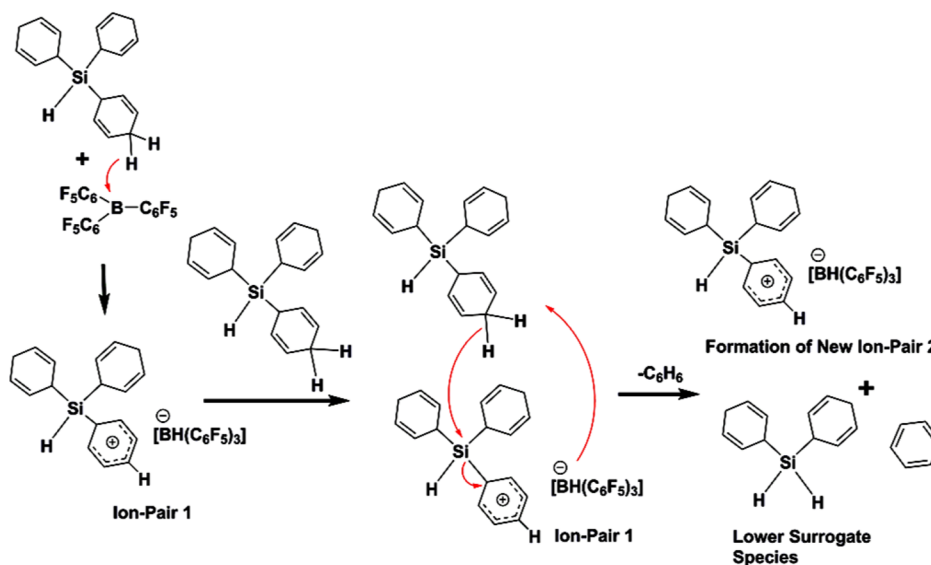


These possibilities, as well as the original proposed mechanism of Simonneau and Oestreich (Scheme 2), have been carefully investigated in their entirety with density functional theory (DFT). As will be shown in the Results and Discussion, we find that the calculations indicate a preference for the autocatalytic³⁶ process, with the $B(C_6F_5)_3$ seen to be more an initiator and a spectator rather than the pure catalyst. The proton source for the reactions is seen to be the silicon complex, analogous to other experimental cases where species such as substituted cyclohexa-1,4-diene were the hydride source.^{37,38} Furthermore, keeping in mind the implications that these results have for $B(C_6F_5)_3$ chemistry, we will also discuss the possibility of $B(C_6F_5)_3$ being more of an initiator in several other reactions where it has, until now, been considered to act as a catalyst.

COMPUTATIONAL DETAILS

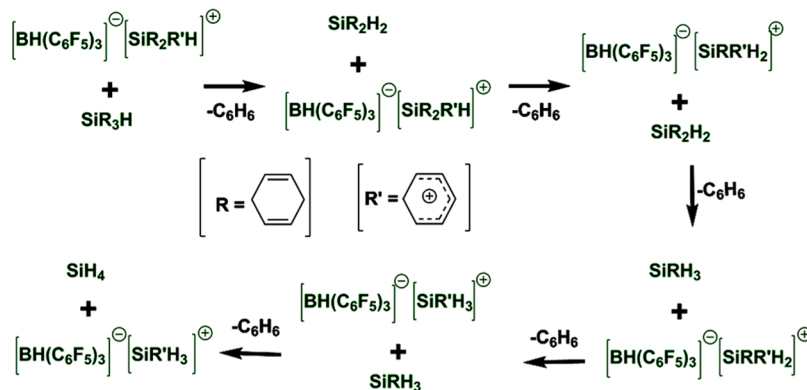
All the calculations for the structures reported herein have been done using DFT.^{39,40} The calculations have been carried out with Turbomole 7.0⁴¹ using the TZVP⁴² basis set. Geometry optimizations were performed using the Perdew, Burke, and Ernzerhof (PBE) functional.⁴³ Dispersion corrections (D3)⁴⁴ have been included in all the calculations. Solvent corrections have also been included in all the calculations using the Cosmo model,⁴⁵ with $\epsilon = 8.93$, to model dichloromethane, CH_2Cl_2 , which had been employed as the solvent in the surrogate-to- SiH_4 ^{27,28} experiments. Therefore, the level of theory employed is PBE-D3/TZVP+COSMO(CH_2Cl_2).^{42,43,45} The resolution of identity (RI)⁴⁶ along with the multipole accelerated RI (marij)⁴⁷ approximations have been used for an accurate and efficient treatment of the electronic Coulomb term in the DFT calculations. Furthermore, in order to underscore the reliability of the calculations, all the geometry optimizations have also been done at the TPSS-D3/def2-TZVP+COSMO(CH_2Cl_2)^{48,49,45} level of theory. The results from both the levels of theory, PBE-D3/TZVP+COSMO(CH_2Cl_2) and TPSS-D3/def2-TZVP+COSMO(CH_2Cl_2), are shown in Tables 1–3. Furthermore, all the figures showing the free energy profiles have two profiles, one for the PBE-D3/TZVP+

Scheme 3. Currently Proposed Autocatalytic Mechanism for the Formation of Di(cyclohexa-2,5-diene-1-yl)silane, a Lower Surrogate of Tri(cyclohexa-2,5-diene-1-yl)silane^a



^aThe $[\text{BH}(\text{C}_6\text{F}_5)_3]^-$ anion remains as a spectator, and shifts to the cation formed to create a new ion-pair.

Scheme 4. *In Situ* Generation of SiH_4 : Currently Proposed Autocatalytic Approach^a



At Every step, a lower surrogate species is formed.

^aThe $[\text{BH}(\text{C}_6\text{F}_5)_3]^-$ anion remains as a spectator. In each step it forms the ion-pair with the new cation which formed from the autocatalytic mechanism. In one step the R' is generated and comes out as a cation in the very next step.

COSMO(CH_2Cl_2) and one for the TPSS-D3/def2-TZVP+ COSMO(CH_2Cl_2) levels of theory. In addition to these calculations, single-point calculations at the PW6B95-D3/def2-QZVP+ COSMO(CH_2Cl_2)^{50,51,45} level of theory have also been done, on the geometries optimized at the TPSS-D3/def2-TZVP+ COSMO(CH_2Cl_2) level. In other words, the TPSS-D3/def2-TZVP+ COSMO(CH_2Cl_2)/PW6B95-D3/def2-QZVP+ COSMO(CH_2Cl_2) level of theory has also been employed to investigate all the catalytic cycles that have been discussed herein. This is the similar level to that employed by Oestreich and co-workers in their investigations into similar systems.³⁸ All the results obtained from the calculations at the TPSS-D3/def2-TZVP+ COSMO(CH_2Cl_2)/PW6B95-D3/def2-QZVP+ COSMO(CH_2Cl_2) level of theory have been included in the SI. For the purpose of clarity, we will henceforth denote PBE-D3/TZVP+ COSMO(CH_2Cl_2) as PTC(DCM) and TPSS-D3/def2-TZVP+ COSMO(CH_2Cl_2) as TDC(DCM). Necessary care was taken to ensure that the

obtained transition state structures possessed only one imaginary frequency corresponding to the correct normal mode, in order to obtain more reliable energy values for the investigated potential energy surface. In addition, intrinsic reaction coordinate (IRC)⁵² calculations were done with all the transition states in order to further confirm that they were the correct transition states, yielding the correct reactant and product structures. The values reported herein are ΔG values, with zero point energy, internal energy, and entropic contributions, with the temperature taken to be 298.15 K. The calculation of the translational entropy in standard software involves assumptions about the volume that may be inaccurate. The translational entropy term can be corrected by a free volume correction introduced by Mammen and co-workers.⁵³ Based on the Sackur–Tetrode equation, the free volume model describes the translational entropy of molecules in the solution ($\Delta S_{\text{trans}}(\text{sol})$); and provides physically intuitive corrections for translational entropy values. In the free volume

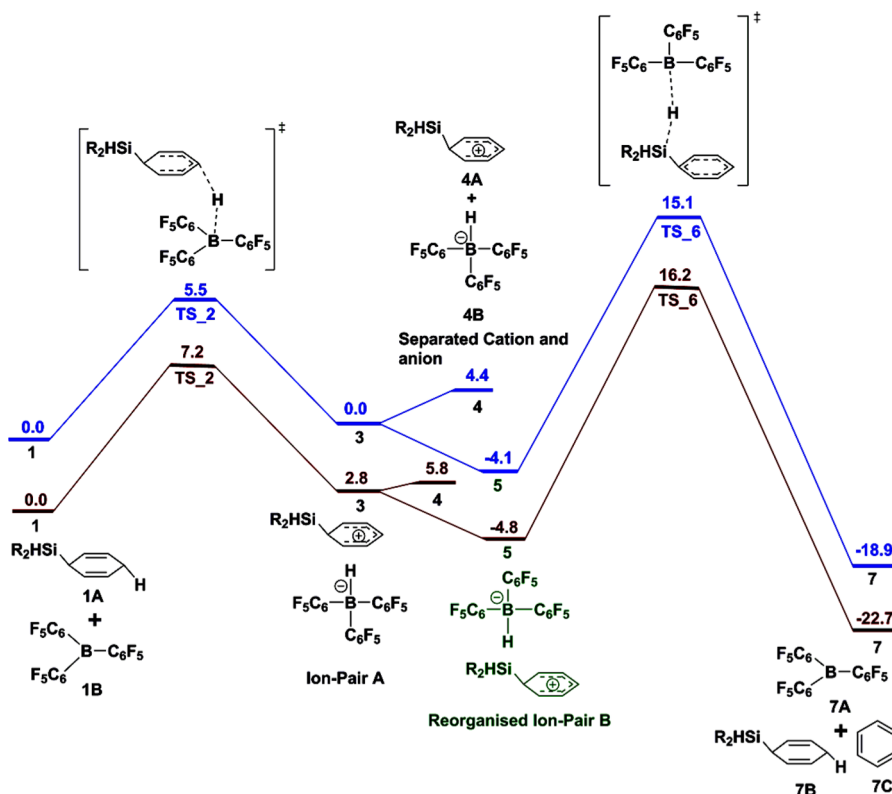


Figure 2. Free energy profile (ΔG in kcal/mol) for the mechanism proposed by Simonneau and Oestreich. R = cyclohexa-1,4-diene. The blue profile is for the PTC(DCM) level of theory, and the brown profile is for the TDC(DCM) level of theory.

model, it has been assumed that the volume available to the molecule in solution is lower than the total volume, and this “free volume” is determined by the eq 1:

$$V_{\text{free}} = C_{\text{free}} \left(\sqrt[3]{\frac{10^{27}}{[X]N_0}} - \sqrt[3]{V_{\text{molec}}} \right)^3 \quad (1)$$

Here, V_{molec} is the molecular volume, $[X]$ is the concentration of molecules (mol/L) in solution, and N_0 is the Avogadro number. The translational entropy can be obtained after considering the free volume correction, and inserting the value of V_{free} in the Sackur–Tetrode equation. The total entropy is then calculated by adding the corrected translational entropy and the entropic contributions from the rotational and vibrational components.

It is to be noted that entropic contributions have been properly handled in every mechanism that has been studied and reported here. For bimolecular reactions where two species had to come together for the reaction to occur, the barrier for the reactions has always been calculated with the reactants assumed initially to have been at infinite separation, and not from a pre-reactive complex.

For the different ion-pairs considered, we have taken the crystal structures, where available, as the starting geometries for the optimization. Solvent corrections have also been included, using the COSMO model,⁴⁵ in the ΔG calculations for the energy of separation of the different ion-pairs. For the reactions done by Oestreich and co-workers,^{26,75} Piers, Tuononen, and co-workers,⁷⁰ Piers and co-workers,⁷⁴ and Stephan and co-workers,^{73,76} we have employed toluene with $\epsilon = 2.38$, in order to model the solvent (toluene) that was employed in these reactions. For the reactions done by Chang and co-workers,⁷²

we have employed $\epsilon = 4.81$ to model chloroform. For the reactions done by Hou and co-workers,⁷¹ we have employed $\epsilon = 5.62$ in order to model chlorobenzene.

Conformational Exploration. The structures of the reactants and products were first optimized with Gaussian 09⁵⁴ at the B3LYP(PCM)/3-21g^{55–57} level of theory. Solvent corrections have been included with PCM,⁵⁶ with the epsilon for dichloromethane, CH_2Cl_2 ($\epsilon = 8.93$), used in all the calculations. For a given structure, a scan to obtain different conformations was done by choosing a dihedral, and different structures were obtained by varying the value of the dihedral. This procedure was repeated with all possible dihedrals for this structure, in order to cover the maximum conformational space. Then the structure with the lowest energy was taken and optimized at the PTC(DCM) level of theory with Turbomole 7.0. This was done with the structures of all the reactants and products. It was seen, in every case, that the geometry obtained by this approach at the PTC(DCM) level of theory with Turbomole 7.0 was lower in energy than other conformations taken and optimized at this level of theory, thereby validating this approach. A similar approach was adopted to scan transition states as well. It is worth mentioning here that, to reduce the computational cost, the transition states involving the autocatalytic pathway were scanned without considering the $[\text{HB}(\text{C}_6\text{F}_5)_3]^-$ ion, as it only remains as a spectator in the entire autocatalytic pathway. For the transition state scanning, the atoms involved in the transition state were fixed. Then, the procedure of scanning with the dihedrals was repeated as before, allowing the sampling of the conformational space for the transition states. The lowest energy transition state obtained by this scanning procedure for all the transition states was then optimized at the PTC(DCM) level of theory with

Turbomole 7.0. As before, this was seen to be lower in energy than other transition state structures. It is worth mentioning here that we have also followed a similar conformational exploration for the ion-pair structures that we have investigated. Hence, the scanning procedure allowed us to obtain reliable reactant, product and transition state structures for the comparison of the reaction mechanism proposed in the literature and the new mechanism(s) that we have proposed.

Energetic Span Model (ESM). The efficiency of the catalytic cycle can be analyzed through the ESM, put into practical use by Shaik and co-workers.^{58,59} The ESM provides a straightforward method to calculate the turnover frequencies (TOFs) of catalytic cycles based on their computed energy profiles. In most cases, the TOF is determined by the TOF-determining transition state (TDTS), the TOF-determining intermediate (TDI), and by the reaction energy, ΔG_r , as shown below:

$$\text{TOF} = \frac{k_B T}{h} e^{-\delta E/RT} \quad (2)$$

where δE is the energy span and is defined as the difference in the Gibbs energy between the TDTS and the TDI, with the addition of the ΔG_r when the TDTS appears before the TDI. δE is the effective activation barrier of the global reaction. The TDTS and TDI are the intermediate and the transition states, respectively, that maximize δE , according to eq 3.

$$\delta E = \begin{cases} \text{TDTS} - \text{TDI} & \text{if TDTS appears after} \\ & \text{TDI} \\ \text{TDTS} - \text{TDI} + \Delta G_r & \text{if TDTS appears before} \\ & \text{TDI} \end{cases} \quad (3)$$

This model has been employed to calculate the TOFs (at 298 K). The ESM can be applied in a user-friendly way with the recently developed AUTOF computer program.^{58,59}

RESULTS AND DISCUSSION

Role of $B(C_6F_5)_3$ in Surrogate Silicon Chemistry. As stated in the Introduction, the possibility of autocatalytic alternatives (see Schemes 3 and 4) to the conventional $B(C_6F_5)_3$ -catalyzed pathways (Scheme 2) for the conversion of SiR_3H to SiH_4 has been considered in our computational studies. Every profile we have shown in the Article and SI have been colored with blue for PTC(DCM) and brown for the TDC(DCM) levels of theory. Figure 2 shows the catalytic cycle proposed by Simonneau and Oestreich,^{27,28} based on a previously proposed mechanism by Sakata and Fujimoto for the formation of the methyl substitute silane ($SiHMe_3$).⁶⁰ In the first step, the Lewis acid $B(C_6F_5)_3$ extracts a hydride from the bisallylic position^{61,62} of SiR_3H to give rise to the ion-pair $[SiR_2R'H]^+[HB(C_6F_5)_3]^-$ (species 3). The calculations indicate that the hydride *anti* to the silicon is the one preferentially taken by the $B(C_6F_5)_3$, as has also been observed by Sakata and Fujimoto.⁶⁰ Here, it is worth mentioning that Sakata and Fujimoto⁶⁰ have discussed a mechanism where methyl substituted cyclohexene behaves as a hydride source, with the hydride being given to the $[SiMe_3(C_6H_6)]^+$ cation. The barrier for the process was found to be higher than for the conventional $[BH(C_6F_5)_3]^-$ pathway and is different from the newly proposed autocatalytic pathway. Now considering the ion-pair A, species 3 can rearrange to species 5, with the boron

now positioned to deliver the hydride to the silicon. For this, a barrier of 15.1 kcal/mol (blue profile in Figure 2) has to be overcome, and yields the lower surrogate species: SiR_2H_2 , the original $B(C_6F_5)_3$ and benzene. However, the alternative route, shown in green in the same figure (see Figure 2), would lead to the autocatalytic pathway. Here, it is noted that 5 is a loosely bound ion-pair species. This is because the energy for completely separating 5 into the cation and anion has been calculated to be only 8.5 kcal/mol at the PTC(DCM) level of theory. This would ensure the availability of the cation for participating in the autocatalytic pathway. This cationic species, $[SiR_2R'H]^+$, can be considered a σ complex cation.^{63,64} Such silicon-substituted cyclohexadienyl cations are low-energy Wheland complexes or, from the perspective of silicon chemistry, arene-stabilized silicon cations.⁶⁵ It has been shown previously⁶⁶ that stabilizing donors are needed in silicon cation generation. Here, cyclohexa-2,5-dien-1-ylsilanes meet this requirement, as they have sufficient hydridic character at the bisallylic position of C(sp³)–H bond due to hyperconjugation with the C(sp³)–Si bond. We also note that the fact that the separation of loosely bound ion-pairs involving a cationic silicon species and the $[HB(C_6F_5)_3]^-$ anion in dichloromethane is very facile has also been reported earlier by Sakata and Fujimoto at the M06-2X(PCM)/6-311++g(d,p)//M06-2X(PCM)/6-311g(d,p) level of theory.⁶⁰ It is also notable that the values obtained at entirely different levels of theory in the current work: the PTC(DCM) and the TDC(DCM) (blue and brown profiles respectively in Figure 2) are quite similar in the values obtained, which suggests that the conclusions that have been reached are reliable and robust, and invariant of the level of theory employed.

Now, the $[SiR_2R'H]^+$ cation, seen to be loosely bound to the anion, can be considered as an independent actor, like in the cases of homogeneous olefin polymerization²⁴ and Friedel–Crafts C–H borylation²⁶ mentioned in the Introduction. The possibility that this species can take part in autocatalytic reactions is explored in Figure 3. The $[SiR_2R'H]^+$ cation can extract a hydride from another SiR_3H substrate molecule to yield SiR_2H_2 , the reaction having a barrier of 10.0 kcal/mol (blue profile in Figure 3). This is 5.1 kcal/mol lower than the corresponding step shown in Figure 2. Therefore, this newly proposed autocatalytic process is significantly more facile than the conventional pathway.

Now, SiR_2H_2 formed can interact with an $[SiR_2R'H]^+$ cation to convert to $[SiRR'H_2]^+$ (with a loosely bound $[HB(C_6F_5)_3]^-$ as a spectator species) to form an SiR_2H_2 species with the release of a benzene molecule. The free energy profile for this is shown in the SI, Figure S6a. As one can see, there can be several permutations and combinations, where different $Si-(R)_xH_y$ species can interact with different $[Si(R)_x(R')H_y]^+$ species (with a spectator $[HB(C_6F_5)_3]^-$ always present), to yield the corresponding lower surrogate silicon intermediates. All of these have been considered in this work, and for each step where the lower surrogate is formed, they have been compared to the $B(C_6F_5)_3$ -catalyzed mechanism proposed in the literature. Shown in Table 1 are the barriers for the formation of the intermediates by the conventional literature mechanism and the corresponding barriers for the formation of the intermediates by different permutations of the newly proposed pathways, independent of $B(C_6F_5)_3$ (the free energy profiles for all the cases are provided in the SI, Figures S4–S6). As the results indicate, not only are the pathways for forming a given intermediate greater by the routes outlined here, the

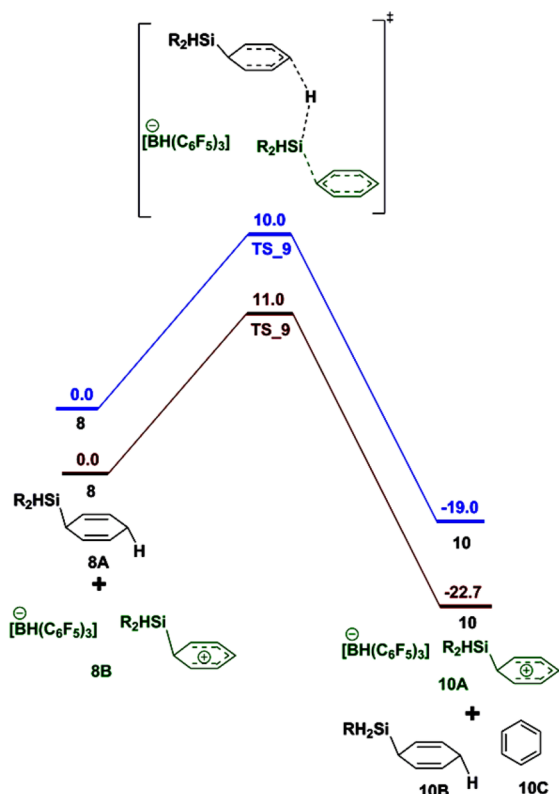


Figure 3. Free energy profile (ΔG in kcal/mol) for the autocatalytic mechanism. The $[\text{BH}(\text{C}_6\text{F}_5)_3]^-$ anion remains as a spectator. $\text{R} =$ cyclohexa-1,4-diene. The blue profile is for the PTC(DCM) level of theory, and the brown profile is for the TDC(DCM) level of theory.

barriers for forming the intermediates are uniformly lower in each case, in comparison to the $\text{B}(\text{C}_6\text{F}_5)_3$ -catalyzed mechanism. While all the cases considered have been comprehensively compared in the SI (see Figures S1–S6), an illustrative case among the lot is shown in Figure 4, which compares the formation of SiH_4 from $[\text{SiR}'\text{H}_3]^+[\text{HB}(\text{C}_6\text{F}_5)_3]^-$ from both the conventional and autocatalytic approaches. The profiles show that the barrier for the autocatalytic mechanism is 4.4 kcal/mol lower than the barrier for the conventional pathway for this step (see Figure 4).

In order to provide a more quantitative estimate of how the newly proposed autocatalytic pathways are more favored over the $\text{B}(\text{C}_6\text{F}_5)_3$ -catalyzed pathways, we have determined the efficiency for the free energy profiles shown in the Figures 2–5 (see the flowchart) as well as Figures S1–S3 in the SI, by employing the ESM.^{58,59} In the present case, for the $\text{B}(\text{C}_6\text{F}_5)_3$ -catalyzed pathway (see Figure 3), the TOF-determining transition state (TDTS) appears after the TOF-determining

intermediate (TDI). The TDI is determined to be species 5 in the energy profile and the TDTS is species 6 (see Figure 2). The TOF for the autocatalytic pathway is calculated to be $1.0 \times 10^9 \text{ h}^{-1}$ at the PTC(DCM) level of theory. This is obtained by considering that the species involved are (5–8–9–10).⁶⁷ The corresponding value for the conventional pathway is $2.6 \times 10^2 \text{ h}^{-1}$; i.e., the newly proposed pathway is 7 orders of magnitude superior in efficiency in comparison to the conventional pathway! This is also seen to be true at the TDC(DCM) level of theory. But this is not all. After the reorganized species has been formed in the initiation step (species 5 in Figure 2), for subsequent cycles, the TOF calculations would involve only a one step pathway. The calculations indicate that the TOF for this would be several orders of magnitude superior to the conventional pathway, at both levels of theory (see Table 2)! Furthermore, in order to make a fairer comparison between the multistep conventional pathway, and the autocatalytic route, we have also calculated the TOF for the complete catalytic cycle, beginning from SiR_3H and ending finally with the formation of SiH_4 , for both the conventional as well as the autocatalytic routes. This will have several steps in all, the flowchart for which has been provided in Figure 5. The ESM results indicate that the autocatalytic pathway for the complete cycle is 10^3 times superior to the conventional pathway for both the PTC(DCM) and the TDC(DCM) levels of theory (see Table 2). Hence, all the ways in which the ESM has been employed to evaluate the conventional and the newly proposed routes for SiH_4 formation all point to significant superiority of the newly proposed pathways over the conventional routes that assume that the $\text{B}(\text{C}_6\text{F}_5)_3$ acts as the catalyst in this process.

These results therefore clearly show that the conventional $\text{B}(\text{C}_6\text{F}_5)_3$ -catalyzed pathway is only a minor route, while the more significant players in this chemistry are the newly proposed routes involving autocatalytic mechanisms. In order to provide further validation of the results, we have also calculated the barriers with full optimization at the PBE-D3/6-311++G**+COSMO(CH_2Cl_2)⁶⁸ level of theory. The results for this are provided in the SI, Table S1. Furthermore, single-point calculations at PW6B95/def2-QZVP+ $\text{COSMO}(\text{CH}_2\text{Cl}_2)$ with the TDC(DCM)-optimized structures have been done, and the results are provided in the SI, Table S2. All these extra calculations show that the conclusions reached, as well as the trends obtained, remain unaltered, thereby underlining the robustness of the level of theory employed.

Furthermore, in order to ensure that there are no other competing pathways, we have also checked another possibility, where the benzene separation from the cationic species of tri(cyclohexa-2,5-dien-1-yl)silane, di(cyclohexa-2,5-dien-1-yl)silane and mono(cyclohexa-2,5-dien-1-yl)silane could take place. The silicon after the benzene dissociation would be stabilized by coordination with the olefinic carbon of the

Table 1. Calculated Free Energy Barriers, ΔG^\ddagger , for All Possible Ways To Form the Lower Surrogate SiR_xH_y Species through the Conventional Mechanism Proposed in the Literature and Our Proposed Mechanism

| intermediate | ΔG^\ddagger , kcal/mol | | | |
|--------------------------------------|---|---|--------------------------------------|--------------------------------------|
| | literature mechanism | proposed cationic autocatalytic mechanism | | |
| | $[\text{HB}(\text{C}_6\text{F}_5)_3]^-$ | SiR_3H | SiR_2H_2 | SiR_3H_3 |
| $[\text{SiR}'_2\text{R}'\text{H}]^+$ | 14.9 ^a /16.2 ^b | 10.0 ^a /11.0 ^b | 10.4 ^a /14.5 ^b | 11.2 ^a /11.3 ^b |
| $[\text{SiRR}'\text{H}_2]^+$ | 14.8 ^a /12.5 ^b | 10.7 ^a /9.0 ^b | 10.3 ^a /10.8 ^b | 12.1 ^a /10.1 ^b |
| $[\text{SiR}'\text{H}_3]^+$ | 14.5 ^a /14.0 ^b | 8.0 ^a /9.0 ^b | 11.0 ^a /12.0 ^b | 9.2 ^a /9.4 ^b |

^aValues for the PTC(DCM) calculations. ^bValues for the TDC(DCM) calculations.

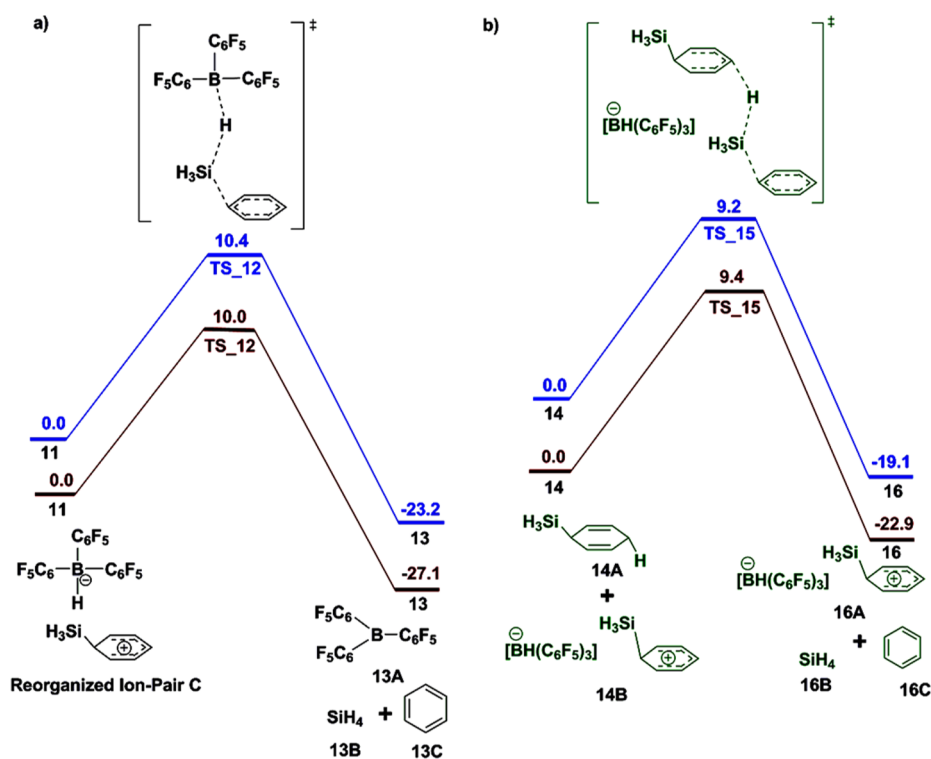


Figure 4. Comparison of the free energy profiles (ΔG , kcal/mol) between (a) the conventional mechanism with mono(cyclohexa-2,5-dien-1-yl)silane and $B(C_6F_5)_3$ and (b) our proposed autocatalytic mechanism. The blue profile is for the PTC(DCM) level of theory, and the brown profile is for the TDC(DCM) level of theory for conventional pathway. The deep green species are the ones pertaining to our newly proposed autocatalytic pathway.

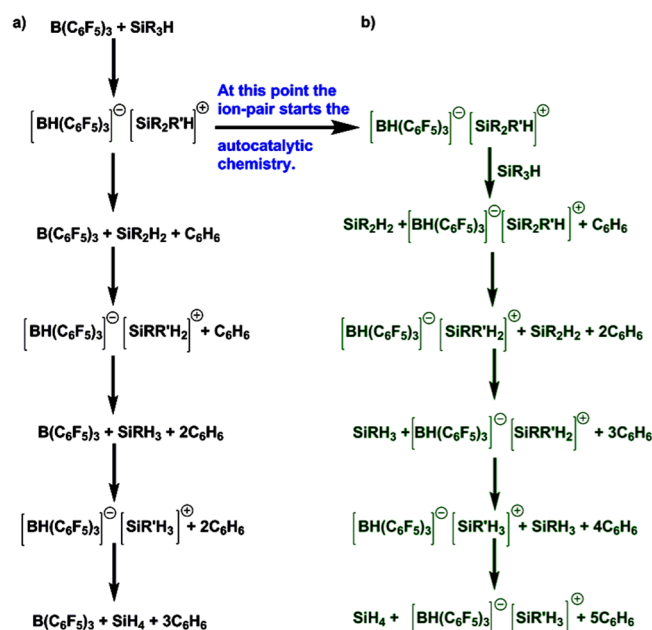


Figure 5. Flowchart for the formation of SiH_4 through (a) the conventional $B(C_6F_5)_3$ -catalyzed pathway and (b) the newly proposed autocatalytic pathway. The autocatalytic pathway is shown in green.

cyclohexadienyl ring (see SI, Figures S7–S9). Subsequently, the silicon cation could participate in new autocatalytic processes. However, such a possibility was found to be unlikely, because the ΔG for the dissociation of benzene for every case was found to be high (9.0 kcal/mol to greater than 30.0 kcal/mol), at both the PTC(DCM) and the TDC(DCM) levels of theory (see SI,

Table S4). Thus, the overall barrier for such processes would become high—higher than the slowest step for our proposed autocatalytic pathways. Hence, this possibility has not been considered further.

What Is the Real Role of $B(C_6F_5)_3$ in Metal-Free Reactions?

What the previous section made clear is the significant difference between the perceived role of $B(C_6F_5)_3$ in the formation of SiH_4 from SiR_3H , and the reality, which is that $B(C_6F_5)_3$ acts less as a pure catalyst, and more as an initiator and then a spectator in the entire, multistep process. This leads to a much larger, and very interesting question: since there are many metal-free chemical transformations that have emerged in recent years where $B(C_6F_5)_3$ has been considered to act as a catalyst,^{1–22} in how many of them is $B(C_6F_5)_3$ really the catalyst, and in how many is it acting more as an initiator? One means of answering the question is by investigating the hydricities of borohydrides,⁶⁹ but a potentially simpler solution lies in looking at the ease of separation of the cation from the ion-pair created when $B(C_6F_5)_3$ reacts with the substrate. In the case of the surrogate silicon chemistry discussed above, for instance, once the zwitterionic complex (ion-pair B), was formed, the total separation of the cation from the ion-pair required only 8.5 kcal/mol additional energy, at the PTC(DCM) level of theory (see Figure 2). Thus, the cation would exist as a loosely bound ion-pair in solution, and the subsequent autocatalytic processes could thus emerge as an alternative. Hence, the ΔG of total separation of the cation from the ion-pair can provide a reliable parameter for how loosely bound the cation would be in solution to the ion-pair. But, what value of the ΔG of total separation can be considered facile? A good indicator for this would be the initiator chemistry for the electrophilic C–H borylation of electron-rich (hetero)arenes

Table 2. TOFs Obtained for the Stepwise and Total Autocatalytic Pathways, as Well as the Conventional B(C₆F₅)₃-Catalyzed Pathway

| pathway | TOF, h ⁻¹ | | | |
|---|--|--|--|--|
| | SiR ₃ H→[SiR ₂ H ₂] | SiR ₂ H→[SiRH ₃] | SiRH ₃ →[SiH ₄] | SiR ₃ H→[SiH ₄] |
| B(C ₆ F ₅) ₃ -catalyzed | 2.6 × 10 ² ^a /8.8 × 10 ⁰ ^b | 1.7 × 10 ⁵ ^a /8.9 × 10 ⁶ ^b | 1.2 × 10 ⁶ ^a /5.2 × 10 ⁵ ^b | 1.4 × 10 ⁶ ^a /9.4 × 10 ⁷ ^b |
| autocatalytic | 1.0 × 10 ⁹ ^a /1.9 × 10 ⁸ ^b | 6.3 × 10 ⁸ ^a /2.7 × 10 ⁸ ^b | 8.8 × 10 ⁸ ^a /2.0 × 10 ⁹ ^b | 2.5 × 10 ⁹ ^a /2.4 × 10 ⁹ ^b |

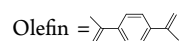
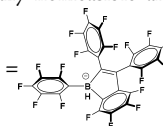
^aValues for the PTC(DCM) calculations. ^bValues for the TDC(DCM) calculations.

Table 3. Calculated Free Energies, ΔG, for the Separation of the Ion-Pairs Formed in the Different Experimentally Studied Reactions Where B(C₆F₅)₃ Has Previously Been Considered To Act as a Catalyst

| | ion-pair | ref | temp | ΔG, kcal/mol |
|----|--|-----|--------|--------------------------------------|
| 1. | (a) [CatB-(NMe ₂ Ph) ₂] ⁺ [HB(C ₆ F ₅) ₃] ⁻ | 26 | RT | 25.2 ^a /28.5 ^b |
| | (b) [CatB-NMe ₂ Ph] ⁺ [HB(C ₆ F ₅) ₃] ⁻ | 26 | RT | 28.3 ^a /30.8 ^b |
| | (c) [CatB-PhNMe ₂] ⁺ [HB(C ₆ F ₅) ₃] ⁻ | 26 | RT | 30.8 ^a /22.3 ^b |
| 2. | [Et ₃ Si] ⁺ [X] ⁻ | 70 | RT | 63.5 ^a /68.8 ^b |
| 3. | (a) [PhSiH ₂] ⁺ [HB(C ₆ F ₅) ₃] ⁻ | 71 | 120 °C | 48.7 ^a /52.2 ^b |
| | (b) [Me ₂ N(Ph-SiH ₂ Ph)] ⁺ [HB(C ₆ F ₅) ₃] ⁻ | 71 | 120 °C | 14.2 ^a /4.8 ^b |
| 4. | (a) [PhSi-Olefin] ⁺ [HB(C ₆ F ₅) ₃] ⁻ | 72 | RT | 40.6 ^a /42.3 ^b |
| | (b) [PhSiMe ₂ -Olefin] ⁺ [HB(C ₆ F ₅) ₃] ⁻ | 72 | RT | 14.2 ^a /13.3 ^b |
| 5. | [NH ₂ (CHMePh) ₂] ⁺ [HB(C ₆ F ₅) ₃] ⁻ | 73 | 100 °C | 31.4 ^a /16.1 ^b |
| 6. | [(PhCH)(Ph)N(SiHMe ₂ Ph)] ⁺ [HB(C ₆ F ₅) ₃] ⁻ | 74 | RT | 24.8 ^a /29.1 ^b |
| 7. | (a) [1,3-dimethyl-2,4-cyclohexadiene] ⁺ [HB(C ₆ F ₅) ₃] ⁻ | 75 | 120 °C | 40.8 ^a /49.7 ^b |
| | (b) [NH(Ph)(CMePh)] ⁺ [HB(C ₆ F ₅) ₃] ⁻ | 75 | 120 °C | 34.7 ^a /36.0 ^b |
| 8. | [2,6-Me ₂ C ₅ H ₃ N] ⁺ [HB(C ₆ F ₅) ₃] ⁻ | 76 | RT | 31.9 ^a /28.0 ^b |

^aValues for the PTC(DCM) calculations. ^bValues for the TDC(DCM) calculations. Cases where the separation is energetically nonfeasible are

shown in bold. Abbreviations: CatB, catecholborane; RT, room temperature; ΔG = {G_[A⁺] + G_{[HB(C₆F₅)₃]⁻]} - G_{[A⁺][HB(C₆F₅)₃]⁻}. X =}}



done at room temperature by Oestreich and co-workers²⁵ that had been mentioned earlier in the Introduction. Here, the B(C₆F₅)₃ had been clearly noted by Oestreich et al. to act as the initiator, and therefore the determination of the ΔG of separation of the ion-pairs for these cases can serve as an upper bound for deciding the ΔG for the facile separation of ions in other reactions. We have therefore calculated the ease of separation of the ion-pairs formed in this case and found them to be 25.2, 28.3, and 30.8 kcal/mol for the ΔG of separation of the ion-pairs [CatB-(NMe₂Ph)₂]⁺[HB(C₆F₅)₃]⁻, [CatB-NMe₂Ph]⁺[HB(C₆F₅)₃]⁻, and [CatB-PhNMe₂]⁺[HB(C₆F₅)₃]⁻, respectively, at the PTC(DCM) level of theory. These values, then, can serve as a benchmark for determining the possibility of ion-pair dissociation at room temperature for other cases. One could also consider slightly higher ΔG values, of up to 35.0 kcal/mol using the PTC(DCM) level of theory, for experiments done at higher temperatures (100–120 °C). One should note that these values provide an *upper bound* to the energy required to separate the ion-pairs in solution. In other words, what these values represent is the complete separation and isolation of the ions by the solvent in question. In reality, what is more likely is that the solvent would only serve to separate the ions and that they would remain in the same vicinity.

However, the ions thus separated would be independent actors, each doing chemistry without interference (or assistance) from the other. In other words, the more likely scenario is that of solvent *separated* ions than solvent *isolated* ions. However, the values shown in Table 3, which represent the latter case, are still of significance, because they serve to provide the relative trend in the ease of ion-pair separation. That is, if an ion-pair in one case separates with ease to completely to form solvent isolated ions, this also indicates that it would show ease in forming solvent-separated ions, in comparison to another case where the complete separation of the ions is less favored.

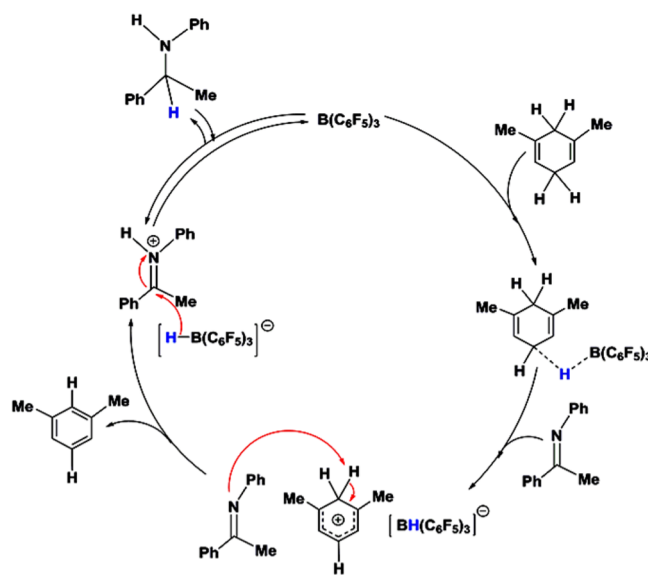
Now, considering the values of about 25.0–30.0 kcal/mol for room-temperature dissociation of ions, and about 35.0 kcal/mol for dissociation at higher temperatures, as discussed above, admittedly, a perusal of the literature shows that there are cases in B(C₆F₅)₃ chemistry where the values for the separation of the cation from the ion-pair fall do not fall within this range. These include the formation of the zwitterionic species [Et₃Si]⁺[X]⁻ {X = 1,2,3-tris(pentafluorophenyl)-4,5,6,7-tetrafluoro-1-boraindene anion; see structure provided in Table 3} studied by Piers, Tuononen, and co-workers,⁷⁰ where the ΔG is found to be 63.5 kcal/mol (see Table 3). In this case, it would be most likely that the ion-pair would not separate, and this is

borne out by the experimental isolation of the $[\text{Et}_3\text{Si}]^+[\text{X}]^-$ crystal structure.⁷⁰ Therefore, $[\text{Et}_3\text{Si}]^+[\text{X}]^-$ would act as a frustrated Lewis pair (FLP), as believed. This fact is further buttressed by the calculations that we have done (at the PTC(DCM) level of theory) that show the energy required to separate the $[\text{Et}_3\text{Si}]^+[\text{X}]^-$ ion-pair by 1.0 Å is as high as 25.3 kcal/mol. This is in contrast to $[\text{SiR}_2\text{R}'\text{H}]^+[\text{HB}(\text{C}_6\text{F}_5)_3]^-$, and $[\text{PhSiMe}_2\text{-Olefin}]^+[\text{HB}(\text{C}_6\text{F}_5)_3]^-$ (discussed below) where the energy required to separate the two ions by 1.0 Å was only 0.7 and 1.2 kcal/mol respectively (the values for other ion-pairs are collected in the SI, Table S3). However, there are several other cases, which are also reported in Table 3, where the ΔG values do fall in the range where separation would be expected. Among these, there are some, like entry 6, where the formation of only a single ion-pair, $[(\text{PhCH})(\text{Ph})\text{N}(\text{SiHMe}_2\text{Ph})]^+[\text{HB}(\text{C}_6\text{F}_5)_3]^-$ is involved, which would yield the $[(\text{PhCH})(\text{Ph})\text{N}(\text{SiHMe}_2\text{Ph})]^+$ cation in a facile manner ($\Delta G = 24.8$ kcal/mol at room temperature) (see Table 3). For such a case, it is highly likely that the cation would be taking part in autocatalytic processes similar to the ones that have been described in the previous section. As shown in the SI, Scheme S1a,b, it is easy to envision an alternative pathway not involving $\text{B}(\text{C}_6\text{F}_5)_3$ as the catalyst that would yield the same products ($[(\text{PhCH})(\text{Ph})\text{N}(\text{SiHMe}_2\text{Ph})]^+$, from toluene) as experimentally observed.⁷¹ There are other cases, however, where two ion-pair species would be formed during the reaction, such as in the case of entry 4 in Table 3, which involves the formation of the $[\text{PhSi-Olefin}]^+[\text{HB}(\text{C}_6\text{F}_5)_3]^-$ and the $[\text{PhSiMe}_2\text{-Olefin}]^+[\text{HB}(\text{C}_6\text{F}_5)_3]^-$ ion-pairs (Olefin = 1,4-diisopropenylbenzene). Here, while the separation of the cation from $[\text{PhSiMe}_2\text{-Olefin}]^+[\text{HB}(\text{C}_6\text{F}_5)_3]^-$ is seen to be very facile ($\Delta G = 14.2$ kcal/mol), the corresponding reaction for $[\text{PhSi-Olefin}]^+[\text{HB}(\text{C}_6\text{F}_5)_3]^-$ is seen to be unfavorable ($\Delta G = 40.6$ kcal/mol) at the PTC(DCM) level of theory.

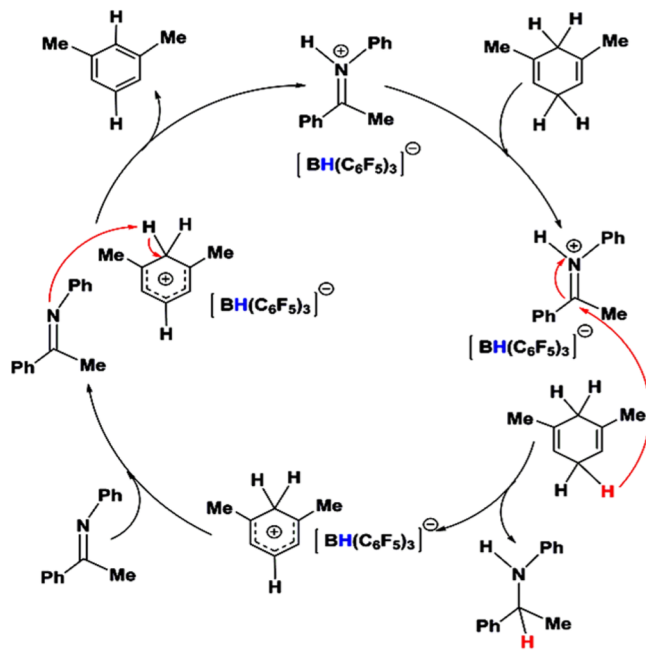
In order to further verify whether the easily separated ion-pair would follow the autocatalytic mechanism or the $\text{B}(\text{C}_6\text{F}_5)_3$ -catalyzed pathway, we have investigated one such system that was experimentally investigated by Oestreich and co-workers.⁷⁵ They proposed the reaction, the hydrogenation of imine, to be a $\text{B}(\text{C}_6\text{F}_5)_3$ -catalyzed process. This is shown in Scheme 5. However, it is easy to envisage a mechanism where the cation $[(\text{PhMeC})\text{NH}(\text{Ph})]^+$ formed would take over and lead to autocatalytic pathways independent of $\text{B}(\text{C}_6\text{F}_5)_3$ (see Scheme 6). Calculations have been done to investigate this possibility. As the free energy profiles shown in Figure 6 indicate, the $\text{B}(\text{C}_6\text{F}_5)_3$ -free pathway is more favorable by 3.6 kcal/mol at the PTC(DCM) level of theory for this case. We have also calculated the barriers at the TDC(DCM) and PBE-D3/6-311++G**+COSMO(CH_2Cl_2) levels of theory. The results are provided in the SI, Table S3, and show the same trend. SI Schemes S1a–S3b show the alternative pathways that are likewise possible for all the cases^{70–76} shown in Table 3.

It is worth mentioning here that Chatterjee and Oestreich have discussed the possibility of Brønsted acid-catalyzed transfer hydrogenation of imines in a separate (experimental) investigation.³⁷ They have proposed a catalytic cycle based on $\text{B}(\text{C}_6\text{F}_5)_3$ and Brønsted acid catalysis. Earlier Grimme, Oestreich, and co-workers had proposed transfer hydrogenation promoted by Ru–S complexes³⁸ based on experimental work supported by computation. It is, thus, important to note that Oestreich and co-workers had laid a path that researchers could follow, pertaining to mechanisms other than the $\text{B}(\text{C}_6\text{F}_5)_3$ Lewis acid-catalyzed pathway.

Scheme 5. Proposed Mechanism by Oestreich and Co-workers⁷⁵ for the Hydrogenation of Imine by $\text{B}(\text{C}_6\text{F}_5)_3$



Scheme 6. Mechanism That We Propose for the Same Reaction: Hydrogenation of Imine by $\text{B}(\text{C}_6\text{F}_5)_3$,⁷⁵ Based on the Facile Separation of the Cation from the Ion-Pair



We would also like to note that the current work, revealing the competition between the initiator and catalytic mechanisms, can also provide impetus for kinetic experiments that would yield insights into which mechanism predominates for a given system. For instance, the conventional mechanism emphasizes the role of $\text{B}(\text{C}_6\text{F}_5)_3$, and involves the formation and breaking of a B–H bond, while the newly proposed mechanism focuses on the formation and breaking of the Si–H bond, with the $\text{B}(\text{C}_6\text{F}_5)_3$ converted to an anion and present more as a spectator. Thus, kinetic isotope effects would be different for the different mechanistic scenarios. Likewise, other kinetic experiments can also be designed in order to test the nature of the reactions in these interesting systems.

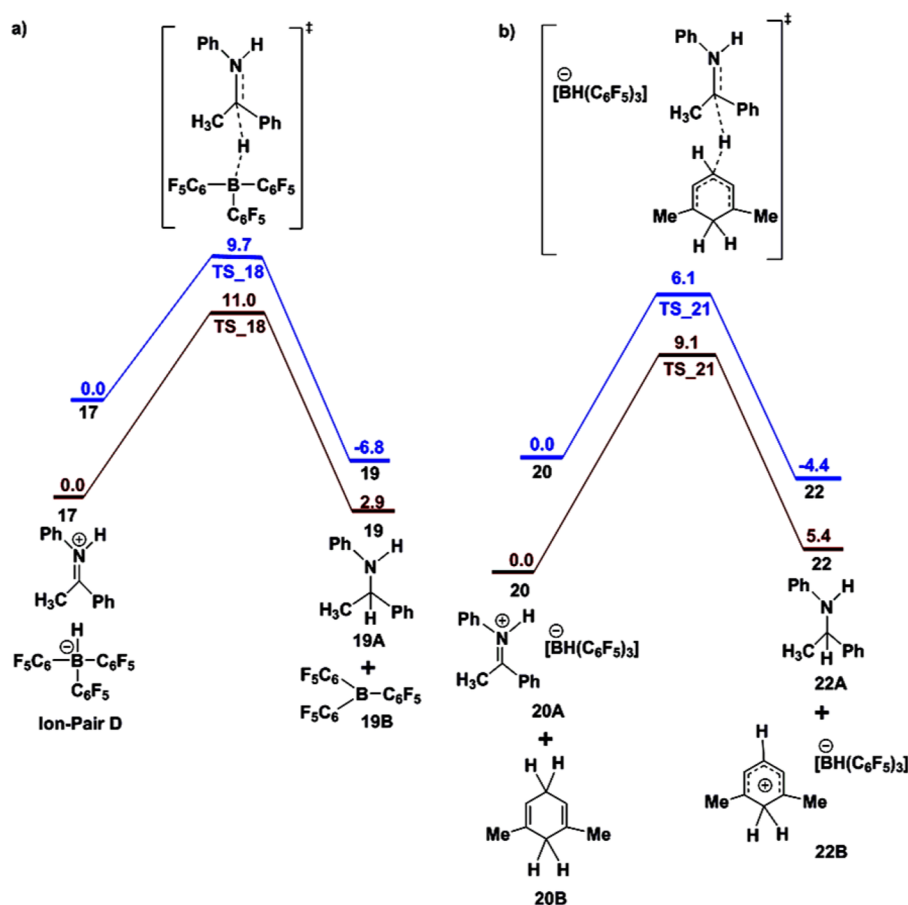


Figure 6. Comparison of the free energy profiles (ΔG , kcal/mol) for the formation of $[\text{PhNH}(\text{HC}(\text{CH}_3)(\text{Ph}))]$ between (a) the conventional mechanism with $[\text{PhNH}(\text{C}(\text{CH}_3)(\text{Ph}))]^+$ cation and $[\text{BH}(\text{C}_6\text{F}_5)_3]^-$ anion and (b) our proposed autocatalytic mechanism. The blue profile is for the PTC(DCM) level of theory, and the brown profile is for the TDC(DCM) level of theory. The autocatalytic mechanism is more favorable than the conventional mechanism.

Therefore, a simple means of determining when $\text{B}(\text{C}_6\text{F}_5)_3$ acts as a catalyst and when it may perform only as an initiator becomes clear: if the formed cation, A^+ , can separate in a facile manner from $[\text{A}]^+[\text{HB}(\text{C}_6\text{F}_5)_3]^-$, then catalytic pathways not involving $\text{B}(\text{C}_6\text{F}_5)_3$ can become competitive in the reaction. Hence, the implications of the current investigations extend well beyond the unravelling of the elegant autocatalytic mechanisms in surrogate silicon chemistry.

CONCLUSIONS

The current work, with density functional theory, showcases the elegant and unheralded nature of surrogate silicon chemistry, dependent not on Lewis acid, $\text{B}(\text{C}_6\text{F}_5)_3$, catalysis but on a series of autocatalytic processes. The computational investigations provide important insights that will be helpful for researchers working in the area of silicon chemistry, as well as for those working with surrogates in allied areas. Indeed, recent work reported by Oestreich and co-workers⁷⁷ converting the surrogate GeR_3H to GeR_2H_2 (R = cyclohexa-1,4-diene) employing $\text{B}(\text{C}_6\text{F}_5)_3$, may also be an example of similar autocatalytic chemistry. Furthermore, the current work shows that cationic autocatalytic processes are not limited to examples in biochemistry⁷⁸ and polymerization,⁷⁹ but are more widespread than had been realized earlier.

However, there is a deeper realization inherent in the findings reported here. This pertains to the exciting and rapidly developing field of Lewis acid-mediated metal-free catalytic

processes. It becomes clear that there are several recently reported chemical transformations^{70–76} where the real mechanism may be significantly different from what is believed, with the $\text{B}(\text{C}_6\text{F}_5)_3$ possibly acting more as the initiator and not the catalyst in these cases. The current work provides a simple means of determining computationally when $\text{B}(\text{C}_6\text{F}_5)_3$ is the former and when it is the latter: by a calculation of the ease of separation of the cation A^+ and anion $[\text{HB}(\text{C}_6\text{F}_5)_3]^-$ from the $[\text{A}]^+[\text{HB}(\text{C}_6\text{F}_5)_3]^-$ ion-pair. In all the cases where A^+ can separate easily, it is possible that alternative mechanisms would become dominant in the reaction medium. The findings are therefore also likely to provide considerable guidance to experimentalists working in this important area of research. For instance, for cases where the real role of $\text{B}(\text{C}_6\text{F}_5)_3$ is to act more as an initiator, it should be possible to substitute it with another Lewis acid, without loss of efficiency in the system. Furthermore, if it is the cationic species, created during the reaction of the precatalyst with $\text{B}(\text{C}_6\text{F}_5)_3$, that is the actual catalyst, then attention can also be focused on investigating means of modifying the precatalyst so that the catalytic process can be made more efficient for analogous systems. Therefore, the current findings represent an important advance in metal-free Lewis acid chemistry.

■ ASSOCIATED CONTENT

S Supporting Information

The Supporting Information is available free of charge on the ACS Publications website at DOI: 10.1021/acscatal.7b04489.

Free energy profiles, schemes for previously proposed and currently proposed mechanisms for different, experimentally studied cases, the formation of different favorable and unfavorable ion-pairs, and the XYZ coordinates of the optimized structures discussed (PDF)

■ AUTHOR INFORMATION

Corresponding Author

*E-mail: k.vanka@ncl.res.in.

ORCID

Kumar Vanka: 0000-0001-7301-7573

Notes

The authors declare no competing financial interest.

■ ACKNOWLEDGMENTS

The authors acknowledge the Centre of Excellence in Scientific Computing (COESC), NCL, Pune, for providing computational facilities. K.V. is grateful to the Department of Science and Technology (DST) (EMR/2014/000013) for providing financial assistance. The authors also acknowledge the Multi-Scale Simulation and Modeling (MSM) project (CSC0129) for providing financial assistance. The authors acknowledge Professor Sebastian Kozuch for helpful discussions with regard to turnover frequency calculations. The authors also acknowledge the comments of the reviewers, which have helped improve the manuscript.

■ REFERENCES

- (1) Oestreich, M.; Hermeke, J.; Mohr, J. A unified survey of Si–H and H–H bond activation catalysed by electron-deficient boranes. *Chem. Soc. Rev.* **2015**, *44*, 2202–2220.
- (2) Massey, A. G.; Park, A. J.; Stone, F. G. A. Tris(pentafluorophenyl)boron. *J. Am. Chem. Soc.* **1963**, *85*, 2021. (b) Massey, A. G.; Park, A. J. Perfluorophenyl derivatives of the elements. I. Tris(pentafluorophenyl)boron. *J. Organomet. Chem.* **1964**, *2*, 245–250. (c) Massey, A. G.; Park, A. J. Perfluorophenyl derivatives of the elements. VII. Further studies on tris(pentafluorophenyl)boron. *J. Organomet. Chem.* **1966**, *5*, 218–225. (d) Piers, W. E.; Chivers, T. Pentafluorophenylboranes: from obscurity to applications. *Chem. Soc. Rev.* **1997**, *26*, 345–354. (e) Jacobsen, H.; Berke, H.; Döring, S.; Kehr, G.; Erker, G.; Fröhlich, R.; Meyer, O. Lewis Acid Properties of Tris(pentafluorophenyl)borane. Structure and Bonding in L–B(C₆F₅)₃ Complexes. *Organometallics* **1999**, *18*, 1724–1735. (f) Piers, W. E. The Chemistry of Perfluoroaryl Boranes. *Adv. Organomet. Chem.* **2004**, *52*, 1–76. (g) Erker, G. Tris(pentafluorophenyl)borane: a special boron Lewis acid for special reactions. *Dalton Trans.* **2005**, 1883–1890. (h) Piers, W. E.; Marwitz, A. J. V.; Mercier, L. G. Mechanistic Aspects of Bond Activation with Perfluoroarylboranes. *Inorg. Chem.* **2011**, *50*, 12252–12262.
- (3) (a) Rokob, T. A.; Hamza, A.; Stirling, A.; Pápai, I. On the Mechanism of B(C₆F₅)₃-Catalyzed Direct Hydrogenation of Imines: Inherent and Thermally Induced Frustration. *J. Am. Chem. Soc.* **2009**, *131*, 2029–2036. (b) Mahdi, T.; Heiden, Z. M.; Grimme, S.; Stephan, D. W. Metal-Free Aromatic Hydrogenation: Aniline to Cyclohexylamine Derivatives. *J. Am. Chem. Soc.* **2012**, *134*, 4088–4091. (c) Zaher, H.; Ashley, A. E.; Irwin, M.; Thompson, A. L.; Gutmann, M. J.; Krämer, T.; O'Hare, D. Structural and theoretical studies of intermolecular dihydrogen bonding in [(C₆F₅)₂(C₆Cl₅)B]–H...H–[TMP]. *Chem. Commun.* **2013**, *49*, 9755–9757. (d) Mahdi, T.;

Stephan, D. W. Enabling Catalytic Ketone Hydrogenation by Frustrated Lewis Pairs. *J. Am. Chem. Soc.* **2014**, *136*, 15809–15812. (e) Scott, D. J.; Fuchter, M. J.; Ashley, A. E. Nonmetal Catalyzed Hydrogenation of Carbonyl Compounds. *J. Am. Chem. Soc.* **2014**, *136*, 15813–15816.

(4) (a) Harrison, D. J.; McDonald, R.; Rosenberg, L. Borane-Catalyzed Hydrosilylation of Thiobenzophenone: A New Route to Silicon–Sulfur Bond Formation. *Organometallics* **2005**, *24*, 1398–1400. (b) Nyhlén, J.; Privalov, T. On the possibility of catalytic reduction of carbonyl moieties with tris(pentafluorophenyl)borane and H₂: a computational study. *Dalton Trans.* **2009**, 5780–5786. (c) Hounjet, L. J.; Bannwarth, C.; Garon, C. N.; Caputo, C. B.; Grimme, S.; Stephan, D. W. Combinations of Ethers and B(C₆F₅)₃ Function as Hydrogenation Catalysts. *Angew. Chem., Int. Ed.* **2013**, *52*, 7492–7495.

(5) For further examples of hydrosilylation of imines catalyzed by electron-deficient boranes: (a) Hog, D. T.; Oestreich, M. B(C₆F₅)₃-Catalyzed Reduction of Ketones and Imines Using Silicon-Stereogenic Silanes: Stereoinduction by Single-Point Binding. *Eur. J. Org. Chem.* **2009**, 5047–5056. (b) Chen, D.; Leich, V.; Pan, F.; Klankermayer, J. Enantioselective Hydrosilylation with Chiral Frustrated Lewis Pairs. *Chem. - Eur. J.* **2012**, *18*, 5184–5187. (c) Zhu, X.; Du, H. A chiral borane catalyzed asymmetric hydrosilylation of imines. *Org. Biomol. Chem.* **2015**, *13*, 1013–1016.

(6) (a) Chase, P. A.; Jurca, T.; Stephan, D. W. Lewis acid-catalyzed hydrogenation: B(C₆F₅)₃-mediated reduction of imines and nitriles with H₂. *Chem. Commun.* **2008**, 1701–1703. (b) Chen, D.; Klankermayer, J. Metal free catalytic hydrogenation of imines with tris(perfluorophenyl)borane. *Chem. Commun.* **2008**, 2130–2131.

(7) Hermeke, J.; Mewald, M.; Oestreich, M. Experimental Analysis of the Catalytic Cycle of the Borane-Promoted Imine Reduction with Hydrosilanes: Spectroscopic Detection of Unexpected Intermediates and a Refined Mechanism. *J. Am. Chem. Soc.* **2013**, *135*, 17537–17546.

(8) (a) Mack, D. J.; Guo, B.; Njardarson, J. T. Synthesis of allylic and homoallylic alcohols from unsaturated cyclic ethers using a mild and selective C–O reduction approach. *Chem. Commun.* **2012**, *48*, 7844–7846. (e) Feghali, E.; Cantat, T. Unprecedented organocatalytic reduction of lignin model compounds to phenols and primary alcohols using hydrosilanes. *Chem. Commun.* **2014**, *50*, 862–865. (f) Mohr, J.; Oestreich, M. B(C₆F₅)₃-Catalyzed Hydrogenation of Oxime Ethers without Cleavage of the N–O Bond. *Angew. Chem., Int. Ed.* **2014**, *53*, 13278–13281. (g) Hounjet, L. J.; Bannwarth, C.; Garon, C. N.; Caputo, C. B.; Grimme, S.; Stephan, D. W. Combinations of Ethers and B(C₆F₅)₃ Function as Hydrogenation Catalysts. *Angew. Chem., Int. Ed.* **2013**, *52*, 7492–7495.

(9) Denis, J. M.; Forintos, H.; Szelke, H.; Keglevich, G. B(C₆F₅)₃-catalyzed silylation versus reduction of phosphonic and phosphinic esters with hydrosilanes. *Tetrahedron Lett.* **2002**, *43*, 5569–5571.

(10) Caputo, C. B.; Stephan, D. W. Activation of Alkyl C–F Bonds by B(C₆F₅)₃: Stoichiometric and Catalytic Transformations. *Organometallics* **2012**, *31*, 27–30.

(11) (a) Shchepin, R.; Xu, C.; Dussault, P. B(C₆F₅)₃-Promoted Tandem Silylation and Intramolecular Hydrosilylation: Diastereoselective Synthesis of Oxasilinanes and Oxasilepanes. *Org. Lett.* **2010**, *12*, 4772–4775. (b) Strašák, T.; Sýkora, J.; Lamač, M.; Kubišta, J.; Horáček, M.; Gyepes, R.; Pinkas, J. Reactivity of a Titanocene Pendant Si–H Group toward Alcohols. Unexpected Formation of Siloxanes from the Reaction of Hydrosilanes and Ph₃COH Catalyzed by B(C₆F₅)₃. *Organometallics* **2013**, *32*, 4122–4129. (c) Simonneau, A.; Friebe, J.; Oestreich, M. Salt-Free Preparation of Trimethylsilyl Ethers by B(C₆F₅)₃-Catalyzed Transfer Silylation by Using a Me₃SiH Surrogate. *Eur. J. Org. Chem.* **2014**, *10*, 2077–2083.

(12) (a) Zhou, D.; Kawakami, Y. Tris(pentafluorophenyl)borane as a Superior Catalyst in the Synthesis of Optically Active SiO-Containing Polymers. *Macromolecules* **2005**, *38*, 6902–6908. (b) Zhang, Z.; Lyons, L. J.; Jin, J. J.; Amine, K.; West, R. Synthesis and Ionic Conductivity of Cyclosiloxanes with Ethyleneoxy-Containing Substituents. *Chem. Mater.* **2005**, *17*, 5646–5650. (c) Hoque, M. A.; Kakihana, Y.; Shinke, S.; Kawakami, Y. Polysiloxanes with Periodically Distributed

Isomeric Double-Decker Silsesquioxane in the Main Chain. *Macromolecules* **2009**, *42*, 3309–3315. (d) Moitra, N.; Ichii, S.; Kamei, T.; Kanamori, K.; Zhu, Y.; Takeda, K.; Nakanishi, K.; Shimada, T. Surface Functionalization of Silica by Si–H Activation of Hydrosilanes. *J. Am. Chem. Soc.* **2014**, *136*, 11570–11573.

(13) Curlless, L. D.; Ingleson, M. J. $B(C_6F_5)_3$ -Catalyzed Synthesis of Benzofused-Siloles. *Organometallics* **2014**, *33*, 7241–7246.

(14) (a) Pérez, M.; Hounjet, L. J.; Caputo, C. B.; Dobrovetsky, R.; Stephan, D. W. Olefin Isomerization and Hydrosilylation Catalysis by Lewis Acidic Organofluorophosphonium Salts. *J. Am. Chem. Soc.* **2013**, *135*, 18308–18310. (b) Holthausen, M. H.; Mehta, M.; Stephan, D. W. The Highly Lewis Acidic Dicationic Phosphonium Salt: $[(SIMES)-PFPh_2][B(C_6F_5)_4]_2$. *Angew. Chem., Int. Ed.* **2014**, *53*, 6538–6541.

(15) (a) Welch, G. C.; Stephan, D. W. Facile Heterolytic Cleavage of Dihydrogen by Phosphines and Boranes. *J. Am. Chem. Soc.* **2007**, *129*, 1880–1881. (b) Sumerin, V.; Schulz, F.; Nieger, M.; Leskelä, M.; Repo, T.; Rieger, B. Facile Heterolytic H_2 Activation by Amines and $B(C_6F_5)_3$. *Angew. Chem., Int. Ed.* **2008**, *47*, 6001–6003. (c) Marwitz, A. J. V.; Dutton, J. L.; Mercier, L. G.; Piers, W. E. Dihydrogen Activation with $tBu_3P/B(C_6F_5)_3$: A Chemically Competent Indirect Mechanism via in Situ-Generated $p-tBu_2P-C_6F_4-B(C_6F_5)_2$. *J. Am. Chem. Soc.* **2011**, *133*, 10026–10029. (d) Lindqvist, M.; Sarnela, N.; Sumerin, V.; Chernichenko, K.; Leskelä, M.; Repo, T. Heterolytic dihydrogen activation by $B(C_6F_5)_3$ and carbonyl compounds. *Dalton Trans.* **2012**, *41*, 4310–4312. (e) Zeonjuk, L. L.; Vankova, N.; Mavrandonakis, A.; Heine, T.; Röschenhaler, G. V.; Eicher, J. On the Mechanism of Hydrogen Activation by Frustrated Lewis Pairs. *Chem. - Eur. J.* **2013**, *19*, 17413–17424.

(16) Adduci, L. L.; McLaughlin, M. P.; Bender, T. A.; Becker, J. J.; Gagné, M. R. Metal-Free Deoxygenation of Carbohydrates. *Angew. Chem., Int. Ed.* **2014**, *53*, 1646–1649. (b) Zhang, Z. Y.; Liu, Z. Y.; Guo, R. T.; Zhao, Y. Q.; Li, X.; Wang, X. C. $B(C_6F_5)_3$ -Catalyzed Ring Opening and Isomerization of Unactivated Cyclopropanes. *Angew. Chem., Int. Ed.* **2017**, *56*, 4028–4032.

(17) Schwier, T.; Gevorgyan, V. *Trans*- and *Cis*-Selective Lewis Acid Catalyzed Hydrogermylation of Alkynes. *Org. Lett.* **2005**, *7*, 5191–5194.

(18) (a) Fasano, V.; Radcliffe, J. E.; Ingleson, M. J. $B(C_6F_5)_3$ -Catalyzed Reductive Amination using Hydrosilanes. *ACS Catal.* **2016**, *6*, 1793–1798. (b) Gandhamsetty, N.; Joung, S.; Park, S. W.; Park, S.; Chang, S. Boron-Catalyzed Silylative Reduction of Quinolines: Selective sp^3 C–Si Bond Formation. *J. Am. Chem. Soc.* **2014**, *136*, 16780–16783.

(19) Schwier, T.; Rubin, M.; Gevorgyan, V. $B(C_6F_5)_3$ -Catalyzed Allylation of Propargyl Acetates with Allylsilanes. *Org. Lett.* **2004**, *6*, 1999–2001.

(20) Chatterjee, I.; Qu, Z. W.; Grimme, S.; Oestreich, M. $B(C_6F_5)_3$ -Catalyzed Transfer of Dihydrogen from One Unsaturated Hydrocarbon to Another. *Angew. Chem., Int. Ed.* **2015**, *54*, 12158–12162.

(21) For a review of transfer hydrosilylation, see: (a) Oestreich, M. Transfer Hydrosilylation. *Angew. Chem., Int. Ed.* **2016**, *55*, 494–499. (b) Simonneau, A.; Friebe, J.; Oestreich, M. Salt-Free Preparation of Trimethylsilyl Ethers by $B(C_6F_5)_3$ -Catalyzed Transfer Silylation by Using a Me_3SiH Surrogate. *Eur. J. Org. Chem.* **2014**, *2014*, 2077–2083.

(22) Keess, S.; Oestreich, M. Cyclohexa-1,4-dienes in transition-metal-free ionic transfer processes. *Chem. Sci.* **2017**, *8*, 4688–4695.

(23) (a) Timoshkin, A. Y.; Frenking, G. Gas-Phase Lewis Acidity of Perfluoroaryl Derivatives of Group 13 Elements. *Organometallics* **2008**, *27*, 371–380. (b) Kim, H. W.; Rhee, Y. M. Dispersion-Oriented Soft Interaction in a Frustrated Lewis Pair and the Entropic Encouragement Effect in its Formation. *Chem. - Eur. J.* **2009**, *15*, 13348–13355. (c) Durfey, B. L.; Gilbert, T. M. Computational Studies of Lewis Acidities of Tris(fluorophenyl)-Substituted Boranes: An Additive Relationship between Lewis Acidity and Fluorine Position. *Inorg. Chem.* **2011**, *50*, 7871–7879. (d) Mück, L. A.; Timoshkin, A. Y.; Frenking, G. Design of Neutral Lewis Superacids of Group 13 Elements. *Inorg. Chem.* **2012**, *51*, 640–646.

(24) (a) Fujimoto, H.; Sakata, K. Quantum Chemical Study of Lewis Acid Catalyzed Allylboration of Aldehydes. *J. Am. Chem. Soc.* **2008**,

130, 12519–12526. (b) Fujimoto, H.; Sakata, K. Quantum Chemical Study of Diels–Alder Reactions Catalyzed by Lewis Acid Activated Oxazaborolidines. *J. Org. Chem.* **2013**, *78*, 3095–3103. (c) Fujimoto, H.; Sakata, K. Quantum Chemical Study of the Reaction of 3-(Trimethylsilyl)cyclohexa-1,4-dienes with $B(C_6F_5)_3$. *Organometallics* **2015**, *34*, 236–241.

(25) (a) Chen, Y. X. E.; Marks, T. J. Cocatalysts for Metal-Catalyzed Olefin Polymerization: Activators, Activation Processes, and Structure–Activity Relationships. *Chem. Rev.* **2000**, *100*, 1391–1434. (b) Delferro, M.; Marks, T. J. Multinuclear Olefin Polymerization Catalysts. *Chem. Rev.* **2011**, *111*, 2450–2485. (c) Duchateau, R. Incompletely Condensed Silsesquioxanes: Versatile Tools in Developing Silica-Supported Olefin Polymerization Catalyst. *Chem. Rev.* **2002**, *102*, 3525–3542. (d) Aoshima, S.; Kanaoka, S. A Renaissance in Living Cationic Polymerization. *Chem. Rev.* **2009**, *109*, 5245–5287.

(26) Yin, Q.; Klare, H. F. T.; Oestreich, M. Catalytic Friedel–Crafts C–H Borylation of Electron-Rich Arenes: Dramatic Rate Acceleration by Added Alkenes. *Angew. Chem., Int. Ed.* **2017**, *56*, 3712–3717.

(27) Simonneau, A.; Oestreich, M. Formal SiH_4 chemistry using stable and easy-to-handle surrogates. *Nat. Chem.* **2015**, *7*, 816–822.

(28) Simonneau, A.; Oestreich, M. PCT International Patent Application WO 2015036309 A1, March 19, 2015.

(29) (a) DHHS. *NIOSH Pocket Guide to Chemical Hazards 279*; Department of Health and Human Services, U.S. Government Printing Office, 2007. (b) Chen, J. R. Characteristics of fire and explosion in semiconductor fabrication processes. *Process Saf. Prog.* **2002**, *21*, 19–25. (c) Wu, C. C.; Lee, Y. C.; Kuan, C. M.; Shen, C. C.; Hu, S. C.; Pan, H. R.; Chen, S. K.; Tsai, H. Y.; Chen, J. R. Analysis of a silane explosion in a photovoltaic fabrication plant. *Process Saf. Prog.* **2006**, *25*, 237–244. (d) Chang, Y. Y.; Peng, D. J.; Wu, H. C.; Tsaor, C. C.; Shen, C. C.; Tsai, H. Y.; Chen, J. R. Revisiting of a silane explosion in a photovoltaic fabrication plant. *Process Saf. Prog.* **2007**, *26*, 155–158.

(30) (a) Matsumura, H. Formation of Silicon-Based Thin Films Prepared by Catalytic Chemical Vapor Deposition (Cat-CVD) Method. *Jpn. J. Appl. Phys.* **1998**, *37*, 3175–3187. (b) Roca i Cabarrocas, P. Plasma enhanced chemical vapor deposition of silicon thin films for large area electronics. *Curr. Opin. Solid State Mater. Sci.* **2002**, *6*, 439–444. (c) Schmidt, V.; Wittemann, J. V.; Senz, S.; Gosele, U. Silicon nanowires. A review on aspects of their growth and their electrical properties. *Adv. Mater.* **2009**, *21*, 2681–2702. (d) Schmidt, V.; Wittemann, J. V.; Gosele, U. Growth, thermodynamics, and electrical properties of silicon nanowires. *Chem. Rev.* **2010**, *110*, 361–388.

(31) (a) Ojima, I.; Patai, S.; Rappoport, Z. *The Chemistry of Organic Silicon Compounds*; Wiley: New York, 1989; pp 1687–1792. (b) Marciniak, B. *Hydrosilylation: A Comprehensive Review on Recent Advances*; Pergamon: New York, 1992; pp 1–407.

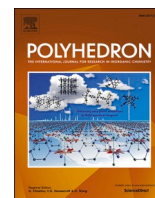
(32) (a) Simonneau, A.; Oestreich, M. 3-Silylated Cyclohexa-1,4-dienes as Precursors for Gaseous Hydrosilanes: The $B(C_6F_5)_3$ -Catalyzed Transfer Hydrosilylation of Alkenes. *Angew. Chem., Int. Ed.* **2013**, *52*, 11905–11907. (b) Keess, S.; Simonneau, A.; Oestreich, M. Direct and Transfer Hydrosilylation Reactions Catalyzed by Fully or Partially Fluorinated Triarylboranes: A Systematic Study. *Organometallics* **2015**, *34*, 790–799.

(33) Rubin, M.; Schwier, T.; Gevorgyan, V. Highly Efficient $B(C_6F_5)_3$ -Catalyzed Hydrosilylation of Olefins. *J. Org. Chem.* **2002**, *67*, 1936–1940.

(34) (a) Blackwell, J. M.; Foster, K. L.; Beck, V. H.; Piers, W. E. $B(C_6F_5)_3$ -Catalyzed Silylation of Alcohols: A Mild, General Method for Synthesis of Silyl Ethers. *J. Org. Chem.* **1999**, *64*, 4887–4892. (b) Gevorgyan, V.; Liu, J. X.; Rubin, M.; Benson, S.; Yamamoto, Y. A novel reduction of alcohols and ethers with a $HSiEt_3$ /catalytic $B(C_6F_5)_3$ system. *Tetrahedron Lett.* **1999**, *40*, 8919–8922. (c) Gevorgyan, V.; Rubin, M.; Benson, S.; Liu, J. X.; Yamamoto, Y. A Novel $B(C_6F_5)_3$ -Catalyzed Reduction of Alcohols and Cleavage of Aryl and Alkyl Ethers with Hydrosilanes. *J. Org. Chem.* **2000**, *65*, 6179–6186. (d) Gevorgyan, V.; Rubin, M.; Liu, J.-X.; Yamamoto, Y. A Direct Reduction of Aliphatic Aldehyde, Acyl Chloride, Ester, and Carboxylic Functions into a Methyl Group. *J. Org. Chem.* **2001**, *66*, 1672–1675.

- (e) Rubin, M.; Gevorgyan, V. $B(C_6F_5)_3$ -Catalyzed Allylation of Secondary Benzyl Acetates with Allylsilanes. *Org. Lett.* **2001**, *3*, 2705–2707. (f) Chojnowski, J.; Rubinsztajn, S.; Cella, J. A.; Fortuniak, W.; Cypriak, M.; Kurjata, J.; Kaźmierski, K. Mechanism of the $B(C_6F_5)_3$ -Catalyzed Reaction of Silyl Hydrides with Alkoxy-silanes. Kinetic and Spectroscopic Studies. *Organometallics* **2005**, *24*, 6077–6084. (g) Hazra, C. K.; Gandhamsetty, N.; Park, S.; Chang, S. Borane catalyzed ring opening and closing cascades of furans leading to silicon functionalized synthetic intermediates. *Nat. Commun.* **2016**, *7*, 13431.
- (35) (a) Lapkin, I. I.; Povarnitsyna, T. N.; Anvarova, G. Y. Organosilicon compounds. IV. Reaction of triethylsilane with α -chlorinated ethers and aldehydes. *Zh. Obshch. Khim.* **1965**, *35*, 1835–1839. (b) Calas, R. Reactivity of silicon-hydrogen silanes in organic chemistry. *Pure Appl. Chem.* **1966**, *13*, 61–79. (c) Lapkin, I. I.; Povarnitsyna, T. N. Organosilicon compounds. V. Mechanism of the reactions of trialkylsilanes with aldehydes and esters. *Zh. Obshch. Khim.* **1968**, *38*, 643–647. (d) Doyle, M. P.; West, C. T.; Donnelly, S. J.; McOsker, C. C. Silane reductions in acidic media: VIII. Boron trifluoride catalyzed organosilane reductions. selectivity and mechanism. *J. Organomet. Chem.* **1976**, *117*, 129–140. (e) Fry, J. L.; Orfanopoulos, M.; Adlington, M. G.; Dittman, W. R., Jr.; Silverman, S. B. Reduction of aldehydes and ketones to alcohols and hydrocarbons through use of the organosilane-boron trifluoride system. *J. Org. Chem.* **1978**, *43*, 374–375. (f) Parks, D. J.; Piers, W. E. Tris-(pentafluorophenyl)boron-Catalyzed Hydrosilylation of Aromatic Aldehydes, Ketones, and Esters. *J. Am. Chem. Soc.* **1996**, *118*, 9440–9441. (g) Parks, D. J.; Blackwell, J. M.; Piers, W. E. Studies on the Mechanism of $B(C_6F_5)_3$ -Catalyzed Hydrosilylation of Carbonyl Functions. *J. Org. Chem.* **2000**, *65*, 3090–3098. (h) Rendler, S.; Oestreich, M. Conclusive Evidence for an S_N2 -Si Mechanism in the $B(C_6F_5)_3$ -Catalyzed Hydrosilylation of Carbonyl Compounds: Implications for the Related Hydrogenation. *Angew. Chem., Int. Ed.* **2008**, *47*, 5997–6000. (i) Fujimoto, H.; Sakata, K. Quantum Chemical Study of $B(C_6F_5)_3$ -Catalyzed Hydrosilylation of Carbonyl Group. *J. Org. Chem.* **2013**, *78*, 12505–12512.
- (36) Ioana, S. *Mechanism of Autocatalytic Reactions*; Lap Lambert Academic Publishing GmbH & Company KG, 2014; pp 1–64.
- (37) Chatterjee, I.; Oestreich, M. Brønsted Acid-Catalyzed Transfer Hydrogenation of Imines and Alkenes Using Cyclohexa-1,4-dienes as Dihydrogen Surrogates. *Org. Lett.* **2016**, *18*, 2463–2466.
- (38) Lefranc, I.; Qu, Z.-W.; Grimme, S.; Oestreich, M. Hydrogenation and Transfer Hydrogenation Promoted by Tethered Ru–S Complexes: From Cooperative Dihydrogen Activation to Hydride Abstraction/Proton Release from Dihydrogen Surrogates. *Chem. - Eur. J.* **2016**, *22*, 10009–10016.
- (39) (a) Hohenberg, P.; Kohn, W. Inhomogeneous Electron Gas. *Phys. Rev.* **1964**, *136*, B864–B871. (b) Kohn, W.; Sham, L. J. Self-Consistent Equations Including Exchange and Correlation Effects. *Phys. Rev.* **1965**, *140*, A1133–A1138.
- (40) (a) Zhao, Y.; Truhlar, D. G. The M06 suite of density functionals for main group thermochemistry, thermochemical kinetics, noncovalent interactions, excited states, and transition elements: two new functionals and systematic testing of four M06-class functionals and 12 other functionals. *Theor. Chem. Acc.* **2008**, *120*, 215–241. (b) Zhao, Y.; Truhlar, D. G. Density Functionals with Broad Applicability in Chemistry. *Acc. Chem. Res.* **2008**, *41*, 157–167.
- (41) TURBOMOLE V7.0, 2015; University of Karlsruhe and Forschungszentrum Karlsruhe GmbH, 1989–2007; TURBOMOLE GmbH, since 2007; <http://www.turbomole.com>.
- (42) Schafer, A.; Huber, C.; Ahlrichs, R. Fully optimized contracted Gaussian basis sets of triple zeta valence quality for atoms Li to Kr. *J. Chem. Phys.* **1994**, *100*, 5829–5835.
- (43) Perdew, J. P.; Burke, K.; Ernzerhof, M. Generalized Gradient Approximation Made Simple. *Phys. Rev. Lett.* **1996**, *77*, 3865–3868.
- (44) (a) Grimme, S.; Antony, J.; Ehrlich, S.; Krieg, H. A consistent and accurate *ab initio* parametrization of density functional dispersion correction (DFT-D) for the 94 elements H–Pu. *J. Chem. Phys.* **2010**, *132*, 154104. (b) Grimme, S.; Ehrlich, S.; Goerigk, L. Effect of the damping function in dispersion corrected density functional theory. *J. Comput. Chem.* **2011**, *32*, 1456–1465.
- (45) Klamt, A.; Schuurmann, G. COSMO: a new approach to dielectric screening in solvents with explicit expressions for the screening energy and its gradient. *J. Chem. Soc., Perkin Trans. 2* **1993**, 799–805.
- (46) (a) Eichkorn, K.; Treutler, O.; Öhm, H.; Häser, M.; Ahlrichs, R. Auxiliary basis sets to approximate Coulomb potentials. *Chem. Phys. Lett.* **1995**, *240*, 283–290. (b) Eichkorn, K.; Weigend, F.; Treutler, O.; Ahlrichs, R. Auxiliary basis sets for main row atoms and transition metals and their use to approximate Coulomb potentials. *Theor. Chem. Acc.* **1997**, *97*, 119–124.
- (47) (a) Sierka, M.; Hoge-kamp, A.; Ahlrichs, R. Fast evaluation of the Coulomb potential for electron densities using multipole accelerated resolution of identity approximation. *J. Chem. Phys.* **2003**, *118*, 9136–9148. (b) Deglmann, P.; May, K.; Furche, F.; Ahlrichs, R. Nuclear second analytical derivative calculations using auxiliary basis set expansions. *Chem. Phys. Lett.* **2004**, *384*, 103–107.
- (48) Tao, J.; Perdew, J. P.; Staroverov, V. N.; Scuseria, G. E. Climbing the Density Functional Ladder: Nonempirical Meta-Generalized Gradient Approximation Designed for Molecules and Solids. *Phys. Rev. Lett.* **2003**, *91*, 146401.
- (49) (a) Weigend, F.; Häser, M.; Patzelt, H.; Ahlrichs, R. RI-MP2: optimized auxiliary basis sets and demonstration of efficiency. *Chem. Phys. Lett.* **1998**, *294*, 143–152. (b) Weigend, F.; Ahlrichs, R. Balanced basis sets of split valence, triple zeta valence and quadruple zeta valence quality for H to Rn: Design and assessment of accuracy. *Phys. Chem. Chem. Phys.* **2005**, *7*, 3297–3305.
- (50) Zhao, Y.; Truhlar, D. G. Design of Density Functionals That Are Broadly Accurate for Thermochemistry, Thermochemical Kinetics, and Nonbonded Interactions. *J. Phys. Chem. A* **2005**, *109*, 5656–5667.
- (51) Weigend, F.; Furche, F.; Ahlrichs, R. Gaussian basis sets of quadruple zeta valence quality for atoms H–Kr. *J. Chem. Phys.* **2003**, *119*, 12753–12762.
- (52) Fukui, K. The path of chemical reactions - the IRC approach. *Acc. Chem. Res.* **1981**, *14*, 363–368.
- (53) Mammen, M.; Shakhnovich, E. I.; Deutch, J. M.; Whitesides, G. M. Estimating the Entropic Cost of Self-Assembly of Multiparticle Hydrogen-Bonded Aggregates Based on the Cyanuric Acid-Melamine Lattice. *J. Org. Chem.* **1998**, *63*, 3821–3830.
- (54) Frisch, M. J.; Trucks, G. W.; Schlegel, H. B.; Scuseria, G. E.; Robb, M. A.; Cheeseman, J. R.; Scalmani, G.; Barone, V.; Mennucci, B.; Petersson, G. A.; Nakatsuji, H.; Caricato, M.; Li, X.; Hratchian, H. P.; Izmaylov, A. F.; Bloino, J.; Zheng, G.; Sonnenberg, J. L.; Hada, M.; Ehara, M.; Toyota, K.; Fukuda, R.; Hasegawa, J.; Ishida, M.; Nakajima, T.; Honda, Y.; Kitao, O.; Nakai, H.; Vreven, T.; Montgomery, J. A., Jr.; Peralta, J. E.; Ogliaro, F.; Bearpark, M.; Heyd, J. J.; Brothers, E.; Kudin, K. N.; Staroverov, V. N.; Kobayashi, R.; Normand, J.; Raghavachari, K.; Rendell, A.; Burant, J. C.; Iyengar, S. S.; Tomasi, J.; Cossi, M.; Rega, N.; Millam, J. M.; Klene, M.; Knox, J. E.; Cross, J. B.; Bakken, V.; Adamo, C.; Jaramillo, J.; Gomperts, R.; Stratmann, R. E.; Yazyev, O.; Austin, A. J.; Cammi, R.; Pomelli, C.; Ochterski, J. W.; Martin, R. L.; Morokuma, K.; Zakrzewski, V. G.; Voth, G. A.; Salvador, P.; Dannenberg, J. J.; Dapprich, S.; Daniels, A. D.; Farkas, Ö.; Foresman, J. B.; Ortiz, J. V.; Cioslowski, J.; Fox, D. J. *Gaussian 09*; Gaussian, Inc.: Wallingford, CT, 2009.
- (55) Binkley, J. S.; Pople, J. A.; Hehre, W. J. Self-consistent molecular orbital methods. 21. Small split-valence basis sets for first-row elements. *J. Am. Chem. Soc.* **1980**, *102*, 939–947.
- (56) Tomasi, J.; Mennucci, B.; Cammi, R. Quantum Mechanical Continuum Solvation Models. *Chem. Rev.* **2005**, *105*, 2999–3094.
- (57) Becke, A. D. Density-functional thermochemistry. III. The role of exact exchange. *J. Chem. Phys.* **1993**, *98*, 5648–5652.
- (58) (a) Kozuch, S.; Shaik, S. A Combined Kinetic–Quantum Mechanical Model for Assessment of Catalytic Cycles: Application to Cross-Coupling and Heck Reactions. *J. Am. Chem. Soc.* **2006**, *128*, 3355–3365. (b) Kozuch, S.; Shaik, S. Kinetic-Quantum Chemical Model for Catalytic Cycles: The Haber–Bosch Process and the Effect of Reagent Concentration. *J. Phys. Chem. A* **2008**, *112*, 6032–6041.

- (59) Uhe, A.; Kozuch, S.; Shaik, S. Automatic analysis of computed catalytic cycles. *J. Comput. Chem.* **2011**, *32*, 978–985.
- (60) Sakata, K.; Fujimoto, H. Quantum Chemical Study of the Reaction of 3-(Trimethylsilyl)cyclohexa-1,4-dienes with $B(C_6F_5)_3$. *Organometallics* **2015**, *34*, 236–241.
- (61) Webb, J. D.; Laberge, V. S.; Geier, S. J.; Stephan, D. W.; Crudden, C. M. Borohydrides from Organic Hydrides: Reactions of Hantzsch's Esters with $B(C_6F_5)_3$. *Chem. - Eur. J.* **2010**, *16*, 4895–4902.
- (62) Gutsulyak, D. V.; van der Est, A.; Nikonov, G. I. Facile Catalytic Hydrosilylation of Pyridines. *Angew. Chem., Int. Ed.* **2011**, *50*, 1384–1387.
- (63) For the crystal structure of the $Et_3Si(toluene)^+$ cation, see: (a) Lambert, J. B.; Zhao, Y. The Trimesitylsilylium Cation. *Angew. Chem., Int. Ed. Engl.* **1997**, *36*, 400–401. (b) Reed, C. A. The Silylium Ion Problem, R_3Si^+ . *Acc. Chem. Res.* **1998**, *31*, 325–332.
- (64) For theoretical studies of the σ complex: (a) Schleyer, P. v. R.; Buzek, P.; Müller, T.; Apeloig, Y.; Siehl, H. U. The Search for an Isolable Silyl Cation Must Continue. *Angew. Chem., Int. Ed. Engl.* **1993**, *32*, 1471–1473. (b) Olsson, L.; Cremer, D. Evidence for the existence of silylium cations in condensed phases. *Chem. Phys. Lett.* **1993**, *215*, 433–443. (c) Olah, G. A.; Rasul, G.; Li, X.-Y.; Buchholz, H. A.; Sandford, G.; Prakash, G. K. S.; Lambert, J. B. Triethylsilyl cations. *Science* **1994**, *263*, 983–984.
- (65) (a) Lambert, J. B.; Zhang, S.; Stern, C. L.; Huffman, J. C. Crystal Structure of a Silyl Cation with No Coordination to Anion and Distant Coordination to Solvent. *Science* **1993**, *260*, 1917–1918.
- (66) For the preparation of donor-stabilized silylium ions from cyclohexa-2,5-dien-1-yl-substituted silanes, see: Simonneau, A.; Biberger, T.; Oestreich, M. The Cyclohexadienyl-Leaving-Group Approach toward Donor-Stabilized Silylium Ions. *Organometallics* **2015**, *34*, 3927–3929.
- (67) As suggested by Prof. Sebastian Kozuch during discussions of the energy profiles shown in Figures 2 and 3.
- (68) Hehre, W. J.; Radom, L.; Schleyer, P. v. R.; Pople, J. A. *Ab Initio Molecular Orbital Theory*; Wiley: New York, 1986.
- (69) Heiden, Z. M.; Lathem, A. P. Establishing the Hydride Donor Abilities of Main Group Hydrides. *Organometallics* **2015**, *34*, 1818–1827.
- (70) (a) Houghton, A. Y.; Hurmalainen, J.; Mansikkamäki, A.; Piers, W. E.; Tuononen, H. M. Direct observation of a borane–silane complex involved in frustrated Lewis-pair-mediated hydrosilylations. *Nat. Chem.* **2014**, *6*, 983–988. (b) Houghton, A. Y.; Karttunen, V. A.; Piers, W. E.; Tuononen, H. M. Hydrogen activation with perfluorinated organoboranes: 1,2,3-tris(pentafluorophenyl)-4,5,6,7-tetrafluoro-1-boraindene. *Chem. Commun.* **2014**, *50*, 1295–1298.
- (71) Ma, Y.; Wang, B.; Zhang, L.; Hou, Z. Boron-Catalyzed Aromatic C–H Bond Silylation with Hydrosilanes. *J. Am. Chem. Soc.* **2016**, *138*, 3663–3666.
- (72) Kim, D. W.; Joung, S.; Kim, J. G.; Chang, S. Metal-Free Hydrosilylation Polymerization by Borane Catalyst. *Angew. Chem., Int. Ed.* **2015**, *54*, 14805–14809.
- (73) Farrell, J. M.; Heiden, Z. M.; Stephan, D. W. Metal-Free Transfer Hydrogenation Catalysis by $B(C_6F_5)_3$. *Organometallics* **2011**, *30*, 4497–4500.
- (74) Blackwell, J. M.; Sonmor, E. R.; Scoccitti, T.; Piers, W. E. $B(C_6F_5)_3$ -Catalyzed Hydrosilylation of Imines via Silyliminium Intermediates. *Org. Lett.* **2000**, *2*, 3921–3923.
- (75) Chatterjee, I.; Oestreich, M. $B(C_6F_5)_3$ -Catalyzed Transfer Hydrogenation of Imines and Related Heteroarenes Using Cyclohexa-1,4-dienes as a Dihydrogen Source. *Angew. Chem., Int. Ed.* **2015**, *54*, 1965–1968.
- (76) Geier, S. J.; Stephan, D. W. Lutidine/ $B(C_6F_5)_3$: At the Boundary of Classical and Frustrated Lewis Pair Reactivity. *J. Am. Chem. Soc.* **2009**, *131*, 3476–3477.
- (77) Keess, S.; Oestreich, M. Access to Fully Alkylated Germanes by $B(C_6F_5)_3$ -Catalyzed Transfer Hydrogermylation of Alkenes. *Org. Lett.* **2017**, *19*, 1898–1901.
- (78) (a) Kamioka, S.; Ajami, D.; Rebek, J., Jr. Synthetic autocatalysts show organocatalysis of other reactions. *Chem. Commun.* **2009**, 7324–7326. (b) Kamioka, S.; Ajami, D.; Rebek, J., Jr. Autocatalysis and organocatalysis with synthetic structures. *Proc. Natl. Acad. Sci. U. S. A.* **2010**, *107*, 541–544. (c) Brook, M. A.; Grande, J. B.; Ganachaud, F. New Synthetic Strategies for Structured Silicones Using $B(C_6F_5)_3$. *Adv. Polym. Sci.* **2010**, *235*, 161–183. (d) Bissette, A. J.; Fletcher, S. P. Mechanisms of Autocatalysis. *Angew. Chem., Int. Ed.* **2013**, *52*, 12800–12826. (e) Plasson, R.; Brandenburg, A.; Jullien, L.; Bersini, H. Autocatalyses. *J. Phys. Chem. A* **2011**, *115*, 8073–8085.
- (79) (a) Valente, A.; Mortreux, A.; Visseaux, M.; Zinck, P. Coordinative Chain Transfer Polymerization. *Chem. Rev.* **2013**, *113*, 3836–3857. (b) Starnes, W. H., Jr.; Ge, X. Mechanism of Autocatalysis in the Thermal Dehydrochlorination of Poly(vinyl chloride). *Macromolecules* **2004**, *37*, 352–359. (c) Thompson, D. B.; Brook, M. A. Rapid Assembly of Complex 3D Siloxane Architectures. *J. Am. Chem. Soc.* **2008**, *130*, 32–33. (d) Moitra, N.; Ichii, S.; Kamei, T.; Kanamori, K.; Zhu, Y.; Takeda, K.; Nakanishi, K.; Shimada, T. Surface Functionalization of Silica by Si–H Activation of Hydrosilanes. *J. Am. Chem. Soc.* **2014**, *136*, 11570–11573.



Computational insights into hydroboration with acyclic α -Borylamido-germylene and stannylene catalysts: Cooperative dual catalysis the key to system efficiency

Subhrashis Banerjee^{a,b}, Kumar Vanka^{a,b,*}

^a Academy of Scientific and Innovative Research (AcSIR), Ghaziabad 201002, India

^b Physical and Materials Chemistry Division, CSIR-National Chemical Laboratory, Dr. Homi Bhabha Road, Pashan, Pune 411 008, India

ARTICLE INFO

Keywords:

Main group chemistry
Computational chemistry
Germynes and stannylenes
Catalysis of hydroboration
New mechanism

ABSTRACT

The chemistry of low valent main group compounds has grown as an alternative to the chemistry of less abundant and less green transition metal complexes. It has been found that low valent compounds such as carbenes, silylenes, stannylenes and germynes are efficient for activating small molecules and for catalysis. However, the reaction mechanism and the factors that affect the rate of reaction are not completely understood. In this computational investigation with density functional theory (DFT), we investigate and demonstrate the efficiency of a new mechanism for the hydroboration of aldehydes by germynes and stannylenes, in the presence of the common hydroborating agent, pinacolborane, HBpin. This mechanism involves an HBpin molecule as an additional catalyst that cooperates with the germylene or stannylene catalyst to efficiently carry out the hydroboration. This mechanism is first demonstrated to work for experimentally reported systems, and then shown to be efficient for newly proposed germylene and stannylene systems. These new systems are α -Borylamido-germylene ((2,6-*i*Pr₂C₆H₃NBCy₂)₂Ge(II)) and α -Borylamido-stannylene((2,6-*i*Pr₂C₆H₃NBCy₂)₂Sn(II)). These new insights will help researchers look into low valent germylene and stannylene chemistry from a new perspective.

1. Introduction

In recent years, the chemistry of low valent main group compounds has become a topic of great interest in the field of catalysis, with main group based catalysts sometimes showing comparable or greater efficiency than transition metal catalysts [1-17]. The central atom of these complexes has a lone pair of electrons, as well as unoccupied orbitals, thereby rendering it capable of being both nucleophilic as well as electrophilic, leading to interesting chemical properties [18]. Generally, carbenes [19-25], silylenes [26-30], germynes [31-37], stannylene [38-41], and borylenes [42-48] have been employed. In these compounds, the central carbon, silicon, germanium or tin atom is stable in a lower oxidation state(II), than the usual (IV), while the boron atom is stable in the (I) oxidation state rather than in (III) (see Fig. 1). Moreover, low valent main group compounds also include compounds in zero oxidation states, such as carbenes [49,50], silylenes [51-61] and germynes [62-70]. The addition of bulky ligands prevent these low valent main group compounds from oligomerizing and polymerizing, thereby

allowing them to act as stable catalysts.

In addition to their catalytic abilities, discussed above, low valent carbenes have also emerged as essential synthetic intermediates for a wide range of organic transformations in recent years [19-25]. This has led to the synthesis of different metal carbene complexes to explore their potential applications in chemistry [26-48]. The pioneering work of Lappert in the 1970s led to the development of persistent group 14 tetrylenes compounds of the type EX₂ [71-75]. In contrast to carbenes, the ground electronic state of their heavier congeners X₂E (with E = Si, Ge and Sn) is usually a singlet state, which is characterised by a high energy lone pair (HOMO) and an energetically accessible vacant p-orbital (LUMO) [76]. But this is not always true for every case of tetrylenes. Triplet carbenes do not have lone pairs and for heavier congeners, the gap can vary substantially. This orbital configuration resembles transition metal frontier d-orbitals and contributes to the dual donor and acceptor character required for bond activation [77]. The reactivity of tetrylenes towards small molecules and strong bonds is largely determined by the nature of the many X substituents that govern

* Corresponding author.

E-mail address: k.vanka@ncl.res.in (K. Vanka).

<https://doi.org/10.1016/j.poly.2022.115907>

Received 31 January 2022; Accepted 11 May 2022

Available online 17 May 2022

0277-5387/© 2022 Elsevier Ltd. All rights reserved.

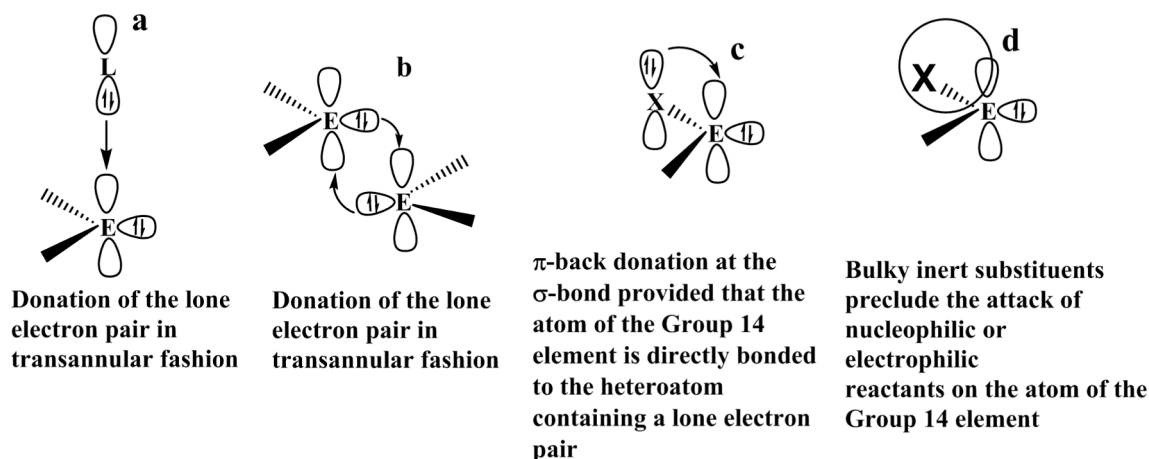


Fig. 1. The ability of low valent main group compounds to act as both electrophiles and nucleophiles.

Table 1

HOMO-LUMO energy gap by using the TDDFT approach for the X_2E type germylene catalyst. For the first three cases, the hydroboration reaction has been investigated experimentally and for the last case, the hydroboration reaction has been investigated computationally in this current work, with a designed catalyst system.

| Catalyst | ΔE (TDDFT) (First Excitation Energy) (ev) |
|---|---|
| 1. Zhao and coworkers germylene [138] | 1.92 |
| 2. Wesemann and coworkers germylene [139] | 2.15 |
| 3. Khan, Pati and coworkers germylene [140] | 2.88 |
| 4. Modeled germylene system in this work | 2.42 |

the energy of the frontier orbitals. Thus, many different substituents with varying steric and electronic properties have been employed to date to tune the ability of tetrylenes to engage in bond activation reactions [78-90]. In general, small HOMO-LUMO gaps lead to higher activity of tetrylenes towards small molecules, as has been demonstrated by Bertrand and coworkers, by means of the different behavior of *N*-heterocyclic carbenes (NHCs) compared to cyclic alkyl (amino) carbenes (CAACs) towards dihydrogen [21]. Two key factors influence this energy separation: the angle created by the substituents at the central group 14 element and the donor/acceptor properties of the substituents [91,92]. It has generally been observed that the acyclic tetrylenes are usually more reactive than their cyclic derivatives. Likewise, bulky groups are beneficial for small molecule activation, since they, too, increase the X-E-X angle. A wide range of substituents have been used for

electronic manipulation, notably for the heavier group 14 analogues of carbenes [83-90]. While amino groups are favoured substituents for stabilising tetrylenes due to their $-I$ and $+M$ donor characteristics, they frequently generate a substantial HOMO-LUMO separation. $-I$ and $+M$ indicate that the amino groups exhibit a negative inductive effect and a positive mesomeric effect respectively on the metal center associated with the group. More reactive species suitable for small molecule activation are thus generated with strongly σ -donating (that is, more electropositive) groups, which leave the empty p-orbital unpopulated. This lowers the energy of the LUMO and makes it available for interactions with the bonding orbitals of further substrates. Thus, besides alkyl moieties, silyl or, more lately, boryl groups have also been employed in this chemistry [83-89]. These bond activation mechanisms for group 14 tetrylenes have been studied in depth [93-95], with the silyl-substituted germylene and the boryl-functionalized silylene described by Aldridge [96] and coworkers serving as examples. Aside from single-site reactivity, E-H bond activation mechanisms have also been reported, including the active engagement of the α -substituent [97].

After the landmark discovery of the hydroboration reaction by H. C. Brown [98], organoboranes have been used extensively for different hydroboration reactions [99-103]. The hydroboration of C=O bonds has been significant, solidifying its reputation as one of the most beneficial and commonly utilised reactions in the pharmaceutical industry [104]. There are a lot of examples of carbonyl hydroboration catalysts, including alkaline earthmetals [105-113], transition metals [114-121], group 13 metal catalysts [13,122-124], lanthanides [125-129], actinides [130] and other unique and sophisticated systems [131-135]. It has always been challenging to develop cost effective and non-toxic p-block based catalysts for the catalytic hydroboration reactions. There are only a few reports on germylenes and stannylenes as catalysts for the

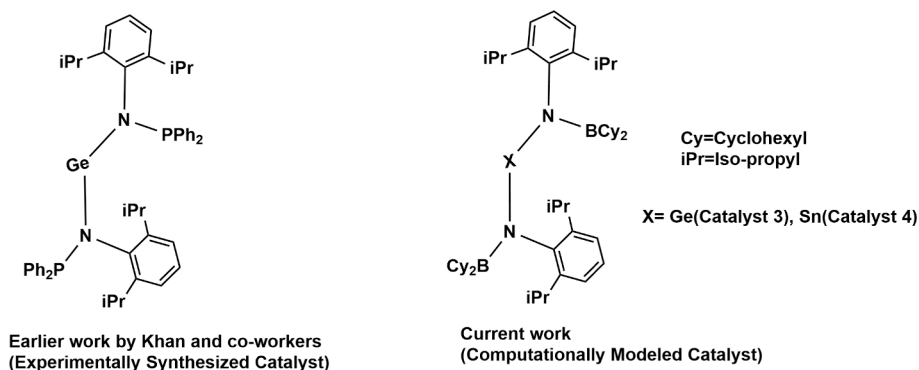


Fig. 2. An experimentally synthesized acyclic germanium based hydroboration catalyst [146] has been modified as shown above into newly proposed catalysts in the current work.

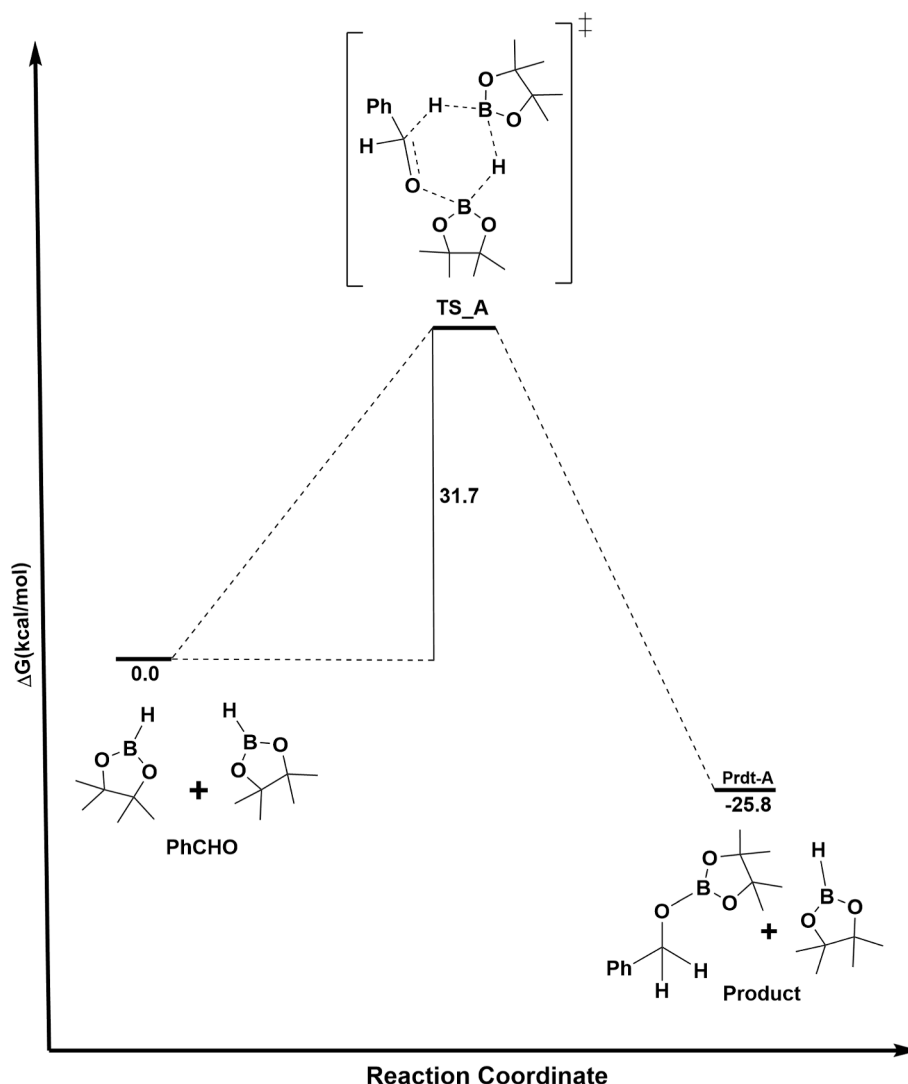


Fig. 3. The free energy profile for the catalytic aldehyde hydroboration passing through a six membered cyclic transition state without the involvement of any catalyst. The values (in kcal/mol) have been calculated at the PBE/TZVP level of theory.

hydroboration of unsaturated substrates, and the most noteworthy examples are the bulky amine substituted germylene hydrides and stannylene hydrides reported by Jones and coworkers [136]. Zhao and coworkers have investigated the hydroboration of aldehydes and ketones with the ylide type *N*-heterocyclic germylene reported by Driess and coworkers [137,138]. Later, Wesemann and coworkers reported the hydroboration of aldehydes and ketones using intramolecular heavier tetrelenes and phosphine based Lewis pairs [139]. Recently, Khan, Pati and coworkers have shown the hydroboration of aldehydes using *N*-heterocyclic germylens and stannylens [140]. However, there have been very few computational studies identifying the role(s) of germylens and stannylens in such reactions [141-145]. Computational investigations on hydroboration reactions with germylene and stannylene catalysts are even fewer [136,138,140]. This has inspired us to model new catalysts and investigate the hydroboration reaction computationally in order to find an efficient mechanistic pathway for the same (Table 1).

It has always been a challenge to model a catalyst and find an

efficient mechanistic pathway using computational tools. In the current work, we have first investigated a catalytic system that has already been proposed in the literature. Our investigations reveal a new mechanistic pathway that can be achieved by changing the concentration of the reacting species: the hydroborating agent pinacolborane (HBpin). Then, by modifying an experimentally synthesized and tested acyclic germanium based catalyst [146], we have modelled new germylene and stannylene catalyst systems, shown in Fig. 2 below, whose design has been directed by taking into consideration the HOMO-LUMO energy gap by using the TDDFT approach. We have then investigated our newly proposed mechanism for the aldehyde hydroboration reaction with the modelled α -Borylamido-germylene ((2,6-*i*Pr₂C₆H₃NBCy₂)₂Ge(II)) (Catalyst 3) and α -Borylamido-stannylene ((2,6-*i*Pr₂C₆H₃NBCy₂)₂Sn(II)) (Catalyst 4) systems, in the presence of the common hydroborating agent, HBpin.

To date, it has been believed that these families of stannylene and germylene systems proceed in the hydroboration reaction with HBpin via a four membered cyclic transition state. The current investigation

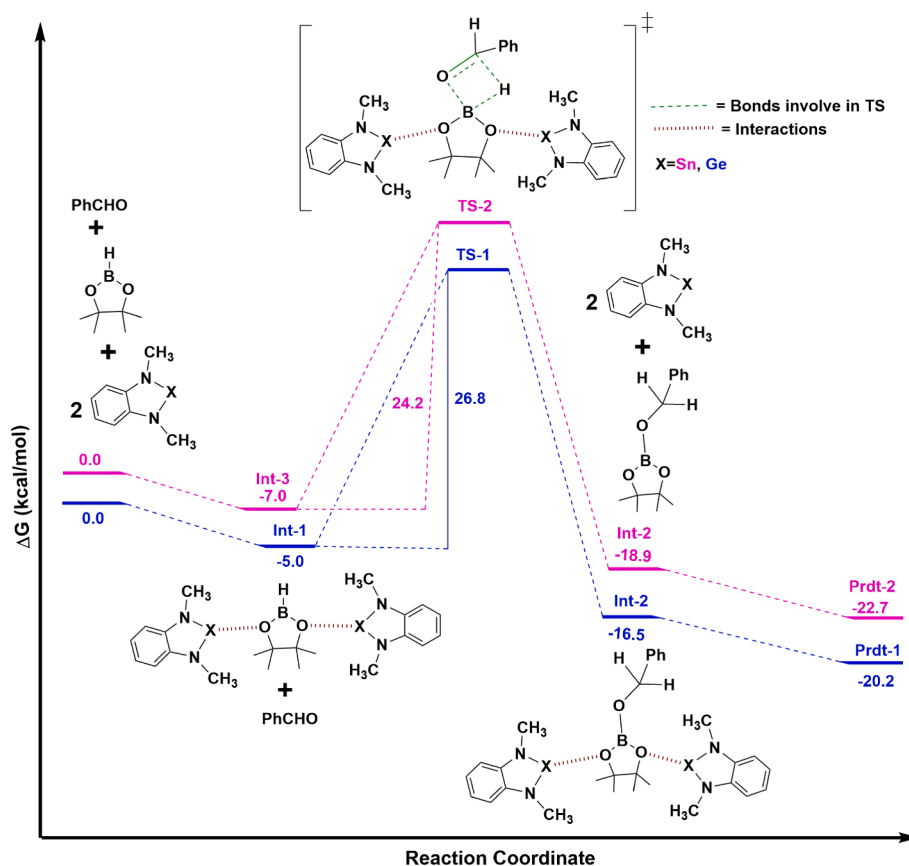


Fig. 4. The free energy profile for the hydroboration reaction with germylene and stannylene catalyst: mechanism proposed in the literature by Khan, Pati and coworkers [140]. The blue colored profile is for when *N*-heterocyclic germylene is used as a catalyst. The pink colored profile corresponds to the *N*-heterocyclic stannylene catalyst case.

shows that the hydroboration reaction proceeds via a six membered cyclic transition state. Along with the external catalyst, a molecule of HBpin assists in facilitating the reaction effectively. The current computational investigation thus finds new insights into the hydroboration reaction with low valent main group catalysts.

2. Computational details

All the calculations for the structures reported herein have been done using DFT [147-150]. The calculations have been carried out with Turbomole 7.4 [151] using the TZVP [152] basis set. Geometry optimizations were performed using the Perdew, Burke, and Ernzerhof (PBE) functional [153]. Dispersion corrections (D3) [154,155] have been included in all the calculations. Solvent corrections have also been included in the calculations using the COSMO model [156], with $\epsilon = 2.38$ to model toluene, PhCH_3 . Therefore, the level of theory employed is PBE-D3/TZVP + COSMO(PhCH_3) [152-156]. The resolution of identity (RI) [157,158] along with the multipole accelerated RI (marij) [159,160] approximations have been used for an accurate and efficient treatment of the electronic Coulomb term in the DFT calculations. Necessary care was taken to ensure that the obtained transition state structures possessed only one imaginary frequency corresponding to the correct normal mode, in order to obtain more reliable energy values for

the investigated potential energy surface. In addition, intrinsic reaction coordinate (IRC) [161] calculations were done with all the transition states in order to further confirm that they were the correct transition states, yielding the correct reactant and product structures. The values reported herein are ΔG values, with zero point energy, internal energy, and entropic contributions, with the temperature taken to be 298.15 K. The calculation of the translational entropy in standard software involves assumptions about the volume that may be inaccurate. The translational entropy term can be corrected by a free volume correction introduced by Mammen and co-workers [162]. Based on the Sackur-Tetrode equation, the free volume model describes the translational entropy of molecules in solution ($\Delta S_{\text{trans}}(\text{sol})$); and provides physically intuitive corrections for translational entropy values. In the free volume model, it has been assumed that the volume available to the molecule in solution is lower than the total volume, and this “free volume” is determined by the equation below:

$$V_{\text{free}} = C_{\text{free}} \left(\sqrt[3]{\frac{10^{27}}{[X]N_0}} - \sqrt[3]{V_{\text{molecule}}} \right)^3$$

here, V_{molecule} is the molecular volume, $[X]$ is the concentration of molecules (mol/L) in solution and N_0 is the Avogadro number. The translational entropy can be obtained after considering the free volume correction, and inserting the value of V_{free} in the Sackur-Tetrode equation. The total entropy is then calculated by adding the corrected translational entropy and the entropic contributions from the rotational and vibrational components.

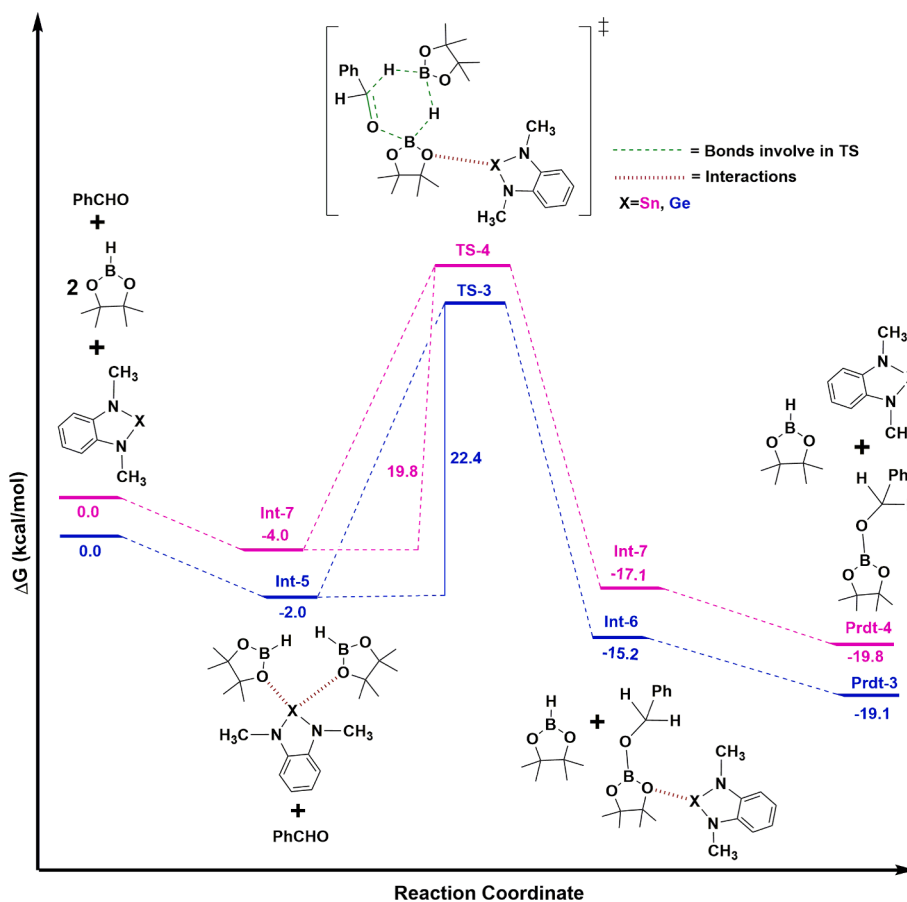


Fig. 5. The free energy profile for a new mechanism that we propose for the hydroboration of benzaldehyde by HBpin, in the presence of one *N*-heterocyclic germylene or the *N*-heterocyclic stannylene catalyst.

3. Results and discussions

At first, we have calculated the barrier for the proton relay mechanism without the stabilizing role of the catalysts. The barrier for this process was found to be 31.7 kcal/mol (see Fig. 3 below). The barrier would have to reduce below 31.7 kcal/mol when catalysts were considered. This was the case when we further investigated the mechanism with the involvement of the catalyst included.

Then we investigated the mechanism proposed by Khan, Pati and co-workers for the hydroboration reaction with *N*-heterocyclic germylene [140]. Initially, two *N*-heterocyclic germylene molecules interact with two oxygens of HBpin and form a stable intermediate. In the next step, the aldehyde reacts with this intermediate to form a borate adduct via a four membered cyclic transition state. This mechanism has been investigated computationally by Khan, Pati and coworkers [140], along with a competing mechanism where only one germylene molecule is involved as a catalyst with the HBpin and aldehyde reactants. The resultant barrier for the mechanism with one catalyst molecule was found by them to be higher than the barrier for the two catalyst case. The intermediate was also confirmed via NMR.

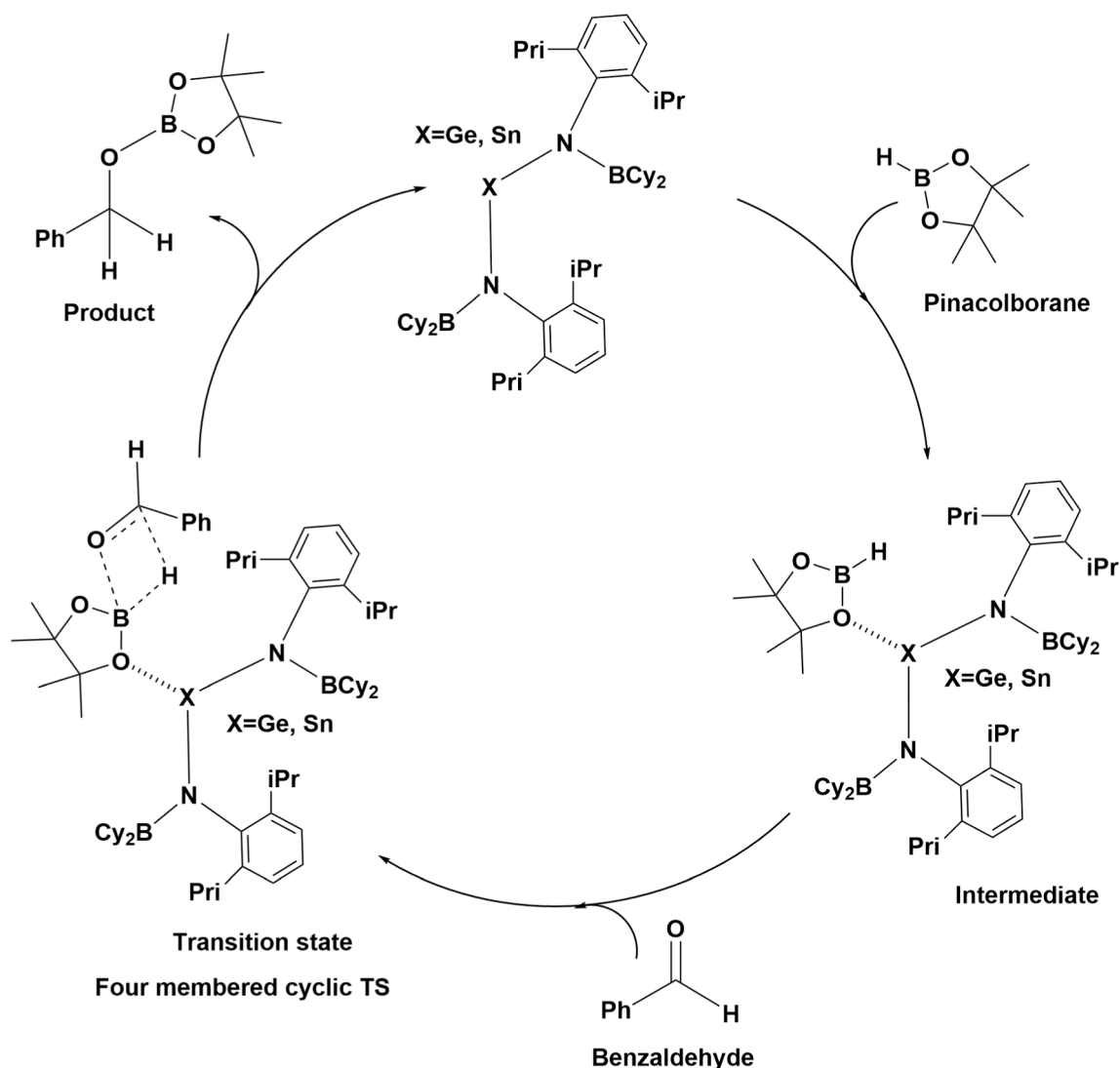
We began by investigating the mechanism where two catalysts were involved in the four membered cyclic transition state as proposed by Khan, Pati and coworkers [140]. In the first step of this mechanism, two catalyst molecules react with two oxygen atoms of HBpin. This forms an intermediate (Int-1) that is stable by 5.0 kcal/mol when *N*-heterocyclic germylene is used as the catalyst. When two molecules of stannylene and one molecule of HBpin are considered, the intermediate (Int-3) is stable

by 7.0 kcal/mol. After this, the aldehyde approaches and forms a four membered cyclic transition state. The barrier for the transition state (TS-1) was calculated to be 26.8 kcal/mol whereas the barrier for the transition state (TS-2) was 24.2 kcal/mol (see Fig. 4 below).

We then proceeded to reinvestigate the mechanism for this conversion. Instead of two germylene molecules acting as catalysts, we propose a system containing one germylene molecule, along with two HBpin and one aldehyde molecules. This is shown in the blue colored profile in Fig. 5 below. The two HBpin molecules form an intermediate with one *N*-heterocyclic germylene molecule. The intermediate (Int-5) is stable by 2.0 kcal/mol. Then, the aldehyde reacts with the intermediate (Int-5) via a six membered cyclic transition state. The barrier for this transition state (TS-3) is 22.4 kcal/mol. This indicates that the six membered transition state is favourable by 4.4 kcal/mol over the four membered cyclic transition state. We have also investigated the same mechanism with the stannylene catalyst. The catalyst forms a stable product via a six membered cyclic transition state. The barrier for the transition state (TS-4) is 19.8 kcal/mol (see pink colored profile in Fig. 5 below).

Then, we estimated the HOMO-LUMO energy gap by using the TDDFT approach for the germylene catalysts that have experimentally been employed for the hydroboration reaction, and discussed above.

We have estimated the HOMO-LUMO energy gap by using TDDFT: the first excitation energy obtained from the TDDFT calculations is taken to represent the HOMO-LUMO gap. It is to be noted that, when comparing different catalysts, the lower the value of the first excitation energy, the greater will be the accessibility of the LUMO to the incoming substrate that will act as the Lewis base in our proposed mechanism.



Scheme 1. The catalytic cycle and reaction mechanism for the aldehyde hydroboration by Catalyst-3 (X = Ge) and Catalyst 4 (X = Sn), via a four membered cyclic transition state.

Subsequent evaluation of the efficacy of different catalysts has been done keeping this aspect in mind. The TDDFT estimated HOMO-LUMO energy gap shows that experimentally synthesized catalyst by Khan, Pati and co-workers has a greater HOMO-LUMO energy gap than the computationally modeled catalyst considered in the current work. In the introduction, we have already mentioned that the lesser the HOMO-LUMO gap, the more is the reactivity of tetrelenes towards small molecules. The estimated HOMO-LUMO energy gap for the experimentally synthesized catalyst for hydroboration is 2.88 eV. Now, it has been found experimentally as well as computationally that the catalyst by Khan, Pati and co-workers can facilitate hydroboration reaction effectively. Therefore, it stands to reason that systems having a HOMO-LUMO gap below 2.88 eV can also catalyze hydroboration effectively, which is actually the case with the modeled catalyst in this work. Recently, Khan and coworkers experimentally obtained a bulky acyclic α -phosphinoamido-germylene ($(2,6\text{-iPr}_2\text{C}_6\text{H}_3\text{NPPh}_2)_2\text{Ge}$), which can be a potential catalyst for the hydroboration reaction [146]. The TDDFT estimated HOMO-LUMO gap for this catalyst was found to be 2.33 eV. Keeping the criterion of the HOMO-LUMO gap in mind, we propose new catalysts for the hydroboration reaction that are modifications of this recently

reported catalyst: α -Borylamido-germylene ($(2,6\text{-iPr}_2\text{C}_6\text{H}_3\text{NBCy}_2)_2\text{Ge}$ (II) (Catalyst-3) and α -Borylamido-stannylyene ($(2,6\text{-iPr}_2\text{C}_6\text{H}_3\text{NBCy}_2)_2\text{Sn}$ (II) (Catalyst-4). The TDDFT estimated HOMO-LUMO energy gap for the newly modeled germylene system is 2.42 eV. The replacement of the phosphorous atom by boron and also the replacement of the phenyl group with a cyclohexyl group leads to the increase in HOMO-LUMO gap by 0.09 eV, in comparison to the α -phosphinoamido-germylene ($(2,6\text{-iPr}_2\text{C}_6\text{H}_3\text{NPPh}_2)_2\text{Ge}$ catalyst mentioned above. Based on the HOMO-LUMO energy gap we hypothesized that the modeled germylene and stannylyene catalysts could further catalyze the hydroboration reaction.

In order to get insights into the hydroboration reaction with the newly designed systems, we have investigated the traditional mechanism of the hydroboration of benzaldehyde with Catalyst-3. As shown in Scheme 1, in the first step, a weakly bound complex (Int-9) between Catalyst-3 and HBpin would be formed, with one of the oxygen atoms of HBpin approaching the germanium atom of Catalyst-3.

Fig. 6 below shows the free energy profile for the proposed reaction. The DFT calculations show that the Ge-O distance (Ge from Catalyst-3 and oxygen from HBpin) is 3.73 \AA , and the intermediate (Int-9) is

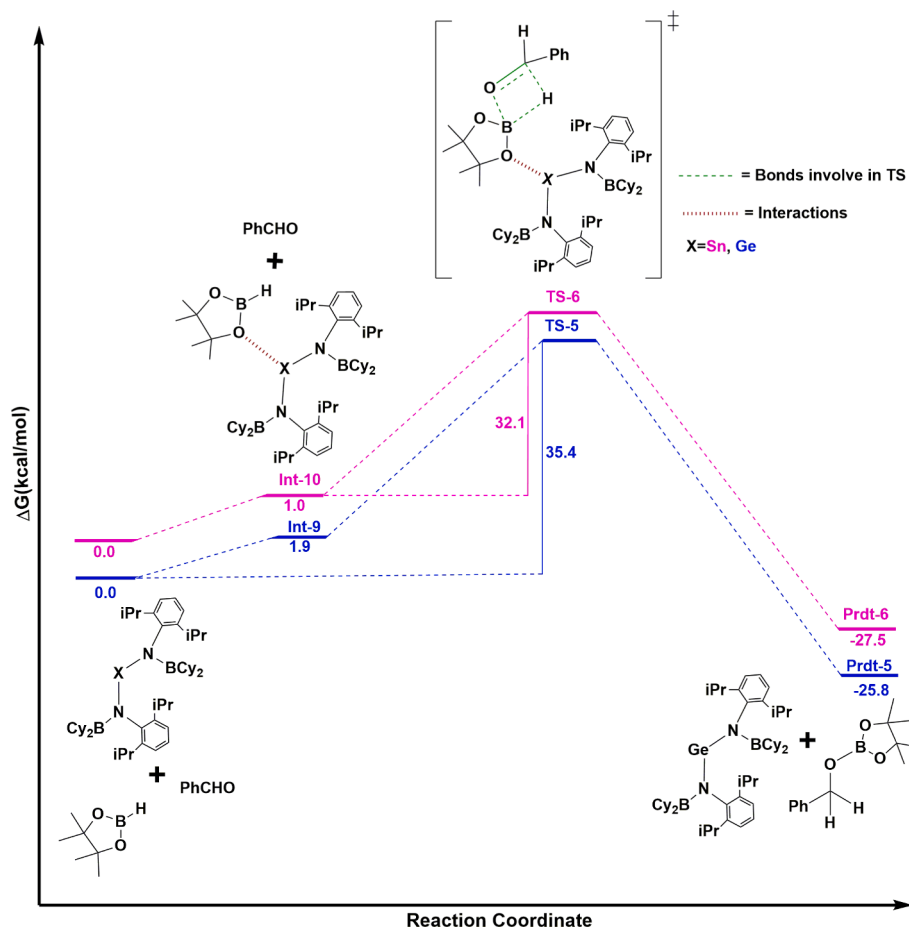


Fig. 6. The free energy profile for the catalytic aldehyde hydroboration by Catalyst-3 and Catalyst-4 with a four-membered cyclic transition state. The values (in kcal/mol) have been calculated at the PBE/TZVP level of theory. The blue colored energy profile is for hydroboration with Catalyst-3 and pink colored profile is for hydroboration with Catalyst-4.

unfavourable by 1.7 kcal/mol (ΔG) in comparison to the separated reactant species, Catalyst-3 and HBpin (see the blue colored profile in Fig. 6 below). Now, the benzaldehyde approaches the B-H bond of Int-9. This leads to nucleophilic attack by the carbonyl oxygen of benzaldehyde to the boron centre of HBpin, with the hydride being transferred from the boron centre to the electrophilic carbonyl carbon of the benzaldehyde. This occurs *via* a four membered cyclic transition state (TS-5) in the traditional mechanism reported in the literature, and leads to the formation of the hydroboration product along with the regeneration of the catalyst (see Fig. 6 below). The barrier (ΔG^\ddagger) corresponding to the transition state is 35.6 kcal/mol, which is high for a reaction that should take place at room temperature. We have also investigated the same pathway with Catalyst-4. The barrier for the four membered cyclic transition state is 32.1 kcal/mol (see the pink colored energy profile in Fig. 6 below).

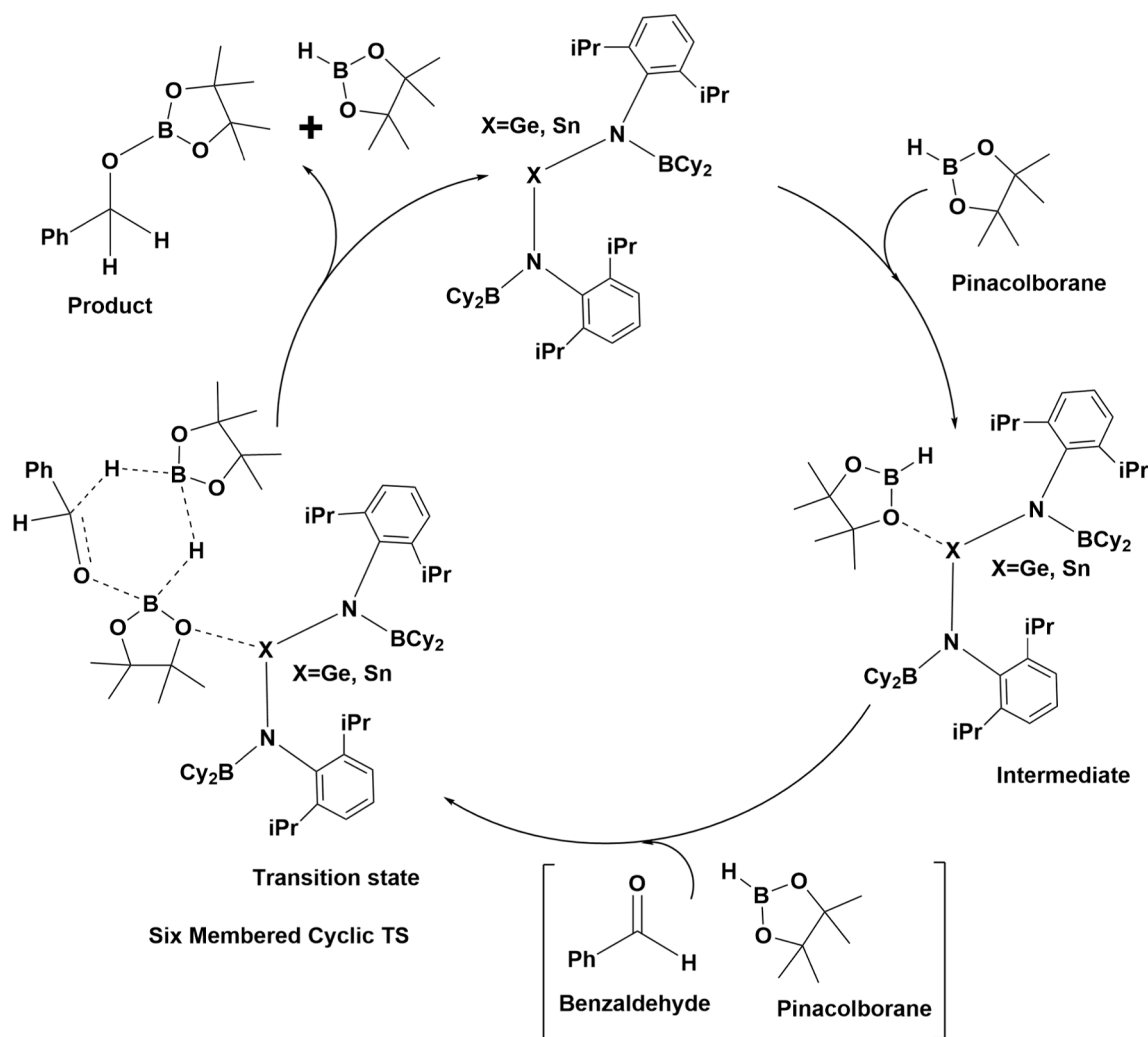
4. Calculations according to the newly proposed mechanism

Since the slowest step of the mechanism discussed above appears to be too high for a room temperature reaction, we have attempted to explore other mechanisms. For this, we have investigated the different

possible interactions between the metal centre (Ge) of the catalyst and pinacolborane. There are no interactions that were found that could stabilise the intermediate more than the Ge-O interaction (between the catalyst and pinacolborane) that we had already studied. Therefore, we considered this interaction to be the most favourable. We thus proceeded to investigate a six membered cyclic transition state, with two pinacolboranes and one aldehyde taking part: the mechanism that we had investigated and discussed above for the reported germylene system (see Fig. 75). This is illustrated in Scheme 2 below.

The transition state (TS-6) involves an HBpin molecule as the catalytic agent for a proton relay mechanism, while the Ge centre of the catalyst employed acts to stabilize the other HBpin molecule in the system. The activation energy (ΔG^\ddagger) barrier corresponding to this transition state is 25.7 kcal/mol, which is significantly lower than the corresponding barrier for the previously proposed mechanism (see Fig. 7 below) and explains why the reaction is feasible at room temperature. We note that the corresponding reaction using the stannylene catalyst also yielded a favourable reaction pathway. The barrier for this process was found to be 23.3 kcal/mol (see Fig. 7 below).

Therefore, the germylene and stannylene catalysts, with the aid of an additional HBpin molecule, allow the reaction to proceed in a facile



Scheme 2. The catalytic cycle and reaction mechanism for aldehyde hydroboration by Catalyst-3(X = Ge) and Catalyst-4(X = Sn), via a six-membered cyclic transition state.

manner under mild conditions. The current report thus reveals an interesting example of “dual” catalysis, where low valent main group compounds, as well as a substrate, both act as catalysts.

5. Conclusion

The current study, employing density functional theory (DFT), sheds light on the mechanism of the hydroboration reaction with low valent main group catalysts: germylenes and stannylenes, with the aid of the hydroborating agent, pinacolborane, HBpin. We have computationally investigated a previously proposed mechanism for a germylene catalyst system that has been experimentally reported. Then, we have compared the free energy profile of this reported mechanism with a newly proposed mechanism, which incorporates an additional HBpin molecule as a second catalyst. Subsequent to this, we have proposed two new catalysts, keeping in mind the electronic structure of previously reported germylenes and stannylenes. Considering the HOMO-LUMO energy gap calculations by using the TDDFT approach, we have computationally designed a new acyclic α -borylamido-germylene, and a stannylene catalyst having an electron deficient boron atom. We have investigated our newly proposed mechanism for the hydroboration reaction with these newly designed catalyst systems, and demonstrated that such a

mechanism would be effective in making these systems good catalysts for the hydroboration of aldehydes in the presence of HBpin as the hydroborating agent. The newly proposed mechanism thus provides new insights for the hydroboration reactions with germylene and stannylene catalysts.

CRediT authorship contribution statement

Subhrashis Banerjee: Data curation, Formal analysis, Investigation, Methodology, Validation, Visualization, Writing – original draft, Writing – review & editing. **Kumar Vanka:** Conceptualization, Formal analysis, Funding acquisition, Investigation, Methodology, Project administration, Resources, Software, Supervision, Writing – review & editing.

Declaration of Competing Interest

The authors declare that they have no known competing financial interests or personal relationships that could have appeared to influence the work reported in this paper.

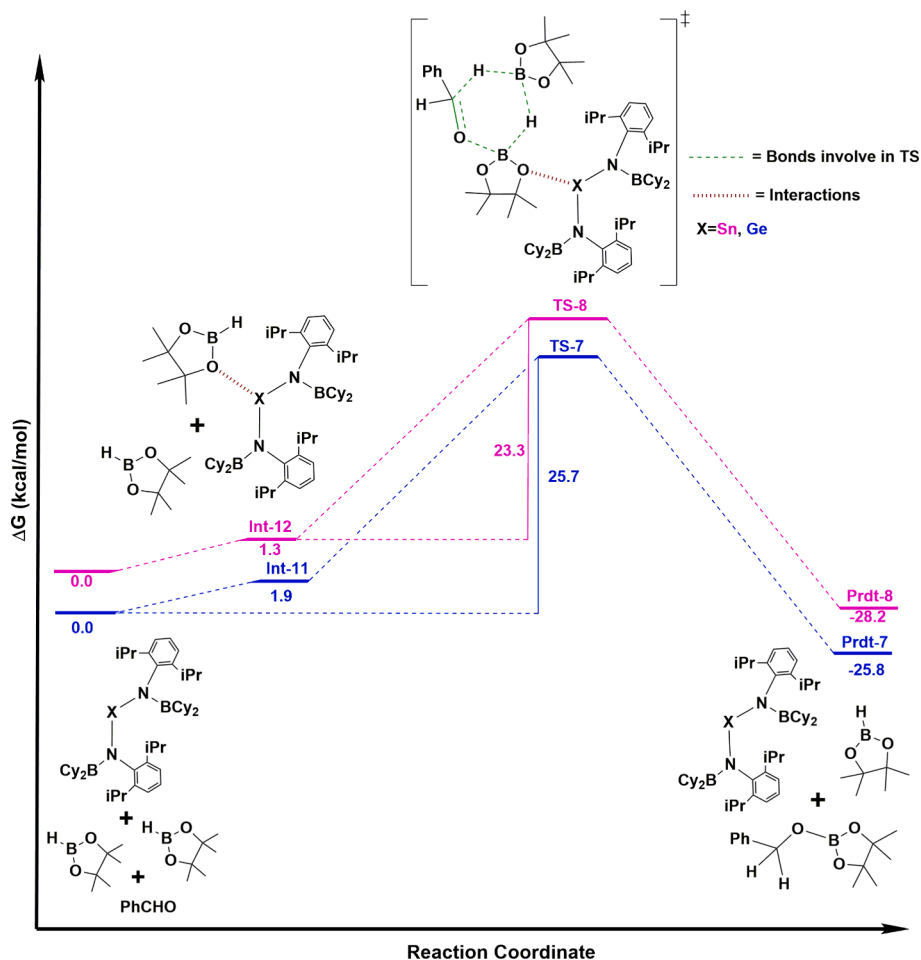


Fig. 7. The free energy profile for the catalytic aldehyde hydroboration by Catalyst-3 and Catalyst-4 passing through a six membered cyclic transition state. The values (in kcal/mol) have been calculated at the PBE/TZVP level of theory. The blue colored energy profile is for hydroboration with Catalyst-3 and pink colored profile is for hydroboration with Catalyst-4.

Acknowledgements

K.V. is grateful to the Department of Science and Technology (DST) (CRG/2021/003255) for providing financial assistance. S.B thanks Council of Scientific and Industrial Research (CSIR) for providing a Research Fellowship. K.V and S.B also thank Param Brahma and CSIR-4PI for providing computational facilities.

Appendix A. Supplementary data

Supplementary data to this article can be found online at <https://doi.org/10.1016/j.poly.2022.115907>.

References

- [1] P.P. Power, *Nature* 463 (2010) 171–177.
- [2] H. Braunschweig, R.D. Dewhurst, F. Hupp, M. Nutz, K. Radacki, C.W. Tate, A. Vargas, Q. Ye, *Nature* 522 (2015) 327–330.
- [3] P. Vasko, S. Wang, H.M. Tuononen, P.P. Power, *Angew. Chem. Int. Ed.* 54 (2015) 3802–3805.
- [4] Y. Peng, J.-D. Guo, B.D. Ellis, Z. Zhu, J.C. Fettingner, S. Nagase, P.P. Power, *J. Am. Chem. Soc.* 131 (2009) 16272–16282.
- [5] Y. Peng, B.D. Ellis, X. Wang, J.C. Fettingner, P.P. Power, *Science* 325 (2009) 1668–1670.
- [6] D. Martin, M. Soleilhavou, G. Bertrand, *Chem. Sci.* 2 (2011) 389–399.
- [7] M. Asay, C. Jones, M. Driess, *Chem. Rev.* 110 (2010) 354–396.
- [8] Y. Xiong, T. Szilvsi, S. Yao, G. Tan, M. Driess, *J. Am. Chem. Soc.* 136 (2014) 11300–11303.
- [9] A.V. Protchenko, J.I. Bates, L.M.A. Saleh, M.P. Blake, A.D. Schwarz, E. L. Kolychev, A.L. Thompson, C. Jones, P. Mountford, S. Aldridge, *J. Am. Chem. Soc.* 138 (2016) 4555–4564.
- [10] M. Hermann, C. Jones, G. Frenking, *Inorg. Chem.* 53 (2014) 6482–6490.
- [11] J. Li, M. Hermann, G. Frenking, C. Jones, *Angew. Chem. Int. Ed.* 2012, 51, 8611–8614; *Angew. Chem.* 124 (2012), 8739–8742.
- [12] M. Usher, A.V. Protchenko, A. Rit, J. Campos, E.L. Kolychev, R. Tirfoin, S. Aldridge, *Chem. Eur. J.* 22 (2016) 11685–11698.
- [13] Z. Yang, M. Zhong, X. Ma, K. Nijesh, S. De, P. Parameswaran, H.W. Roesky, *J. Am. Chem. Soc.* 138 (2016) 2548–2551.
- [14] S.K. Mandal, H.W. Roesky, *Acc. Chem. Res.* 45 (2012) 298–307.
- [15] A. Jana, H.W. Roesky, C. Schulzke, A. Dçring, *Angew. Chem. Int. Ed.* 48 (2009) 1106–1109.
- [16] M. Reißmann, A. Schfer, S. Jung, T. Müller, *Organometallics* 32 (2013) 6736–6744.
- [17] E. Rivard, *Chem. Soc. Rev.* 45 (2016) 989–1003.
- [18] V. Nesterov, D. Reiter, P. Bag, P. Frisch, R. Holzner, A. Porzelt, S. Inoue, *Chem. Rev.* 118 (2018) 9678–9842.
- [19] A.J. Arduengo III, R.L. Harlow, M. Kline, *J. Am. Chem. Soc.* 113 (1991) 361–363.
- [20] A.J. Arduengo III, J.R. Goerlich, W.J. Marshall, *J. Am. Chem. Soc.* 117 (1995) 11027–11028.
- [21] G.D. Frey, V. Lavallo, B. Donnadieu, W.W. Schoeller, G. Bertrand, *Science* 316 (2007) 439–441.
- [22] D.J. Nelsona, S.P. Nolan, *Chem. Soc. Rev.* 42 (2013) 6723–6753.
- [23] S.C. Sau, P.K. Hota, S.K. Mandal, M. Soleilhavou, G. Bertrand, *Chem. Soc. Rev.* 49 (2020) 1233–1252.
- [24] Á. Vivanos, C. Segarra, M. Albrecht, *Chem. Rev.* 118 (2018) 9493–9586.
- [25] E. Peris, *Chem. Rev.* 118 (2018) 9988–10031.
- [26] R. Becerra, N. Goldberg, J.P. Cannady, M.J. Almond, J.S. Ogden, R. Walsh, *J. Am. Chem. Soc.* 126 (2004) 6816–6824.
- [27] A. Jana, C. Schulzke, H.W. Roesky, *J. Am. Chem. Soc.* 131 (2009) 4600–4601.
- [28] N. Kuriakose, K. Vanka, *Dalton Trans.* 43 (2014) 2194–2201.
- [29] T. Chu, G.I. Nikonov, *Chem. Rev.* 118 (2018) 3608–3680.
- [30] M.M.D. Roy, A.A. Omaña, A.S.S. Wilson, M.S. Hill, S. Aldridge, E. Rivard, *Chem. Rev.* 121 (2021) 12784–12965.
- [31] P. Jutzi, N. Burford, *Chem. Rev.* 99 (1999) 969–990.
- [32] M. Kira, S. Ishida, T. Iwamoto, *Chem. Rec.* 4 (2004) 243–253.
- [33] M. Kira, *J. Organomet. Chem.* 689 (2004) 4475–4488.

- [34] A. Jana, I. Objartel, H.W. Roesky, D. Stalke, *Inorg. Chem.* 48 (2009) 798–800.
- [35] W. Wang, S. Inoue, S. Yao, M. Driess, *Chem. Commun.* (2009) 2661–2663.
- [36] W. Wang, S. Inoue, S. Yao, M. Driess, *Organometallics* 30 (2011) 6490–6494.
- [37] W. Wang, S. Inoue, S. Enthaler, M. Driess, *Angew. Chem., Int. Ed.* 51 (2012) 6167–6171.
- [38] Y. Mizuhata, T. Sasamori, N. Tokitoh, *Chem. Rev.* 109 (2009) 3479–3511.
- [39] T.J. Hadlington, M. Driess, C. Jones, *Chem. Soc. Rev.* 47 (2018) 4176–4197.
- [40] D.L. Kaysa, *Chem. Soc. Rev.* 45 (2016) 1004–1018.
- [41] K. Ota, R. Kinjo, *Chem. Soc. Rev.* 50 (2021) 10594–10673.
- [42] H. Braunschweig, R.D. Dewhurst, A. Schneider, *Chem. Rev.* 110 (2010) 3924–3957.
- [43] E.C. Neeve, S.J. Geier, I.A.I. Mkhaliid, S.A. Westcott, T.B. Marder, *Chem. Rev.* 116 (2016) 9091–9161.
- [44] M.-A. L egar e, C. Prankeviccius, H. Braunschweig, *Chem. Rev.* 119 (2019) 8231–8261.
- [45] H. Braunschweig, R.D. Dewhurst, V.H. Gessner, *Chem. Soc. Rev.* 42 (2013) 3197–3208.
- [46] G. Frenking, M. Hermann, D.M. Andrad a, N. Holzmann, *Chem. Soc. Rev.* 45 (2016) 1129–1144.
- [47] Y. Sua, R. Kinjo, *Chem. Soc. Rev.* 48 (2019) 3613–3659.
- [48] T. Taniguchi, *Chem. Soc. Rev.* 50 (2021) 8995–9021.
- [49] R. Tonner, G. Frenking, *Pure Appl. Chem.* 81 (2009) 597–614.
- [50] G. Frenking, *Angew. Chem. Int. Ed.* 53 (2014) 6040–6046.
- [51] Y. Xiong, S. Yao, S. Inoue, J.D. Epping, M. Driess, *Angew. Chem. Int. Ed.* 52 (2013) 7147–7150.
- [52] K.C. Mondal, S. Roy, H.W. Roesky, *Chem. Soc. Rev.* 45 (2016) 1080–1111.
- [53] B. Niep otter, R. Herbst-Irmer, D. Kratzert, P.P. Samuel, K.C. Mondal, H. W. Roesky, P. Jerabek, G. Frenking, D. Stalke, *Angew. Chem. Int. Ed.* 53 (2014) 2766–2770.
- [54] K.C. Mondal, H.W. Roesky, F. Klinke, M.C. Schwarzer, G. Frenking, B. Niep otter, H. Wolf, R. Herbst-Irmer, D. Stalke, *Angew. Chem. Int. Ed.* 52 (2013) 2963–2967.
- [55] Y. Wang, M. Karni, S. Yao, A. Kaushansky, Y. Apeloig, M. Driess, *J. Am. Chem. Soc.* 141 (2019) 12916–12927.
- [56] T. Koike, T. Nukazawa, T. Iwamoto, *J. Am. Chem. Soc.* 143 (2021) 14332–14341.
- [57] S. Karwasara, L.R. Maurer, B. Peerless, G. Schnakenburg, U. Das, A.C. Filippou, *J. Am. Chem. Soc.* 143 (2021) 14780–14794.
- [58] J. Keuter, A. Hepp, C. M uck-Lichtenfeld, F. Lips, *Angew. Chem. Int. Ed.* 58 (2019) 4395–4399.
- [59] S. Yao, A. Kostenko, Y. Xiong, A. Ruzicka, M. Driess, *J. Am. Chem. Soc.* 142 (2020) 12608–12612.
- [60] A. Burchert, S. Yao, R. M uller, C. Schattenberg, Y. Xiong, M. Kaupp, M. Driess, *Angew. Chem. Int. Ed.* 56 (2017) 1894–1897.
- [61] Y. Xiong, S. Yao, R. M uller, M. Kaupp, M. Driess, *Angew. Chem. Int. Ed.* 54 (2015) 10254–10257.
- [62] B. Su, R. Ganguly, Y. Li, R. Kinjo, *Angew. Chem. Int. Ed.* 53 (2014) 13106–13109.
- [63] T. Chu, L. Belding, A. van der Est, T. Dudding, I. Korobkov, G.I. Nikonov, *Angew. Chem. Int. Ed.* 53 (2014) 2711–2715.
- [64] T. Sugahara, T. Sasamori, N. Tokitoh, *Angew. Chem. Int. Ed.* 56 (2017) 9920–9923.
- [65] Y. Wang, M. Karni, S. Yao, Y. Apeloig, M. Driess, *J. Am. Chem. Soc.* 141 (2019) 1655–1664.
- [66] Y. Xiong, S. Yao, M. Karni, A. Kostenko, A. Burchert, Y. Apeloig, M. Driess, *Chem. Sci.* 7 (2016) 5462–5469.
- [67] G. Frenking, R. Tonner, S. Klein, N. Takagi, T. Shimizu, A. Krapp, K.K. Pandey, P. Parameswaran, *Chem. Soc. Rev.* 43 (2014) 5106–5139.
- [68] Y. Li, K.C. Mondal, H.W. Roesky, H. Zhu, P. Stollberg, R. Herbst-Irmer, D. Stalke, D.M. Andrad a, *J. Am. Chem. Soc.* 135 (2013) 12422–12428.
- [69] S. Yao, Y. Xiong, M. Driess, *Acc. Chem. Res.* 50 (2017) 2026–2037.
- [70] Y. Xiong, S. Yao, G. Tan, S. Inoue, M. Driess, *J. Am. Chem. Soc.* 135 (2013) 5004–5007.
- [71] P.J. Davidson, M.F. Lappert, *J. Chem. Soc., Chem. Commun.*, 1973, pp. 317a–317a.
- [72] D.H. Harris, M.F. Lappert, *J. Chem. Soc., Chem. Commun.* (1974) 895–896.
- [73] M.J.S. Gynane, M.F. Lappert, S.J. Miles, P.P. Power, *J. Chem. Soc., Chem. Commun.* (1976) 256–257.
- [74] D.E. Goldberg, D.H. Harris, M.F. Lappert, K.M. Thomas, *J. Chem. Soc., Chem. Commun.* (1976) 261–262.
- [75] M.F. Lappert, *J. Organomet. Chem.* 100 (1975) 139–159.
- [76] Y. Apeloig, R. Pauncz, M. Karni, R. West, W. Steiner, D. Chapman, *Organometallics* 22 (2003) 3250–3256.
- [77] C. Weetman, S. Inoue, *ChemCatChem* 10 (2018) 4213–4228.
- [78] M. Haaf, T.A. Schmedake, R. West, *Acc. Chem. Res.* 33 (2000) 704–714.
- [79] M.D. Roy, E. Rivard, *Acc. Chem. Res.* 50 (2017) 2017–2025.
- [80] S. Fujimori, S. Inoue, *Eur. J. Inorg. Chem.* 2020 (2020) 3131–3142.
- [81] R.L. Melen, *Science* 363 (2019) 479–484.
- [82] S. Yadav, S. Saha, S.S. Sen, *ChemCatChem* 8 (2016) 486–501.
- [83] A.V. Protchenko, K.H. Birjumar, D. Dange, A.D. Schwarz, D. Vidovic, C. Jones, N. Kaltsoyannis, P. Mountford, S. Aldridge, *J. Am. Chem. Soc.* 134 (2012) 6500–6503.
- [84] M. Kira, S. Ishida, T. Iwamoto, C. Kabuto, *J. Am. Chem. Soc.* 121 (1999) 9722–9723.
- [85] B.D. Rekker, T.M. Brown, J.C. Fettinger, H.M. Tuononen, P.P. Power, *J. Am. Chem. Soc.* 134 (2012) 6504–6507.
- [86] C. Hering-Junghans, P. Andreiuk, M.J. Ferguson, R. McDonald, E. Rivard, *Angew. Chem. Int. Ed.* 56 (2017) 6272–6275.
- [87] T. Ochiai, T. Szilv asi, D. Franz, E. Irran, S. Inoue, *Angew. Chem. Int. Ed.* 55 (2016) 11619–11624.
- [88] A.V. Protchenko, A.D. Schwarz, M.P. Blake, C. Jones, N. Kaltsoyannis, P. Mountford, S. Aldridge, *Angew. Chem. Int. Ed.* 52 (2013) 568–571.
- [89] D. Wendel, A. Porzelt, F.A.D. Herz, D. Sarkar, C. Jandl, S. Inoue, B. Rieger, *J. Am. Chem. Soc.* 139 (2017) 8134–8137.
- [90] L. Kristinsd ottir, N.L. Oldroyd, R. Grabner, A.W. Knights, A. Heilmann, A. V. Protchenko, H. Niu, E.L. Kolychev, J. Campos, J. Hicks, K.E. Christensena, S. Aldridge, *Dalton Trans.* 48 (2019) 11951–11960.
- [91] D. Munz, *Organometallics* 37 (2018) 275–289.
- [92] D.M. Andrad a, N. Holzmann, T. Hamadi, G. Frenking, *Beilstein J. Org. Chem.* 11 (2015) 2727–2736.
- [93] Y. Wang, J. Ma, *J. Organomet. Chem.* 694 (2009) 2567–2575.
- [94] M. Denk, R. Lennon, R. Hayashi, R. West, A.V. Belyakov, H.P. Verne, A. Haaland, M. Wagner, N. Metzler, *J. Am. Chem. Soc.* 116 (1994) 2691–2692.
- [95] R. Dasgupta, S. Khan, *Adv. Organomet. Chem.* 74 (2020) 105–152.
- [96] A.V. Protchenko, M.P. Blake, A.D. Schwarz, C. Jones, P. Mountford, S. Aldridge, *Organometallics* 34 (2015) 2126–2129.
- [97] L. Greb, F. Ebner, Y. Ginzburg, L.M. Sigmund, *Eur. J. Inorg. Chem.* 2020 (2020) 3030–3047.
- [98] H.C. Brown, B.C.S. Rao, *J. Am. Chem. Soc.* 81 (1959) 6423–6428.
- [99] A. Suzuki, *Proc. Japan Acad. Ser. B Phys. Biol. Sci.*, 80 (2004), pp. 359–371.
- [100] R.B. King, *Chem. Rev.* 101 (2001) 1119–1152.
- [101] W.E. Piers, *Adv. Organomet. Chem.* 52 (2004) 1–77.
- [102] A. Staubitz, A.P.M. Robertson, M.E. Sloan, I. Manners, *Chem. Rev.* 110 (2010) 4023–4078.
- [103] D.P. Curran, A. Solovveyev, M. Makhlof Brahm, L. Fensterbank, M. Malacria, E. Lacote, *Angew. Chem. Int. Ed.* 50 (2011) 10294–10317.
- [104] M. Arrowsmith, T.J. Hadlington, M.S. Hill, G. Kociok-Kohn, *Chem. Commun.* 48 (2012) 4567–4569.
- [105] G. Zhang, H. Zeng, J. Wu, Z. Yin, S. Zheng, J.C. Fettinger, *Angew. Chem. Int. Ed.* 55 (2016) 14369–14372.
- [106] K. Kuciński, G. Hreczycho, *Green Chem.* 21 (2019) 1912–1915.
- [107] J.H. Kim, A.K. Jaladi, H.T. Kim, D.K. An, *Bull. Korean Chem. Soc.* 40 (2019) 971–975.
- [108] S.J. Yang, A.K. Jaladi, J.H. Kim, S. Gundeti, D.K. An, *Bull. Korean Chem. Soc.* 40 (2019) 34–38.
- [109] A. Harinath, J. Bhattacharjee, H.P. Nayek, T.K. Panda, *Dalt. Trans.* 47 (2018) 12613–12622.
- [110] D.H. Ma, A.K. Jaladi, J.H. Lee, T.S. Kim, W.K. Shin, H. Hwang, D.K. An, *ACS Omega* 4 (2019) 15893–15903.
- [111] S. Yadav, S. Pahar, S.S. Sen, *Chem. Commun.* 53 (2017) 4562–4564.
- [112] Y. Wu, C. Shan, J. Ying, J. Su, J. Zhu, L.L. Liu, Y. Zhao, *Green Chem.* 19 (2017) 4169–4175.
- [113] R. McLellan, A.R. Kennedy, R.E. Mulvey, S.A. Orr, S.D. Robertson, *Chem.–A Eur. J.* 23 (2017) 16853–16861.
- [114] C. Gunanathan, M. Holscher, F. Pan, W. Leitner, *J. Am. Chem. Soc.* 134 (2012) 14349–14352.
- [115] Y.N. Liu, H.F. Su, Y.W. Li, Q.Y. Liu, Z. Jaglić, W.G. Wang, C.H. Tung, D. Sun, *Inorg. Chem.* 58 (2019) 4574–4582.
- [116] H. Zeng, J. Wu, S. Li, C. Hui, A. Ta, S.Y. Cheng, S. Zheng, G. Zhang, *Org. Lett.* 21 (2019) 401–406.
- [117] G. Zhang, J. Cheng, K. Davis, M.G. Bonifacio, C. Zajackowski, *Green Chem.* 21 (2019) 1114–1121.
- [118] C. Cop eret, B. Ghaffari, J. Mendes Burak, K.W. Chan, *Chem.–A Eur. J.* 25 (2019) 13869–13873.
- [119] K.A. Gudun, M. Segizbayev, A. Adamov, P.N. Plessow, K.A. Lyssenko, M. P. Balanay, A.Y. Khalimon, *Dalt. Trans.* 48 (2019) 1732–1746.
- [120] R. Ar evalo, C.M. Vogels, G.A. Macneil, L. Riera, J. P erez, S.A. Westcott, *Dalt. Trans.* 46 (2017) 7750–7757.
- [121] T. Bai, T. Janes, D. Song, *Dalt. Trans.* 46 (2017) 12408–12412.
- [122] Y. Ding, X. Ma, Y. Liu, W. Liu, C. Ni, B. Yan, L. Yan, Z. Yang, *Inorg. Chim. Acta* 497 (2019), 119091.
- [123] D. Jin, X. Ma, Y. Liu, J. Peng, Z. Yang, *Appl. Organomet. Chem.* 33 (2019), e4637.
- [124] A.J. Woodside, M.A. Smith, T.M. Herb, B.C. Manor, P.J. Carroll, P.R. Rablen, C. R. Graves, *Organometallics* 38 (2019) 1017–1020.
- [125] V.L. Weidner, C.J. Barger, M. Delferro, T.L. Lohr, T.J. Marks, *ACS Catal.* 7 (2017) 1244–1247.
- [126] W. Wang, X. Shen, F. Zhao, H. Jiang, W. Yao, S.A. Pullarkat, L. Xu, M. Ma, *J. Org. Chem.* 83 (2018) 69–74.
- [127] S. Chen, D. Yan, M. Xue, Y. Hong, Y. Yao, Q. Shen, *Org. Lett.* 19 (2017) 3382–3385.
- [128] D. Yan, P. Dai, S. Chen, M. Xue, Y. Yao, Q. Shen, X. Bao, *Org. Biomol. Chem.* 16 (2018) 2787–2791.
- [129] Z. Zhu, P. Dai, Z. Wu, M. Xue, Y. Yao, Q. Shen, X. Bao, *Catal. Commun.* 112 (2018) 26–30.
- [130] T. Ghatak, K. Makarov, N. Fridman, M.S. Eisen, *Chem. Commun.* 54 (2018) 11001–11004.
- [131] D. Mukherjee, H. Osseili, T.P. Spaniol, J. Okuda, *J. Am. Chem. Soc.* 138 (2016) 10790–10793.
- [132] N.A. Phillips, J. O’Hanlon, T.N. Hooper, A.J.P. White, M.R. Crimmin, *Org. Lett.* 21 (2019) 7289–7293.
- [133] J.L. Carden, L.J. Gierlich, D.F. Wass, D.L. Browne, R.L. Melen, *Chem. Commun.* 55 (2019) 318–321.
- [134] W. Wang, M. Luo, W. Yao, M. Ma, S.A. Pullarkat, L. Xu, P.H. Leung, *New J. Chem.* 43 (2019) 10744–10749.

- [135] T. Li, J. Zhang, C. Cui, *Chinese J. Chem.* 37 (2019) 679–683.
- [136] T.J. Hadlington, M. Hermann, G. Frenking, C. Jones, *J. Am. Chem. Soc.* 136 (2014) 3028–3031.
- [137] M. Driess, S. Yao, M. Brym, C.V. Willen, *Angew. Chem. Int. Ed.* 45 (2006) 4349–4352.
- [138] Y. Wu, C. Shan, Y. Sun, P. Chen, J. Ying, J. Zhu, L. Liu, Y. Zhao, *Chem. Commun.* 52 (2016) 13799–13802.
- [139] J. Schneider, C.P. Sindlinger, S.M. Freitag, H. Schubert, L. Wesemann, *Angew. Chem. Int. Ed.* 56 (2017) 333–337.
- [140] R. Dasgupta, S. Das, S. Hiwase, S.K. Pati, S. Khan, *Organometallics* 38 (2019) 1429–1435.
- [141] L. Zhong-yang, H. Long-qiang, S. Ahmadi, *J. Phys. Org. Chem.* 34 (2021), e4266.
- [142] N. Abedini, M.Z. Kassaei, *J. Phys. Org. Chem.* 34 (2021), e4208.
- [143] K.J. Iversen, J.L. Dutton, D.J.D. Wilson, *Chem. Asian J.* 12 (2017) 1499–1508.
- [144] M. Elveny, N.A. Alrazzak, A.M. Aljeboree, A.F. Alkaim, A.G. Ebadi, *J. Phys. Org. Chem.* 34 (2021), e4262.
- [145] H. Steinert, J. Löffler, V.H. Gessner, *Eur. J. Inorg. Chem.* 2021 (2021) 5004–5013.
- [146] S. Pal, R. Dasgupta, S. Khan, *Organometallics* 35 (2016) 3635–3640.
- [147] P. Hohenberg, W. Kohn, *Phys. Rev.* 136 (1964) B864–B871.
- [148] W. Kohn, L. Sham, *J. Phys. Rev.* 140 (1965) A1133–A1138.
- [149] Y. Zhao, D.G. Truhlar, *Theor. Chem. Acc.* 120 (2008) 215–241.
- [150] Y. Zhao, D.G. Truhlar, *Acc. Chem. Res.* 41 (2008) 157–167.
- [151] TURBOMOLE V7.4 2019, a development of University of Karlsruhe and Forschungszentrum Karlsruhe GmbH, 1989-2007, TURBOMOLE GmbH, since 2007; available from <http://www.turbomole.com>.
- [152] S. Ansgar, H. Christian, A. Reinhard, *J. Chem. Phys.* 100 (1994) 5829–5835.
- [153] J.P. Perdew, K. Burke, M. Ernzerhof, *Phys. Rev. Lett.* 77 (1996) 3865–3868.
- [154] S. Grimme, J. Antony, S. Ehrlich, H. Krieg, *J. Chem. Phys.*, 132 (2010), pp. 154104/1–154104/19.
- [155] S. Grimme, S. Ehrlich, L. Goerigk, *J. Comput. Chem.* 32 (2011) 1456–1465.
- [156] A. Klamt, G. Schuurmann, *J. Chem. Soc. Perkin Trans.* (1993) 799–805.
- [157] K. Eichkorn, O. Treutler, H. Öhm, M. Häser, R. Ahlrichs, *Chem. Phys. Lett.* 240 (1995) 283–290.
- [158] K. Eichkorn, F. Weigend, O. Treutler, F. Ahlrichs, *Theor. Chem. Acc.* 97 (1997) 119–124.
- [159] M. Sierka, A. Hogekamp, R. Ahlrichs, *J. Chem. Phys.* 118 (2003) 9136–9148.
- [160] P. Deglmann, K. May, F. Furche, R. Ahlrichs, *Chem. Phys. Lett.* 384 (2004) 103–107.
- [161] K. Fukui, *Acc. Chem. Res.* 14 (1981) 363–368.
- [162] M. Mammen, E.I. Shakhnovich, J.M. Deutch, G.M. Whitesides, *J. Org. Chem.* 63 (1998) 3821–3830.